UNIVERSITY OF OKLAHOMA

GRADUATE COLLEGE

NOVEL BIOMARKER APPLICATION REVEALS THE MICROBIAL ECOLOGICAL DYNAMICS SURROUNDING OCEANIC ANOXIC EVENT II (OAE-2)

A DISSERTATION

SUBMITTED TO THE GRADUATE FACULTY

in partial fulfillment of the requirements for the

Degree of

DOCTOR OF PHILOSOPHY

By

GREGORY THOMAS CONNOCK
Norman, Oklahoma
2021

NOVEL BIOMARKER APPLICATION REVEALS THE MICROBIAL ECOLOGICAL DYNAMICS SURROUNDING OCEANIC ANOXIC EVENT II (OAE-2)

A DISSERTATION APPROVED FOR THE

UNIVERSITY OF OKLAHOMA

SCHOOL OF GEOSCIENCES

BY THE COMMITTEE CONSISTING OF

Dr. Xiao-Lei Liu

Dr. Michael H. Engel

Dr. Gerilyn S. Soreghan

Dr. Lee R. Krumholz

Dr. Roger E. Summons

"Life is not a problem to be solved, but rather a mystery to be lived."
- adapted from Søren Kierkegaard

Abstract

Biomarkers are established facets of paleoenvironmental study, yet significant untapped potential remains. Conventional methods (e.g. GC-MS) fail to characterize large, polar molecules, which often possess greater biological specificity than saturated or aromatized hydrocarbons, while approaches leveraging the expanded analytical window intrinsic to LC-MS are frequently focused on a single compound class. Here, application of a novel LC-qTOF-MS method enabled simultaneous monitoring of numerous biomarkers, leading to the concept of a biomarker inventory populated with biosynthetic derivatives of marine microbial communities spanning the epipelagic to benthic realms. This comprehensive approach granted unparalleled insight into microbial ecological dynamics surrounding OAE-2, addressing outstanding enigmas related to the spatiotemporal evolution of organic carbon burial drivers. An extensive reassessment of previously discounted biomarkers revealed significant paleoreconstructive potential by tracking pelagic redox fluctuations in a menagerie of depositional settings, especially useful for delineating periods of marine deoxygenation (i.e. OAEs) in the geologic record. Critical evaluation of a potential OAE-2 trigger revealed both transient and enduring biochemical shifts relevant to an apparent association with enhanced organic carbon burial. However, the relationship between cause (i.e. trigger) and effect (OAE-2) was substantiated by currently unconsidered mechanisms that fundamentally alter the invocation of this trigger in paleoenvironmental research. This dissertation, documenting the incipient findings of method application, highlights the immense potential of LC-qTOF-MS as a cipher to decode the molecular signatures bound in the sedimentary archives.

Table of Contents

List of Figures

List of Tables

Acknowledgements

I am forever grateful to my advisor, Dr. Xiao-Lei Liu, for everything he did for me over the past three years. You always entertained my tangential thoughts and ramblings, were patient and understanding, and cultivated a collaborative relationship that I will cherish for years to come. Thank you for everything.

My sincere thanks to Dr. Jeremy Owens for your time, input, and engaging discussions about everything OAE-2. Your generosity sharing so many precious DSDP, ODP, and IODP samples is not taken for granted, and I hope I can return the favor one day.

I would also like to extend my gratitude to Dr. Engel. Our small talk, which often ascended to 'long' talks, was such a refreshing part of my day and I always looked forward to our paths crossing in the depths of Sarkeys.

I greatly appreciate my committee members, Dr. Gerilyn Soreghan, Dr. Lee Krumholz, and Dr. Roger Summons, in addition to my advisor and Dr. Engel, for providing me with valuable guidance throughout my progression from a PhD student to candidate and finally graduate. Thank you for the time you sacrificed serving on my committee and helping mold me into a better scientist along the way.

I am very grateful to Dr. R. Paul Philp, who not only introduced me to the field of organic geochemistry and focused my raw curiosity, but also aided in funding during my first year and served as an irreplaceable outlet for both technical and personal challenges I encountered.

I also would like to acknowledge the kindness of Dr. Roger Summons for sharing the cyanobacterial culture TLE, Dr. Yuichiro Kashiyama for the 17-nor-DPEP standards, and Dr.

Walter Vetter for the tocomonoenol isolates. Also, thank you Ms. Nikki Potter for entertaining my highly specific sampling requests for the RKB core.

My gratitude extends to the graduate students of the Geobiology Lab and Organic Geochemistry Groups at OU. Our conversations and seminars were always a bright spot in the week.

I would also like to thank the faculty in the School of Geosciences. I gained an alternative, more comprehensive perspective from every class I took, directly impacting the work in this dissertation. Additionally, many thanks to the office staff on the 7th floor, you do so much and never fail to have an answer for any question I would throw your way.

My sincerest gratitude goes out to my family for their everlasting support and love. Thank you for teaching me the value of hard work from an early age. Without it, I would likely not be where I am today, and am forever grateful.

Thank you Mandy, my wife and puzzle piece that makes me whole. Teaching me how to automatically generate the table of contents was a lifesaver, but more importantly, thank you for supporting me in this endeavor. Your love, willingness to listen to my biomarker chatter, and sheer existence mean more than you could ever know. You are my best friend and the love of my life. I am so lucky to be with you every day.

Finally, to my other two best friends Teddy and Finn, thank you for your endless happiness and love. You never failed to lift me up when I needed it the most.

Introduction

Why study the rock record?

The Earth is in a constant, natural state of change driven by gradual processes punctuated by geologically instantaneous and catastrophic events. Earth systems (geosphere, biosphere, atmosphere, hydrosphere, cryosphere) operate in tandem to maintain the semblance of an equilibrium amidst the backdrop of greater forcings (e.g. orbital 'Milankovitch' cycles) imposing an overriding control on the planetary state through time. The relatively rapid and incipient climate change initiated during the Industrial Era in the 1830s (Figure 1; Abram et al., 2016) has been exacerbated by continued societal demands today. Model simulations grant invaluable insight into projections of future climatic states, but represent a composite signal of multiple scenarios with a range of outcomes undermined by inherent biases (e.g. Liang et al., 2008) and uncertainties (e.g. Knutti and Sedlacek, 2013). This is compounded by the brevity of the pre-industrial and historical records used in model parameterization tuning (Schmidt et al., 2017), which may compromise output relevance in a warming world as highlighted by inaccurate model-based reconstructions of past periods of warm climate (e.g. early Eocene; Huber and Caballero, 2011). Thus, one answer to the question, 'why study the rock record?', emerges.

The sedimentary archives are vast, recording a wide variety of climatic states spanning millions of years. The reductionist phrase 'the present is the key to the past' stemming from the principle of uniformitarianism (Hutton, 1788; Lyell, 1830; Whewell, 1832) may also be reworded as 'the past is the key to the present and future' (Doe, 1983). Study of the past may grant insight into how various Earth systems operated and responded to natural change before and [potentially] will in the future. The temporal heterogeneity of paleoclimates, affording an abundance of potential analogs for theoretical climate scenarios, is underscored by the immense climatic

variability observed over the last 100 Ma (Figure 2; Tierney et al., 2020). From the extremes of the mid-Cretaceous hothouse to the late Pleistocene Last Glacial Maximum, an abundance of distinct paleoclimatic scenarios is at the disposal of scientists today. Significantly, the results of these natural climate experiments are encoded into the rock record, and are readily accessible via geoscientific investigations which generate valuable context and/or proxy data to aid model calibrations. Continued integration of model and proxy/contextual information is paramount to improve climate forecasts and mitigate attendant impacts, with improved interpretations of the rock record equally as important as computational advances furthering model sophistication. This work focuses on the former, empowering the past as an analog for the future by reimagining the application of an established geochemical proxy for ancient microbial life referred to as 'biomarkers.'

Biomarkers

Biomarkers are molecular fossils of past [predominantly] microbial life preserved in sediments and rocks. Although intimidating to those unfamiliar with the concept, biomarkers can be thought of as partially degraded geological fossils of biosynthetic products just as macrofossils represent the recalcitrant remains (e.g. bones) of defunct organisms (Figure 3). The concept of a 'biomarker' in organic geochemical research was born when molecular signatures of exclusively biological origin were characterized in sedimentary organic matter and oils (Treibs, 1936). Subsequent instrumental advancements led to the advent of gas chromatograph (GC) mass spectrometers (MS) interfaced with an on-line computer system (e.g. Hites and Biemann, 1967; Burlingame and Schnoes, 1969), which greatly accelerated the detection and identification of biomarkers in the geosphere. This was further propelled by the petroleum industry (e.g. Philp, 1985; Seifert and Moldowan, 1986; Peters et al., 2005) following the discovery of molecular

evidence for the biogenic origin of petroleum (Whitehead, 1973). The allure of biomarkers extended into academic pursuits as well, particularly origins of life studies, given these 'chemical fossils' do not require the preservation of intact organisms or parts of organisms (Eglinton and Calvin, 1967), leading to significant insight into early life on Earth (e.g. Summons et al., 1988; Brocks et al., 2005). Later analytical advances, such as liquid chromatography-mass spectrometry (LC-MS), enabled the detection of larger, more polar compounds (e.g. glycerol dialkyl glycerol tetraethers, GDGTs) of [potentially] greater biological, and by extension, environmental specificity (Hopmans et al., 2000; Sturt et al., 2004). Continued progression has arisen via the integration of organic geochemistry with other disciplines, such as molecular biology and phylogenetics, which has fostered the application of lipidomics (Pearson, 2014) in geochemical study that is challenging and refining the proposed, potential origins of many biomarkers (e.g. 2-methylhopanoids; Rashby et al., 2007; Elling et al., 2020). These advances are conceivable due to the highly conserved nature of membrane lipid biosynthesis through time (Summons et al., 2006), which has enabled many of these molecular fossils to be correlated to extant life, ultimately enhancing their inherent paleoreconstructive potential.

Life is a function of the surrounding environment [and vice versa to an extent], which is why biomarker distributions are powerful tools in paleoenvironmental reconstructions. Biological specificity may vary, with some biomarkers linked to a certain taxonomic family (e.g. isorenieratane and the green sulfur bacteria, *Chlorobiaceae*; Liaaen-Jensen et al., 1964), and others ubiquitously produced by a specific domain of life (e.g. hopanoids and Bacteria; Rohmer et al., 1979; 1984; Ourisson et al., 1987). This imparts varying degrees of paleoenvironmental insight to individual biomarkers or biomarker classes. For example, isorenieratane is a widely observed fossil pigment in marine deposits spanning the Phanerozoic (French et al., 2015; Cui et al., 2020),

signifying the relatively pervasive recurrence of photic zone euxinia (PZE; Summons and Powell, 1987) in the geologic record. Environmental deductions of PZE may be inferred from sedimentary occurrences of isorenieratane due to the clear derivation from isorenieratene biosynthesized by *Chlorobiaceae* that require light and hydrogen sulfide (i.e. PZE) as obligately anaerobic phototrophic sulfur bacteria (Truper and Genovese, 1968; van Gemerden, 1983). Thus, detection of isorenieratane in sediments and rocks provides strong evidence for the presence of PZE during deposition. Biomarkers may record both qualitative (e.g. redox conditions, water column chemistry and structure, microbial community compositions) and quantitative (e.g. sea surface temperatures, SSTs) information of paleoenvironmental relevance. Greater perspectives on biogeochemical cycling, the origins of life, and the biotic response following major climatic and/or extinction events may be achieved using biomarkers as means to reanimate past interactions between life and the environment. Yet, a variety of processes may alter the molecular signal post-senescence (e.g. diagenesis, catagenesis, contamination), with the conversion of living biomass to fossilized organic matter particularly poorly constrained, which must be considered and minimized when possible to limit misinterpretation of biomarker records. Thermal maturity is easily determined via pyrolysis methods (e.g. Rock Eval; Espitalie et al., 1977), and contamination by living organisms, exogenous migrated hydrocarbons, and anthropogenic sources can be ruled out using applied logic and appropriate handling procedures. For example, the presence of intact polar lipids or branched alkanes with quaternary carbons may indicate contamination from living communities and plastics (Brocks et al., 2008; Liu et al., 2011), respectively, while assessing the regional structural and stratigraphic history of a basin may identify a potential risk for allochthonous hydrocarbon charge contaminating the indigenous biomarker signature. However, the poorly defined diagenetic pathways remain a concern for any organic geochemical study, as

biased degradation may mask the genetic environmental signal and undermine subsequent interpretations (e.g. Wakeham et al., 1997). The subsequent section will address how I attempted to mitigate potential preservation biases through application of a structurally diverse biomarker inventory.

Study novelty, objectives, and outline

The chapters in this work were produced by implementing a novel analytical method and approach to provide an updated perspective on biomarkers in paleoenvironmental study. Development of a new liquid chromatography – quadrupole time-of-flight – mass spectrometry (LC-qTOF-MS) method, outlined in Chapter 1, enabled two common shortcomings in many biomarker studies to be addressed and explored. Most biomarker studies employ a GC-MS and/or GC-MS/MS that limits investigations to defunctionalized molecules, typically fully saturated and aromatic hydrocarbons, and is appropriate for many settings subjected to post-depositional processes (e.g. thermal stress, weathering) whereby only carbon skeletons remain. However, if any large, polar [potentially] functionalized compounds were present (e.g. crenarchaeol), then the relatively narrow analytical window of GC-MS ionization methods (e.g. electron impact in GC-MS vs. electrospray in LC-MS; Figure 4) would preclude detection and result in an incomplete characterization of the molecular signal and underrepresentation of biomarker diversity. This is especially relevant in pristine samples (e.g. Integrated Ocean Drilling Program, IODP, cores) characterized by exceptional biomarker preservation as demonstrated by the preservation of functionalized chlorins in ~100 Ma black shales (Junium et al., 2011). Utilization of LC-MS circumvents this inherent limitation of GC-MS, but many studies using LC-MS are highly focused on a single compound class (e.g. GDGTs) targeting a specific question (e.g. sea surface

temperature history). Thus, the potential of LC-MS and biomarkers in paleoenvironmental study remains to be realized and forms the core objective of this work.

The development of a novel LC-qTOF-MS method greatly expanded the targeted analytes in this study, overcoming analytical limitations intrinsic to GC-MS. In addition, an attempt was made to identify as many biomarker classes as possible, leading to the population of a diverse biomarker inventory that contrasts the narrow scopes of conventional LC-MS biomarker investigations. It should be noted that the novelty of the analytical method outlined here afforded a more comprehensive biomarker assessment to be conducted. All compounds were measured in a single run, simultaneously, which has not been achieved before and partially explains why a paucity of comprehensive LC-based biomarker studies exist. Method novelty was amplified by minimal sample requirements and preparation that accelerated sample processing and data acquisition.

The initial objective of this study was to assess LC-qTOF-MS viability in biomarker-driven paleoenvironmental reconstructions. Preliminary screening of Cenomanian-Turonian black shales from ODP Site 1258 on the Demerara Rise revealed exceptional biomarker preservation and spawned the term ‘biomarker inventory.’ This term, biomarker inventory, is used throughout this work to encapsulate the diverse biomarker classes detected in mid-Cretaceous strata across the globe. At its core, it is intended to signify the comprehensive biomarker profiling ability enabled by this new method and how it affords the organic geochemist unparalleled insight into microbial ecological dynamics in the past. Simultaneous detection of distinct microbial derivatives, and in some cases unaltered biosynthetic products (e.g. tocopherols, see Chapter 2), hailing from specific marine habitats (e.g. epipelagic vs. benthic) is a new, potent tool for paleoenvironmental research.

Demonstrating the effectiveness and investigative capacity of this method and approach is critical for further adoption and application to be realized, and forms the core objective of this work.

The mid-Cretaceous was marked by one of the largest carbon cycle perturbations of the Phanerozoic referred to as Oceanic Anoxic Event-2 (OAE-2; Scholle and Arthur, 1980; Owens et al., 2018). Extensive study of the most widely observed OAE (OAE-2) has revealed additional, coeval changes across multiple Earth systems, such as biogeochemical cycling disturbances (Kuypers et al., 2004; Mort et al., 2007; Higgins et al., 2012; Raven et al., 2019), trace metal drawdown (Hetzel et al., 2009; Owens et al., 2016), rapid SST fluctuations (Forster et al., 2007; O'brien et al., 2017), and regional development of PZE (Sinninghe Damsté and Köster, 1998; Kuypers et al., 2002). This pronounced environmental dynamicity surrounding OAE-2 likely imparted significant effects that cascaded through marine microbial communities, which was ultimately preserved in the biomarker record. Thus, OAE-2 and its lasting enigmas, despite decades of study, provided an ideal testing bed to assess the viability of the LC-qTOF-MS method and biomarker inventory approach in paleoenvironmental study. Key questions were:

1. What initiated the progressive deoxygenation preceding OAE-2 as defined by the positive carbon isotope excursion?
2. How do proposed triggers for enhanced organic carbon burial impact marine environments? What is the extent and duration of these effects as inferred from stratigraphic trends in biomarker inventories?
3. How do organic carbon burial drivers, principally productivity and preservation, vary over time and across space? What are the implications for the positive carbon isotope excursion, OAE-2, and other periods of widespread deoxygenation in Earth history?

Chapter 1 forms the foundational work of this study from which all other chapters stem. It confirmed the anticipated potential of the LC-qTOF-MS method, underscored by the discovery of an expansive biomarker inventory capturing microbial ecological dynamics spanning the entire water column and sediments. The recognition of an extended period of enhanced primary productivity in the southern proto-North Atlantic, termed the pre-OAE biotic perturbation (pre-OAE BP), provided the first direct evidence of a causal mechanism initiating pre-OAE marine deoxygenation. Furthermore, a distinct compositional shift in microbial communities coincident with the OAE-2 interval was identified and tied to evolving organic carbon burial drivers at Demerara Rise. This presented some of the first evidence that these processes may operate along a continuum locally, setting up the multi-site study in Chapter 4.

Chapter 2 leverages the greater analytical window inherent to LC-MS to detect and assess the paleoenvironmental significance of tocopherols (i.e. Vitamin E) and associated derivatives, frequently overlooked and discounted by past organic geochemical study. For the first time methylphytylbenzoquinones (MPBQs), products of tocopherol recycling, were reported in geologic samples in exceptionally high abundance. This chapter also explores the rare cooccurrence of tocopherols and MTTCs, discussing potential implications for MTTC origin, which is timely given the increasing popularity of MTTCs in paleoenvironmental study. Most significantly, a series of tocol derivative ratios were developed that bracket the OAE-2 interval exceptionally well due to an apparent sensitivity to shallow water (i.e. photic zone) anoxia, and situationally, may record a phytoplanktonic stress response. These findings are applied to subsequent chapters and form a key part of later interpretations.

Chapter 3 assesses the biotic and chemical impacts of subaerial volcanism on marine environments in the mid-Cretaceous Western Interior Seaway of North America. Growing

invocation of volcanism as a mechanism to enhance carbon burial during OAE-2, as well as other periods of widespread black shale deposition, provided an impetus to evaluate the duration of volcanogenic effects on marine systems. High-resolution sampling across three mid-Cretaceous ash beds enabled both short- and long-term trends to be evaluated following major eruptions. Transient increases in primary production were limited to the immediate aftermath of ash deposition, challenging current thinking reliant on enduring stimulatory effects (e.g. iron fertilization). However, a pronounced and lasting transition towards anoxia/euxinia near the sediment-water interface was observed after the two largest eruptive events. Thus, a link between volcanism and enhanced organic carbon burial was confirmed, but via a different mechanism (i.e. enhanced preservation) than currently proposed (i.e. enhanced productivity).

Chapter 4 represents the spatial extrapolation of Chapter 1, incorporating aspects of the preceding chapters to address fundamental questions surrounding OAE-2 initiation, perpetuation, and termination. A latitudinal transect spanning distinct depositional settings across the proto-North Atlantic revealed basin-wide microbial ecological dynamics elucidating the spatial character of the pre-OAE BP and diachroneity of organic carbon burial drivers surrounding OAE-2. Spatiotemporal evolution of depth-specific microbial communities highlighted how nutrient distributions were governed by water column redox gradients, ultimately affecting the production and preservation of organic carbon. Differential propagation of oxygen minimum zones across the proto-North Atlantic through time imposed significant control on predominant organic carbon burial drivers locally, exposing undocumented complexities generalized by the positive carbon isotope excursion and detailing the lifecycle of OAE-2.

References

1. Abram, N. J., McGregor, H. V., Tierney, J. E., Evans, M. N., McKay, N. P., Kaufman, D. S., & the PAGES 2k Consortium. (2016). Early onset of industrial-era warming across the oceans and continents. Nature, 536, 411-418.
2. Burlingame, A. L., & Schnoes, H. K. (1969). Mass spectrometry in organic geochemistry. Organic Geochemistry, Springer, Berlin, Heidelberg, 89-160.
3. Brocks, J.J., Love, G.D., Summons, R.E., Knoll, A.H., Logan, G.A., & Bowden, S.A. (2005). Biomarker evidence for green and purple sulphur bacteria in a stratified Palaeoproterozoic sea. Nature, 437, 866–870.
4. Brocks, J.J., Grosjean, E., & Logan, G.A. (2008). Assessing biomarker syngeneity using branched alkanes with quaternary carbon (BAQCs) and other plastic contaminants. Geochimica et Cosmochimica Acta, 72, 871–888.
5. Cui, X., Liu, X.-L., Shen, G., Ma, J., Husain, F., Rocher, D., Zumberge, J. E., Bryant, D. A., & Summons, R. E. (2020). Niche expansion for phototrophic sulfur bacteria at the Proterozoic-Phanerozoic transition. Proceedings of the National Academy of Sciences, 117, 17599-17606.
6. Doe, B. R. (1983). The past is the key to the future. Geochimica et Cosmochimica Acta, 47, 1341-1354.
7. Eglinton, G., & Calvin, M. (1967). Chemical fossils. Scientific American, 261, 32-43.
8. Elling, F. J., Hemingway, J. D., Evans, T. W., Kharbush, J. J., Spieck, E., Summons, R. E., & Pearson, A. (2020). Vitamin B_{12}-dependent biosynthesis ties amplified 2-methylhopanoid production during oceanic anoxic events to nitrification. Proceedings of the National Academy of Sciences, 117, 32996-33004.
9. Espitalie, J., Laporte, J. L., Madec, M., Marquis, F., Leplat, P., Paulet, J., & Boutefeu, A. (1977). Rapid method for source rock characterization and for determination of their petroleum potential and degree of evolution. Revue de l'Institut Francais du Petrole et Annales des Combustibes Liquides, 32, 23-42.
10. Forster, A., Schouten, S., Moriya, K., Wilson, P. A., & Sinninghe Damsté, J.S. (2007). Tropical warming and intermittent cooling during the Cenomanian/Turonian oceanic anoxic event 2: Sea surface temperature records from the equatorial Atlantic. Paleoceanography, 22, PA1219.
11. French K. L., Rocher D., Zumberge J. E. & Summons R. E. (2015). Assessing the distribution of sedimentary C_{40} carotenoids through time. Geobiology, 13, 139–151.
12. Hetzel, A., Böttcher, M. E., Wortmann, U. G., & Brumsack, H.-J. (2009). Paleo-redox conditions during OAE 2 reflected in Demerara Rise sediment geochemistry (ODP Leg 207). Palaeogeography, Palaeoclimatology, Palaeoecology, 273, 302-328.
13. Higgins, M. B., Robinson, R. S., Husson, J. M., Carter, S. J., & Pearson, A. Dominant eukaryotic export production during ocean anoxic events reflects the importance of recycled NH_4^+. Proceedings of the National Academy of Sciences, 109, 2269-2274.
14. Hites, R. A., & Biemann, K. (1967). Mass spectrometer-computer system particularly suited for gas chromatography of complex mixtures. Analytical Chemistry, 40, 1217-1221.
15. Hopmans, E. C., Schouten, S., Pancost, R. D., van der Meer, M. T. J., Sinninghe Damsté, J. S. (2000). Analysis of intact tetraether lipids in archaeal cell material and sediments by high performance liquid chromatography/atmospheric pressure chemical ionization mass spectrometry. Rapid Communications in Mass Spectrometry, 14, 585–589.

16. Huber, M., & Caballero, R. (2011). The early Eocene equable climate problem revisited. Climate of the Past, 7, 603-633.
17. Hutton, J. (1788). Theory of the Earth. Transactions of the Royal Society of Edinburgh, 1.
18. Junium, C. K., Keely, B. J., Freeman, K. H., & Arthur, M. A. (2011). Chlorins in mid-Cretaceous black shales of the Demerara Rise: The oldest known occurrence. Organic Geochemistry, 42, 856-859.
19. Knutti, R., & Sedlacek, J. (2013). Robustness and uncertainties in the new CMIP5 climate model projections. Nature Climate Change 3, 369-373.
20. Kuypers, M. M. M., Pancost, R. D., Nijenhuis, I. A., & Sinninghe Damsté, J. S. (2002). Enhanced productivity led to increased organic carbon burial in the euxinic North Atlantic basin during the late Cenomanian oceanic anoxic event. Paleoceanography, 17, PA000569.
21. Kuypers, M. M. M., van Breugel, Y., Schouten, S., Erba, E., and Sinninghe Damsté, J. S. (2004). N_2-fixing cyanobacteria supplied nutrient N for Cretaceous oceanic anoxic events. Geology, 32, 853-856.
22. Liaaen-Jensen, S., Hegge, E., & Jackman, L. M. (1964). Bacterial carotenoids XVIII, The carotenoids of photosynthetic bacteria, Acta Chemica Scandinavica, 18, 1703-1718.
23. Liang X. Z., Kunkel K. E., Meehl G. A., Jones R. G. & Wang J. X. L. (2008). Regional climate models downscaling analysis of general circulation models present climate biases propagation into future change projections. Geophysical Research Letters, 35, 1–5.
24. Liu, X.-L., Lipp, J. S., & Hinrichs, K.-U. (2011). The distribution of intact and core GDGTs in marine sediments. Organic Geochemistry, 42, 368-375.
25. Lyell, C. (1830). Principles of Geology. John Murray, Albemarle street, London.
26. Mort, H.P., Adatte, T., Föllmi, K.B., Keller, G., Steinmann, P., Matera, V., Berner, Z., & Stüben, D. (2007). Phosphorus and the roles of productivity and nutrient recycling during oceanic anoxic event 2. Geology, 35, 483-486.
27. O'Brien, C. L., Robinson, S. A., Pancost, R. D., Sinninghe Damsté, J. S., Schouten, S., Lunt, D. J., Alsenz, H., Bornemann, A., Bottini, C., Brassell, S. C., Farnsworth, A., Forster, A., Huber, B. T., Inglis, G. N., Jenkyns, H. C., Linnert, C., Littler, K., Markwick, P., McAnena, A., Mutterlose, J., Naafs, B. D. A., Püttmann, W., Sluijs, A., van Helmond, N. A. G. M., Vellekoop, J., Wagner, T., & Wrobel N. E. (2017). Cretaceous sea-surface temperature evolution: Constraints from TEX 86 and planktonic foraminiferal oxygen isotopes. Earth-Science Reviews, 172, 224–247.
28. Ourisson, G., Rohmer, M., & Poralla, K. (1987). Prokaryotic hopanoids and other polyterpenoid sterol surrogates. Annual Review of Microbiology, 41, 301-333.
29. Owens, J. D., Reinhard, C. T., Rohrssen, M., Love, G. D., & Lyons T. W. (2016). Empirical links between trace metal cycling and marine microbial ecology during a large perturbation to Earth's carbon cycle. Earth Planet. Sci. Lett. 449, 407–417.
30. Owens, J. D., Lyons, T. W., & Lowery, C. M. (2018). Quantifying the missing sink for global organic carbon burial during a Cretaceous oceanic anoxic event. Earth and Planetary Science Letters, 499, 83-94.
31. Pearson, A. (2014). Lipidomics for Geochemistry. Treatise on Geochemistry 2nd Edition, 12, 291-336.
32. Peters, K.E., Walters, C.C., & Moldowan, J.M. (2005). The biomarker guide (Volume 1). Cambridge university press.
33. Philp, R. P. (1985). Fossil fuel biomarkers. Methods in Geochemistry and Geophysics, 23, 1-294.

34. Rashby, S. E., Sessions, A. L., Summons, R. E., & Newman, D. K. (2007). Biosynthesis of 2-methylbacteriohopanepolyols by an anoxygenic phototroph. Proceedings of the National Academy of Sciences, 104, 15099-15104.
35. Raven, M. R., Fike, D. A., Bradley, A. S., Gomes, M. L., Owens, J. D., & Webb. S. A. (2019). Paired organic matter and pyrite $\delta^{34}S$ records reveal mechanisms of carbon, sulfur, and iron cycle disruption during Oceanic Anoxic Event 2. Earth and Planetary Science Letters, 512, 27-38.
36. Rohmer, M., Bouvier, P., & Ourisson, G. (1979). Molecular evolution of biomembranes: structural equivalents and phylogenetic precursors of sterols. Proceedings of the National Academy of Sciences, 76, 847-851.
37. Rohmer, M., Bouvier-Nave, P., & Ourisson, G. (1984). Distribution of hopanoid triterpanes in prokaryotes. Journal of General Microbiology, 130, 1137-1150.
38. Schmidt, G.A., Bader, D., Donner, L.J., Elsaesser, G.S., Golaz, J.C., Hannay, C., Molod, A., Neale, R.B., & Saha, S. (2017). Practice and philosophy of climate model tuning across six US modeling centers. Geoscientific Model Development, 10, 3207-3223.
39. Scholle, P. A., & Arthur, M. A. (1980). Carbon isotope fluctuations in Cretaceous pelagic limestones: potential stratigraphic and petroleum exploration tool. American Association of Petroleum Geologists Bulletin, 64, 67-87.
40. Seifert, W. K., & Moldowan, J. M. (1986). Use of biological markers in petroleum exploration. Methods in Geochemistry and Geophysics, 24, 261-290.
41. Sinninghe Damsté, J. S., & Köster, J. (1998). A euxinic southern North Atlantic Ocean during the Cenomanian/Turonian oceanic anoxic event. Earth and Planetary Science Letters, 158, 165-173.
42. Sturt, H. F., Summons, R. E., Smith, K., Elvert, M., Hinrichs, K.-U. (2004). Intact polar membrane lipids in prokaryotes and sediments deciphered by high-performance liquid chromatography/electrospray ionization multistage mass spectrometry-new biomarkers for biogeochemistry and microbial ecology. Rapid Communications in Mass Spectrometry, 18, 617–628.
43. Summons, R. E., & Powell, T. G. (1987). Identification of aryl isoprenoids in source rocks and crude oils: Biological markers for the green sulphur bacteria. Geochimica et Cosmochimica Acta, 51, 557-566.
44. Summons, R.E., Brassell, S.C., Eglinton, G., Evans, E., Horodyski, R.J., Robinson, N., & Ward, D.M. (1988) Distinctive hydrocarbon biomarkers from fossiliferous sediment of the Late Proterozoic Walcott Member, Chuar Group, Grand Canyon, Arizona: Geochimica et Cosmochimica Acta, 52, 2625–2637.
45. Summons, R. E., Bradley, A. S., Jahnke, L. L., & Waldbauer, J. R. (2006). Steroids, triterpenoids, and molecular oxygen. Philosophical Transactions of the Royal Society B, 361, 951-968.
46. Tierney, J. E., Poulsen, C. J., Montañez, I. P., Bhattacharya, T., Feng, R., Ford, H. L., Hönisch, B., Inglis, G. N., Petersen, S. V., Sagoo, N., Tabor, C. R., Thirumalai, K., Zhu, J., Burls, N. J., Foster, G. L., Goddéris, Y., Huber, B. T., Ivany, L. C., Kirtland Turner, S., Lunt, D. J., McElwain, J. C., Mills, B. J. W., Otto-Bliesner, B. L., Ridgwell, A., & Zhang, Y. G. (2020). Past climates inform our future. Science, 370, eaay3701.
47. Treibs, A. (1936). Chlorophyll and heme derivatives in organic mineral materials. Angewandte Chem, 49, 682-686.

48. Truper, H. G., & Genovese, S. (1968). Characterization of photosynthetic sulfur bacteria causing red water in Lake Faro. Woods Hole Oceanographic Institution, 225-232.
49. van Gemerden, H. (1983). Physiological ecology of purple and green bacteria. Annals of the Institut Pasteur / Microbiology, 134, 73-92.
50. Wakeham, S.G., Hedges, J.I., Lee, C., Peterson, M.L., & Hernes, P.J. (1997). Compositions and transport of lipid biomarkers through the water column and surficial sediments of the equatorial Pacific Ocean. Deep Sea Research Part II: Topical Studies in Oceanography, 44, 2131-2162.
51. Whewell, W. (1832). Review of Lyell's Principles of Geology. Quarterly Reviews, 103-132.
52. Whitehead, E. V. (1973). Molecular evidence for the biogenesis of petroleum and natural gas. Proceedings of Symposium on Hydrogeochemistry and Biogeochemistry, 2, 158-211.

Figures

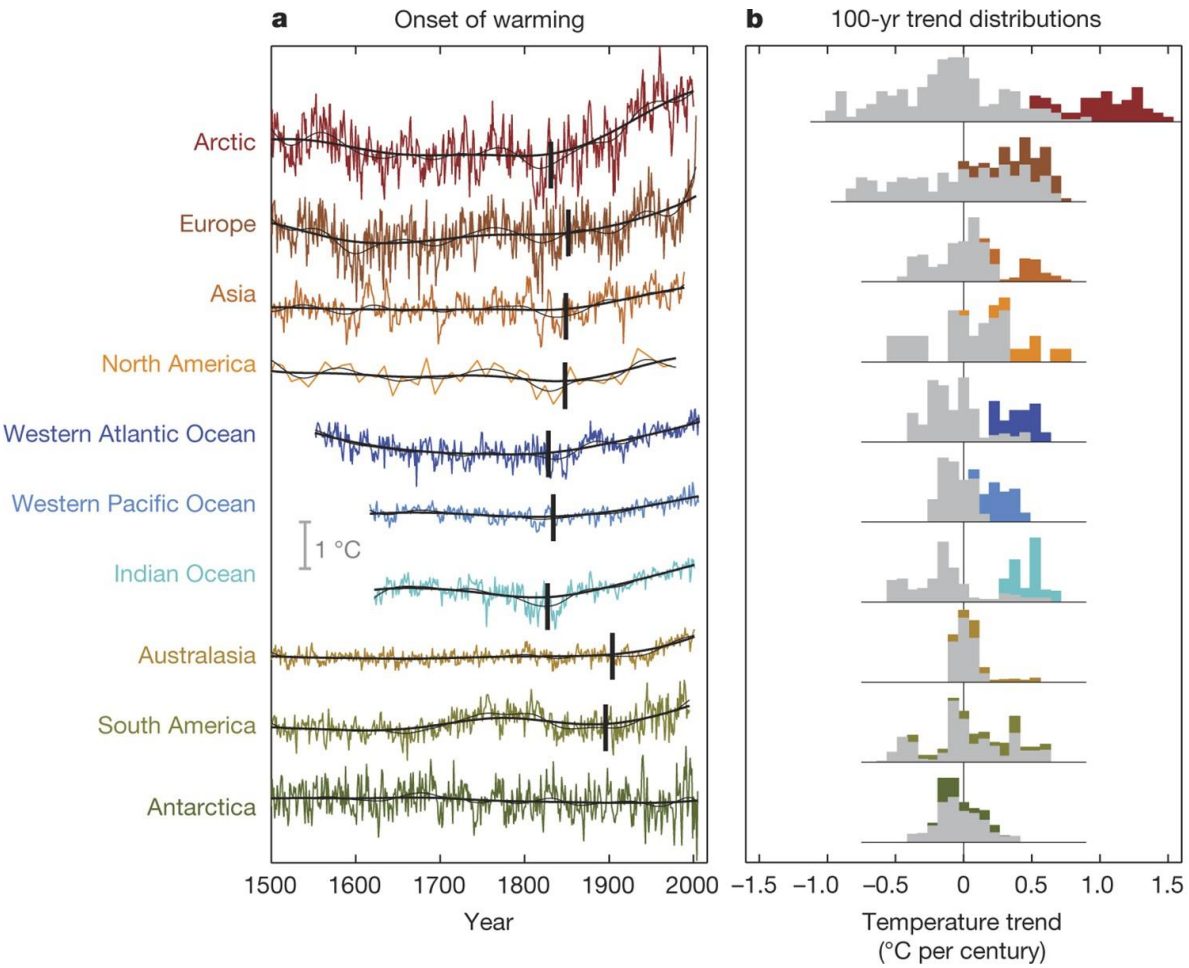

Figure 1. Regional changes in temperature over the past half millennium. (A) Averaged 15-year (thin lines) and 50-year (thick lines) trends. The vertical black rectangle denotes the onset of warming coeval with the Industrial Era. (B) Histograms depicting the pre-industrial temperature change (gray) to the post-industrial temperature change (colored) over each century. From Abram et al., (2016).

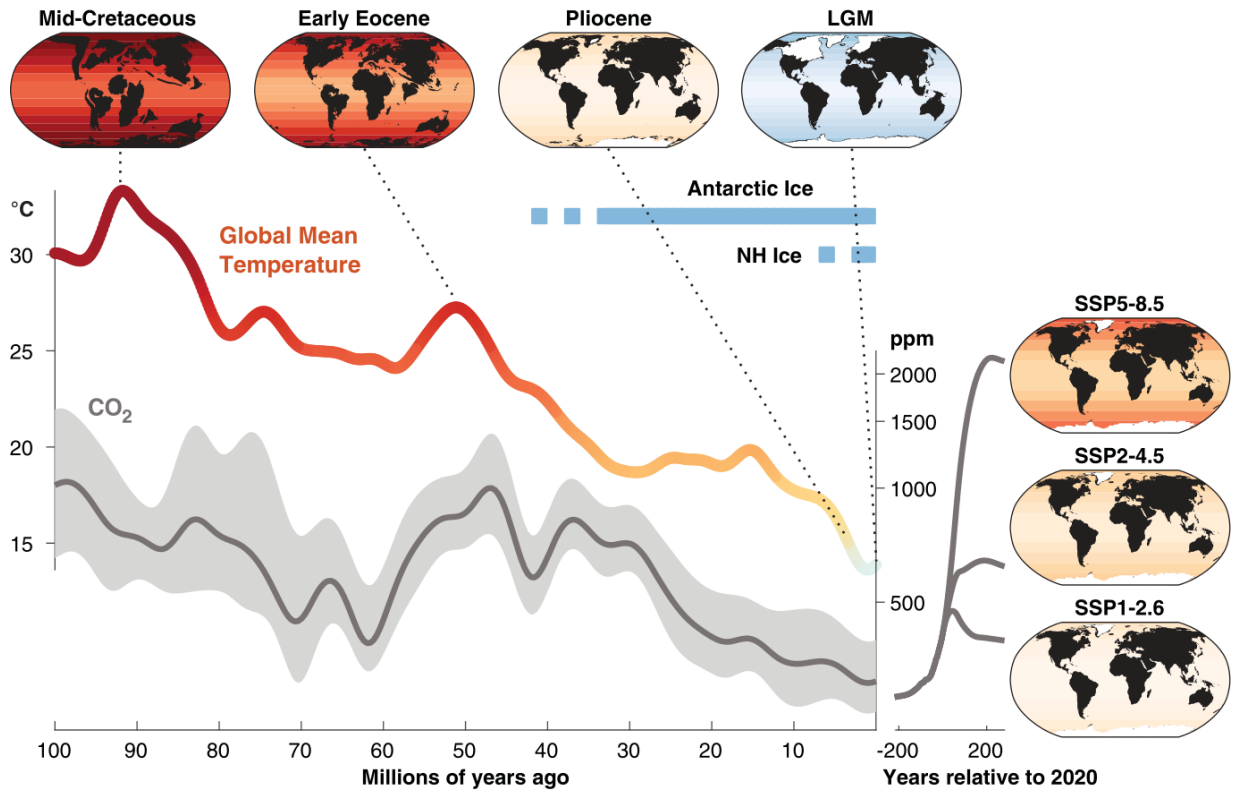

Figure 2. Comparison of reconstructed paleoclimates in the past 100 Ma and potential climate scenarios of future Earth. From Tierney et al., (2020). For information on origin and calculation of temperature and CO_2 data, as well as future projections, please see Tierney et al., (2020).

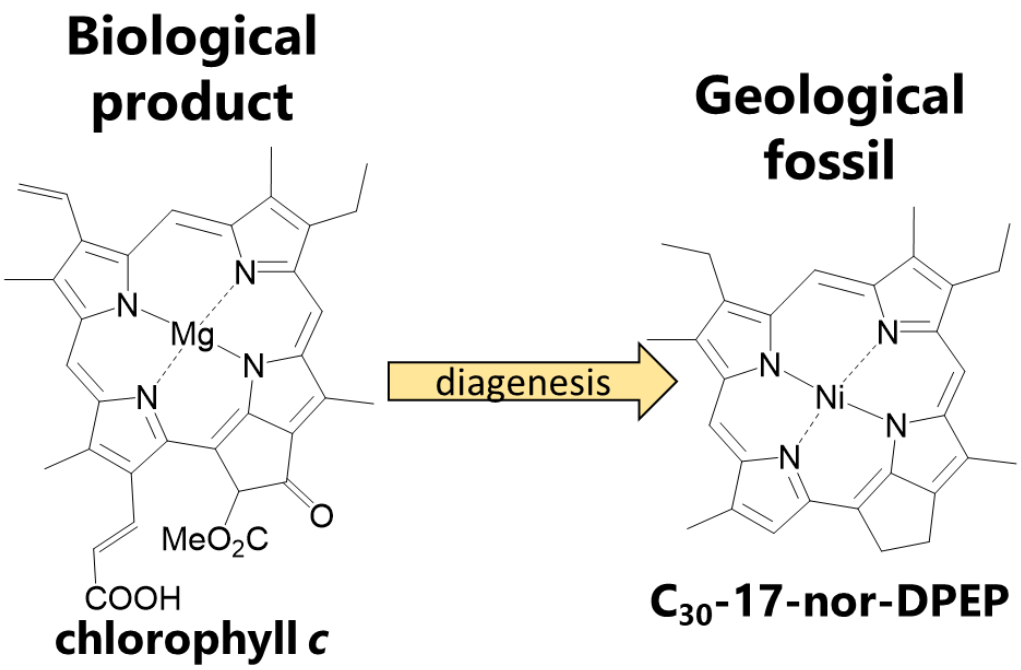

Figure 3. A simplified illustration of the biomarker concept. Biological products (e.g. chlorophyll c) are degraded during diagenesis producing biomarkers (e.g. C_{30}-17-nor-DPEP) that retain sufficient structural information to be correlated back to biosynthetic precursors.

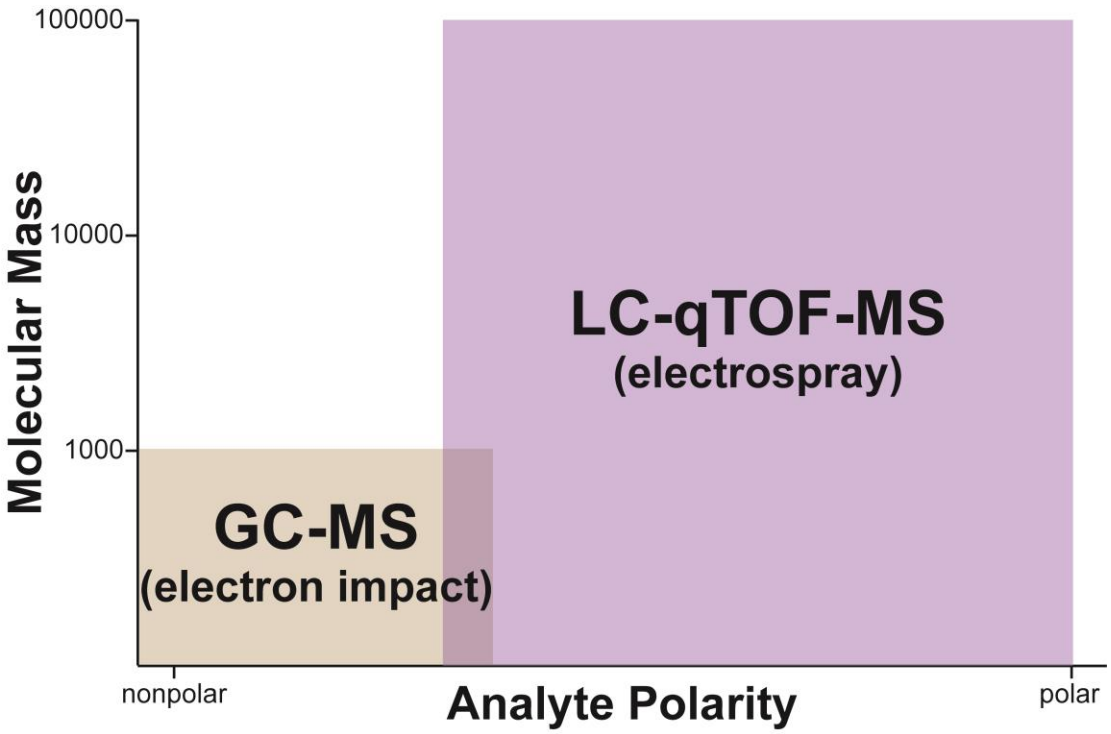

Figure 4. Analytical windows of ionization methods used in GC-MS and LC-MS. Note the greatly expanded analyte range of LC-qTOF-MS (purple) relative to GC-MS (brown). This is not intended to imply method inferiority, as both instruments are exceedingly valuable to organic geochemical studies, with targeted analyte properties (e.g. size and polarity) governing instrument selection.

Chapter 1: Biotic induction and microbial ecological dynamics of Oceanic Anoxic Event 2 (OAE-2)

Authors: Gregory T. Connock[1*], Jeremy D. Owens[2], and Xiao-Lei Liu[1]

Affiliations: [1]School of Geosciences, University of Oklahoma, Norman, Oklahoma 73019, USA. [2]Department of Earth, Ocean, and Atmospheric Science, Florida State University, and National High Magnetic Field Laboratory, Tallahassee, Florida 32306, USA.

Abstract: Understanding the mechanisms for past marine deoxygenation are paramount as consistencies between projections of global climate and oceanic anoxic events (OAEs) emerge. Still, the events preceding widespread carbon burial coincident with OAEs remain indeterminate and must be constrained to better predict the long-term Earth systems response to climate change. Here, we report a biomarker inventory enveloping OAE-2 (~94Ma), a global carbon cycle perturbation, generated by a novel LC-qTOF-MS (liquid chromatography – quadrupole time-of-flight – mass spectrometry) method capturing microbial communities spanning the entire water column in the southern proto-North Atlantic Ocean (ODP Leg 207 Site 1258, Demerara Rise). Detection of tetrapyrroles (free base chlorins/porphyrins and metalloporphyrins), glycerol ether lipids, and a diaromatic carotenoid (isorenieratane) enabled reconstruction of the variations in specific microbial communities through time, elucidating undocumented paleoceanographic dynamics. Our record revealed an abrupt, sustained increase in primary productivity preceded OAE-2 by ~220 ± 4 kyr, well before other geochemical proxies register biogeochemical perturbations. This destabilized carbon cycling and initiated the progressive marine deoxygenation recently found to antedate OAE-2, revealing how organic carbon burial drivers operate along a continuum in concert with microbial ecological changes. During OAE-2, recurring photic zone euxinia, supported by high rates of microbial sulfate reduction and density stratification, triggered a major marine microbial reorganization defined by a decrease in primary production and proliferation of taxa tolerant to the expanding euxinic environment. Recognition of the antecedent, protracted biotic induction of OAE-2 fundamentally alters how OAEs are assessed and may serve as a presage to assess the trajectory of modern oceans subjected to continued anthropogenic forcings.

1.1 Introduction

Global climate change, principally driven by increasing atmospheric CO_2 fueled by societal sustainment, is a widely accepted phenomenon afflicting modern Earth. Anticipatory efforts seeking to characterize the oceanographic response to anthropogenic forcings may benefit from an improved understanding of analogous periods in Earth history. Oceanic anoxic events (OAEs; Schlanger and Jenkyns, 1976) are oft-employed models of future climate, given the high pCO_2 (Witkowski et al., 2018 and references therein) and temperatures (Schouten et al., 2002; Forster et

al., 2007; O'brien et al., 2017 and references therein) facilitating the development of expansive marine deoxygenation (Owens et al., 2016; Ostrander et al., 2017).

OAE-2 is the most well studied and widely observed OAE, as defined by a global positive carbon isotope excursion (+CIE) immediately preceding the Cenomanian-Turonian boundary (~93.9 Ma; Scholle and Arthur, 1980; Erbacher et al., 2005). The +CIE, observed in both organic and inorganic carbon reservoirs, represents a major perturbation to the global biogeochemical carbon cycle whereby enhanced productivity and/or preservation led to significant organic carbon burial (Scholle and Arthur, 1980; Owens et al., 2018). However, the causal mechanisms initiating and sustaining rampant deoxygenation of the marine realm remain poorly constrained. Recent investigations revealed progressive deoxygenation, potentially associated with large igneous province (LIP) activity, presaged OAE-2 (Ostrander et al., 2017; Raven et al., 2019). Yet direct evidence of heightened primary productivity, a mechanism producing progressive deoxygenation via organic carbon remineralization, prior to OAE-2 is lacking.

Biomarkers, molecular fossils of past microbial life, possess the potential to elucidate the microbial ecological response bounding the OAE-2 interval. Previous biomarker studies provided critical insight into OAE-2, such as the spatiotemporal extents of photic zone euxinia (PZE; Kuypers et al., 2002; van Bentum et al., 2009), and primary producer composition (Kuypers et al., 2004; Higgins et al., 2012; Junium et al., 2015; Owens et al., 2016;), or estimates of sea surface temperature (SST; Schouten et al., 2002; Forster et al., 2007) and pCO_2 (e.g. Witkowski et al., 2018 and references therein), but all primarily reflect surface ocean processes which inherently limited paleoenvironmental reconstructions. Likewise, organic geochemical surveys of the Demerara Rise have been limited in scope, unable to capitalize on the unprecedented, continuous, and exceptionally preserved (Junium et al., 2011) record enveloping OAE-2 due to deposition in

relatively persistent reducing bottom waters (Owens et al., 2016). Coarse sampling (Kuypers et al., 2002; Owens et al., 2016), the narrow analytical window of GC-MS (gas chromatography-mass spectrometry) limiting interpretations to relatively nondescript biomarkers (Kuypers et al., 2002; van Bentum et al., 2009; Owens et al., 2016), and a singular focus restricted to a specific biomarker class representative of a specific region of the water column (e.g. porphyrins or archaeal lipids; Forster et al., 2007; Junium et al., 2015) precludes a comprehensive understanding of the potential process(es) influencing microbial communities, and by extension, proxies reliant on specific biomarker distributions (e.g. TEX_{86}-derived SST). Thus, the impact of dynamic climatic states on the total marine microbial ecology, pillars of biogeochemical cycling, is under-constrained and remains critical for local and global interpretations of OAE-2.

Here, we present unparalleled results generated by a novel LC-qTOF-MS (liquid chromatography – quadrupole time-of-flight – mass spectrometry) method comprising a holistic biomarker inventory of OAE-2, capturing the temporal evolution of microbial communities spanning the entire marine water column (i.e. surface to sediment). This new record allows us to leverage marine microbial variations to clarify the biotic response to and [potential] function in progressive deoxygenation antecedent to OAE-2, as well as to characterize the microbial ecological reorganization during, and recovery after, the event.

1.2 Materials and Methods

1.2.1 Site description and novelty

Ocean Drilling Program (ODP) Leg 207 recovered mid-Cretaceous (Albian) to mid-Paleogene (Lutetian) strata from 5 sites (1257-1261) on the Demerara Rise, a gently dipping (1.5^{o}) submarine plateau ~375 km north of Suriname (Erbacher et al., 2004). At present, the Demerara Rise is submerged ~700 mbsl, but the northwestern edge where site 1258 was drilled transitions

to a ramp reaching depths of nearly 4000 mbsl. site 1258, the source of samples in this study, captures the entirety of OAE-2 (~426-422 mcd) as delineated by carbon isotope stratigraphy (Erbacher et al., 2005), and is comprised of predominantly laminated black shales deposited in the equatorial proto-North Atlantic at intermediate water depths (500-1500 m). Organic matter is abundant, thermally immature, and marine in origin within the Cenomanian-Turonian interval (Erbacher et al., 2004; Forster et al., 2004; Meyers et al., 2006). Pervasive deposition of laminated black shales is not exclusive to OAE-2, signifying highly reducing bottom water conditions were a consistent feature at site 1258 (Erbacher et al., 2005). A constant redox state favoring organic matter preservation is rarely observed in coeval localities, providing an advantageous framework for geochemical interpretation.

The molecular fossil record is presumed to primarily reflect a microbial signal given the locally anoxic to euxinic conditions that enveloped OAE-2. Relatively invariant carbonate-corrected total organic carbon (TOC) values prior to, during, and after OAE-2 (Owens et al., 2016; Figure S1-1) highlight a consistent balance between production, preservation, and sedimentary dilution of organic matter. Black shale deposition at other localities (e.g. Furlo, Italy) is restricted to solely the OAE due to a combination of dynamic, site-specific bottom water redox conditions and sedimentation rates. Contrasting redox states preceding OAE-2 at these sites may compromise the integrity of the microbial signal, underlining the novelty of the exceptional biomarker preservation observed at the Demerara Rise (e.g. Junium et al., 2011). Therefore, the biotic response to dynamic oceanographic conditions preceding OAE-2 is likely not ubiquitously encoded in the sedimentary archive, with the Demerara Rise an extraordinary resource for OAE research. As a result, our interpretations are not intended to be global in extent due to locality-induced preservation biases, but rather global in effect.

1.2.2 Sample preparation

Forty-three composite core samples from ODP Leg 207 Site 1258 (cores A, B, and C, Demerara Rise) were provided in pre-cleaned micro-centrifuge tubes to the Geobiology Lab at the University of Oklahoma as powdered sample splits with methods for sample processing previously outlined (Owens et al., 2016). For ease of communication, a visual is provided depicting the preparatory procedure (Figure S1-2).

Approximately 150 mg of powdered core sample was transferred from the centrifuge tube to a glass 4 mL vial. Two internal standards, 100 ng of C_{46} glycerol trialkyl glycerol tetraether (GTGT) and 1 μg of β-carotene, were introduced to the sediment powder for relative quantification of target compounds integrated from LC-qTOF-MS scans. A 1.5 mL 1:1 azeotrope of DCM:MeOH was added to the 4 mL vial, which was then vortexed prior to 20 minutes of ultrasonication for sample extraction. Post-sonication, samples were centrifuged at 3000 rpm for 5 minutes. The supernatant of each sample was transferred to a 2 mL vial and dried under a gentle stream of N_2. The introduction of 1.5 mL of DCM:MeOH (1:1), sonication, centrifugation, transferring, and drying were repeated twice more for a total of three extractions. The final combined extract of each sample was blown to complete dryness and massed to yield quantitative results of the total lipid extract (TLE). The weighed TLE was brought up in 1 mL of 100% MeOH, ultrasonicated for 5 minutes, and centrifuged at 3000 rpm for 5 minutes. The supernatant was transferred to a new 2 mL vial for LC-qTOF-MS analysis.

1.2.3 LC-qTOF-MS

LC-MS was performed with an Agilent 1290 series UPLC system coupled to Agilent 6530 qTOF mass spectrometer through an Agilent jet stream dual electrospray ionization (AJS-ESI) interface. The ESI drying gas (N_2) temperature was set at 300°C, the N_2 flow rate was 8 L min^{-1},

and the nebulizer gas (N_2) pressure was 35 psi. The qTOF parameters were set to: capillary voltage 3.5 kV, fragmentor voltage 175 V; skimmer voltage 65 V and octupole voltage 750 V in auto MS/MS scanning mode with MS^1 range of *m/z* 100-2000 and MS^2 mass range of *m/z* 50-2000. Separation of compounds was achieved by dissolving the TLE in methanol and injecting 10 µl onto two Agilent Poroshell 120 EC-C18 columns (1.8 µm, 2.1 × 150 mm) in series maintained at 35°C. The LC program was set at a flow rate of 0.2 mL min^{-1}, first from 100% A to 90% A and 10% B in 5 min, followed by a gradient to 35% B at 30 min, and to 50% B at 70 min, and finally re-equilibrated with 100% A for 10 min, where the eluent A was 95: 5: 0.04 :0.10 of methanol/H_2O/formic acid/14.8 M NH_3(aq.) and B was 50: 50: 0.04: 0.10 of hexane/2-propanol/formic acid/14.8 M NH_3(aq.).

1.2.4 Biomarker identification and quantification

Biomarkers discussed in the text are identified based on accurate masses, chromatographic behavior (retention time compared with authentic standards), and characteristic fragmentation patterns of MS^2. Extracted ion chromatograms (EICs) and representative molecular structures of major compounds shown in Figure 1-1 are presented in Figure S1-3A-D. Hydroxychlorophyllones-a and meso-hydroxychlorophyllones-a are C_{33} chlorins, each containing two isomer peaks (Figure S1-3A), detected in all analyzed samples. The exceptional preservation of meso-hydroxychlorophyllones-a in Demerara Rise black shales has been previously documented (Junium et al., 2011). Major free based porphyrins include C_{33} BiCAP, C_{32} Etio, C_{32} DPEP, and C_{30} DPEP (Figure S1-3A). Metalloporphyrins associated with vanadyl (VO), nickel (Ni), zinc (Zn), and iron (Fe) are recognized in analyzed samples (Figure S1-3B). The VO^{2+}, Ni^{2+}, and Zn^{2+} chelated to porphyrins are divalent, and these metalloporphyrins are detected as protonated ions, $[M+H]^+$, while Fe-porphyrins occur as M^+ due to the presence of the trivalent

metal ion, Fe^{3+}. The Chl-c specific C_{30}-17-nor-DPEP, C_{30}-VO-17-nor-DPEP and C_{30}-Ni-17-nor-DPEP are assigned to the latest isomer peak of C_{30} DPEP, C_{30}-VO-DPEP and C_{30}-Ni-DPEP based on the retention time of 17-nor-DPEP standards (generously provided by Dr. Kashiyama of the Fukui University of Technology, see initial identification of 17-nor-DPEP in Kashiyama et al., 2008a). Glycerol ether lipids (Figure S1-3C and D) including the tetraethers (isoGDGTs, brGDGTs, obGDGTs, BDGT and PDGT) and diethers (archaeol, extended archaeol, and DAGEs) are identified by MS^2 fingerprints reported in previous works (Liu et al., 2012; Zhu et al., 2014; Coffinet et al., 2020). The OH-GDGT and S-GDGT were not discussed in the text but are shown in Figure S1-3C to illustrate the distinct retention time of isoGDGT-1. The soil-derived 5-methyl brGDGTs and aquatic bacterial 6- and 7-methyl brGDGTs isomers were distinguished by comparing results of a soil extract containing only the 5-methyl brGDGTs and a modern marine sediment sample with all isomers. The distribution of 7-methyl brGDGTs is not discussed in this work. Extended archaeols synthesized by cultured halophilic archaeal species are known to contain a phytane and a C_{25} ($C_{20,25}$ ext. Ar), or two C_{25} isoprenoids hydrocarbons ($C_{25,25}$ ext. Ar; DeRosa et al., 1983). Novel extended archaeol derivatives with up to C_{40} isoprenoid are tentatively identified based on their MS^2 in this study (Figure S1-3D). The occurrence of isorenieratane in the Demerara Rise black shales is confirmed by MS^2 and retention times of C_{40} aromatic carotenoids previously identified in the Woodford Shale extracts (Connock et al., 2018).

1.3 Results and Discussion

1.3.1 Biomarker inventory

Biomarkers were analyzed in 43 samples over a ~10m depth transect of pre-OAE, OAE, and post-OAE strata at ODP Site 1258 on the Demerara Rise. Application of a novel LC-qTOF-MS method revealed a diverse molecular fossil record (Figure 1-1) comprised of cyclic

tetrapyrroles (herein referred to as 'tetrapyrroles', including free base chlorins, porphyrins, and metalloporphyrins), isorenieratane, dialkyl glycerol ethers (DAGEs), extended archaeols ($C_{20/25}$, $C_{20/30}$, $C_{20/35}$, and $C_{20/40}$), butanetriol/pentanetriol dialkyl glycerol tetraethers (BDGT/PDGT), and glycerol dialkyl glycerol tetraethers (GDGTs), including isoprenoidal GDGTs (isoGDGTs, such as crenarchaeol), branched GDGTs (brGDGTs) and overly-branched GDGTs (obGDGTs; see Figure S1-3 for biomarker identifications).

Microbial ecological reconstruction of the epipelagic to benthic realms was possible given the depth-specific biological origins of individual biomarkers (Figure 1-2). Generalized residence depth was used to categorize biomarkers for ease of discussion. 'Shallow' (epipelagic) refers to the tetrapyrroles, 'intermediate' (mesopelagic) to crenarchaeol, isorenieratane, and obGDGTs, and 'deep' (bathypelagic to benthic) to DAGEs, extended archaeols, and BDGT/PDGT. Tetrapyrroles, derived from chlorophylls present in photoautotrophs (Treibs, 1936; Junium et al., 2011), record depths extending from the sea surface to the top of the chemocline or base of the euphotic zone. Crenarchaeol, produced by the ammonia oxidizing archaea *Thaumarchaeota* (Sinninghe Damsté et al., 2002; Zeng et al., 2019), primarily monitors the zone immediately above the chemocline or base of the photic zone. Isorenieratane, a degradation product of isorenieratene biosynthesized predominantly by the anoxygenic photosynthetic sulfur-oxidizing bacteria *Chlorobiaceae* (Liaaen-Jensen et al., 1964), reflects the relative depth of the chemocline within the photic zone (Summons and Powell, 1987). The development of an oxygen minimum zone (OMZ) or expanded bottom water anoxia is captured by the obGDGTs, sourced from unidentified anaerobic bacteria within or below the chemocline (Liu et al., 2014). At greater depths beyond the photic zone and extending into the sediments, DAGEs (Grossi et al., 2015), extended archaeols (Bale et al., 2019), and

BDGT/PDGT (Coffinet et al., 2020) track deep water microbial compositions of sulfate-reducing bacteria, halophilic archaea, and methanogenic archaea, respectively.

A series of principal component analyses (PCA, see Supplementary Information) highlighted the utility of our biomarker inventory to discern differences imposed by contrasting biogeochemical regimes. Biomarkers derived from intermediate and deep waters were most effective at delineating OAE from non-OAE strata (Figure S1-4). Tetrapyrroles were the predominant biomarker class followed by crenarchaeol and isorenieratane. A sharp drop in tetrapyrrole fractional abundance, primarily due to a relative increase in crenarchaeol and isorenieratane contribution, occurred immediately before the +CIE and was sustained through OAE-2 (Figure 1-3). Other features defining OAE-2 include relatively low, invariant tetrapyrroles and crenarchaeol concentrations accompanied by elevated amounts of isorenieratane, obGDGTs, DAGEs, and extended archaeols (Figure 1-4). The initial deposition of pre-OAE (429.91-427.63 mcd) and post-OAE strata was relatively similar based on PCA results, biomarker profiles and fractional abundances, excluding a period from 421.19-421.04 mcd where an abrupt increase of isorenieratane was observed. Spikes in tetrapyrroles, crenarchaeol, obGDGTs, and DAGEs at 427.54 mcd defined the latter phase of the pre-OAE interval. The DAGEs declined rapidly, but a gradual decrease in the tetrapyrroles, crenarchaeol, and obGDGTs, punctuated by brief positive excursions, extended into OAE-2 as isorenieratane concentrations progressively rose (Figure 1-4). This signifies a previously undocumented pre-OAE biotic event predating the +CIE commonly used to demarcate OAE-2 initiation.

1.3.2 The biotic induction of OAE-2

The rapid proliferation of select microbial communities at 427.54 mcd likely represents a pre-OAE biotic perturbation (pre-OAE BP) presaging the protracted period of widespread marine

deoxygenation during OAE-2, and progressive deoxygenation predating the +CIE (Figure 1-4; Ostrander et al., 2017). At the beginning of the pre-OAE BP, abruptly elevated tetrapyrrole and crenarchaeol concentrations signify a spike in primary production by photoautotrophs and chemoautotrophs residing above the chemocline. Increased volumes of precipitating biogenic snow concordantly consumed oxygen, expanding the preexisting oxygen minimum zone (OMZ) as anaerobic bacteria thrived based on accelerated obGDGTs synthesis. Microbial sulfate reduction (MSR), inferred from the DAGEs profile, temporarily facilitated organic carbon oxidation as accelerated biomass production exceeded the degradation capability of the pelagic OMZ. However, euxinia did not penetrate the photic zone at the outset of the productivity bloom as isorenieratane was not detected and heightened rates of MSR were transient, limited to pre-OAE BP initiation. The lack of a well-stratified water column, evinced by absent to low concentrations of halophilic archaeal lipids (extended archaeols), relatively low rates of MSR, and a dense oxygenic microbial plate initially precluded the development of PZE.

Establishing a definitive causal mechanism for the pre-OAE BP is difficult, but the concomitance of large igneous province (LIP) activity with the productivity spike is intriguing. Application of a linear sedimentation rate from OAE-2 to the pre-OAE BP interval following previous works (Owens et al., 2016; Ostrander et al., 2017) approximated the pre-OAE BP occurring 220 ± 4 kyr before OAE-2, lasting for ~100 kyr (427.54-426.88 mcd). Event duration was estimated based on the onset of the productivity spike (427.54 mcd), nearly synchronous with a minor positive $\delta^{13}C_{org}$ excursion (0.83 ‰ at 427.49 mcd, Figure S1-1; Erbacher et al., 2005) observed until tetrapyrrole concentrations return to pre-perturbation values at 426.88 mcd (Figure 1-4). Given elevated primary production played a role in producing the +CIE of OAE-2 through enhanced organic carbon burial, we attribute the smaller positive $\delta^{13}C_{org}$ excursion to the pre-OAE

BP invoking a similar rationale and leverage the higher resolution $\delta^{13}C_{org}$ record to constrain pre-OAE BP duration. Importantly, this event was roughly coincident with the onset of LIP activity (~200-300 kyr before OAE-2) inferred from marine osmium isotope stratigraphy (Du Vivier et al., 2014). Similarities in the modern planktonic community response to the 2018 Kilauea eruption (Wilson et al., 2019) and the pre-OAE BP, such as elevated primary production and microbial ecological shifts, reinforce the inference of a potential magmatic driver (see Supplementary Information for additional details).

A constant, yet overall lower, nutrient and trace metal inventory (Figure S1-5; Hetzel et al., 2009; Owens et al., 2016) and redox-driven shift in fixed N species leading to a fixed N shortage (Lam et al., 2007) were probable culprits in the failure to sustain prolific rates of primary production beyond 100 kyr at Demerara Rise. The gradual decline in biomass production, indicated by decreasing tetrapyrrole and crenarchaeol profiles, (Figure 1-4), was accompanied by a notable shift in deep water communities. Sulfate-reducing bacteria exerted increasing predominance over methanogenic archaea, a trend coeval with the primary productivity spike and extending well into the OAE (Figure 1-3). A collapse of autotrophic communities to pre-perturbation levels was concordant with the progressive shoaling of H_2S-laden waters fueled by elevated rates of MSR. Continued vertical migration of the chemocline intruded the photic zone, producing PZE which spawned anoxygenic photosynthesis by *Chlorobiaceae* (Figure 1-4). Unlike the overall oscillatory character of PZE throughout the studied section, this protracted phase of PZE persisted until the onset of OAE-2 (426.43-426.00 mcd, Figures 1-3 & 1-4) and is approximately contemporaneous with the thallium (Tl) isotope excursion (426.40-426.30 mcd; Ostrander et al., 2017).

The positive Tl isotope excursion captures a progressive expansion of bottom water anoxia predating OAE-2 by 43 ± 11 kyr (Ostrander et al., 2017). However, evidence for a causal

mechanism of pre-OAE deoxygenation remains indeterminate. Our holistic biomarker inventory provides an interpreted sequence of events culminating in the regional to global expansion of anoxia predating OAE-2. Protracted enhanced primary productivity began ~220 ± 4 kyr prior to OAE-2, increasing localized production and export of organic carbon at Demerara Rise. Similar productivity spikes likely occurred in settings of comparable paleogeographic configuration (e.g. equatorial, continental margins/shelves), seeding the oceans with fixed carbon. Continued scavenging of marine oxygen via organic carbon remineralization resulted in OMZ expansion locally, and likely initiated oxygen drawdown in much of the proto-North Atlantic Ocean. Stratigraphic records of sulfur isotopes of pyrite ($\delta^{34}S_{pyrite}$) from the proto-North Atlantic and Tethys Oceans (Raven et al., 2019) validate the areal extrapolation of our interpretations. A gradual decline in $\delta^{34}S_{pyrite}$ values at Demerara Rise begins at 427.50 mcd, nearly identical to the onset of the pre-OAE BP (427.54 mcd, Figure 1-4). Correlation of $\delta^{34}S_{pyrite}$ in a global transect (Western Interior Seaway, proto-North Atlantic, Tethys) revealed consistent behavior in $\delta^{34}S_{pyrite}$ prior to the +CIE, indicating increasingly expansive marine deoxygenation on a global scale (Raven et al., 2019). Over ~100 kyr, increased regional biomass production induced pervasive marine anoxia, inhibiting Mn-oxide formation, producing the observed positive Tl isotope excursion, and ultimately, the globally observed +CIE reflecting enhanced organic carbon burial signaling the onset of OAE-2. Thus, the local biotic signal recorded at ODP Site 1258 underlines the significant role the Demerara Rise, and similar undocumented settings, played in initiating deoxygenation of the global ocean.

1.3.3 Microbial ecological dynamics during and after OAE-2

Changes in microbial community compositions during OAE-2 were apparent, signified by an abrupt reorganization of the normalized total biomarker pool (Figure 1-3) and variations in the

absolute concentrations of individual biomarkers (Figure 1-4). In general, OAE-2 was defined by an expansion and diversification of intermediate and deep water communities (426.00-423.07 mcd), followed by a period of instability leading to the termination of the OAE (423.07-422.00 mcd). Photo- and chemoautotrophs residing above the chemocline were adversely affected, evinced by relatively low, invariant tetrapyrrole and crenarchaeol profiles (Figure 1-4). Based on these observations, we divided OAE-2 into two periods defined by contrasting paleoenvironmental conditions modulating the microbial inhabitants of Demerara Rise.

The first period of OAE-2 (426.00-423.07 mcd, Figure 1-4) was marked by the intrusion of a euxinic OMZ into the photic zone (Figure 1-5). Elevated, yet fluctuating isorenieratane concentrations suggest shallow, relatively persistent PZE of varying vertical extent, in agreement with previous work at nearby sites (Kuypers et al., 2002; van Bentum et al., 2009). During this interval, high rates of MSR were sustained as DAGEs continually increased, aligning with estimates of expanded seafloor euxinia (Owens et al., 2013). The co-occurrence of abundant extended archaeols and isorenieratane indicates the role that density stratification served in maintaining the protracted PZE of OAE-2, substantiating concurrent findings based on neodymium (Martin et al., 2012) and oxygen isotopes (Friedrich et al., 2008). Vertical nutrient advection via upwelling (Trabucho Alexandre et al., 2010) led to preferential exposure to and consumption by expanding intermediate water communities tolerant to sulfidic conditions in the OMZ. Scavenging of an already depleted fixed N inventory (Lam et al., 2007) and inhibition of efficient nutrient transfer by pronounced density stratification likely induced severe N deficiency in surface water communities, explaining the relatively muted productivity of oxygenic photoautotrophs (i.e. tetrapyrroles) and chemoautotrophs (i.e. crenarchaeol) observed (Figure 1-4). The concentration and predominant utilization of fixed N in the OMZ led to the proliferation

and diversification of intermediate and deep water microbial taxa, challenging previous interpretations of highly productive, predominantly eukaryotic primary producers reliant on the upwelling of isotopically depleted NH_4^+ (Higgins et al., 2012). Instead, the decline of C_{30}-17-nor-DPEP (Figure S1-1), a source-specific tetrapyrrole diagenetically derived from algal chlorophyll-*c* (Kashiyama et al., 2008a), and reconstructed water column conditions during OAE-2 indirectly support a rise in cyanobacteria, diazotrophs able to fix N_2, in oxygenated, nutrient-depleted shallow waters. Cyanobacterial ascendancy is further supported by C and N stable isotopes (Kashiyama et al., 2008b; Junium et al., 2015) and phylum-specific biomarkers (e.g. 2-methylhopanoids; Kuypers et al., 2002; Owens et al., 2016).

A reversal from the formerly outlined conditions typified the second period of OAE-2 (423.07-421.99 mcd, Figure 1-4). Destabilization of the stratified water column and reduced production of H_2S led to rapid deepening and contraction of the euxinic OMZ. The observed decline in halophilic archaea, coincident with a collapse in *Chlorobiaceae* populations, is roughly coeval with positive neodymium isotopic excursions observed across the proto-North Atlantic (Martin et al., 2012) attributed to enhanced latitudinal commingling of proto-North Atlantic water masses (Zheng et al., 2013). Although detrimental to sustained PZE, the persistence of a well-developed anaerobic bacterial community (i.e. obGDGTs) suggests the lasting presence of a non-euxinic OMZ despite improved bottom water circulation. A premature recovery of the chemoautotrophic *Thaumarchaeota*, inhabiting the base of the photic zone, relative to the shallower dwelling obligately oxygenic phototrophs (Figure 1-3) likely reflects reduced toxicity associated with retreating euxinic waters, lessened resource competition with [primarily] *Chlorobiaceae,* and a competitive advantage tied to preferential exposure to upwelled nutrients and tolerance to low O_2 conditions. A brief (one data point, 422.31 mcd, Figure 1-4) relapse of

PZE and associated density stratification punctuates the ultimate collapse of the unique microbial ecology defining OAE-2.

The termination of OAE-2 was marked by the temporary re-establishment of microbial community compositions mirroring those observed prior to the pre-OAE BP (Figures 1-3 & 1-4). Contraction of the OMZ led to a deep chemocline, with PZE restricted to the basal photic zone as the production of reduced sulfide species diminished. Methanogenic archaea thrived relative to sulfate-reducing bacteria in less sulfidic bottom waters (Figure 1-3). The *Thaumarchaeota* continued the recovery initiated towards the latter half of OAE-2, accompanied by the rebounding oxygenic photoautotrophs. However, the recovery of shallow autotrophic communities was halted by an episode of PZE (421.19-421.04 mcd) comparable to the protracted PZE observed during the first half of OAE-2 based on isorenieratane concentrations (Figure 1-4). Temporary development of pronounced density stratification likely facilitated the accumulation of H_2S in the lower to intermediate photic zone, producing the short-lived PZE episode. Interestingly, covariant responses observed in additional biomarker profiles (e.g. obGDGTs) to PZE during OAE-2 were not evident in this isolated event.

This brief episode of post-OAE PZE (421.19-421.04 mcd) corresponds to a positive organic carbon isotope excursion (Figure S1-1; Erbacher et al., 2005), trace metal drawdown (Figure S1-5; Hetzel et al., 2009; Owens et al., 2016), and minor positive Tl isotope excursion (Ostrander et al., 2017). Prior study tentatively attributed this geochemical perturbation to enhanced carbon burial during a post-OAE deoxygenation event of smaller magnitude (Ostrander et al., 2017), with subsequent work revealing continued pyrite burial post-OAE 2 (Raven et al., 2019). Our biomarker inventory revealed some environmental consistencies (e.g. PZE) between

this event and OAE-2, but the overall biotic response to the post-OAE event was relatively subdued.

1.3.4 Broader implications

The recognition of the pre-OAE BP and evolving water column conditions at Demerara Rise highlights additional complexities of a dynamic ocean relevant to interpretations of OAE-2 and the +CIE. Enhanced, sustained, and widespread carbon burial is required to produce the +CIE used to define OAE-2 (Scholle and Arthur, 1980, Owens et al., 2018). Still, the principal forcing, productivity or preservation, remains enigmatic, although evidence for the former mounts (e.g. Pedersen and Calvert, 1990; Kuypers et al., 2002).

Based on the tetrapyrrole profiles (Figure 1-4) primary production was greatest during the pre-OAE BP and relatively muted throughout OAE-2 at Demerara Rise, assuming minimal alteration to the genetic tetrapyrrole stratigraphic signal. Biomass preservation was presumedly enhanced during OAE-2 through sulfurization (Raven et al., 2019), as the OMZ transitioned from anoxic to euxinic and penetrated the photic zone (Figure 1-5), yet low tetrapyrrole concentrations persisted. Previous work noted a similar discrepancy between preservation potential and porphyrin abundance, postulating a paucity of trace metals to chelate with the free-base porphyrins induced poor preservation as desulfurization did not reveal additional porphyrin content (Junium et al., 2015). However, both the pre-OAE BP and OAE-2 were characterized by relatively depleted trace metal inventories (Figure S1-5, Hetzel et al., 2009; Owens et al., 2016), suggesting productivity as the predominant control on porphyrin abundance at Demerara Rise.

The strong covariance between tetrapyrrole and crenarchaeol concentrations reinforces the interpretation that tetrapyrroles faithfully reflect primary production (Figure S1-6). Crenarchaeol, a biosynthetic product of chemoautotrophic archaea (*Thaumarchaeota*) comprising up to 20% of

all archaea and bacteria in the modern ocean (Karner et al., 2001), is structurally distinct from the tetrapyrroles making it likely that diagenetic alteration of the two biomarkers is not consistent in rate or form. Thus, the positive correlation between key proxies for major contributors to primary production, the photoautotrophs and chemoautotrophs, minimizes concern for the integrity of the biotic signal at Demerara Rise (see Supplementary Information for additional details). This permits a crude approximation of the relative temporal change in primary productivity if we assume chlorophyll production, represented by the summed chlorophyll derivatives (i.e. tetrapyrroles), varies linearly with primary production in response to evolving environmental factors (e.g. light intensity, nutrient availability, temperature). Therefore, the pre-OAE BP (427.54-426.88 mcd) represents a threefold increase in primary productivity relative to the average preceding this event (429.91-427.63 mcd), and was fivefold greater than levels observed during OAE-2 based on averaged tetrapyrrole concentrations.

These findings provide direct evidence for a causal mechanism resulting in both the Tl isotope excursion and +CIE as previously described. It is highly probable the pre-OAE BP was not exclusive to Demerara Rise based on the immense and presently unconstrained organic carbon burial required to produce the +CIE (Owens et al., 2018). Further characterization of comparable localities to Demerara Rise may reveal similar productivity spikes, as primed, highly productive settings likely capitalized on exogenous nutrient delivery via efficient upwelling to the photic zone prior to stratification during OAE-2. Hence, OAE-2 and the +CIE were not coincident with heightened surface water productivity, relative to the pre-OAE BP. Rather, antecedent spikes in primary productivity locally facilitated the initiation of the OAE as a mechanism to consume marine oxygen and subsequently enhance organic carbon preservation globally.

A transition from a productivity- to preservation-dominant system during OAE-2 at Demerara Rise, and possibly similar paleogeographic settings experiencing the pre-OAE BP, facilitated substantial organic carbon burial producing the +CIE. Distinct shifts in water column chemistry and structure from the pre-OAE BP to OAE-2 induced considerable changes in microbial life (Figure 1-5), which altered the primary driver governing biomass sequestration. Yet, both intervals reveal relatively comparable carbonate-corrected TOC values (total organic carbon; Figure S1-1; Owens et al., 2016), signifying enhanced preservation as a critical component of organic carbon burial during OAE-2 at Demerara Rise. Consequently, this work suggests that sustained increases in primary production prior to OAE-2 initiated and regulated pre-OAE deoxygenation, resulting in a progressive shift to preservation as the primary control on organic carbon accumulation in sediments. Expanding euxinia and attendant changes to biogeochemical cycling adversely affected primary producers while simultaneously enhancing organic matter preservation via sulfurization (Raven et al., 2019). Flourishment of *Thaumarchaeota* in oligotrophic settings in the modern open ocean (Könneke et al., 2014), and lack thereof during OAE-2 based on diminished crenarchaeol concentrations, underscores the paucity of bioessential elements (e.g. nutrient N) caused by microbial descension of the redox ladder due to intensified anoxia, ultimately limiting primary production. The switch from a productivity to preservation model, reconstructed using biomarkers (Figure 1-5) and initially suggested based on drawdown of the trace metal inventory (Owens et al., 2016), was also concomitant with relative warming inferred from the GDGT-based TEX^{H}_{86} SST calculations (Figure S1-1; Forster et al., 2007). Simulated projections of the marine microbial response to continued global warming in the future revealed similar biotic trends (e.g. decreased primary productivity) to warming-induced oceanographic changes (e.g. intensified stratification; Steinacher et al., 2010) observed during

OAE-2. Thus, an abundance of proxy- and model-based results paired with conceptual evidence suggest relatively low production and enhanced preservation of organic carbon throughout OAE-2 at Demerara Rise.

The pre-OAE BP may foreshadow greater regional trends observed during OAE-2. Equatorial upwelling centers, like Demerara Rise, are spatially restricted and represent regions of already high primary production prior to OAE-2. Climatic shifts concurrent with OAE-2 may have produced favorable conditions for elevated primary productivity in regions unable to capitalize on or exposed to allochthonous nutrient delivery prior to the +CIE. While the pre-OAE BP offers a causal mechanism for the Tl isotope excursion and +CIE initiation, areal expansion of organic carbon preservation and production is necessary to sustain enhanced organic carbon burial for the duration of the +CIE.

1.4 Conclusions

Application of a new LC-qTOF-MS method on exceptionally preserved rock samples revealed an unparalleled, diverse biomarker inventory that enabled greater insight into oceanographic conditions before, during, and after OAE-2. Efficient transmission of exogenous, potentially LIP-derived nutrients to the upper euphotic zone prior to OAE-2 led to a protracted phase of elevated primary productivity at equatorial coastal upwelling centers, leading to progressive marine deoxygenation. Over time, enhanced biomass production and attendant remineralization depleted marine oxygen levels, priming the marine realm for the rapid organic carbon sequestration defining the onset of OAE-2. Expanding anoxic and euxinic conditions, combined with pronounced water column stratification, fundamentally altered microbial ecological compositions during OAE-2 by perturbing the flow of key nutrients (e.g. N) throughout

the water column. This ultimately influenced organic carbon burial drivers, with preservation supplanting productivity to perpetuate the +CIE.

Continued development of preexisting proxies is critical to extract and clarify current understandings of major climatic events in Earth history. Although reliant on preservation of the microbial signal, this new analytical method enables simultaneous examination of a wide array of biomarkers, producing a more holistic reconstruction of oceanographic changes inferred from microbial ecological variations spanning the surface to the sediment. This is timely, as investigations of the sedimentary archives become increasingly valuable analogs to understand the response of modern oceans to natural and anthropogenic forcings. Similarities between the pre-OAE biotic perturbation and modern, climate-driven marine deoxygenation are concerning, while particular attention to preexisting highly productive settings may hold the key to forecasting the geologically rapid transition to a global OAE. Even though natural processes are beyond our control, stifling anthropogenic catalysts of climate change may decelerate the unfortunate, progressive suitability of OAEs in studies of future Earth.

1.5 References

1. Bale, N. J., Sorokin, D. Y., Hopmans, E. C., Koenen, M., Rijpstra, W. I. C., Villanueva, L., Wienk, H., & Sinninghe Damsté, J. S. (2019). New insight into the polar lipid composition of extremely halo(alkali)philic Euryarchaea from hypersaline lakes. Frontiers in Microbiology, 10, 1-24.
2. Breit, G. N., & Wanty, R. B. (1991). Vanadium accumulation in carbonaceous rocks – a review of geochemical controls during deposition and diagenesis. Chemical Geology, 91, 83-97.
3. Coffinet, S., Meador, T, B., Mühlena, L., Becker, K. W., Schröder, J., Zhu, Q.-Z., Lipp, J. S., Heuer, V. B., Crump, M. P., & Hinrichs, K.-U. (2020). Structural elucidation and environmental distributions of butanetriol and pentanetriol dialkyl glycerol tetraethers (BDGTs and PDGTs). Biogeosciences, 17, 317-330.
4. Connock, G.T., Nguyen, T.X., & Philp, R.P. (2018). The development and extent of photic-zone euxinia concomitant with Woodford Shale deposition. American Association of Petroleum Geologists Bulletin, 102, 959-986.

5. De Rosa, M., Gambacorta, A., Nicolaus, B., Ross, H.N.M., Grant, W.D., & Bu'Lock, J.D. (1982). An asymmetric archaebacterial diether lipid from alkaliphilic halophiles. Microbiology, 128, 343-348.
6. Du Vivier, A. D. C., Selby, D., Sageman, B. B., Jarvis, I., Gröcke, D. R. & Voigt, S. (2014). Marine $^{187}Os/^{188}Os$ isotope stratigraphy reveals the interaction of volcanism and ocean circulation during Oceanic Anoxic Event 2. Earth Planet. Sci. Lett. 389, 23–33.
7. Erbacher, J., Mosher, D. C., Malone, M. J., & Expedition 207 Scientists. (2004). Chapter 5, Site 1258. Proceedings of the Ocean Drilling Program, Initial Reports, 207, 1-117.
8. Erbacher, J., Friedrich, O., Wilson, P. A., Birch, H. & Mutterlose, J. (2005). Stable organic carbon isotope stratigraphy across Oceanic Anoxic Event 2 of Demerara Rise, western tropical Atlantic. Geochemistry, Geophysics Geosystems, 6, 1–9.
9. Forster, A., Sturt, H., Meyers, P. A., & Expedition 207 Scientists. (2004). Molecular biogeochemistry of Cretaceous blacks shales from Demerara Rise: Preliminary shipboard results from sites 1257 and 1258, Leg 207. Proceedings of the Ocean Drilling Program, 207, 1-22.
10. Forster, A. Schouten, S., Moriya, K., Wilson, P. A., & Sinninghe Damsté, J. S. (2007). Tropical warming and intermittent cooling during the Cenomanian/Turonian oceanic anoxic event 2: Sea surface temperature records from the equatorial Atlantic. Paleoceanography, 22, PA1219.
11. Friedrich, O., Erbacher, J., Moriya, K., Wilson, P. A., & Kuhnert, H. (2008). Warm saline intermediate waters in the Cretaceous tropical Atlantic Ocean. Nature Geoscience, 1, 453-457.
12. Grossi, V., Mollex, D., Vinçon-Laugier, Hakil, F., Pacton, M., & Cravo-Laureau, C. (2015). Mono-and dialkyl glycerol ether lipids in anaerobic bacteria: Biosynthetic insights from the mesophilic sulfate reducer *Desulfatibacillum alkenivorans* PF2803. Applied Environmental Microbiology, 81, 3157-3168.
13. Hetzel, A., Böttcher, M. E., Wortmann, U. G., & Brumsack, H.-J. (2009). Paleo-redox conditions during OAE 2 reflected in Demerara Rise sediment geochemistry (ODP Leg 207). Palaeogeography, Palaeoclimatology, Palaeoecology, 273, 302-328.
14. Higgins, M. B., Robinson, R. S., Husson, J. M., Carter, S. J., & Pearson, A. (2012). Dominant eukaryotic export production during ocean anoxic events reflects the importance of recycled NH_4^+. Proceedings of the National Academy of Sciences, 109. 2269-2274.
15. Hopmans, E. C., Weijers, J. W. H., Schefuß, E., Herfort, L., Sinninghe Damsté, & Schouten, S. (2004). A novel proxy for terrestrial organic matter in sediments based on branched and isoprenoid tetraether lipids. Earth and Planetary Science Letters, 224, 107-116.
16. Junium, C. K., Keely, B. J., Freeman, K. H., & Arthur, M. A. (2011). Chlorins in mid-Cretaceous black shales of the Demerara Rise: The oldest known occurrence. Organic Geochemistry, 42, 856-859.
17. Junium, C. K., Freeman, K. H., & Arthur, M. A. (2015). Controls on the stratigraphic distribution and nitrogen isotopic composition of zinc, vanadyl and free base porphyrins through Oceanic Anoxic Event 2 at Demerara Rise. Organic Geochemistry, 80, 60-71.
18. Karner, M. B., DeLong, E. F., & Karl, D. M. (2001). Archaeal dominance in the mesopelagic zone of the Pacific Ocean. Nature, 409, 507-510.
19. Kashiyama, Y., Ogawa, N. O., Shiro, M., Tada, R., Kitazato, H., & Ohkouchi, N. (2008a). Reconstruction of the biogeochemistry and ecology of photoautotrophs based on nitrogen

and carbon isotopic compositions of vanadyl porphyrins from Miocene siliceous sediments. Biogeosciences, 5, 797-816.
20. Kashiyama, Y., Ogawa, N. O., Kuroda, J., Shiro, M., Nomoto, S., Tada, R., Kitazato, H., & Ohkouchi, N. (2008b). Diazotrophic cyanobacteria as the major photoautotrophs during mid-Cretaceous oceanic anoxic events: Nitrogen and carbon isotope evidence from sedimentary porphyrin. Organic Geochemistry, 39, 532-549.
21. Kim, J. H., Van der Meer, J., Schouten, S., Helmke, P., Willmott, V., Sangiorgi, F., Koç, N., Hopmans, E. C., & Sinninghe Damsté, J. S. (2010). New indices and calibrations derived from the distribution of crenarchaeal isoprenoid tetraether lipids: Implications for past sea surface temperature reconstructions. Geochimica et Cosmochimica Acta, 74, 4639-4654.
22. Könneke, M., Schubert, D.M., Brown, P.C., Hügler, M., Standfest, S., Schwander, T., von Borzyskowski, L.S., Erb, T.J., Stahl, D.A., & Berg, I.A. (2014). Ammonia-oxidizing archaea use the most energy-efficient aerobic pathway for CO2 fixation. Proceedings of the National Academy of Sciences, 111, 8239-8244.
23. Kuypers, M. M. M., Pancost, R. D., Nijenhuis, I. A. & Sinninghe Damsté, J. S. (2002). Enhanced productivity led to increased organic carbon burial in the euxinic North Atlantic basin during the late Cenomanian oceanic anoxic event. Paleoceanography, 17, 3, 3–13.
24. Kuypers, M. M. M., van Breugel, Y., Schouten, S., Erba, E. & Sinninghe Damsté, J. S. (2004). N_2-fixing cyanobacteria supplied nutrient N for Cretaceous oceanic anoxic events. Geology, 32, 853-856.
25. Lam, P., Jensen, M. M., Lavik, G., McGinnis, D. F., Müller, B., Schubert, C. J., Amann, R., Thamdrup, B., & Kuypers, M. M. M. (2007). Linking crenarchaeal and bacterial nitrification to anammox in the Black Sea. Proceedings of the National Academy of Sciences, 104, 7104-7109.
26. Lee, C.-T. A., Jiang, H., Ronay, E., Minisini, D., Stiles, J., & Neal, M. (2018). Volcanic ash as a driver of enhanced carbon burial in the Cretaceous. Scientific Reports, 8, 4197.
27. Lewan, M. D. (1984). Factors controlling the proportionality of vanadium to nickel in crude oils. Geochimica et Cosmochimica Acta, 48, 2231-2238.
28. Liaaen-Jensen, S., Hegge, E., & Jackman, L. M. (1964). Bacterial carotenoids XVIII, The carotenoids of photosynthetic bacteria, Acta Chemica Scandinavica, 18, 1703-1718.
29. Liu, X.-L., Summons, R.E., & Hinrichs, K.U. (2012). Extending the known range of glycerol ether lipids in the environment: structural assignments based on tandem mass spectral fragmentation patterns. Rapid Communications in Mass Spectrometry, 26, 2295-2302.
30. Liu, X-L., Zhu, C., Wakeham, S. G., & Hinrichs, K-U. (2014). In situ production of branched glycerol dialkyl glycerol tetraethers in anoxic water columns. Marine Chemistry, 166, 1-8.
31. Martin, E. E., MacLeod, K. G., Jiménez Berrocoso, A., & Bourbon, E. (2012). Water mass circulation on Demerara Rise during the Late Cretaceous based on Nd isotopes. Earth and Planetary Science Letters, 327-328, 111-120.
32. Meyers, P.A., Bernasconi, S.M., & Forster, A. (2006). Origins and accumulation of organic matter in expanded Albian to Santonian black shale sequences on the Demerara Rise, South American margin. Organic Geochemistry, 37, 1816-1830.
33. O'Brien, C. L., Robinson, S. A., Pancost, R. D., Sinninghe Damsté, J. S., Schouten, S., Lunt, D. J., Alsenz, H., Bornemann, A., Bottini, C., Brassell, S. C., Farnsworth, A., Forster,

A., Huber, B. T., Inglis, G. N., Jenkyns, H. C., Linnert, C., Littler, K., Markwick, P., McAnena, A., Mutterlose, J., Naafs, B. D. A., Püttmann, W., Sluijs, A., van Helmond, N. A. G. M., Vellekoop, J., Wagner, T., & Wrobel N. E. (2017). Cretaceous sea-surface temperature evolution: Constraints from TEX 86 and planktonic foraminiferal oxygen isotopes. Earth-Science Reviews, 172, 224–247.

34. Ostrander, C. M., Owens, J. D., & Nielsen, S. G. (2017). Constraining the rate of oceanic deoxygenation leading up to a Cretaceous oceanic Anoxic Event (OAE-2: ~94Ma). Science Advances, 3e1701020.
35. Owens, J. D., Gill, B. C., Jenkyns, H. C., Bates, S. M., Severmann, S., Kuypers, M. M. M., Woodfine, R. G., & Lyons T. W. (2013). Sulfur isotopes track the global extent and dynamics of euxinia during Cretaceous Oceanic Anoxic Event 2. Proc. Natl. Acad. Sci. 110, 18407–18412.
36. Owens, J. D., Reinhard, C. T., Rohrssen, M., Love, G. D., & Lyons T. W. (2016). Empirical links between trace metal cycling and marine microbial ecology during a large perturbation to Earth's carbon cycle. Earth Planet. Sci. Lett. 449, 407–417.
37. Owens, J. D., Lyons, T. W., & Lowery, C. M. (2018). Quantifying the missing sink for global organic carbon burial during a Cretaceous oceanic anoxic event. Earth Planet. Sci. Lett. 499, 83–94.
38. Raven, M. R., Fike, D. A., Bradley, A. S., Gomes, M. L., Owens, J. D., & Webb, S. A. (2019). Paired organic matter and pyrite $\delta^{34}S_{pyrite}$ records reveal mechanisms of carbon, sulfur, and iron cycle disruption during Oceanic Anoxic Event 2. Earth and Planetary Science Letters, 512, 27-38.
39. Pedersen, T. F., & Calvert, S. E. (1990). Anoxia vs. Productivity: What controls the formation of organic-carbon-rich sediments and sedimentary rocks? AAPG Bulletin, 74, 454-466.
40. Schlanger, S. O., & Jenkyns, H. C. (1976). Cretaceous Oceanic Anoxic Events: Causes and consequences. Geologie en Mijnbouw, 55, 179-184.
41. Scholle, P. A., & Arthur, M. A. (1980). Carbon isotope fluctuations in Cretaceous pelagic limestones: potential stratigraphic and petroleum exploration tool. American Association of Petroleum Geologists Bulletin, 64, 67-87.
42. Schouten, S., Hopmans, E. C., Schefuß, E., & Sinninghe Damsté, J. S. (2002). Distributional variations in crenarchaeotal membrane lipids: A new tool for reconstructing ancient sea water temperatures? Earth and Planetary Science Letters, 204, 265-274.
43. Sinninghe Damsté, J. S., Schouten, S., Hopmans, E. C., van Duin, A. C. T., & Geenevasen, J. A. J. (2002). Crenarchaeol: the characteristic core glycerol dibiphytanyl glycerol tetraether membrane lipid of cosmopolitan pelagic crenarchaeota. Journal of Lipid Research, 43, 1641-1651.
44. Steinacher, M., Joos, F., Frölicher, T.L., Bopp, L., Cadule, P., Cocco, V., Doney, S.C., Gehlen, M., Lindsay, K., Moore, J.K., & Schneider, B. (2010). Projected 21st century decrease in marine productivity: a multi-model analysis. Biogeosciences, 7, 979-1005.
45. Summons, R. E., & Powell, T. G. (1987). Identification of aryl isoprenoids in source rocks and crude oils: Biological markers for the green sulphur bacteria. Geochimica et Cosmochimica Acta, 51, 557-566.
46. Trabucho Alexandre, J., Tuenter, E., Henstra, G.A., van der Zwan, K.J., van de Wal, R.S., Dijkstra, H.A., & de Boer, P.L. (2010). The mid-Cretaceous North Atlantic nutrient trap: black shales and OAEs. Paleoceanography, 25, PA4201.

47. Treibs, A. (1936). Chlorophyll and heme derivatives in organic mineral materials. Angewandte Chem, 49, 682-686.
48. van Bentum, E. C., Hetzel, A., Brumsack, H.-J., Forster, A., Reichart, G.-J., & Sinninghe Damsté, J. S. (2009). Reconstruction of water column anoxia in the equatorial Atlantic during the Cenomanian-Turonian oceanic anoxic event using biomarker and trace metal proxies. Palaeogeography, Palaeoclimatology, Palaeoecology, 280, 489-498.
49. Wilson, S.T., Hawco, N.J., Armbrust, E.V., Barone, B., Björkman, K.M., Boysen, A.K., Burgos, M., Burrell, T.J., Casey, J.R., DeLong, E.F., & Dugenne, M. (2019). Kīlauea lava fuels phytoplankton bloom in the North Pacific Ocean. Science, 365, 1040-1044.
50. Witkowski, C. R., Weijers, J. W. H., Blais, B., Schouten, S., & Sinninghe Damsté, J. S. (2018). Molecular fossils from phytoplankton reveal secular pCO_2 trend over the Phanerozoic. Science Advances, 4, eaat4556.
51. Xiao, W., Wang, Y., Zhou, S., Hu, L., Yang, H., & Xu, Y. (2016). Ubiquitous production of branched glycerol dialkyl glycerol tetraethers (brGDGTs) in global marine environments: a new source indicator for brGDGTs. Biogeosciences, 13, 5883-5894.
52. Zeng, Z., Liu, X.-L., Farley, K. R., Wei, J. H., Metcalf, W. W., Summons, R. E., & Welander, P, V. (2019). GDGT cyclization proteins identify the dominant archaeal sources of tetraether lipids in the ocean. Proceedings of the National Academy of Sciences, 116, 22505-22511.
53. Zheng, X.-Y., Jenkyns, H. C., Gale, A. S., Ward, D. J., & Henderson, G. M. (2013). Changing ocean circulation and hydrothermal inputs during Oceanic Anoxic Event 2 (Cenomanian-Turonian): Evidence from Nd-isotopes in the European shelf sea. Earth and Planetary Science Letters, 375, 338-348.
54. Zhu, C., Yoshinaga, M.Y., Peters, C.A., Liu, X.-L., Elvert, M., & Hinrichs, K.U. (2014). Identification and significance of unsaturated archaeal tetraether lipids in marine sediments. Rapid Communications in Mass Spectrometry, 28, 1144-1152.

1.6 Figures

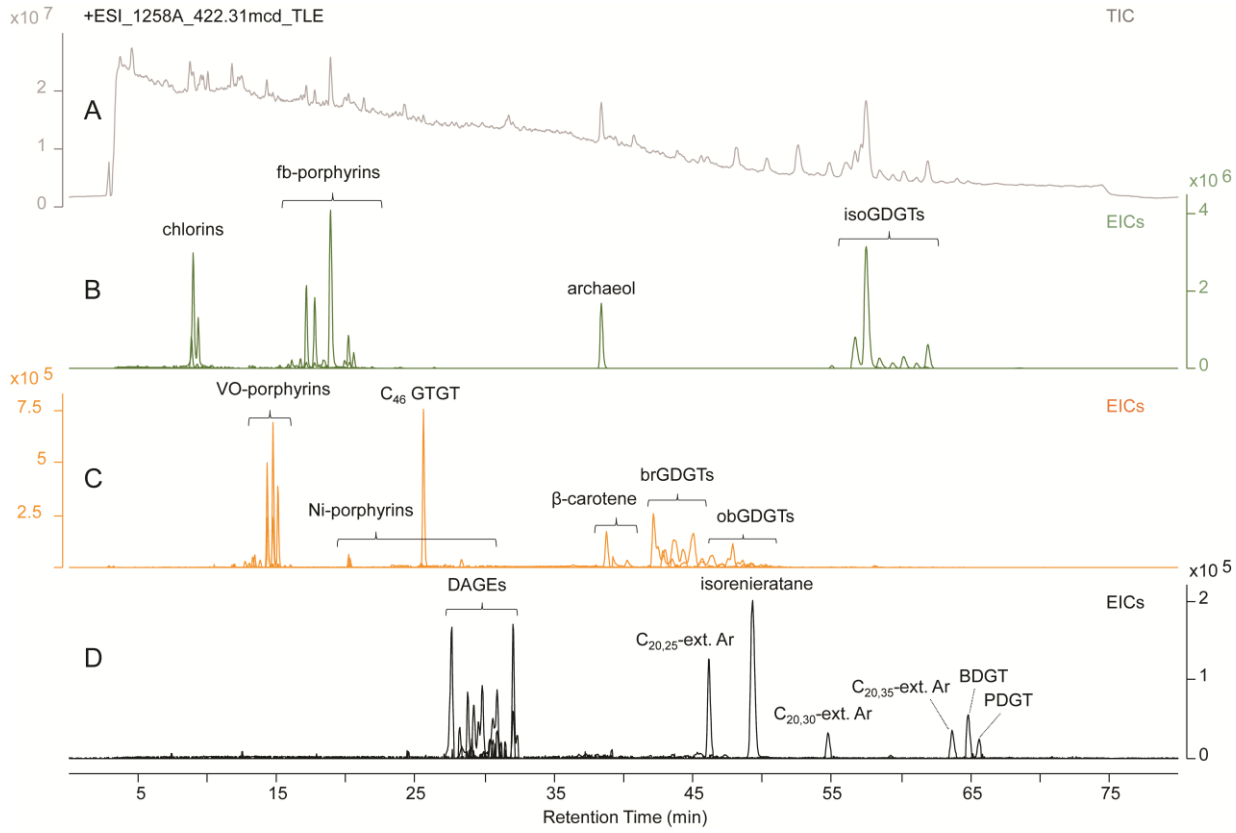

Figure 1-1. Total ion chromatogram (TIC) and summed extracted ion chromatograms (EIC) from LC-qTOF-MS analysis for sample 1258A 42-6 82-83. (A) TIC depicting the overall signal intensity of major biomarkers and background metrics. (B to D) Combined EICs based on the relative abundance of targeted biomarker classes to show compound separation and abundance.

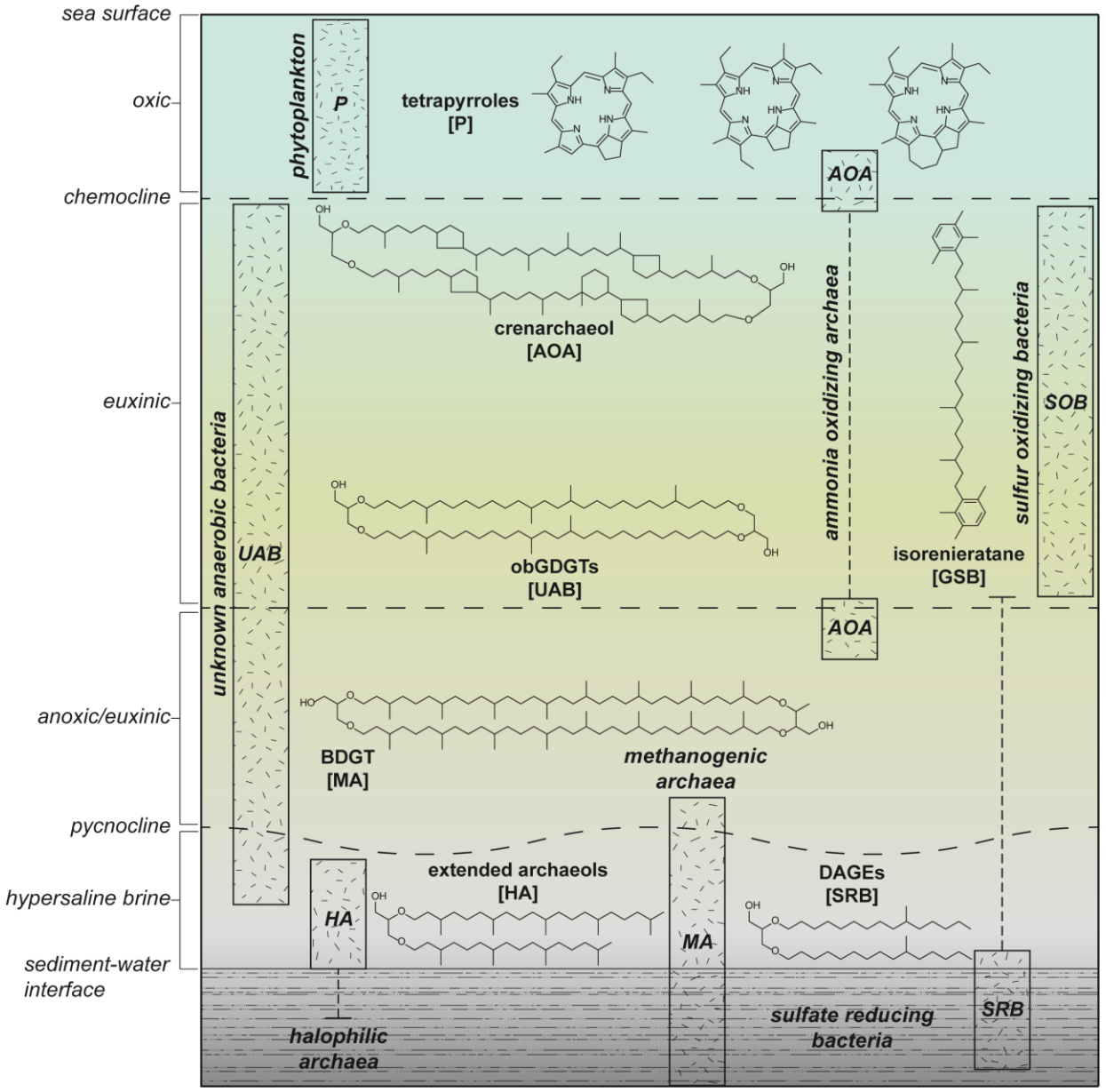

Figure 1-2. An idealized 2-D water column portraying the depth distribution and source organisms of biomarkers detected in mid-Cretaceous strata from site 1258, Demerara Rise. The residence depths of specific microbes are illustrated using rectangles, spanning habitable depth ranges, and containing relevant abbreviations (e.g. sulfur-oxidizing bacteria = SOB). Vertical hashed lines represent regions potentially occupied by a specific organism but beyond their ideal depth range. Selected biomarker structures are depicted to portray the compound diversity hosted in sediments from the Demerara Rise, with the source organism abbreviation in brackets.

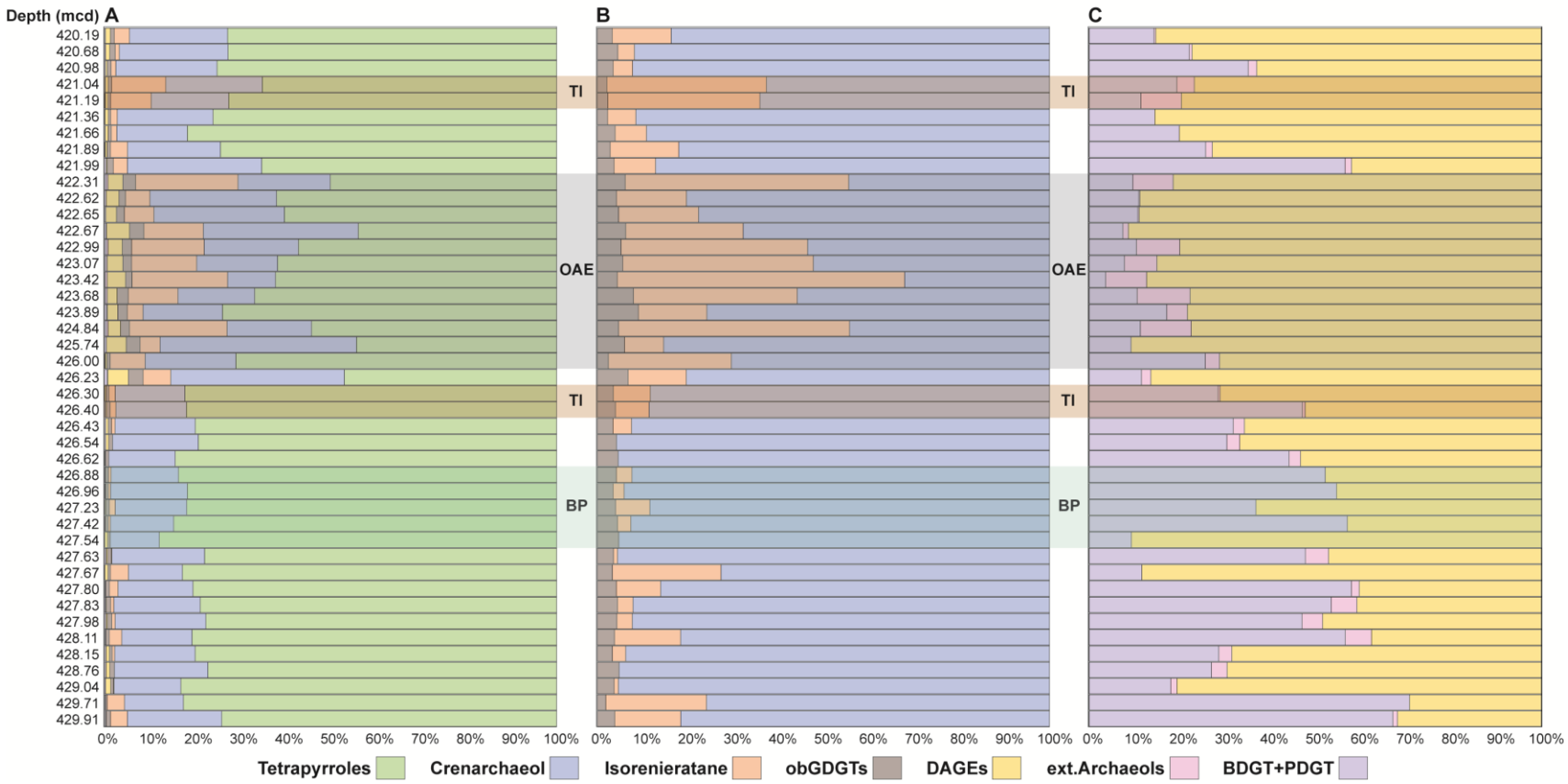

Figure 1-3. Biomarker fractional abundances preceding, during, and following OAE-2. (A) The fractional abundance of individual biomarkers, representative of the entire water column. (B) The fractional abundance of biomarkers derived exclusively from intermediate depths. (C) The fractional abundance of lipids produced by deep water microbial communities. The color shaded intervals represent the timing and duration of the pre-OAE biotic perturbation (BP), thallium isotope excursions (Tl), and OAE-2 (OAE).

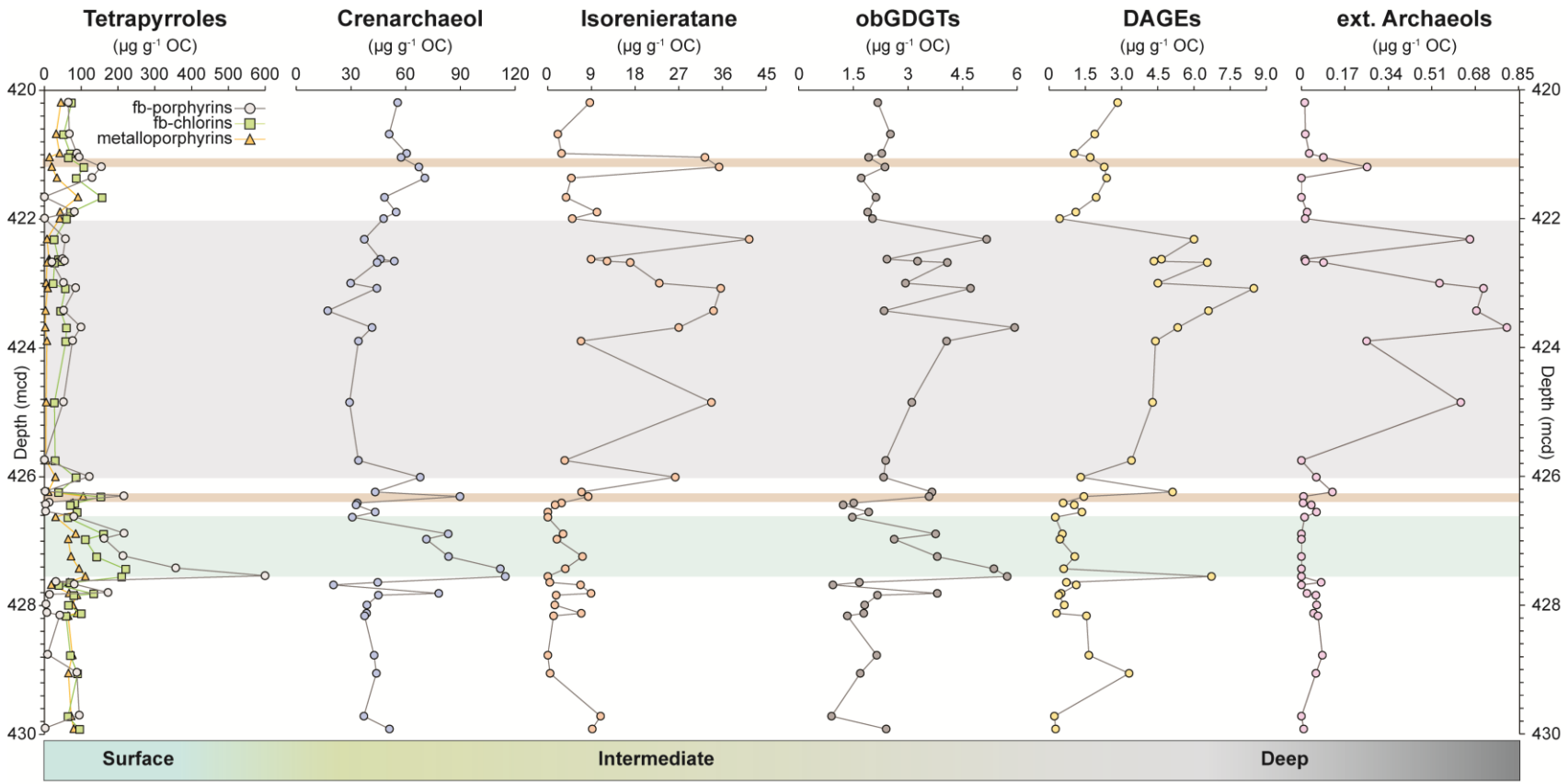

Figure 1-4. Depth profiles of biomarkers through the studied section. Biomarkers are ordered from left to right by increasing residence depth, indicated by the shaded rectangle and associated labels 'Surface', 'Intermediate', and 'Deep'. The blue shaded interval represents the pre-OAE biotic perturbation, the gray shaded interval represents OAE-2, and the brown shaded intervals represent the positive Tl isotopic excursions. The tetrapyrroles are comprised of three individual logs, the free base porphyrins (fb-porphyrins), free base chlorins (fb-chlorins) and summed VO-, Ni-, Fe-, and Zn-metalloporphyrins. The obGDGTs, DAGEs, extended archaeols, and individual tetrapyrrole profiles are comprised of multiple compounds (see Supplementary Information for additional details).

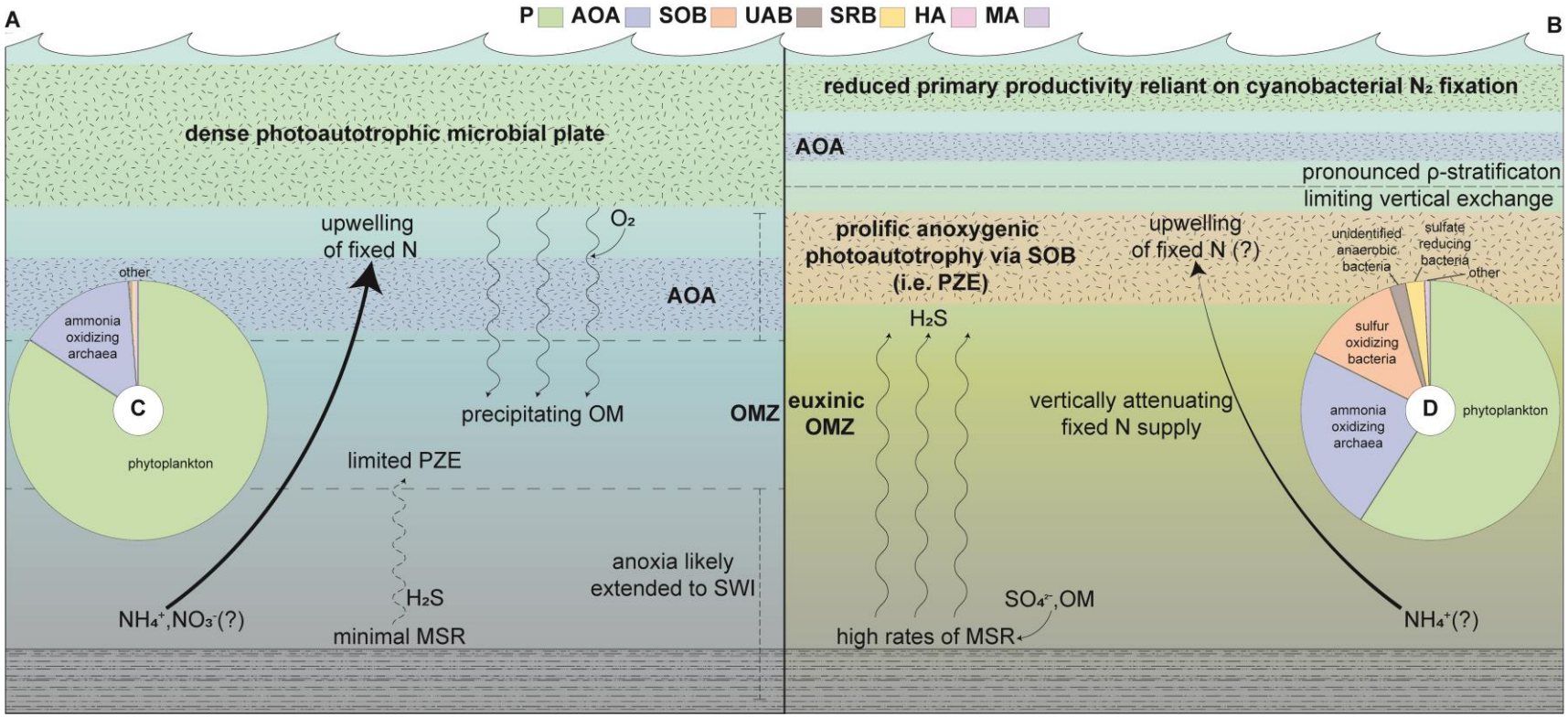

Figure 1-5. Contrasting biogeochemical conditions between the pre-OAE BP and OAE-2. (A-B) Microbial ecology and water column conditions during the pre-OAE BP, reflecting high primary production of organic carbon (A) and OAE-2, characterized by relatively lower organic carbon production, but substantially enhanced biomass preservation (B). (C-D) Averaged fractional abundances of individual biomarkers throughout the pre-OAE BP (C) and OAE-2 (D).

1.7 Supplementary Information

1.7.1 Principal component analysis

Principal component analysis (PCA) was performed on the entire dataset using RStudio Desktop (available at https://rstudio.com), an integrated development environment for R (R Core Team 2020, available at https://www.R-project.org/). Data exploration and interpretative validation were the primary motives to conduct PCA on our biomarker inventory. The prcomp() function was favored given the greater numerical accuracy of singular value decomposition compared to spectral decomposition, called by the princomp() function. Data were centered and scaled in the prcomp() function. Biplot visualization (Figure S1-4) was achieved by modification of the plot() function following publicly available online guides.

1.7.2 Evidence for LIP trigger of the pre-OAE biotic perturbation

A spike in bioessential trace metals, (e.g. V, Mo; Hetzel et al., 2009; Owens et al., 2016), immediately precedes (427.63 mcd) the biotic perturbation at 427.54 mcd, where trace metals are in relatively low abundance (Figure S1-5). This combined with the relative timing of LIP activity (Du Vivier et al., 2014) and continental arc volcanism (Lee et al., 2018) suggests exogenous nutrient delivery by sources as a possible trigger for the pre-OAE BP. In addition, an abrupt increase in TEX^{H}_{86} equating to a ~1^{o}C sea surface temperature rise coincides with the pre-OAE event (Figure S1-1), underlining the possible role LIP-sourced and/or volcanogenic greenhouse gases played in stimulating continental erosion and runoff enriched in nutrients (e.g. PO_4^{3-}). Continental derivation of nutrients, at least at the onset, is further validated by a spike in the BIT index (branched/isoprenoid tetraether), indicative of terrestrial organic matter input (Hopmans et al., 2004), coeval with the precipitate trace metal incursion. Consistency between trace metal and

BIT index behavior throughout the pre-OAE biotic shift (427.54-426.40 mcd, Figures S1-1 & S1-5) implies similar controlling processes, something unobserved during OAE-2. The departure from trace metal (e.g. V) and BIT index covariance during OAE-2 (Figure S1-7) is likely a result of increased production of aquatic brGDGTs in an expanded OMZ, which adversely affected crenarchaeol production by *Thaumarchaeota*. Relative increases in 6-methyl penta- and hexamethylated brGDGTs to 5-methyl penta- and hexamethylated brGDGTs, previously used to differentiate soil vs. aquatic brGDGT synthesis (Xiao et al., 2016), coincided with elevated BIT values and provided evidence for multiple controls on brGDGT distributions (Figure S1-7). This results in an increase in the numerator (brGDGTs) and decrease in the denominator (crenarchaeol) of the BIT index, explaining the elevated BIT indices observed during OAE-2. Regarding the pre-OAE trigger mechanism(s), either fluvial discharge was the primary source of trace metals or was coincidental with ocean fertilization by LIP-related hydrothermal fluids rich in trace metals. Nevertheless, one or both processes provided an injection of nutrients [partially] culpable for initiating the pre-OAE biotic perturbation.

1.7.3 Tetrapyrroles as a record of primary production

It is critical to provide a complete discussion outlining our rationale to employ the tetrapyrroles (free base chlorins, porphyrins and metalloporphyrins) as a record of productivity in the Cenomanian-Turonian equatorial North Atlantic Ocean. Tetrapyrrole investigations are disconnected in time, as initial popularity of these fossil chlorophylls diminished until relatively recent pursuits targeted reconstruction of ancient N cycling dynamics. A previous study of free base and metallo (VO, Zn) C_{33} bicycloalkanoporphyrins (BiCAPs) at ODP site 1261 of the Demerara Rise concluded tetrapyrrole stratigraphic abundance was primarily a function of metal accessibility, and not bottom water redox or maturity (Junium et al., 2015). We agree maturity and

redox state exerted a minimal effect on tetrapyrrole preservation. The narrow stratigraphic window of the studied section (~10 m) ensures comparable levels of thermal stress imparting a consistent, albeit negligible, influence on tetrapyrrole distribution. Similarly, the exceptional preservation present at the Demerara Rise before, during, and after OAE-2 limits preservation biases. However, a shift to euxinic conditions likely impacted the availability of metals reactive with sulfides (e.g. Ni; Lewan, 1984), which will in turn affect relevant metalloporphyrin formation. Other metals (e.g. V) will complex with organic matter under reducing conditions (Breit and Wanty, 1991), competing with porphyrin chelation. Although expanded euxinia and enhanced organic matter preservation typify OAE-2, characterized by relatively low concentrations of trace metals, free base chlorins, porphyrins, and metalloporphyrins, our observations suggest chlorophyll production exerts greater control on tetrapyrrole abundance.

Overall, high tetrapyrrole concentrations was not exclusively linked to high metal concentrations. The free base chlorins and porphyrins should not be sensitive to metal availability and display no significant relationship with V (Figure S1-8), Zn, Mo, or Fe. Identified metalloporphyrins (VO, Ni, Zn, Fe) also exhibit a weak correlation to formerly mentioned metals. High metalloporphyrin concentrations are observed at relatively low and high metal abundances. If a group of samples, partially composed of data from the pre-OAE biotic perturbation, with high metalloporphyrin concentrations relative to depressed trace metal (e.g. V) values is removed, then a strong positive relationship emerges (Figure S1-8). This suggests metal availability does play a role in metalloporphyrin abundance, but to what extent remains unconstrained as other processes (e.g. supply of free base porphyrins) may also impact the absolute metalloporphyrin concentrations. Despite the ambiguity surrounding the impact of metal availability on tetrapyrrole preservation, the presence of metals, particularly V, clearly facilitates the metalation of free bases.

A strong negative linear relationship was observed between the ratio of free bases to metalloporphyrins and V (R^2 = 0.86, Figure S1-8). Therefore, metal abundance plays a key role in metalloporphyrin formation if sufficient precursor is available but does not influence the absolute concentration of porphyrins in sediments.

On average, concentrations of free base tetrapyrroles (chlorins + porphyrins) are an order of magnitude greater relative to metalloporphyrins in our study (Figure 1-4, Data S1-1). Given that free base tetrapyrroles lack any significant relationship to metal supply and the Cenomanian-Turonian at site 1258 was deposited under relatively constant reducing conditions, the total tetrapyrrole profile (free base + metallo, Figure 1-4) is primarily indicative of chlorophyll production and therefore reflective of primary production. Inclusion of the metalloporphyrins, which mostly mirror the free base tetrapyrroles over the analyzed section (Figures 1-4 & S1-5), helps diminish diagenetic alteration of the primary producer signal. However, uncharacterized complexity influencing metalloporphyrin distributions precludes application in isolation of free base tetrapyrroles. For example, the metalloporphyrins were present in greatest concentrations prior to OAE-2 and do not recover to comparable levels post-OAE as trace metals and free base tetrapyrroles rebound (Figures 1-4 & S1-5). It is beyond the scope of this study to elucidate additional controls on metalloporphyrin formation, but the progressive alteration of the original chlorophyll risks deterioration of the original primary producer signal.

1.8 Supplementary Figures and Tables

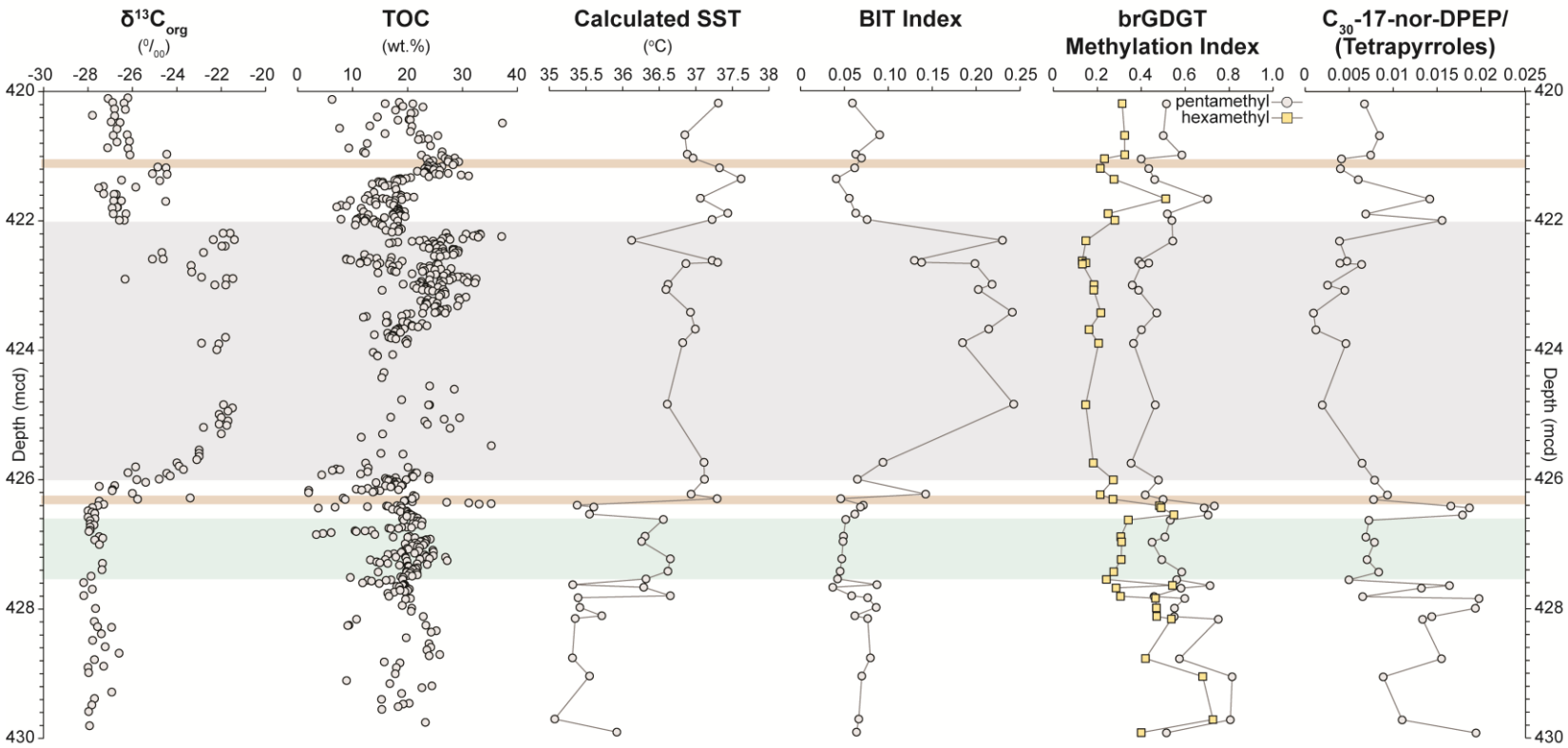

Figure S1-1. Various geochemical profiles from site 1258, Demerara Rise. The $\delta^{13}C_{org}$ and TOC values are compiled from previous studies (Erbacher et al., 2005; Hetzel et al. 2009; Owens et al., 2016). Sea surface temperatures (SST) were calculated from TEX^{H}_{86} using published methods (Schouten et al., 2002; Kim et al., 2010). Similarly, BIT indices were calculated based on previously published work (Hopmans et al., 2004). The brGDGT methylation index is simply the ratio of the 5-methyl normalized to the 6-methyl penta-/hexa-methyl brGDGTs, similar to prior reports (Xiao et al., 2016). The C_{30}-17-nor-DPEP is normalized to the total summed tetrapyrroles, including free base chlorins, porphyrins, and metalloporphyrins. The blue shaded interval represents the pre-OAE biotic perturbation, the gray shaded interval represents OAE-2, and the brown shaded intervals represent the positive Tl isotopic excursions.

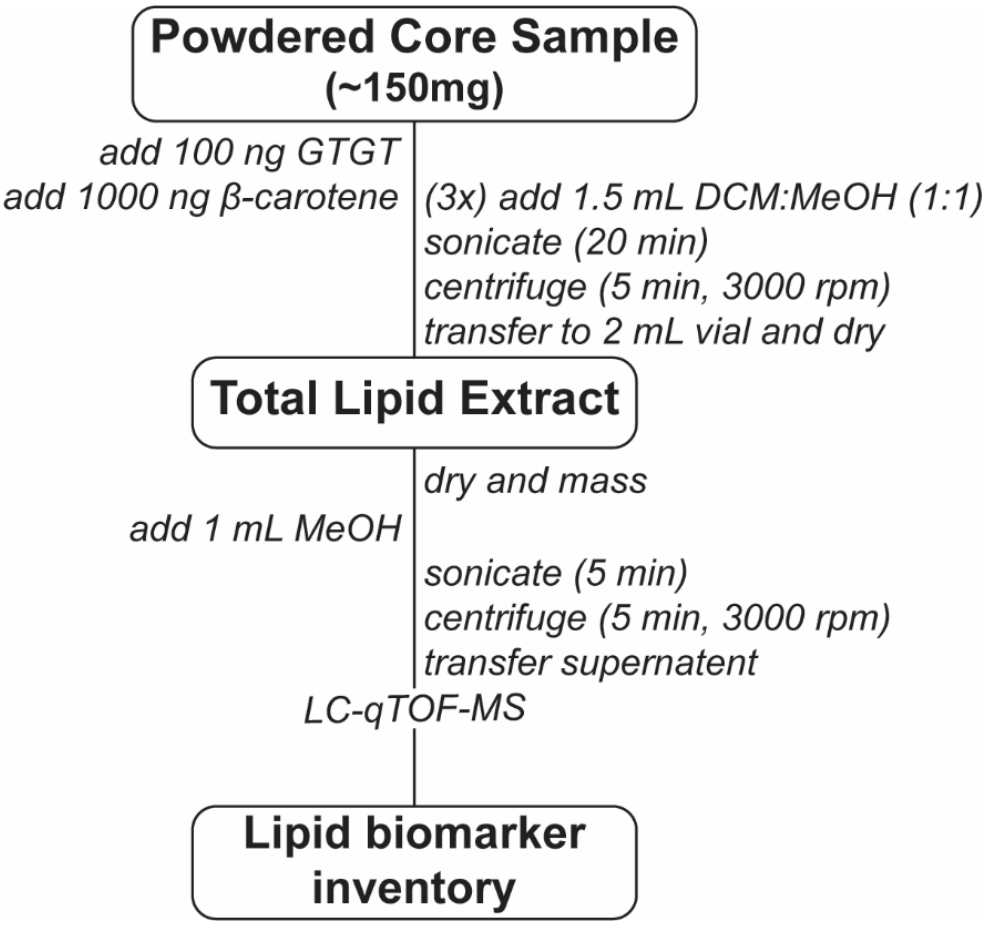

Figure S1-2. Preparatory procedure for extraction and analysis of biomarkers.

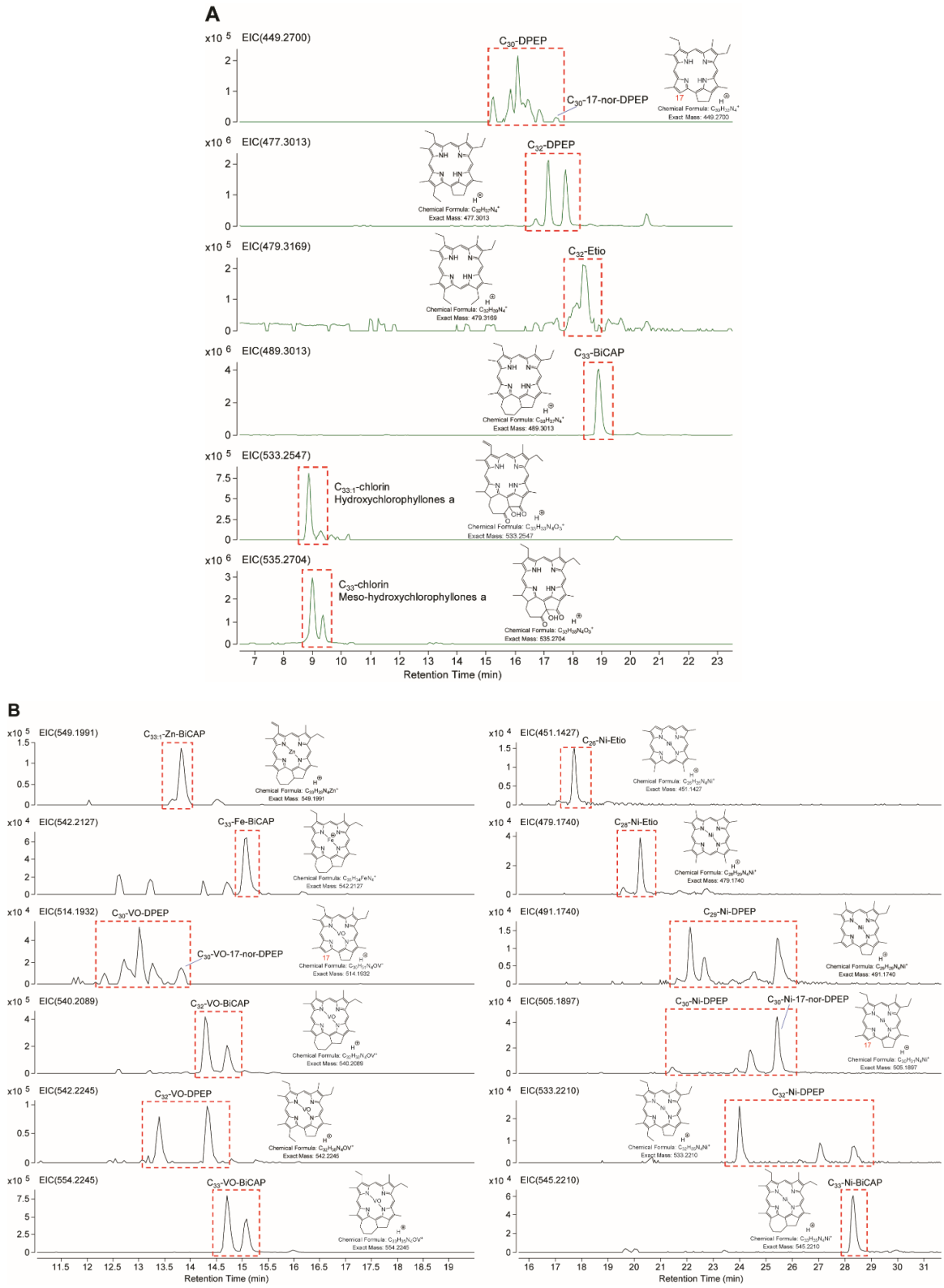
A
EIC(449.2700)
C30-DPEP
C30-17-nor-DPEP
EIC(477.3013)
C32-DPEP
EIC(479.3169)
C32-Etio
EIC(489.3013)
C33-BiCAP
EIC(533.2547)
C33:1-chlorin
Hydroxychlorophyllones a
EIC(535.2704)
C33-chlorin
Meso-hydroxychlorophyllones a
Retention Time (min)
B
EIC(549.1991)
C33:1-Zn-BiCAP
EIC(542.2127)
C33-Fe-BiCAP
EIC(514.1932)
C30-VO-DPEP
C30-VO-17-nor-DPEP
EIC(540.2089)
C32-VO-BiCAP
EIC(542.2245)
C32-VO-DPEP
EIC(554.2245)
C33-VO-BiCAP
EIC(451.1427)
C28-Ni-Etio
EIC(479.1740)
C28-Ni-Etio
EIC(491.1740)
C29-Ni-DPEP
EIC(505.1897)
C30-Ni-DPEP
C30-Ni-17-nor-DPEP
EIC(533.2210)
C32-Ni-DPEP
EIC(545.2210)
C33-Ni-BiCAP
Retention Time (min)

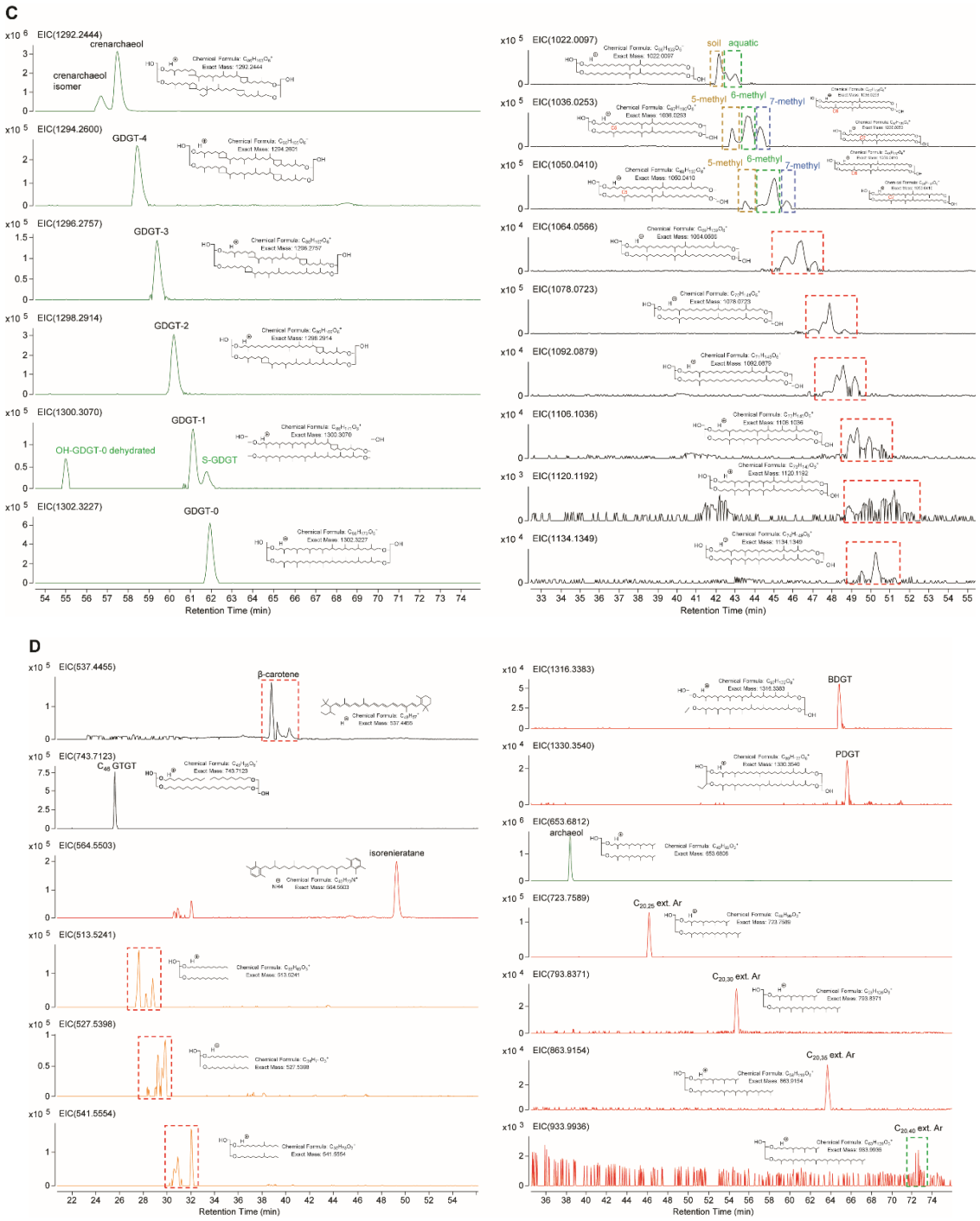

Figure S1-3. Extracted ion chromatograms (EICs) of identified biomarkers. (A) Free base porphyrins and chlorins detected in sample 1258A 42-6 82-83. (B) Major VO-, Zn-, Fe- and Ni-porphyrins detected in sample 1258A 42-6 17-18. (C) isoGDGTs, brGDGTs and obGDGTs detected in sample 1258A 42-6 82-83. (D) Internal standards (β-carotene and C_{46} GTGT), isorenieratane, DAGEs, BDGT, PDGT, archaeol, and extended archaeols shown in sample 1258A 42-6 82-83.

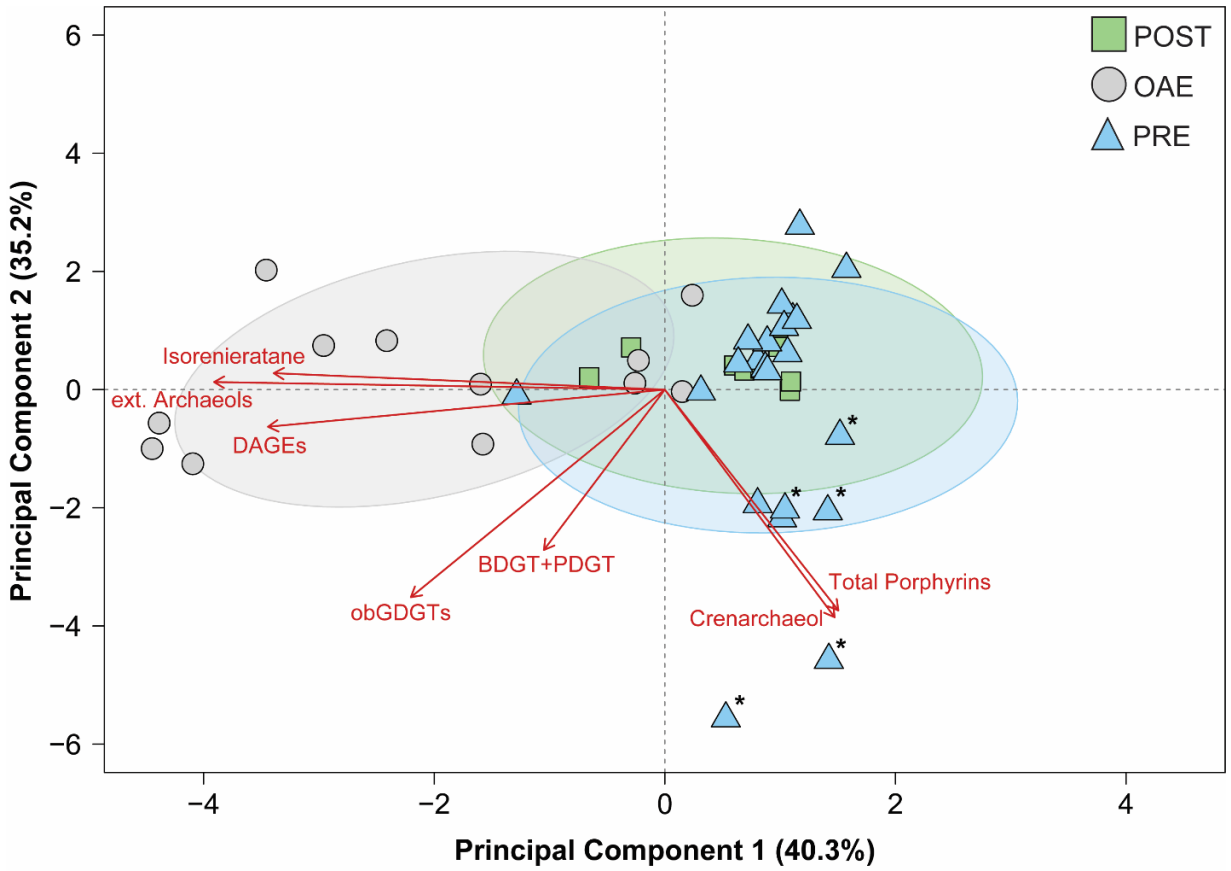

Figure S1-4. PCA results of biomarkers utilized in this study. Note the separation, driven primarily by biomarkers sourced from intermediate and deep waters, of pre- and post-OAE strata from samples deposited during the OAE. Samples with a '*' are from the pre-OAE biotic perturbation.

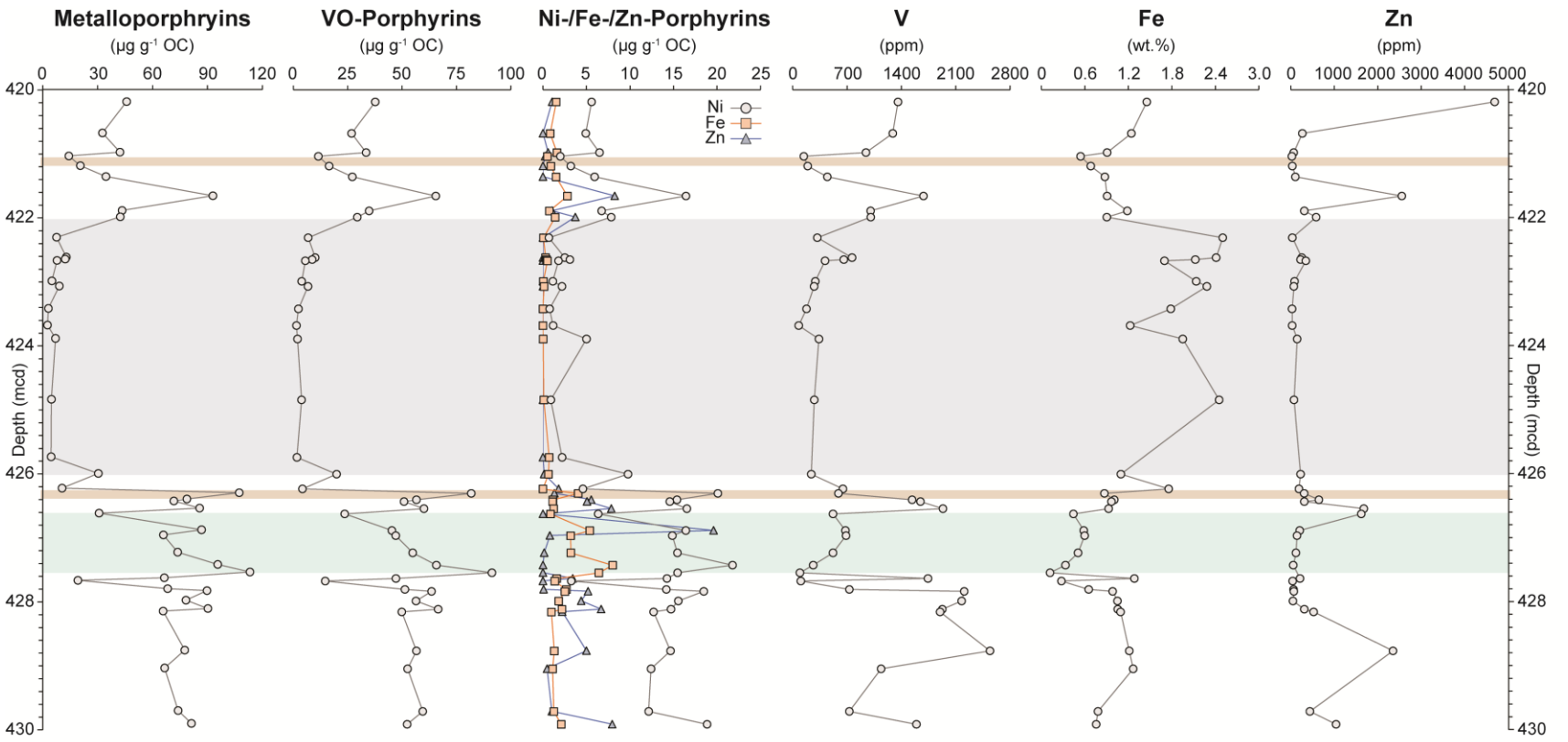

Figure S1-5. Depth profiles of metalloporphyrins and trace metals through the studied section. All metalloporphyrin data were generated in this study, with trace metal data from previous work (Owens et al., 2016). The blue shaded interval represents the pre-OAE biotic perturbation, the gray shaded interval represents OAE-2, and the brown shaded intervals represent the positive Tl isotopic excursions.

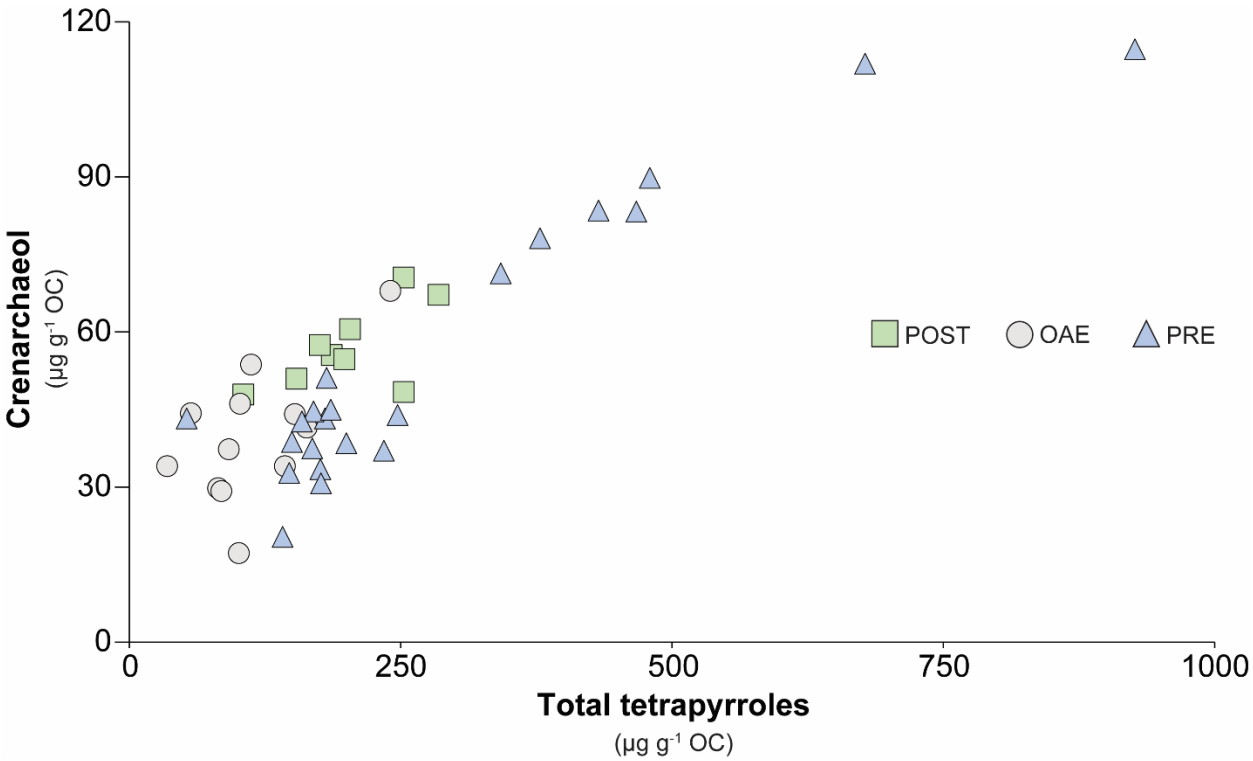

Figure S1-6. Cross plot of crenarchaeol and summed tetrapyrrole (chlorins, free base porphyrins, and metalloporphyrins) concentrations.

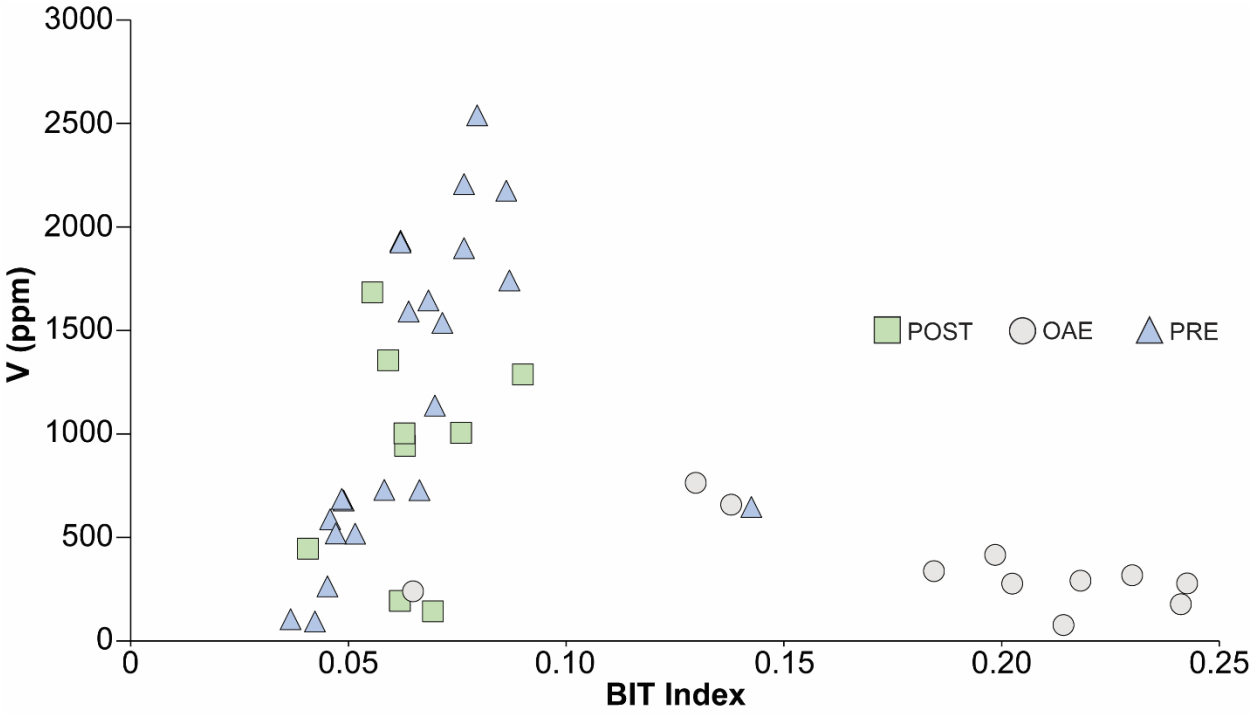

Figure S1-7. Cross plot of V and BIT Index. Note the duality of the relationship between BIT indices and V concentrations. Pre- and post-OAE strata predominantly exhibited a positive relationship between trace metal abundance and BIT indices, whereas most OAE-2 samples displayed a negative correlation between the two variables.

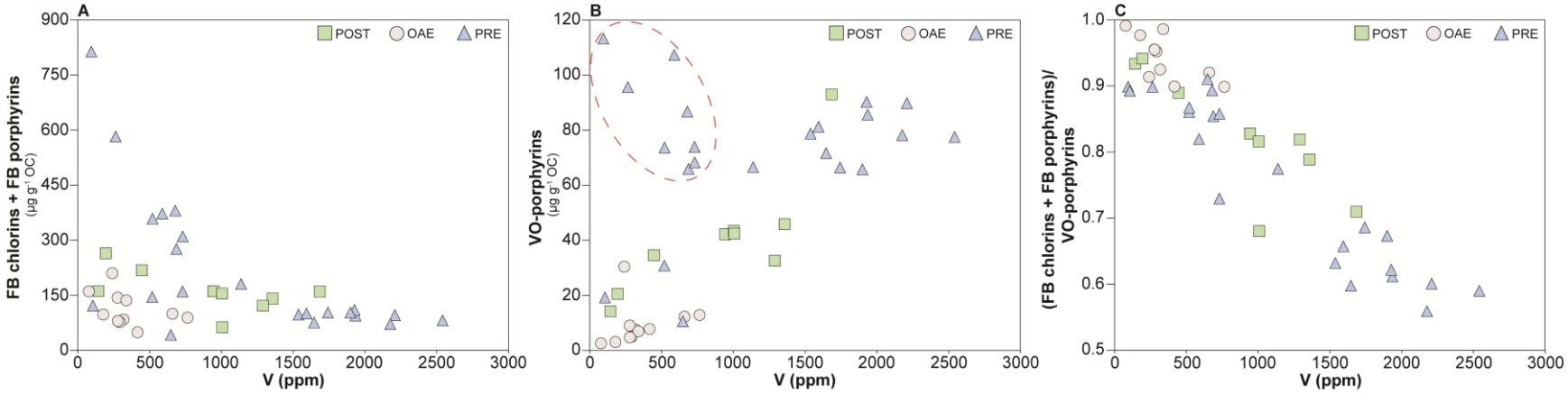

Figure S1-8. Cross plots of various tetrapyrroles and V. (A) Cross plot of the free base chlorins and porphyrins with V. (B) Cross plot of the VO-metalloporphyrins and V. Note the cluster of pre-OAE samples, encircled by the red hashed outline, exhibiting relatively high metalloporphyrin content for a given range of V concentrations. Otherwise, a clear positive correlation would exist between metalloporphyrins and V. (C) The ratio of free base chlorins and porphyrins to metalloporphyrins against V levels.

Sample	Depth (mcd)	FB-chlorins (µg g-1 OC)	FB-Porphyrins (µg g-1 OC)	Metalloporphyrins (µg g-1 OC)	Crenarchaeol (µg g-1 OC)	Isorenieratane (µg g-1 OC)	obGDGTs (µg g-1 OC)	DAGEs (µg g-1 OC)	ext. Archaeols (µg g-1 OC)	BDGT+PDGT (µg g-1 OC)
207-1258B 45R-3 1-2	420.19	75.65	64.96	45.84	55.54	8.65	2.17	2.84	0.01	0.48
207-1258A 42-5 51-53	420.68	53.41	68.00	32.57	50.94	2.03	2.52	1.89	0.02	0.54
207-1258B 45-3 80-81	420.98	72.82	88.24	42.18	60.55	2.82	2.28	1.03	0.03	0.58
207-1258A 42-5 87-88	421.04	66.82	94.39	14.22	57.47	32.40	1.92	1.71	0.09	0.43
207-1258A 42-5 102-103	421.19	109.63	154.62	20.55	67.18	35.29	2.37	2.28	0.26	0.33
207-1258A 42-5 119-121	421.36	88.53	129.58	34.53	70.51	4.83	1.72	2.39	n.d.	0.41
207-1258A 42-6 17-18	421.66	159.98	n.d.	92.95	48.36	3.76	2.12	1.95	n.d.	0.49
207-1258B 45-4 30-31	421.89	73.08	81.65	43.39	54.75	10.12	1.89	1.10	0.02	0.39
207-1258B 45R-4 40-41	421.99	61.84	0.78	42.39	47.90	5.04	2.03	0.44	0.02	0.59
207-1258A 42-6 82-83	422.31	27.10	56.99	7.58	37.32	41.53	5.16	6.00	0.66	0.71
207-1258A 42-6 113-114	422.62	39.89	49.25	12.85	46.14	8.90	2.42	4.66	0.01	0.57
207-1258B 45R-4 106-107	422.65	45.16	54.63	12.25	53.70	12.20	3.26	4.34	0.02	0.52
207-1258A 42-6 118-119	422.67	28.55	20.33	7.77	44.27	16.98	4.08	6.55	0.09	0.53
207-1258A 42-7 10-11	422.99	24.82	51.84	5.01	29.80	22.98	2.93	4.51	0.54	0.59
207-1258B 45R-4 148-149	423.07	58.57	84.76	9.01	44.11	35.65	4.72	8.48	0.71	0.78
207-1258A 42-7 53-54	423.42	45.46	52.21	3.07	17.21	34.17	2.34	6.60	0.68	0.28
207-1258A 42-7 79-80	423.68	61.47	99.34	2.57	41.50	26.97	5.93	5.33	0.80	0.73
207-1258A 42-7 100-101	423.89	59.84	76.43	6.95	34.04	6.82	4.06	4.41	0.26	0.97
207-1258C 17R-1 5-6	424.84	28.13	51.84	4.76	29.20	33.73	3.10	4.29	0.62	0.63
207-1258C 17R-1 95-96	425.74	30.16	n.d.	4.56	34.06	3.46	2.39	3.42	n.d.	0.35
207-1258C 17R-1 121-122	426.00	87.96	122.07	30.39	67.94	26.26	2.33	1.31	0.06	0.47
207-1258A 42-7 114-115	426.23	39.95	2.36	10.55	43.27	6.94	3.66	5.12	0.12	0.69
207-1258C 17R-2 12-13	426.30	156.28	215.92	107.30	89.80	8.32	3.58	1.44	0.01	0.58
207-1258C 17R-2 22-23	426.40	84.18	13.13	78.69	33.43	2.80	1.51	0.58	0.01	0.53
207-1258C 17R-2 25-26	426.43	72.30	3.29	71.64	32.72	1.46	1.22	1.05	0.04	0.51
207-1258A 42-CCW 4-5	426.54	90.90	3.67	85.63	43.25	n.d.	1.92	1.36	0.06	0.62
207-1258A 43-1 14-15	426.62	65.73	79.91	30.80	30.69	n.d.	1.47	0.26	0.01	0.21
207-1258C 17R-2 70-71	426.88	164.07	216.34	86.70	83.28	3.13	3.76	0.55	n.d.	0.60
207-1258A 43-1 41-42	426.96	114.04	162.15	65.92	71.30	1.85	2.62	0.45	n.d.	0.55
207-1258A 43-1 75-76.5	427.23	145.11	213.46	73.67	83.48	7.14	3.80	1.06	n.d.	0.62
207-1258C 17R-3 4-5	427.42	225.33	356.91	95.60	111.88	3.59	5.36	0.61	n.d.	0.81
207-1258A 43-1 106-107	427.54	214.09	599.19	113.21	114.68	n.d.	5.72	6.73	n.d.	0.69
207-1258C 17R-3 25-26	427.63	71.98	31.15	66.43	44.65	0.40	1.67	0.72	0.08	0.73
207-1258A 43-1 119-120	427.67	40.73	81.07	19.25	20.37	6.73	0.94	1.13	n.d.	0.15
207-1258A 43-2 4-5	427.80	137.03	172.97	68.24	78.13	8.90	3.80	0.50	0.02	0.72
207-1258C 17R-3 45-46	427.83	81.86	13.83	89.76	44.96	1.69	2.16	0.40	0.06	0.53
207-1258C 17R-CC 2-3	427.98	67.16	4.44	78.19	38.72	1.43	1.81	0.64	0.06	0.62
207-1258C 17R-CC 15-16	428.11	102.69	6.88	90.20	38.48	6.89	1.79	0.31	0.05	0.47
207-1258A 43-2 39-41	428.15	60.64	42.09	65.73	37.49	1.17	1.34	1.55	0.07	0.65
207-1258A 43-2 100-105	428.76	72.58	8.88	77.53	42.66	n.d.	2.14	1.65	0.08	0.64
207-1258A 43-3 2-3	429.04	92.25	88.33	66.54	43.92	0.44	1.69	3.32	0.06	0.74
207-1258A 43-3 68.5-70	429.71	65.57	94.94	73.91	37.03	10.86	0.90	0.22	n.d.	0.53
207-1258A 43-3 88.5-90	429.91	98.22	2.18	81.24	51.13	9.14	2.40	0.27	0.01	0.57

Table S1-1. Biomarker concentrations from site 1258, Demerara Rise. Free base- (FB) chlorins, FB-porphyrins, metalloporphyrins, obGDGTs, DAGEs, and ext. Archaeols are summed concentrations of multiple compounds shown in Figure S1-3. Horizontal black lines bracket the OAE 2 interval.

Sample	Depth (mcd)	Metalloporphyrins (µg g-1 OC)	VO-Porphyrins (µg g-1 OC)	Ni-Porphyrins (µg g-1 OC)	Fe-Porphyrins (µg g-1 OC)	Zn-Porphyrins (µg g-1 OC)	V (ppm)	Fe (wt. %)	Zn (ppm)
207-1258B 45R-3 1-2	420.19	45.84	37.68	5.58	1.52	1.05	1356.67	1.45	4689.12
207-1258A 42-5 51-53	420.68	32.57	26.81	4.91	0.84	n.d	1288.65	1.24	267.54
207-1258B 45-3 80-81	420.98	42.18	33.49	6.50	1.61	0.58	943.36	0.91	68.51
207-1258A 42-5 87-88	421.04	14.22	11.46	1.98	0.52	0.26	143.28	0.54	28.41
207-1258A 42-5 102-103	421.19	20.55	16.46	3.19	0.91	n.d	194.18	0.68	36.89
207-1258A 42-5 119-121	421.36	34.53	27.10	5.93	1.50	n.d	446.42	0.88	108.21
207-1258A 42-6 17-18	421.66	92.95	65.46	16.42	2.82	8.24	1684.64	0.91	2555.90
207-1258B 45-4 30-31	421.89	43.39	34.87	6.74	0.73	1.05	1003.50	1.18	314.62
207-1258B 45R-4 40-41	421.99	42.39	29.43	7.84	1.40	3.72	1006.13	0.90	584.21
207-1258A 42-6 82-83	422.31	7.58	6.83	0.68	0.07	n.d	317.84	2.50	38.12
207-1258A 42-6 113-114	422.62	12.85	10.05	2.50	0.30	n.d	764.21	2.41	254.31
207-1258B 45R-4 106-107	422.65	12.25	8.64	3.09	0.41	0.11	659.09	2.12	226.84
207-1258A 42-6 118-119	422.67	7.77	5.48	1.78	0.51	n.d	416.21	1.70	347.21
207-1258A 42-7 10-11	422.99	5.01	3.85	1.12	0.04	n.d	291.87	2.14	89.26
207-1258B 45R-4 148-149	423.07	9.01	6.71	2.17	0.13	n.d	277.34	2.28	72.01
207-1258A 42-7 53-54	423.42	3.07	2.31	0.77	0.00	n.d	177.77	1.79	29.84
207-1258A 42-7 79-80	423.68	2.57	1.42	1.15	0.00	n.d	77.31	1.22	36.24
207-1258A 42-7 100-101	423.89	6.95	1.94	5.00	0.02	n.d	338.13	1.95	149.23
207-1258C 17R-1 5-6	424.84	4.76	3.76	0.90	0.10	n.d	278.60	2.45	75.24
207-1258C 17R-1 95-96	425.74	4.56	1.65	2.19	0.72	n.d	-	-	-
207-1258C 17R-1 121-122	426.00	30.39	19.87	9.76	0.63	0.13	239.71	1.10	226.34
207-1258A 42-7 114-115	426.23	10.55	4.17	4.58	n.d	1.79	647.39	1.76	187.98
207-1258C 17R-2 12-13	426.30	107.30	81.84	20.09	4.06	1.31	588.13	0.87	309.74
207-1258C 17R-2 22-23	426.40	78.69	56.59	15.40	1.15	5.55	1537.31	1.01	646.93
207-1258C 17R-2 25-26	426.43	71.64	50.88	14.57	1.12	5.07	1645.63	0.97	312.46
207-1258A 42-CCW 4-5	426.54	85.63	60.03	16.53	1.23	7.85	1934.51	0.93	1679.66
207-1258A 43-1 14-15	426.62	30.80	23.59	6.34	0.87	n.d	518.90	0.44	1623.12
207-1258C 17R-2 70-71	426.88	86.70	45.29	16.41	5.39	19.61	678.95	0.58	208.12
207-1258A 43-1 41-42	426.96	65.92	47.08	14.87	3.17	0.79	687.20	0.60	146.43
207-1258A 43-1 75-76.5	427.23	73.67	54.88	15.44	3.22	0.13	520.10	0.51	122.18
207-1258C 17R-3 4-5	427.42	95.60	65.80	21.79	8.01	n.d	264.23	0.33	58.68
207-1258A 43-1 106-107	427.54	113.21	91.30	15.47	6.44	n.d	94.13	0.12	-
207-1258C 17R-3 25-26	427.63	66.43	47.19	14.25	1.57	3.42	1742.22	1.28	214.09
207-1258A 43-1 119-120	427.67	19.25	14.64	3.25	1.36	n.d	105.12	0.28	46.12
207-1258A 43-2 4-5	427.80	68.24	51.31	14.18	2.69	0.07	730.29	0.65	64.03
207-1258C 17R-3 45-46	427.83	89.76	63.58	18.48	2.52	5.18	2208.25	0.98	72.05
207-1258C 17R-CC 2-3	427.98	78.19	56.43	15.56	1.82	4.38	2175.84	1.05	52.15
207-1258C 17R-CC 15-16	428.11	90.20	66.63	14.71	2.18	6.68	1926.94	1.05	312.74
207-1258A 43-2 39-41	428.15	65.73	49.85	12.71	0.97	2.20	1898.24	1.09	525.58
207-1258A 43-2 100-105	428.76	77.53	56.59	14.65	1.30	4.99	2540.30	1.21	2353.98
207-1258A 43-3 2-3	429.04	66.54	52.54	12.42	1.11	0.46	1137.49	1.27	-
207-1258A 43-3 68.5-70	429.71	73.91	59.50	12.14	1.25	1.02	729.67	0.78	440.65
207-1258A 43-3 88.5-90	429.91	81.24	52.32	18.85	2.11	7.96	1592.82	0.76	1043.45

Table S1-2. Metalloporphyrin concentrations and selected metal abundances from site 1258, Demerara Rise. Metalloporphyrins, and metal-specific porphyrins (e.g. VO-porphyrins), are summed concentrations of multiple compounds shown in Figure S1-3. Metal abundances are from previous work (Owens et al., 2016). Horizontal black lines bracket the OAE 2 interval.

Sample	Depth (mcd)	Calculated SST (°C)	BIT Index	brGDGT Methylation Index (pentamethylated)	brGDGT Methylation Index (hexamethylated)	C_{30}-17-nor-DPEP /tetrapyrroles
207-1258B 45R-3 1-2	420.19	37.31	0.06	0.39	0.24	2.17
207-1258A 42-5 51-53	420.68	36.85	0.09	0.38	0.24	2.52
207-1258B 45-3 80-81	420.98	36.88	0.06	0.44	0.24	2.28
207-1258A 42-5 87-88	421.04	36.96	0.07	0.30	0.17	1.92
207-1258A 42-5 102-103	421.19	37.32	0.06	0.33	0.16	2.37
207-1258A 42-5 119-121	421.36	37.62	0.04	0.35	0.21	1.72
207-1258A 42-6 17-18	421.66	37.06	0.06	0.53	0.38	2.12
207-1258B 45-4 30-31	421.89	37.44	0.06	0.39	0.19	1.89
207-1258B 45R-4 40-41	421.99	37.22	0.08	0.41	0.21	2.03
207-1258A 42-6 82-83	422.31	36.12	0.23	0.41	0.11	5.16
207-1258A 42-6 113-114	422.62	37.22	0.13	0.30	0.10	2.42
207-1258B 45R-4 106-107	422.65	37.30	0.14	0.33	0.11	3.26
207-1258A 42-6 118-119	422.67	36.86	0.20	0.30	0.10	4.08
207-1258A 42-7 10-11	422.99	36.62	0.22	0.27	0.14	2.93
207-1258B 45R-4 148-149	423.07	36.59	0.20	0.29	0.14	4.72
207-1258A 42-7 53-54	423.42	36.93	0.24	0.36	0.16	2.34
207-1258A 42-7 79-80	423.68	36.99	0.21	0.30	0.12	5.93
207-1258A 42-7 100-101	423.89	36.82	0.18	0.28	0.15	4.06
207-1258C 17R-1 5-6	424.84	36.61	0.24	0.35	0.11	3.10
207-1258C 17R-1 95-96	425.74	37.11	0.09	0.27	0.14	2.39
207-1258C 17R-1 121-122	426.00	37.12	0.06	0.36	0.20	2.33
207-1258A 42-7 114-115	426.23	36.93	0.14	0.32	0.16	3.66
207-1258C 17R-2 12-13	426.30	37.29	0.05	0.38	0.20	3.58
207-1258C 17R-2 22-23	426.40	35.38	0.07	0.55	0.36	1.51
207-1258C 17R-2 25-26	426.43	35.61	0.07	0.52	0.37	1.22
207-1258A 42-CCW 4-5	426.54	35.55	0.06	0.53	0.41	1.92
207-1258A 43-1 14-15	426.62	36.56	0.05	0.40	0.26	1.47
207-1258C 17R-2 70-71	426.88	36.31	0.05	0.38	0.23	3.76
207-1258A 43-1 41-42	426.96	36.26	0.05	0.34	0.23	2.62
207-1258A 43-1 75-76.5	427.23	36.65	0.05	0.37	0.23	3.80
207-1258C 17R-3 4-5	427.42	36.62	0.05	0.44	0.21	5.36
207-1258A 43-1 106-107	427.54	36.32	0.04	0.42	0.18	5.72
207-1258C 17R-3 25-26	427.63	35.32	0.09	0.54	0.41	1.67
207-1258A 43-1 119-120	427.67	36.29	0.04	0.44	0.21	0.94
207-1258A 43-2 4-5	427.80	36.65	0.06	0.35	0.23	3.80
207-1258C 17R-3 45-46	427.83	35.39	0.08	0.45	0.35	2.16
207-1258C 17R-CC 2-3	427.98	35.42	0.09	0.42	0.35	1.81
207-1258C 17R-CC 15-16	428.11	35.72	0.06	0.42	0.35	1.79
207-1258A 43-2 39-41	428.15	35.35	0.08	0.57	0.40	1.34
207-1258A 43-2 100-105	428.76	35.31	0.08	0.43	0.31	2.14
207-1258A 43-3 2-3	429.04	35.55	0.07	0.61	0.51	1.69
207-1258A 43-3 68.5-70	429.71	35.07	0.07	0.61	0.54	0.90
207-1258A 43-3 88.5-90	429.91	35.92	0.06	0.39	0.30	2.40

Table S1-3. Miscellaneous geochemical parameters calculated from quantified biomarker concentrations. Calculated SSTs, BIT indices, and brGDGT methylation indices were generated using published methods (Schouten et al., 2002; Hopmans et al., 2004; Kim et al., 2010; Xiao et al., 2016). Horizontal black lines bracket the OAE 2 interval.

Chapter 2: Clarifying the significance of tocol derivatives in the geosphere

Authors: Gregory T. Connock[1*] and Xiao-Lei Liu[1]

Affiliations: [1]School of Geosciences, University of Oklahoma, Norman, Oklahoma 73019, USA.

Abstract: Tocopherols serve a critical role as antioxidants inhibiting lipid peroxidation in photosynthetic organisms yet are seldomly used by organic geochemical studies in deep time. The ubiquity of tocopherols in all photosynthetic lifeforms is often cited as an impediment to any diagnostic paleoenvironmental potential, while the inability to readily analyze these compounds via conventional methods (i.e. GC-MS) further diminishes the capacity to serve as a 'biomarker'. Here, we reexamined the utility of tocopherols and associated derivatives (i.e. tocol derivatives) by applying a novel LC-qTOF-MS method to an exceptionally preserved black shale sequence spanning the mid-Cretaceous Oceanic Anoxic Event 2 (OAE-2). Additional sites defined by contrasting depositional conditions and ages (late Devonian to mid-Pleistocene) were analyzed to determine preservation potential. Tocol derivatives included two tocopherol variants (α, γ), α-tocopherol quinone, 5,7,8-trimethylated methyltrimethyltridecylchroman (α-MTTC), and the first reported detection of methylphytylbenzoquinones (DMPBQ and TMPBQ) in geologic samples. Significantly, α-MTTC, DMPBQ and TMPBQ exhibited no depositional or temporal exclusivity, present in all analyzed samples where TMPBQ was often one of the most predominant compounds. Strong correlations between tocopherols, MPBQs and α-MTTC provided empirical evidence of a common origin. Tocopherol concentrations and ratios, normalizing tocopherols to potential degradation products (α-T/α-TQ, α-T/TMPBQ, γ-T/DMPBQ, α-T/α-MTTC), revealed distinct temporal trends coincident with OAE-2. Both absolute and relative increases in tocopherols defined OAE-2, which afforded two interpretative perspectives dependent on depositional setting. Shoaling euxinic waters during OAE-2 likely forced an upward migration of oxygenic photoautotrophs, increasing reactive oxygen species production and eliciting heightened tocopherol biosynthesis to mitigate oxidative cellular damage. However, this may also have simultaneously enhanced tocopherol preservation given the relatively high lability of tocopherols in the water column. Thus, tocopherols are highly sensitive to vertical fluctuations in pelagic redox, and may be applied to infer the presence of shallow water anoxia in paleoenvironmental studies, but also may reflect a phytoplanktonic stress response in specific settings defined by persistent anoxia (e.g. laminated black shales). Additionally, the strong covariation of tocopherols and α-MTTC, which are typically not observed together due to instrumental and preservation biases, provides strong empirical evidence for a precursor-product relationship and reignites the ongoing enigma surrounding the origin(s) of MTTCs.

2.1 Introduction

Tocopherols (i.e. Vitamin E) are lipophilic nonenzymatic antioxidants primarily biosynthesized and concentrated in the plastid membranes of all photosynthetic lifeforms (Wang and Quinn, 2000; Atkinson et al., 2010; Muñoz and Munné-Bosch, 2019). The localization of tocopherols in chloroplasts is not a coincidence, as they serve critical roles in mitigating oxidative

damage inherent to operation of the photosynthetic apparatus (Lichtenhaler et al., 1981; Soll et al., 1985; Arango and Heise, 1998). Generation of harmful reactive oxygen species (ROS, e.g. lipid peroxyl radicals, singlet oxygen) is inevitable and exacerbated by exposure to abiotic stresses, but ROS may be physically quenched or chemically scavenged by tocopherols, which also inhibit lipid peroxidation, act as photoprotectants, physically stabilize lipid bilayers, and play an under-constrained role in cell signaling (Fahrenholzt et al., 1974; Burton and Ingold, 1981; Kagan et al., 1990; Fryer, 1993; Trebst et al., 2002; Havaux et al., 2005; Krieger-Liszkay and Trebst, 2006; Hincha, 2008; Miret and Munné-Bosch; 2015). These functions are entirely dependent on the molecular structure of tocopherols, comprised of a phytyl tail linked to a chromanol ring of varying methylation corresponding to δ-(monomethyl), β-/γ-/ζ- (dimethyl), and α-tocopherols (trimethyl). Antioxidant potential is granted by the hydroxyl group on the chromanol moiety either through donation of one electron to produce the tocopheryoxyl radical (i.e. physical quenching; Fahrenholzt et al., 1974) or two electrons which results in ring opening and formation of tocopherol quinones (i.e. chemically scavenging; Neely et al,. 1988). This proclivity to act as an antioxidant simultaneously limits the preservation of tocopherols in sediments, compounding fundamental issues as a traditional 'biomarker' given the ubiquity of these compounds in photosynthetic organisms.

Few reports of tocopherols in ancient sediments and rocks exist. Widespread application and discussion of pristane and phytane in rocks and oils (e.g. Brooks et al., 1969; Powell et al., 1973; Didyk et al., 1978) initially stimulated interest in tocopherols, which are potential precursors of pristane (Goossens et al., 1984). One of the first reports of tocopherols as standalone biomarkers suggested some potential as a proxy for phototrophic biomass flux to the sediments (Brassell et al., 1983), although this gained minimal traction (e.g. Dumitrescu and Brassell, 2005) and no

published accounts of tocopherols in geologic samples followed. This was likely a result of the extra step (i.e. derivatization) required for tocopherol analysis on a gas chromatograph-mass spectrometer (GC-MS) and apparent lack of utility in paleoenvironmental studies. Conventional thinking discounted tocopherols as useful proxies given that they are required by all phototrophs which precludes biological source specificity beyond primary producers and, by extension, ties to specific environmental states. However, an improved understanding over the past 20 years of the biophysiochemical role tocopherols play (Muñoz and Munné-Bosch, 2019 and references therein) and an ideal depositional setting minimizing post-senescence degradation granted an opportunity to reexamine tocopherols as a viable resource in paleoenvironmental investigations.

Here, we employed a novel liquid chromatography – quadrupole time-of-flight – mass spectrometry (LC-qTOF-MS) method on exceptionally preserved Cenomanian-Turonian samples from the southern proto-North Atlantic Ocean (ODP Site 1258, Demerara Rise) to reassess the potential of tocopherols and associated derivatives as geochemical proxies. Utilization of LC-qTOF-MS circumvented limitations inherent to GC-MS systems that are unable to directly analyze tocopherols without derivatization, while preservation biases were minimized by the relatively persistent, highly reducing bottom waters spanning Cenomanian-Turonian deposition at the Demerara Rise. Our primary aim focused on leveraging tocopherol lability in the water column and antioxidant function in photosynthetic organisms to reconstruct environmental and microbial ecological changes spanning oceanic anoxic event 2 (OAE-2), a period of widespread marine deoxygenation and climatic change that induced major perturbations to biogeochemical cycling (e.g. C, N). Cooccurrence of tocopherol derivatives (e.g. tocopherol quinone), potential degradation products (e.g. methyltrimethyltridecylchromans, MTTCs), and intact tocopherols enabled the development of new ratios sensitive to oceanographic changes and a critical evaluation

of the origin and paleoenvironmental significance of MTTCs. We also screened additional sites of varying depositional histories and ages to determine the preservation potential of tocopherols and related derivatives in deep time.

2.1.1 Depositional setting and significance for paleoenvironmental study

See section 1.2.1 in Chapter 1 for site description and review of the geologic setting. See Figure S2-1 of this chapter for graphical overview of paleogeography and depositional environment.

2.2 Materials and Methods

For details regarding sample preparation and analysis see section 1.2 in Chapter 1.

2.3 Results

2.3.1 Identification and occurrence

A diverse suite of tocopherols and associated, potential derivatives (herein simply referred to as 'tocol derivatives') were detected in the Demerara Rise samples (Figure 2-1; see Appendix for structures). Both α- and γ-tocopherols (α-T and γ-T), and α-tocopherol quinone (α-TQ) were identified based on accurate masses ($[M+H]^+$, *m/z*: 417.3727, 431.3884, 447.3833), chromatographic behavior, and diagnostic fragmentation patterns of MS^2 consistent with authentic standards (Figure 2-1). Two intermediates in the recycling of α-TQ and γ-TQ back to α-T and γ-T (Kobayashi and DellaPenna, 2008; Mène-Saffrané and DellaPenna, 2010; Eugeni Piller et al., 2014), trimethylphytylbenzoquinone (TMPBQ) and dimethylphytylbenzoquinone (DMPBQ)[1], were tentatively identified and found to predominate the tocol derivative inventory. The structure

[1] Not to be confused with the dimethylphytylbenzoquinol (i.e. $DMPBQH_2$ with ketone groups reduced to hydroxyl groups) as is commonly reported in the literature as a precursor to γ-T in the α-T biosynthetic pathway.

of these two derivatives was determined by comparison of measured and theoretical masses ($[M+H]^+$, *m/z*: 429.3727, 415.3571) combined with the presence of key fragments (e.g. 165Da; Figure 2-1). Initial interpretations of MS^2 assigned α- and γ-tocomonoenol (α-T_1 and γ-T_1) as likely structures, given that cleavage of the oxygen-bearing ring of the chromanol moiety yielded primary fragments of 165Da and 151Da for α-T and γ-T; however, retention times were inconsistent with α-T_1 and γ-T_1 isolates (kindly provided by Dr. Walter Vetter of the University of Hohenheim; Figure S2-2). Acetylation revealed the apparent lack of a 6-chromanol moiety for these two derivatives, whereas both α-T and γ-T were readily acetylated. This eliminated unsaturated tocopherols (i.e. tocomonoenols or marine-derived tocopherol) as possible configurations, leaving methylated phytylbenzoquinones as the likely structures. Both TMPBQ and DMPBQ exhibited multiple isomers (3 and 2, respectively; Figure 2-1). The DMPBQ is presumed to be methylated at C-7 and C-8 (γ) due to the confirmed presence of γ-T, but lack of an authentic standard does not preclude methylation at C-5 and C-8 (β). In addition, the 5,7,8-triMeMTTC (herein referred to as α-MTTC) was recognized in all samples based on accurate mass ($[M+H]^+$, *m/z*: 415.3934), characteristic fragmentation producing a pronounced primary fragment at 149Da (similar cleavage as observed in α-T; Figure 2-1), and consistent retention time with a Woodford Shale extract containing high concentrations of MTTCs as confirmed previously by GC-MS/MS (Connock et al., unpublished results). Other tocopherols and potential derivatives, such as *δ*-tocopherol, *δ*-/γ-/β-/ζ-MTTC, and tocotrienols, were not detected in the Demerara Rise samples.

Additional samples were analyzed to assess the preservation potential of intact tocopherols and derivatives. Coeval sites (OAE-2) from the Cape Verde Basin (DSDP 367), Tarfaya Basin (Shell International/Office National de Recherches et d'Exploitations Pétrolières S75), Newfoundland Basin (IODP U1407), and Western Interior Seaway (Kansas, US, Amoco 1

Rebecca K. Bounds, RKB) were selected to assess the impact of contrasting depositional environments on tocol derivative preservation. Localities including mid-Pleistocene (offshore NW Australia, IODP 1483) and upper Devonian (Oklahoma, US, Wyche-1) strata were chosen to substantiate possible environmental biases identified in the coeval sites and determine the temporal range of both tocopherols and subsequent degradation products. However, a detailed review of stratigraphic trends at each individual site is beyond the scope of this study. The TMPBQ and α-MTTC were ubiquitously observed at all sites, and DMPBQ was not present in the Wyche-1 or site 1483 cores. Dimethylated MTTCs (β-/γ-/ζ-MTTC) were identified in the Wyche-1 and RKB cores. Tocopherols were not as well preserved, with α-T detected at sites 1258, 367, S75, and in the RKB core, while γ-T and α-TQ were exclusive to 1258 and RKB. The most dominant tocol derivative was TMPBQ at all sites, excluding the RKB and Wyche-1 where α-MTTC predominated over TMPBQ. Furthermore, a TLE from a cyanobacterial culture, *Synechococcus* sp. PCC 7002, was analyzed for tocol derivative composition and found to predominantly produce 3 isomers of TMPBQ, with trace amounts of α-T, that displayed identical mass spectra and retention times to the isomers detected in natural samples (Figure 2-1). No tocotrienols, tocopherol quinones, or MTTCs were detected in the cyanobacteria culture TLE.

2.3.2 Stratigraphic trends spanning OAE-2

The tocol derivatives exhibited significant stratigraphic variations at the Demerara Rise. Overall, concentrations of tocopherols, α-TQ, methylated phytylbenzoquinones and α-MTTC displayed similar depth trends. Invariant, relatively low values were observed prior to OAE-2, excluding a single sample at 427.54 mcd where a pronounced increase in TMPBQ and DMPBQ occurred. A rise in all tocol derivatives immediately before the +CIE preceded the predominantly elevated concentrations found to characterize OAE-2 (Figure 2-2), which was clearly defined by

an abrupt reorganization of the tocol derivative pool (Figure 2-3). The fractional abundance of both α-T and γ-T increased markedly at the expense of TMPBQ, still the predominant tocol derivative during OAE-2. A progressive decline in all tocol derivatives marked the latter half of the OAE, while the post-OAE interval was characterized by variable tocol derivative concentrations that were slightly higher than those observed pre-OAE. Akin to the onset of OAE-2, the termination of the event, marked by the cessation of the +CIE, coincided with a rapid shift in tocol derivatives comparable to pre-OAE compositions primarily driven by decreasing α-T and γ-T concentrations (Figures 2-2 & 2-3).

2.3.3 Statistical tests

A series of statistical methods were employed to evaluate the significance of stratigraphic trends and potential for tocol derivatives to delineate the OAE-2 interval. One-tailed unequal variance *t*-tests were used in tandem with principal component analysis (PCA) and hierarchical cluster analysis (HCA) to assess the significance of tocol derivative variations across OAE-2 and ability to delineate contrasting biogeochemical states in the water column. In addition, two-tailed unequal variance *t*-tests assessed the existence of significant differences between structural classes (e.g. tocopherols vs. MTTCs) to determine possible precursor-product relationships or derivation from a similar source.

Initial PCA and HCA results using solely the concentrations of tocol derivatives were relatively ineffective at statistically delineating OAE-2, despite observable variations over the studied interval. To further assess the statistical significance of stratigraphic trends, samples were grouped into three categories (pre-OAE, OAE, and post-OAE) for one-tailed unequal variance *t*-tests. Significant differences (defined as $p < 0.05$) were observed in tocopherols and α-MTTC between pre-OAE and OAE samples, as well as between the pre-OAE and post-OAE interval.

Weakly significant ($0.05 < p < 0.10$) differences existed in tocopherol variations between OAE and post-OAE strata, which were characterized by no significant differences ($0.10 < p$) in α-MTTC concentrations and significant differences in α-TQ values. No statistically significant differences in TMPBQ or DMPBQ were present between pre-OAE and OAE samples, and only a weakly significant difference was observed for these compounds when comparing the OAE and post-OAE intervals. However, removal of a TMPBQ/DMPBQ outlier corresponding to the concentration spike at 427.54 mcd (Figure 2-2) improves the *p*-values dramatically for each respective comparison, producing weakly significant and significant differences for the pre-OAE vs. OAE and OAE vs. post-OAE samples, respectively. All tocol derivatives exhibited significant variations between pre- and post-OAE deposition. While these results do support the challenge of using exclusively tocol derivative concentrations to demarcate OAE-2, caution must be stressed due to the small sample size, presence of outliers, and non-normal distribution of some compounds. Still, tocopherols, α-TQ, methylated phytylbenzoquinones, and α-MTTC did exhibit statistically significant fluctuations that implied underlying potential as paleoenvironmental tools.

Additional PCA and HCA was conducted using ratios of tocol derivatives based on conceptual evidence for sensitivity to biological, ecological, and chemical changes in the water column (Figure 2-4). These included α-T/TMPBQ, γ-T/DMPBQ, α-T/α-TQ, and α-T/α-MTTC. Tocol derivatives were also normalized to well-established biomarker proxies of varying source specificity, including the tetrapyrroles (summed free-base chlorins, porphyrins, and metalloporphyrins), crenarchaeol and isorenieratane. In addition to supplementing tocol derivatives in delineation of OAE-2, inclusion of conventional biomarker proxies granted insight into the paleoenvironmental control(s) on tocol derivative distributions. Inputting these variables into PCA produced a relatively tight cluster of data points exclusive to OAE-2 distinct from pre-

and post-OAE samples, which was substantiated by the clusters comprising the dendrogram generated by HCA of the same variables (Figure 2-4). Thus, significant statistical evidence and effective delineation of OAE from non-OAE strata suggests that tocol derivatives were sensitive to the oceanographic changes coincident with OAE-2 at the Demerara Rise and may hold some utility as 'biomarkers' in paleoenvironmental reconstructions.

2.4. Discussion

2.4.1 Origin of tocol derivatives

As previously stated, tocopherols are produced by all photosynthetic life. While these compounds are relatively more concentrated in vascular land plants (Esteban et al., 2009), tocopherols are predominantly derived from marine primary producers in this study based on the depositional setting (distal shelf, ~1000 mbsl, Figure S2-1; Erbacher et al., 2004) and rapid autoxidation (i.e. degradation) of intact tocopherols if transported to the depocenter via riverine influx (Rontani et al., 2008). Thus, α-T and γ-T were biosynthesized by all phytoplankton (e.g. eukaryotic microalgae and prokaryotic cyanobacteria) inhabiting the surface waters at the Demerara Rise during the Cenomanian-Turonian. There was likely no unique source responsible for the varying methylation of α-T and γ-T given the strong, positive linear relationship between both tocopherol variants (R^2 = 0.91, Figure 2-5). By extension, α-TQ was also derived from a similar source as the tocopherols, as it is an oxidation product of chemical scavenging of singlet oxygen by α-T (Neely et al., 1988). Higher concentrations of α-T generally correlated with higher concentrations of α-TQ, in agreement with the reported formation of α-TQ from α-T (Figure 2-5). This rationale is not compromised by the seemingly poor correlation between α-T and α-TQ over the entire OAE-2 interval, predominantly driven by separation between pre-OAE, OAE, and post-OAE sample groups subject to variable oxidation rates related to contrasting depositional states.

There is no known report documenting the occurrence of the tentatively identified methylated phytylbenzoquinones in rocks or sediments. However, the overwhelming predominance of these compounds over other tocol derivatives at the Demerara Rise, as well as robust preservation to at least the late Devonian, necessitated an attempt to elucidate potential biological sources or formation pathways. A strong relationship emerged between TMPBQ and α-TQ (Figure 2-5), which was not entirely unexpected given both occupy key steps in α-T recycling (Figure S2-3). First, α-T is oxidized, forming an α-tocopheroxyl radical, which is subsequently oxidized yielding α-TQ. A recently characterized NAD(P)H-dependent quinone oxidoreductase reduces α-TQ to α-tocopherol quinol, with TMPBQ produced from α-tocopherol quinol via an unknown plastid-dehydratase. Regeneration of α-T is completed via cyclization of TMPBQ by a tocopherol cyclase (Kobayashi and DellaPenna, 2008; Mène-Saffrané and DellaPenna, 2010; Eugeni Piller et al., 2014). Comparable correlations between both TMPBQ, α-TQ, and α-T (Figure 2-5) support similar formation mechanisms (i.e. tocopherol oxidation and recycling), but the detection of predominantly TMPBQ, with relatively low α-T and no α-TQ, in a cyanobacterial culture TLE (*Synechococcus* sp. PCC 7002) introduced further complexity (Figure 2-1). The low concentrations of α-T and lack of α-TQ in the culture TLE presented two possibilities: 1) *Synechococcus* sp. PCC 7002 primarily produces methylated phytylbenzoquinones via an uncharacterized biosynthetic pathway or 2) *Synechococcus* sp. PCC 7002 does produce tocopherols, but the majority were oxidized to tocopherol quinones that were ubiquitously recycled to methyl phytylbenzoquinones not subject to extensive cyclization, leaving no detectable α-TQ and low regenerated α-T. It is beyond the scope of this study to clearly define the origin of TMPBQ, but the latter scenario is unlikely unless TMPBQ accumulated due to the absence or shortage of tocopherol cyclase. This may explain the distribution of tocol derivatives in the cyanobacterial

TLE. Tocopherol cyclase, in addition to the recycling of α-T, plays a key role in the formation of the oxygen-bearing ring connecting the hydroxylated aromatic moiety to the phytyl group (Soll et al., 1980; Arango and Heise, 1998a). Thus, a lack of detectable α-TQ, low α-T, and high concentrations of TMBPQ in the cyanobacterial culture may reflect tocopherol cyclase deficiency for an unknown reason, leading to low α-T production and an accumulation of TMPBQ over time. However, the predominance of TMPBQ in most geological samples representing a myriad of oceanographic conditions separated by millions of years precludes tocopherol cyclase deficiency as a likely blanket resolution, especially given the higher relative amounts of α-T detected at some localities. This leaves two plausible explanations for the prominence of TMPBQ over other tocol derivatives: 1) TMPBQ, and the related DMPBQ, are biosynthetic products of cyanobacteria and possibly other phytoplankton or 2) TMPBQ and DMPBQ are post-senescence degradation products (e.g. diagenetic) of α-T and α-TQ via an uncharacterized degradation pathway.

If TMPBQ and DMPBQ are biosynthetic products of photosynthetic life, then the high concentrations observed in sediments, rocks, and culture TLEs implies a relatively important function. Like tocopherols, quinones serve a critical role in photosynthesis. While tocopherols primarily act as electron donors to inhibit lipid peroxidation by physically quenching or chemically scavenging singlet oxygen produced during photosynthesis (Qin et al., 2009), quinones may act as a shuttle for electrons and protons in the electron transport chains of photosynthetic and respiratory processes, as well as serve as an antioxidant in reduced form (Nowicka and Kruk, 2010). It is possible TMPBQ was not as efficiently recycled by primary producers nearly 100Ma, either as a stress response to environmental factors not widely observed in today's oceans or compared to the relatively improved α-T regeneration by phylogenetic descendants. This explains the lack of TMPBQ accumulation in most extant life, and the strong association with the progenitor of

chloroplasts (i.e. endosymbiotic cyanobacteria) in this study. Alternatively, TMPBQ may represent an uncharacterized breakdown product of α-T or degradation of α-TQ by loss of the isoprenoid hydroxyl group during diagenesis. However, the introduction of a double bond during diagenesis is highly unlikely. Therefore, we favor the direct biosynthesis of TMPBQ by photosynthetic organisms, serving a comparable role as the structurally similar phylloquinone (i.e. Vitamin K1). For context, phylloquinone is a key cofactor in the electron transfer chain of photosystem I, acts as an electron donor and acceptor to modulate ROS, and plays a role in cell signaling (Lochner et al., 2003). We are unable to rule out TMPBQ formation from α-T or α-TQ post-cell senescence though, and will consider this as a possibility when evaluating the paleoenvironmental significance. It is puzzling why this compound has not been previously reported in sediments and rocks, and more frequently discussed in biological studies, given the high abundance in all analyzed geological samples and the cyanobacterial culture TLE. Further work is required to fully characterize the prevalence and distribution of TMPBQ in microbial life, and we do not claim TMPBQ as an exclusive biomarker for cyanobacteria. Instead, we encourage future study to screen for these compounds to assess formation pathways and refine the temporal window of occurrence.

The origin of DMPBQ is also unknown, and even more challenging to determine given no report of the DMPBQ identified in this study was found in published literature. A peak with the correct mass and similar (but not identical) retention time was present in the cyanobacterial culture TLE, but did not possess the diagnostic fragmentation associated with the DMPBQ in the rock and sediment extracts. However, there was a strong, positive linear relationship between TMPBQ and DMPBQ ($R^2 = 0.82$, Figure 2-5), interpreted to reflect a common origin and/or formation pathway. This is further substantiated by a positive correlation between ratios of precursors and products,

namely γ-T/DMPBQ and α-T/TMPBQ (R^2 = 0.77, Figure 2-6). Lack of γ-TQ precluded further assessment, but correlation between DMPBQ and γ-T, in combination with a strong covariation with TMPBQ (Figure 2-5), granted confidence that DMPBQ is likely associated with γ-T recycling and inherently recorded comparable information as TMPBQ.

The MTTCs are an enigmatic suite of compounds frequently used as indicators for elevated salinity and stratification in paleoenvironmental reconstructions (e.g. Sinninghe Damsté et al., 1993; Bechtel et al., 2007; Tulipani et al., 2015). Initial work discounted tocopherols as likely precursors based on the high energy required to remove the hydroxyl group at C-6 on the chromanol moiety and identification of a monomethyl MTTC methylated at C-6 in a single sample (Sinninghe Damsté et al., 1987). Still, the structural resemblance between MTTCs and tocopherols (see Appendix for structures) merits further investigation, especially given the rare reported cooccurrence of the two compound classes.

There is strong evidence that α-MTTC and tocopherols were controlled by similar processes at the Demerara Rise. The α-MTTC correlates with all tocol derivatives to varying extents (Figure 2-7), with the most robust relationships between α-MTTC and α-T, γ-T, and α-TQ. Two-tailed unequal variance *t*-tests were performed to assess the presence of significant differences, or similarities, between individual tocol derivatives over the entire stratigraphic interval. No significant differences ($p > 0.10$) between α-MTTC and α-T, γ-T, and α-TQ existed, substantiating the empirical relationships previously outlined. Based on these results, either α-MTTC was derived from the diagenetic alteration of α-T, or α-MTTC was associated with the synthesis of tocopherols in the organism. Any direct assessment of these two theories would greatly benefit from compound specific isotopic analysis (CSIA), which is not reported here, to address any potential intracellular associations or precursor-product relationships. However, both

scenarios could result in an overlapping range of carbon isotopic compositions. Only in the event of contrasting $\delta^{13}C$ values would CSIA elucidate an unlikely possibility of distinct sources of α-MTTC and tocopherols at the Demerara Rise. Thus, it is proposed here α-MTTC is either a diagenetic product of α-T or biosynthesized in response to similar stimuli as the tocopherols.

The observed affiliation of α-MTTC with tocopherols in this study provides a fresh perspective to evaluate previous interpretations of MTTC origin and [potentially] fundamentally shift the interpretation of MTTCs in the geologic record. No definitive source has been confirmed, despite the initial identification of MTTCs over three decades ago (Sinninghe Damsté et al., 1987). Nevertheless, continued application of MTTCs as indicators for hypersalinity and/or salinity-induced stratification persists (e.g. Sinninghe Damsté et al., 1993; Schwark et al., 1998; Bechtel et al., 2007; Wang et al., 2011; Tulipani et al., 2015). The MTTCs were originally attributed to non-photosynthetic bacteria (Sinninghe Damsté et al., 1987). This was later revised based on high MTTC concentrations and similar carbon isotopic compositions to known algal lipids (e.g. steroids), suggesting derivation from a photosynthetic organism in the upper water column (Sinninghe Damsté et al., 1993). An alternative MTTC formation pathway was proposed involving the condensation of phytol with alkyl phenols (Li et al., 1995) that was immediately contested (Sinninghe Damsté and de Leeuw, 1995), but still favored by some recent applications of MTTCs (e.g. Tulipani et al., 2015). However, widespread consistency between carbon isotopic compositions of MTTCs and other known potential photosynthetic biomarkers (e.g. phytane, steranes, hopanes; Grice et al., 1998; van Breugel et al., 2007; Zhang et al., 2012; Tulipani et al., 2013; Tulipani et al., 2015) substantiates the apparent link between MTTCs and phytoplankton. The strong correlations between α-MTTC and tocol derivatives at the Demerara Rise provides additional evidence for derivation from primary producers (Figure 2-7), be it via biosynthesis of

α-MTTC or degradation of α-T to produce α-MTTC. Although the covariation of α-MTTC and tocol derivatives could support the formation of α-MTTC by condensation of higher plant phenols and phytol[2] (Li et al., 1995), it is unlikely α-T was terrigenous in origin given the depositional setting and relatively high concentrations of tocol derivatives detected. While the source of α-MTTC is reaffirmed by strong relationships with tocol derivatives of phytoplanktonic origin in this study, the implications of its occurrence in sediments and rocks is fundamentally altered (see section 2.4.4 for further discussion).

2.4.2 Preservation potential of tocol derivatives

Assessing the preservation of tocol derivatives in the geologic record is paramount to determine the viability of individual derivatives as paleoenvironmental proxies. Of all tocol derivatives reported in this study, α-MTTC and TMPBQ exhibited the widest spatiotemporal range of occurrence. This was not entirely surprising given MTTCs have been reported in sediments, rocks, and oils spanning the Pleistocene (this study; Sinninghe Damsté et al., 1987) to the early Cambrian (Dutta et al., 2013). However, the ubiquity and predominance of TMPBQ, and to a lesser extent DMPBQ, at all sites was unexpected, especially since there is no previous report documenting its occurrence in the geologic record, and no study on extant life has revealed methylated phytylbenzoquinones as prominent tocol derivatives. The observed limited preservation of α-T, γ-T, and α-TQ undermines broad application of these specific tocol derivatives, likely due to a combination of biodegradation and a tendency for rapid photo- and autoxidation prior to diagenesis (Yamauchi and Matsushita, 1979; Rontani et al., 2008; Rontani et

[2] Tocopherols and alkylphenols in terrigenous organic matter may be transported to marine environments via riverine input, whereby alkylphenols may subsequently undergo condensation reactions with phytol during early diagenesis (Li et al., 1995). Thus, a correlation between tocol derivatives and MTTCs may not signify a precursor-product relationship, but rather a common depositional, and not necessarily biological, origin. However, this is unlikely considering the depositional context of the Demerara Rise.

al., 2010). Previous study placed the oldest occurrence of α-T ~30Ma prior to the oldest α-T reported in this study (early Aptian OAE 1a, ~121.5Ma; Dumitrescu and Brassell, 2005). The apparent exclusivity of α-T, γ-T, and α-TQ to localities subject to extended periods of deoxygenation (e.g. sites 144 & 367, Kuypers et al., 2002; site S75, Kuhnt et al., 2017; site 1258, Ostrander et al., 2017; Connock et al., in review, Chapter 1; RKB, Chapter 4) reinforces experimental evidence that preservation of these compounds likely relied on pervasive anoxia extending well above the sediment-water interface (SWI). This does not explain the absence of α-T in the late Devonian Wyche-1 core though, suggesting additional factors may influence tocopherol preservation (e.g. meteoric weathering, Wyche-1 core was ~30m below ground). In contrast, the prevalent detection of α-MTTC, TMPBQ, and DMPBQ may reflect the relatively enhanced preservation potential inherent to these three compounds lacking a hydroxyl group. Previous postulation on the origin of α-MTTC, TMPBQ, and DMPBQ as degradation products of the more labile α-T, γ-T, and α-TQ or biosynthetic products of photosynthetic life is consistent with the relatively high concentrations detected at all sites regardless of depositional environment. As a result, α-MTTC, TMPBQ, and DMPBQ may inherently possess greater viability as reconstructive tools in paleoenvironmental investigations. Further study is needed to better constrain the temporal range of TMPBQ, and DMPBQ, which may also aid efforts to understand the corresponding biological and/or environmental significance.

2.4.3 Paleoenvironmental implications of tocol derivatives spanning OAE-2

The Demerara Rise, although highly reducing prior to OAE-2, exhibited relatively dynamic water chemistry and structure that caused a significant marine microbial ecological reorganization during OAE-2 (Connock et al., in review; Chapter 1). Enhanced rates of microbial sulfate reduction (MSR) led to a transition from anoxia to euxinia that frequently extended into the euphotic zone

due to stratification of the water column caused by water mass density contrasts (Kuypers et al., 2002; van Bentum et al., 2009; Jiménez Berrocoso et al., 2010; Martin et al., 2012; Owens et al., 2013; Raven et al., 2019; Connock et al., in review, Chapter 1). Consequently, the distinct changes in tocol derivatives coincident with OAE-2 at the Demerara Rise may be an artifact of evolving redox conditions and/or attendant biological responses to the shoaling euxinic waters.

Tocopherols are very labile compounds, prone to both rapid abiotic degradation (e.g. autoxidation and photooxidation; Grams et al., 1972; Liebler et al., 1990, Rontani et al., 2007; Nassiry et al., 2009) and biodegradation (e.g. aerobic and anaerobic; Rontani et al., 2008; Rontani et al., 2010) within the water column and sediments. Preservation of these compounds in ancient sediments and rocks must reflect either an absence of these degradative processes, which is unlikely, or a more plausible scenario whereby extensive anoxia/euxinia and/or rapid settling rates mitigated tocopherol breakdown. There is no indication of variable sedimentation rates within the study interval at the Demerara Rise, with no major lithologic changes or unconformities reported. Thus, the occurrence of α-T and γ-T in every sample is indicative of relatively persistent anoxia, in agreement with the nearly ubiquitous deposition of laminated black shales throughout the Cenomanian-Turonian interval (Erbacher et al., 2004).

Elevations in α-T and γ-T concentrations, primarily confined to OAE-2, may reflect the enhanced preservation of biomass presumed to accompany photic zone euxinia (PZE) due to the absence of aerobic and inhibition of anaerobic biodegradation by high levels of sulfide (Khan and Trottier, 1978; McCartney and Oleszkiewicz, 1991). This is underscored by similar, albeit relatively slight, increases in other tocol derivatives during OAE-2 (Figure 2-2). Relative enrichments in α-T and γ-T were nearly exclusive to the OAE interval, which was also defined by a ~400% and ~200% increase in the fractional abundance of α-T and γ-T (i.e. relative to all tocol

derivatives) relative to pre-OAE strata (Figure 2-3). Normalization of the tocopherols to both known (α-TQ) and potential (TMPBQ, DMPBQ, α-MTTC) degradation products substantiated interpretations founded on concentration profiles. All tocol derivative ratios (α-T/α-TQ, α-T/TMPBQ, γ-T/DMPBQ, α-T/α-MTTC) clearly delineated OAE-2 as defined by carbon isotope stratigraphy (Figure 2-8; Erbacher et al., 2005). Given that α-TQ is an oxidation product of α-T, α-T/α-TQ values may reflect the relative oxicity of the water column, with higher values indicative of more reducing conditions. Strong correlations between α-T/α-TQ and other tocol derivative ratios (Figure 2-6) evinces redox sensitivity, or some related process, as an underlying control on tocol derivative distributions. This is consistent with the association of α-TQ, TMPBQ, and [presumedly] DMPBQ, in tocopherol recycling (Figure S2-3), as well as the potential derivation of α-MTTC from α-T. Therefore, we propose that the mere presence of tocopherols and specific tocol derivative ratios (α-T/TMPBQ, γ-T/DMPBQ, α-T/α-TQ, α-T/α-MTTC) may be viable redox proxies, sensitive to both the development and expansion of anoxia/euxinia.

An empirical evaluation of tocol derivative ratios with well-constrained biomarkers sensitive to marine redox variations granted further insight into the potential mechanism(s) modulating tocol derivative distribution when preserved in sediments and rocks. A previous assessment of site 1258 on the Demerara Rise revealed the preservation of a diverse biomarker inventory capturing under-constrained pelagic redox dynamicity enveloping OAE-2 (Connock et al., in review, Chapter 1). Of relevance for this discussion are the overly branched glycerol dialkyl glycerol tetraethers (obGDGTs) produced by unknown anaerobic bacteria within or below the chemocline (Liu et al., 2014), diagnostic lipids of sulfate reducing bacteria associated with MSR (dialkyl glycerol ethers, DAGEs; Grossi et al., 2015), and the diaromatic carotenoid isorenieratane, a characteristic fossil pigment of anoxygenic phototrophic sulfur bacteria indicative of PZE

(*Chlorobiaceae*; Liaaen-Jensen et al., 1964; Summons and Powell, 1987). Each biomarker is associated with a distinct residence depth, with DAGEs, obGDGTs, and isorenieratane reflective of redox conditions spanning the benthic to epipelagic zones.

Cross plots between the tocol derivative ratios and the obGDGTs, DAGEs, and isorenieratane revealed empirical relationships of varying strength (Figure 2-9). Weak and loose positive correlations between all ratios and obGDGTs immediately indicated tocol derivative distributions may not solely be governed by marine deoxygenation. Slightly improved positive correlations were observed between the tocol derivative ratios and isorenieratane, but substantial deviation from the fitted linear regression line precluded a confident assessment of this relationship. A strong positive relationship between DAGEs and all tocol derivative ratios substantiated correlations with isorenieratane and revealed a potential connection between enhanced tocopherol production/preservation and marine hydrogen sulfide (H_2S) concentrations. While enhanced preservation of organic matter via sulfurization is established (Werne et al., 2004), the rapid degradation of α-T in the water column (e.g. Nassiry et al., 2009) suggests elevated rates of MSR and H_2S-rich bottom waters likely have little direct influence on α-T breakdown near the surface. Instead, the presence of H_2S in the euphotic zone (i.e. PZE) may inhibit potential degradation processes and facilitate the improved retention of α-T in sediments. This implies tocol derivative ratios respond to not only the development of anoxia, but are possibly more sensitive proxies for the transition to euxinia, especially PZE. The PCA biplot corroborated an association between the tocol derivative ratios and established biomarkers for anoxia (e.g. obGDGTs, brGDGTs), euxinia (e.g. DAGEs), stratification (e.g. extended archaeols, extARs; DeRosa et al., 1983; Bale et al., 2019), and PZE (isorenieratane), which by extension, qualified the ratios as excellent tools in differentiating OAE from non-OAE strata as highlighted in the HCA dendrogram

(Figure 2-4). However, it is important to evaluate an alternative explanation for the observed trends that considers the role tocol derivatives may serve in the physiological stress response related to PZE and the greater oceanographic state during OAE-2.

Previous work using molecular fossil stratigraphy discovered that OAE-2 was defined by a major microbial ecological reorganization induced by pervasive, recurrent PZE. Primary productivity markedly decreased due to fundamental alterations to essential nutrient cycling (e.g. N; Higgins et al., 2012; Naafs et al., 2019) and habitat constriction by the shoaling chemocline, ultimately leading to nutrient shortages in the upper, oxygenated portion of the photic zone (Connock et al., in review, Chapter 1). As a result, oxygenic photosynthetic organisms were likely subjected to higher light intensities, nutrient deficiencies, and other environmental stressors known to trigger elevated tocopherol biosynthesis. Thus, the perceived redox sensitivity of tocopherol preservation at the Demerara Rise may be compounded by additional, coincident modulatory processes acting on tocopherol production during OAE-2.

The development of inhospitable conditions in, minimally, the lower euphotic zone likely forced an upward migration of obligate aerobes, increasing light exposure and intensity. It is likely production of ROS increased due to the presence of excess excitation energy in the thylakoids caused by light stress, necessitating compensatory mechanisms, such as an increase in α-T, to mitigate oxidative damage (Krieger-Liszkay and Trebst, 2006; Gruszka et al., 2008; Qin et al., 2009), improve photoprotection (Fryer, 1993; Havaux et al., 2005), and aid the physical stabilization of thylakoid membranes (Hincha, 2008). Increases in tocol derivative concentrations during OAE-2 (Figure 2-2) may reflect a phytoplanktonic response to photooxidative stress, which may also be elicited from heightened exposure to UV-B radiation (DeLong and Steffen, 1997) inherent to the inferred shallower residence depth. A decrease in primary productivity, inferred

from relatively low tetrapyrrole concentrations throughout OAE-2 at Demerara Rise (Connock et al., in review, Chapter 1), substantiates the presence of enhanced oxidative stress throughout OAE-2. It is possible that high chlorophyll turnover and breakdown produced excess free phytol that may be recycled and used in tocopherol biosynthesis (Ischebeck et al., 2006), leading to the rise in tocol derivative concentrations observed. Although speculative, it is worth reconciling the behavior of α-T/α-TQ with the established roles of both compounds in ROS scavenging (Kobayashi and DellaPenna, 2008; Mène-Saffrané and DellaPenna, 2010; Eugeni Piller et al., 2014). Elevated production of ROS associated with exposure to high light intensities would lead to greater consumption of α-T via chemical scavenging, producing α-TQ, and physical quenching, which destroys the α-T molecule. The precipitous rise and fall in α-T/α-TQ values leading into the early stages of OAE-2 (426.43-425.74 mcd, Figure 2-8) may record the physiological response of phytoplankton to progressive deoxygenation and the advent of established PZE at Demerara Rise. An attempt to adapt to the evolving oceanographic conditions is reflected by the initial rise in α-T/α-TQ values, but a lack of stress tolerance to the sustained environmental changes by the preexisting phytoplanktonic community is illustrated by a rapid decline in α-T/α-TQ values (Figure 2-8). This is consistent with observed behavior of α-T in plants when a stressor is encountered. Initial exposure to stress is marked by increased α-T production, followed by α-T loss as stress-intolerant species fail to remediate oxidative damage to critical cellular components, leading to cell senescence if other protective agents (i.e. carotenoids) are unable to fulfill similar roles as α-T (Munné-Bosch, 2005). Therefore, the subsequent return and maintenance of relatively elevated α-T/α-TQ values observed for the remainder of the OAE suggests an ecological shift to stress-tolerant phytoplankton capable of synthesizing and maintaining sufficient α-T concentrations to guard against increased oxidative damage. Laboratory culture experiments on

phytoplankton (e.g. cyanobacteria, diatoms, green algae, dinoflagellates) demonstrated stress tolerance and α-T contents do vary between strains (Haubner et al., 2014), substantiating interpretation of a phytoplanktonic compositional shift during OAE-2 based on tocol derivatives. While increased photon flux density led to increased α-T biosynthesis in some strains, elevated salinities were also found to lead to higher α-T concentrations in culture experiments (Haubner et al., 2014). As a result, it is important to consider other forms of abiotic stress that could trigger enhanced production of ROS that stimulated α-T biosynthesis, such as elevated salinities (Skłodowska et al., 2009; Haubner et al., 2014; Jin and Daniell, 2014) and limited nitrate concentrations (Mudimu et al., 2017), which were likely present during OAE-2 (Kuypers et al., 2004; Kashiyama et al., 2008; Jiménez Berrocoso et al., 2010; Martin et al., 2012). Previous investigations of OAE-2 also revealed a phototrophic ecological shift favoring cyanobacteria in nutrient N-depleted waters (Kuypers et al., 2004; Kashiyama et al., 2008; Junium et al., 2015; Owens et al., 2016; Connock et al., in review, Chapter 1), although this is not unequivocally confirmed and alternative, valid models exist (e.g. Higgins et al., 2012). If true though, this ecological reorganization may have favored phytoplankton capable of heightened α-T production, explaining trends in tocol derivatives spanning OAE-2.

In summary, it is challenging to disentangle potential controls on tocol derivative distributions. Major climatic and oceanographic changes (e.g. PZE) concurrent with OAE-2 likely imparted significant environmental stress onto primary producers, selecting organisms capable of prolific α-T synthesis to cope with elevated concentrations of ROS. It is also probable that the same changes (i.e. PZE) facilitated the enhanced preservation of tocol derivatives by minimizing potential degradative processes. Both the elevated tocol derivative concentrations, and pronounced increases in α-T and γ-T relative to other tocol derivatives, may be explained by both scenarios

(Figure 2-10). However, the preservation of tocol derivatives depends on redox state and for most studies the presence of extensive anoxia and/or euxinia will be the primary paleoenvironmental information gleaned from their occurrence. Persistently reducing intervals, like the Cenomanian-Turonian at Demerara Rise, may exhibit adequate biomarker preservation to extract vertical redox fluctuations in the water column and/or a potential phytoplanktonic stress response from the tocol derivative signal as proposed here, but only in conjunction with other biomarkers and additional geochemical context. Thus, the occurrence of tocopherols and tocopherol quinones in the geosphere is diagnostic for highly reducing conditions, likely extending well above the SWI. Yet, tocopherols may reflect the phytoplanktonic stress response to increased ROS in intervals defined by sustained anoxia (e.g. laminated black shales; Figure 2-10). It is clear that tocopherols do not simply track the photosynthetic biomass flux to the sediments as presumed by initial studies, especially given the lack of any correlation with fossil chlorophylls (i.e. free base chlorins/porphyrins, metalloporphyrins) in this study (Figure 2-4). Further delineation of formation pathways for potential tocopherol derivatives (TMPBQ, DMPBQ, α-MTTC) may permit inference of the phytoplanktonic stress response in older deposits and different depositional settings.

2.4.4 Reexamination of MTTCs in the geologic record

Covariation between α-MTTC and other tocol derivatives (Figure 2-7) in this study suggests MTTCs are either diagenetic products of tocopherols or biosynthesized in response to similar stimuli promoting tocopherol synthesis. This finding necessitates a critical reevaluation of MTTCs occurrence in sediments and rocks, especially given this is one of a few reported cooccurrences of MTTCs and tocopherols in the geologic record (e.g. Barakat and Rullkötter, 1997). Conventional paleoenvironmental interpretations founded on MTTCs will be briefly

reviewed, followed by a discussion on how these may be reassessed and aligned with the updated framework on MTTCs origin presented here.

Initial work noted the association of specific MTTCs with hypersaline facies or biomarkers previously linked to hypersaline environments, resulting in the oft-employed MTTC ratio (α-MTTC/total MTTCs; Sinninghe Damsté et al., 1987; Sinninghe Damsté et al., 1993). Lower values are conventionally interpreted to reflect higher paleosalinity, as α-MTTC is a common constituent of sediments deposited under 'normal' salinities. However, consistent with the variable application of MTTCs and the MTTC ratio in paleoenvironmental investigations, later work attributed relative increases in α-MTTC to rising paleosalinities as well (Schwark and Püttmann, 1990; Bechtel and Püttmann, 1997). Despite early caution on ubiquitous application of MTTCs and the MTTC ratio as a reliable paleosalinity proxy (Barakat and Rullkötter, 1997), these compounds have gained increasing popularity in paleoenvironmental studies. Additional ratios of MTTCs (Wang et al., 2011), cross plots with other biomarker parameters (Schwark et al., 1998; Bechtel et al., 2007; Tulipani et al., 2015), and ternary diagrams (Jiang et al., 2019) have been developed in a wide range of depositional settings, but all lack a clear conceptual basis underpinning MTTC distributions and are weakly linked to paleosalinity.

There is no documented physiological response to elevated salinity that would favor reduced methylation on the chroman ring; MTTCs and the MTTC ratio are purely qualitative, empirically based proxies somewhat correlative to lithologies or geochemical proxies associated with heightened salinities. Here, α-MTTC exhibited relatively indistinct depth trends compared to α-T, α-TQ, and TMPBQ (Figure 2-2), interpreted to represent a common origin. Regardless of how α-MTTC is produced (biologically or diagenetically), a clear relationship exists between α-MTTC and α-T, as well as other tocol derivatives (Figure 2-7). By extension α-MTTC (and

MTTCs in general) may record comparable paleoenvironmental information as α-T as previously discussed. The apparent link between MTTCs and elevated salinities may be founded on the coincident development of photic zone anoxia/euxinia aided by the formation of a pycnocline. Introduction of attendant, abiotic stressors may prompt accelerated antioxidant biosynthesis leading to elevation of endogenous MTTCs (if biological) and tocopherols, which may ultimately degrade to MTTCs and yield high MTTC concentrations in sediments. Alternatively, these same conditions will minimize tocopherol degradation in the water column, leading to elevated MTTC concentrations in the sediments if formed diagenetically. It is an unlikely coincidence that reports of MTTCs also document the presence of PZE, irrespective of depositional environment or time interval (e.g. Schwark and Püttmann, 1990; Bechtel and Püttmann, 1997; Schwark et al., 1998; Bechtel et al., 2007; van Breugel et al., 2007; Tulipani et al., 2015; Jiang et al., 2018). All sites screened for tocol derivatives in this study also possessed detectable C_{40} aromatic carotenoids, excluding site 1483 which did possess α-MTTC, corroborating published results of α-MTTC cooccurrence with PZE. Instead of a proxy for paleosalinity, MTTCs may be better indicators for phytoplankton community health and response to environmental stressors, such as hypersalinity, over time. Elevated salinities may induce increased tocopherol biosynthesis (Skłodowska et al., 2009; Haubner et al., 2014; Jin and Daniell, 2014), which will potentially lead to relatively high MTTC concentrations, although it is difficult to reconcile the MTTC ratio with salinity variations.

Few studies examine the effectiveness of individual tocopherol variants (α, γ, δ) in preventing oxidative damage, and those that do are hardly representative of marine phytoplankton. However, some evidence suggests both δ-T and γ-T exhibit greater antioxidant potential than α-T in rapeseed oil, tobacco plants, and as lard preservatives (Wagner et al., 2004; Voll and Abbasi, 2007; King et al., 2011), which may explain the low MTTC ratios (if derived from tocopherols)

tied to hypersaline settings. Even in the absence of hypersalinity, sufficient oxidative stress may be present to produce low MTTC ratios, though this does contradict the consensus α-T is the most effective antioxidant among tocopherol variants (Hussain et al., 2013). Inclusion of tocol derivative methylation ratios (α-T/γ-T and TMPBQ/DMPBQ) in the PCA revealed slight covariation between α-T/γ-T and previously discussed tocol derivative ratios, in contrast (i.e. inverse) to the tentative relationship between MTTCs and paleosalinities. In other words, if lower MTTC ratios (α-MTTC/total MTTCs) are tied to higher paleosalinities and/or elevated oxidative stress, and MTTCs are [potential] tocopherol derivatives, then other methylation ratios of potential precursors and associated derivatives (e.g. α-T/γ-T and TMPBQ/DMPBQ) should behave similarly to the MTTC ratio, which was not observed. Interestingly, TMPBQ/DMPBQ values varied independently from all other biomarker proxies and did drive separation between the pre-OAE and post-OAE 95% confidence ellipses in the biplot, but had little effect in OAE sample delineation (Figure 2-4). While no significant or systematic stratigraphic changes in the ratios of α-T/γ-T or TMPBQ/DMPBQ were observed over the study interval (Figure S2-4), this does not preclude the utility of tocol derivative isoforms to elucidate paleoenvironmental trends in other settings. Thus, the occurrence and distribution of MTTCs is more likely sensitive to the presence of environmental conditions that induce a phytoplanktonic stress response, which include but are not limited to hypersalinity. This finding does not impede the continued application of MTTCs in paleoenvironmental study, but rather refines the current understanding and may facilitate the application of MTTCs in a broader sense while improving integration with other biomarker and geochemical proxies.

Regardless of the origin(s) of MTTCs, a clear association between MTTCs and tocopherols exists and aligns with previous reports of MTTCs in deep time. Derivation from tocopherols

explains the wide temporal occurrence of MTTCs given the critical role tocopherols serve in all photosynthetic organisms, while the association between MTTCs and stratified, hypersaline water columns may be a byproduct of improved tocopherol preservation in those settings. Further work is required to establish potential tocopherol degradation routes terminating in MTTCs formation, and additional screening of extant life is critical to support a biological origin of these compounds. Continued application of MTTCs in paleoenvironmental studies must consider alternative interpretations and leverage a multi-proxy or at the least, multi-biomarker, approach to assess the significance of MTTCs stratigraphic occurrence and distribution.

2.4.5 Implications

Pervasive, enhanced organic carbon burial was a hallmark feature of OAE-2 that produced distinct global imprint in the organic and inorganic carbon isotopic record referred to as the +CIE (Scholle and Arthur, 1980; Owens et al., 2018). Recent study suggested organic carbon burial drivers (productivity, preservation, and sedimentation rate, where relevant) operated along a continuum before, during, and after OAE-2, exhibiting a temporal dependence on the local-regional oceanographic state. At the Demerara Rise, elevated primary productivity prior to OAE-2 primarily drove organic carbon sequestration, while during the OAE evolving water column conditions adversely affected primary production yet simultaneously enhanced biomass preservation (Connock et al., in review, Chapter 1). This aligned well with the relatively invariant carbonate-corrected TOC values spanning the studied interval (Owens et al,. 2016). However, the observed enrichment in tocopherols and other tocol derivatives exclusive to OAE-2 may elucidate additional mechanisms facilitating the enhanced preservation of organic carbon.

Although a causality dilemma, the following proposed scenario is grounded in conceptual evidence and supported by established interpretations of OAE-2. Today, tocopherols are used as

natural food preservatives given the innate antioxidant potential these molecules possess (Seppanen et al., 2010), and may have acted in a similar capacity by inhibiting oxidative degradation of precipitating organic matter during OAE-2. Elevated tocopherol concentrations likely enhanced organic carbon preservation accordingly, but tocopherol production could have been triggered by vertical advection of sulfidic waters (i.e. PZE), which will also reduce avenues for organic carbon degradation (Figure 2-10). Regardless of the sequence of events, there is no way to discount the role tocopherols likely served in augmenting depositional systems primed for rampant organic carbon burial during OAE-2, demonstrated by the strong positive correlation between tocopherols (α-T, γ-T) normalized to associated degradation products (α-TQ, TMPBQ, α-MTTC, and DMPBQ) and organic carbon isotopic compositions (Figure 2-11). Therefore, it is probable that widespread marine deoxygenation and the regional development of PZE, paired with other environmental changes, created ideal conditions for organic carbon burial, simultaneously increasing tocopherol biosynthesis that only amplified organic carbon retention during OAE-2 and perpetuated the +CIE.

2.5 Conclusions

The paleoenvironmental potential of tocopherols and associated derivatives remains untapped, with this study elucidating numerous applications of these overlooked compounds detected in multiple environments spanning ~400 My. Two explanations for tocol derivative distributions spanning a major OAE were proposed. The presence of tocopherols in geologic samples is a strong indication that highly reducing conditions were present at deposition, and likely extended well above the SWI. In certain scenarios dominated by pervasive and sustained anoxia (i.e. Demerara Rise) stratigraphic variations in absolute and relative tocopherol abundances may capture temporal variations in primary producer health and exposure to external stressors. Intact

tocopherols hold the greatest promise as indicators for shallow water anoxia in the immediate future due to an unequivocal source and established formation and degradation pathways. However, improved characterization of potential degradation products, such as MPBQs and MTTCs, will empower application of tocopherols in deep time reconstructions across a variety of depositional settings. Additional screening of extant life may confirm TMPBQ as a biomarker exclusive to cyanobacteria or a ubiquitous product in photosynthetic organisms, which may support the currently uncharacterized diagenetic origin from tocopherol precursors. Continued application of the increasingly popular MTTCs is urged to consider the potential derivation from tocopherols based on strong empirical evidence presented here, which may alter the paleoenvironmental significance extracted from these enigmatic compounds. Contrary to the conclusions by prior studies, the findings presented here indicate that tocopherols hold great promise in future paleoenvironmental investigations, especially if more stable derivatives can be elucidated.

2.6 References

1. Arango, Y., & Heise, K. P. (1998). Localization of alpha-tocopherol synthesis in chromoplast envelope membranes of *Capsicum annuum* L. fruits. Journal of Experimental Botany, 49, 1259-1262.
2. Atkinson, J. Harroun, T., Wassall, S. R., Stillwell, W., & Katsaras, J. (2010). The location and behavior of α-tocopherol in membranes. Molecular Nutrition and Food Research, 54, 641-651.
3. Bale, N. J., Sorokin, D. Y., Hopmans, E. C., Koenen, M., Rijpstra, W. I. C., Villanueva, L., Wienk, H., & Sinninghe Damsté, J. S. (2019). New insight into the polar lipid composition of extremely halo(alkali)philic Euryarchaea from hypersaline lakes. Frontiers in Microbiology, 10, 1-24.
4. Barakat, A. O., & Rullkötter, J. (1997). A comparative study of molecular paleosalinity indicators: chromans, tocopherols and C_{20} isoprenoid thiophenes in Miocene lake sediments (Nördlinger Ries, Southern Germany). Aquatic Geochemistry, 3, 169-190.
5. Bechtel, A., & Püttmann, W. (1997). Palaeoceanography of the early Zechstein Sea during Kupferschiefer deposition in the Lower Rhine Basin (Germany): A reappraisal from stable isotope and organic geochemical investigations. Palaeogeography, Palaeoclimatology, Palaeoecology, 136, 331-358.

6. Bechtel, A., Gawlick, H.-J., Gratzer, R., Tomaselli, M., & Püttmann, W. (2007). Molecular indicators of palaeosalinity and depositional environment of small scale basins within carbonate platforms: The Late Triassic Hauptdolomite Wiestalstausee section near Hallein (Northern Calcareous Alps, Austria). Organic Geochemistry, 38, 92-111.
7. van Bentum, E. C., Hetzel, A., Brumsack, H.-J., Forster, A., Reichart, G.-J., & Sinninghe Damsté, J. S. (2009). Reconstruction of water column anoxia in the equatorial Atlantic during the Cenomanian-Turonian oceanic anoxic event using biomarker and trace metal proxies. Palaeogeography, Palaeoclimatology, Palaeoecology, 280, 489-498.
8. Brassell, S. C., Eglinton, G., & Maxwell, J. R. (1983). The geochemistry of terpenoids and steroids. Biochemical Society Transactions, 11, 575-586.
9. van Breugel, Y., Schouten, S., Tsikos, H., Erba, E., Price, G. D., & Sinninghe Damsté, J. S. (2007). Synchronous negative carbon isotope shifts in marine and terrestrial biomarkers at the onset of the early Aptian oceanic anoxic event 1a: Evidence for the release of ^{13}C-depleted carbon into the atmosphere. Paleoceanography, 22, PA1210.
10. Brooks, J. D., Gould, K., & Smith, J. W. (1969). Isoprenoid hydrocarbons in coal and petroleum. Nature, 222, 257-259.
11. Burton, G. W., & Ingold, K. U. (1981). Autoxidation of biological molecules. 1. Antioxidant activity of vitamin E and related chain-breaking phenolic antioxidants in vitro. Journal of the American Chemical Society, 103, 6472-6477.
12. Connock, G. T., Owens, J. D., & Liu, X.-L. (in review). Biotic induction and microbial ecological dynamics of Oceanic Anoxic Event 2 (OAE-2). Communications Earth & Environment.
13. DeLong, J. M., & Steffen, K. L. (1997) Photosynthetic function, lipid peroxidation, and α-tocopherol content in spinach leaves during exposure to UV-B radiation. Canadian Journal of Plant Science, 77, 453-459.
14. De Rosa, M., Gambacorta, A., Nicolaus, B., Ross, H.N.M., Grant, W.D., & Bu'Lock, J.D. (1982). An asymmetric archaebacterial diether lipid from alkaliphilic halophiles. Microbiology, 128, 343-348.
15. Didyk, B. M., Simoneit, B. R. T., Brassell, S. C., & Eglinton, G. (1978). Organic geochemical indicators of palaeoenvironmental conditions of sedimentation. Nature, 272, 216-222.
16. Dumitrescu, M., & Brassell, S. C. (2005). Biogeochemical assessment of sources of organic matter and paleoproductivity during the early Aptian Oceanic Anoxic Event at Shatsky Rise, ODP Leg 198. Organic Geochemistry, 36, 1002-1022.
17. Dutta, S., Hartkopf-Fröder, C., Witte, K., Brocke, R., & Mann, U. (2013). Molecular characterization of fossil palynomorphs by transmission micro-FTIR spectroscopy: Implications for hydrocarbon source evaluation. International Journal of Coal Geology, 115, 13-23.
18. Erbacher, J., Mosher, D. C., & Malone, M. J. (2004). Shipboard Scientific Party, Chapter 5, Site 1258. Proceedings of the Ocean Drilling Program, Initial Reports, 207, 1-117.
19. Erbacher, J., Friedrich, O., Wilson, P. A., Birch, H., & Mutterlose, J. (2005). Stable organic carbon isotope stratigraphy across Oceanic Anoxic Event 2 of Demerara Rise, western tropical Atlantic. Geochemistry, Geophysics, Geosystems, 6, Q06010.
20. Esteban, R., Olano, J. M., Castresana, J., Fernández-Marín, B., Hernández, A., Becerril, J. M., García-Plazaola, J. I. (2009). Distribution and evolutionary trends of photoprotective

isoprenoids (xanthophylls and tocopherols) within the plant kingdom. Physiologia Plantarum, 135, 379-389.
21. Eugeni Piller, L., Glauser, G., Kessler, F., & Besagni, C. (2014). Role of plastoglobules in metabolite repair in the tocopherol redox cycle. Frontiers in Plant Science, 5, 1-10.
22. Fahrenholzt, S. R., Doleiden, F. H., Trozzolo, A. M., & Lamola, A. A. (1974). On the quenching of singlet oxygen by alpha-tocopherol. Photochemistry and Photobiology, 20, 505-509.
23. Forster, A., Sturt, H., & Meyers, P. A. (2004). Chapter 10, Molecular biogeochemistry of Cretaceous black shales from the Demerara Rise: Preliminary shipboard results from Sites 1257 and 1258, Leg 207. Proceedings of the Ocean Drilling Program, Initial Reports, 207, 1-22.
24. Fryer, M. J. (1993). Evidence for the photoprotective effects of Vitamin E. Photochemistry and Photobiology, 58, 304-312.
25. Goossens, H., de Leeux, J. W., Schenck, P. A., & Brassell, S. C. (1984). Tocopherols as likely precursors of pristane in ancient sediments and crude oils. Letters to Nature, 312, 440-442.
26. Grams, G. W., Eskins, K., & Inglett, G. E. (1972). Dye-sensitized photooxidation of α-tocopherol. Journal of the American Chemical Society, 94, 866-868.
27. Grice, K., Schouten, S., Peters, K. E., & Sinninghe Damsté, J. S. (1998). Molecular isotopic characterization of hydrocarbon biomarkers in Palaeocene-Eocene evaporitic, lacustrine source rocks from the Jianghan Basin, China. Organic Geochemistry, 29, 1745-1764.
28. Grossi, V., Mollex, D., Vinçon-Laugier, Hakil, F., Pacton, M., & Cravo-Laureau, C. (2015). Mono-and dialkyl glycerol ether lipids in anaerobic bacteria: Biosynthetic insights from the mesophilic sulfate reducer *Desulfatibacillum alkenivorans* PF2803. Applied Environmental Microbiology, 81, 3157-3168.
29. Gruszka, J., Pawlak, A., & Kruk, J. (2008). Tocochromanols, plastoquinol, and other biological prenyllipids as singlet oxygen quenchers – determination of singlet oxygen quenching rate constants and oxidation products. Free Radical Biology and Medicine, 45, 920-928.
30. Häubner, N., Sylvander, P., Vuori, K., & Snoeijs, P. (2014). Abiotic stress modifies the synthesis of alpha-tocopherol and beta-carotene in phytoplankton species. Journal of Phycology, 50, 753-759.
31. Havaux, M., Eymery, F., Porfirova, S., Rey, P., & Dörmann, P. (2005). Vitamin E Protects against Photoinhibition and Photooxidative Stress in *Arabidopsis thaliana*. The Plant Cell, 17, 3451-3469.
32. Higgins, M. B., Robinson, R. S., Hussson, J. M., Carter, S. J., & Pearson, A. Dominant eukaryotic export production during ocean anoxic events reflects the importance of recycled NH_4^+. Proceedings of the National Academy of Sciences, 109, 2269-2274.
33. Hincha, D. K. (2008). Effects of α-tocopherol (vitamin E) on the stability and lipid dynamics of model membranes mimicking the lipid composition of plant chloroplast membranes. FEBS Letters, 582, 3687-3692.
34. Hussain, N., Irshad, F., Jabeen, Z., Shamsi, I. H., Li, Z., & Jiang, L. (2013). Biosynthesis, structural, and functional attributes of tocopherols in plants: past, present, and future perspectives. Journal of Agricultural Food Chemistry, 61, 6137-6149.

35. Ischebeck, T., Zbierzak, A. M., Kanwischer, M., & Dörmann, P. (2006). A salvage pathway for phytol metabolism in *Arabidopsis*. Journal of Biological Chemistry, 281, 2470-2477.
36. Jiménez Berrocoso, A., MacLeod, K. G., Martin, E. E., Bourbon, E., Londoño, C. I., & Basak, C. (2010). Nutrient trap for Late Cretaceous organic-rich black shales in the tropical North Atlantic. Geology, 38, 1111-1114.
37. Jiang, K., Lin, C., Zhang, X., Cai, C., Xiao, F., He, W., & Peng, L. (2018). Variations in abundance and distribution of methyltrimethyltridecylchromans (MTTCs) in sediments from saline lacustrine settings in Cenozoic lacustrine basins, China. Organic Geochemistry, 121, 58-67.
38. Jiang, K., Lin, C., Cai, C., Zhang, Z., Huang, S., & Fan, Z. (2019). Current status and challenges of methyltrimethyltridecylchromans research in source rocks and crude oils. American Chemical Society Omega, 4, 9835-9842.
39. Jin, S., & Daniell, H. (2014). Expression of γ-tocopherol methyltransferase in chloroplasts results in massive proliferation of the inner envelope membrane and decreases susceptibility to salt and metal-induced oxidative stresses by reducing reactive oxygen species. Plant Biotechnology Journal, 12, 1274-1285.
40. Junium, C. K., Keely, B. J., Freeman, K. H., & Arthur, M. A. (2011). Chlorins in the mid-Cretaceous black shales of the Demerara Rise: The oldest known occurrence. Organic Geochemistry, 42, 856-859.
41. Junium, C. K., Freeman, K. H., & Arthur, M. A. (2015). Controls on the stratigraphic distribution and nitrogen isotopic composition of zinc, vanadyl, and free base porphyrins through Oceanic Anoxic Event 2 at Demerara Rise. Organic Geochemistry, 80, 60-71.
42. Kagan, V. E., Serbinova, E. A., Bakalova, R. A., Stoytchev, Ts. S., Erin, A. N., Prilpko, L. L., & Evstigneeva, R. P. (1990). Mechanisms of stabilization of biomembranes by alpha-tocopherol. Biochemical Pharmacology, 40, 2403-2413.
43. Kashiyama, Y., Ogawa, N. O., Kuroda, J., Shiro, M., Nomoto, S., Tada, R., Kitazato, H., & Ohkouchi, N. (2008). Diazotrophic cyanobacteria as the major photoautotrophs during mid-Cretaceous oceanic anoxic events: Nitrogen and carbon isotope evidence from sedimentary porphyrin. Organic Geochemistry, 39, 532-549.
44. Khan, A. W., & Trottier, T. M. (1978). Effect of sulfur-containing compounds on anaerobic degradation of cellulose to methane by mixed cultures obtained from sewage sludge. Applied and Environmental Microbiology, 35, 1027-1034.
45. King, R. E., Min, D. B., & Min, S. C. (2011). Study of α-T, γ-, and δ-tocopherols in the oxidative stability of lard. Food Science and Biotechnology, 20, 817-822.
46. Kobayashi, N., & DellaPenna, D. (2008). Tocopherol metabolism, oxidation and recycling under high light stress in Arabidopsis. The Plant Journal, 55, 607-618.
47. Krieger-Liszkay, A., & Trebst, A. (2006). Tocopherol is the scavenger of singlet oxygen produced by the triplet states of chlorophyll in the PSII reaction centre. Journal of Experimental Botany, 57, 1677-1684.
48. Kuhnt, W., Holbourn, A. E., Beil, S., Aquit, M., Krawczyk, T., Flögel, S., Chellai, EH., & Jabour, H. (2017). Unraveling the onset of Cretaceous Oceanic Anoxic Event 2 in an extended sediment archive from the Tarfaya-Laayoune Basin, Morocco. Paleoceanography, 32, 923-946.

49. Kuypers, M. M. M., Pancost, R. D., Nijenhuis, I. A., & Sinninghe Damsté, J. S. (2002). Enhanced productivity led to increased organic carbon burial in the euxinic North Atlantic basin during the late Cenomanian oceanic anoxic event. Paleoceanography, 17, PA000569.
50. Kuypers, M. M. M., van Breugel, Y., Schouten, S., Erba, E., and Sinninghe Damsté, J. S. (2004). N_2-fixing cyanobacteria supplied nutrient N for Cretaceous oceanic anoxic events. Geology, 32, 853-856.
51. Li, M., Larter, S. R., Taylor, P., Jones, D. M., Bowler B., & Bjoroy, M. (1995) Biomarkers or not biomarkers? A new hypothesis on the origin of pristane involving derivation from methyltrimethyltridecylchromans formed during diagenesis from chlorophyll and alkylphenols. Organic Geochemistry, 23, 159-167.
52. Liaaen-Jensen, S., Hegge, E., & Jackman, L. M. (1964). Bacterial carotenoids XVIII, The carotenoids of photosynthetic bacteria, Acta Chemica Scandinavica, 18, 1703-1718.
53. Lichtenhaler, H. K., Prenzel, U., Douce, R., & Joyard, J. (1981). Localization of prenylquinones in the envelope of spinach chloroplasts. Biochimica et Biophysica Acta, 641, 99-105.
54. Liebler, D. C., Baker, P. F., & Kaysen, K. L. (1990). Oxidation of vitamin E: evidence for competing autoxidation and peroxyl radical trapping reactions of the tocopheryl radical. Journal of the American Chemical Society, 112, 6995-7000.
55. Liu, X-L., Zhu, C., Wakeham, S. G., & Hinrichs, K-U. (2014). In situ production of branched glycerol dialkyl glycerol tetraethers in anoxic water columns. Marine Chemistry, 166, 1-8.
56. Lochner, K., Döring, Böttger, M. (2003). Phylloquinone, what can we learn from plants? Biofactors, 18, 73-78.
57. Martin, E. E., MacLeod, K. G., Jiménez Berrocoso, A., & Bourbon, E. (2012). Water mass circulation on Demerara Rise during the Late Cretaceous based on Nd isotopes. Earth and Planetary Science Letters, 327-328, 111-120.
58. McCartney, D. M., & Oleszkiewicz, J. A. (1991). Sulfide inhibition of anaerobic degradation of lactate and acetate. Water Research, 25, 203-209.
59. Mène-Saffrané, L., & DellaPenna, D. (2010). Biosynthesis, regulation and functions of tocochromanols in plants. Plant Physiology and Biochemistry, 48, 301-309.
60. Meyers, P. A., Bernasconi, S. M., & Forster, A. (2006). Origins and accumulation of organic matter in expanded Albian to Santonian black shale sequences on the Demerara Rise, South America margin. Organic Geochemistry, 37, 1816-1830.
61. Miret, J. A., & Munné-Bosch, S. (2015). Redox signaling and stress tolerance in plants: a focus on vitamin E. Annals of the New York Academy of Sciences: Cellular and Environmental Stressors in Biology and Medicine, 1340, 29-38.
62. Mudimu, O., Koopmann, I. K., Rybalka, N., Friedl, T., Schulz, R., & Bilger, W. (2017). Screening of microalgae and cyanobacteria strains for α-tocopherol content at different growth phases and the influence of nitrate reduction on α-tocopherol production. Journal of Applied Phycology, 29, 2867-2875.
63. Munné-Bosch, S. (2005). The role of α-tocopherol in plant stress tolerance. Journal of Plant Physiology, 162, 743-748.
64. Muñoz, P., & Munné-Bosch, S. (2019). Vitamin E in Plants: Biosynthesis, Transport, and Function. Trends in Plant Science, 24, 1040-1051.
65. Naafs, B. D. A., Monteiro, F. M., Pearson, A., Higgins, M. B., Pancost, R. D., & Ridgwell, A. (2019). Fundamentally different global marine nitrogen cycling in response to severe

ocean deoxygenation. Proceedings of the National Academy of Sciences, 116, 24979-24984.
66. Nassiry, M., Aubert, C., Mouzdahir, A., & Rontani, J.-F. (2009). Generation of isoprenoid chromans, notably prist-1-ene, via photo- and autoxidative degradation of vitamin E. Organic Geochemistry, 40, 38-50.
67. Neely, W. C., Martin, J. M., & Barker, S. A. (1988). Products and relative reaction rates of the oxidation of tocopherols with singlet molecular oxygen. Photochemistry and Photobiology, 48, 423-428.
68. Nowicka, B., & Kruk, J. (2010). Occurrence, biosynthesis and function of isoprenoid quinones. Biochimica, et Biophysica Acta, 1797, 1587-1605.
69. Ostrander, C. M., Owens, J. D., & Nielsen, S. G. (2017). Constraining the rate of oceanic deoxygenation leading up to a Cretaceous oceanic Anoxic Event (OAE-2: ~94Ma). Science Advances, 3:e1701020.
70. Owens, J. D., Gill, B. C., Jenkyns, H. C., Bates, S. M., Severmann, S., Kuypers, M. M. M., Woodfine, R. G., & Lyons, T. W. (2013). Sulfur isotopes track the global extent and dynamics of euxinia during Cretaceous Oceanic Anoxic Event 2. Proceedings of the National Academy of Sciences, 110, 18407-18412.
71. Owens, J. D., Reinhard, C. T., Rohrssen, M., Love, G. D., & Lyons, T. W. (2016). Empirical links between trace metal cycling and marine microbial ecology during a large perturbation to Earth's carbon cycle. Earth and Planetary Science Letters, 449, 407-417.
72. Owens, J. D., Lyons, T. W., & Lowery, C. M. (2018). Quantifying the missing sink for global organic carbon burial during a Cretaceous oceanic anoxic event. Earth and Planetary Science Letters, 499, 83-94.
73. Powell, T. G., & McKirdy, D. M. (1973). Relationship between ratio of pristane to phytane, crude oil composition and geological environment in Australia. Nature Physical Science, 243, 37-39.
74. Qin, S. S., Yu, Z-W., Yu, Y-X. (2009). Structural and kinetic properties of α-tocopherol in phospholipid bilayers, a molecular dynamics simulation study. Journal of Physical Chemistry B, 113, 16537-16546.
75. Raven, M. R., Fike, D. A., Bradley, A. S., Gomes, M. L., Owens, J. D., & Webb. S. A. (2019). Paired organic matter and pyrite $\delta^{34}S$ records reveal mechanisms of carbon, sulfur, and iron cycle disruption during Oceanic Anoxic Event 2. Earth and Planetary Science Letters, 512, 27-38.
76. Rontani, J-F., Nassiry, M., & Mouzdahir, A. (2007). Free radical oxidation (autoxidation) of α-tocopherol (vitamin E): a potential source of 4,8,12-16-tetramethylheptadecan-4-olide in the environment. Organic Geochemistry, 38, 37-47.
77. Rontani, J-F., Nassiry, M., Guasco, S., Mouzdahir, A., & Bonin, P. (2008). Aerobic metabolism of vitamin E by marine bacteria: Interaction with free radical oxidation (autoxidation) processes. Organic Geochemistry, 39, 676-688.
78. Rontani, J-F., Nassiry, M., Michotey, V., Guasco, S., Bonin, P. (2010). Formation of pristane from α-tocopherol under simulated anoxic sedimentary conditions: A combination of biotic and abiotic degradative processes. Geochimica et Cosmochimica Acta, 74, 252-263.
79. Scholle, P. A., & Arthur, M. A. (1980). Carbon isotope fluctuations in Cretaceous pelagic limestones: potential stratigraphic and petroleum exploration tool. American Association of Petroleum Geologists Bulletin, 64, 67-87.

80. Schwark, L., & Püttmann, W. (1990). Aromatic hydrocarbon composition of the Permian Kupferschiefer in the Lower Rhine Basin, NW Germany. Advances in Organic Geochemistry, 16, 749-761.
81. Schwark, L., Vliex, M., & Schaeffer, P. (1998). Geochemical characterization of Malm Zeta laminated carbonates from the Franconian Alb, SW-Germany (II). Organic Geochemistry, 29, 1921-1952.
82. Seppanen, C. M., Song, Q., & Csallany, A. S. (2010). The antioxidant functions of tocopherol and tocotrienol homologues in oils, fats, and food systems. Journal of the American Oil Chemists' Society, 87, 469-481.
83. Sinninghe Damsté, J. S., & de Leeuw, J. W. (1995). Comments on "Biomarkers or not biomarkers? A new hypothesis on the origin of pristane involving derivation from methyltrimethyltridecylchromans formed during diagenesis from chlorophyll and alkylphenols" by Li, M., Larter, S. R., Taylor, P., Jones, D. M., Bowler B., & Bjoroy, M. Organic Geochemistry, 23, 1085-1087.
84. Sinninghe Damsté, J. S., Kock-van Dalen, A. C., de Leeuw, J. W., Schenck, P. A., Guoying, S., & Brassell, S. C. (1987). The identification of mono-, di- and trimethyl 2-methyl-2-(4,8,12-trimethyltridecyl)chromans and their occurrence in the geosphere. Geochimica et Cosmochimica Acta, 51, 2393-2400.
85. Sinninghe Damsté, J. S., Keely, B. J., Betts, S. E., Baas, M., Maxwell, J. R., & de Leeuw, J. W. (1993). Variations in the abundances and distributions of isoprenoid chromans and long-chain alkylbenzenes in sediments of the Mulhouse Basin: a molecular sedimentary record of paleosalinity. Organic Geochemistry, 20, 1201-1215.
86. Skłodowska, M., Gapińska, M., Gajewska, E., & Gabara, B. (2009). Tocopherol content and enzymatic antioxidant activities in chloroplasts from NaCl-stressed tomato plants. Acta Physiologiae Plantarum, 31, 393-400.
87. Soll, J., Kemmerling, M., & Schultz, G. (1980). Tocopherol and plastoquinone synthesis in spinach chloroplast subfractions. Archives of Biochemistry and Biophysics, 204, 544-550.
88. Soll, J., Schultz, G., Joyard, J., Douce, R., & Block, M. A. (1985). Localization and synthesis of prenylquinones in isolated outer and inner envelope membranes from spinach chloroplasts. Archives of Biochemistry and Biophysics, 238, 290-299.
89. Summons, R. E., & Powell, T. G. (1987). Identification of aryl isoprenoids in source rocks and crude oils: Biological markers for the green sulphur bacteria. Geochimica et Cosmochimica Acta, 51, 557-566.
90. Trebst, A., Depka, B., & Holländer-Czytko, H. (2002). A specific role for tocopherol and of chemical singlet oxygen quenchers in the maintenance of photosystem II structure and function in *Chlamydomonas reinhardtii*. FEBS Letters, 516, 156-160.
91. Tulipani, S., Grice, K., Greenwood, P. F., & Schwark, L. 2013. A pyrolysis and stable isotopic approach to investigate the origin of methyltrimethyltridecylchromans (MTTCs). Organic Geochemistry, 61, 1-5.
92. Tulipani, S., Grice, K., Greenwood, P. F., Schwark, L., Böttcher, M. E., Summons, R. E., & Foster, C. B. (2015). Molecular proxies as indicators of freshwater incursion-driven salinity stratification. Chemical Geology, 409, 61-68.
93. Voll, L. M., & Abbasi, A.-R. (2007). Are there specific in vivo roles for α- and γ-tocopherol in plants? Plant Signaling & Behavior, 2:6, 486-488.

94. Wagner, K.-H., Isnardy, B., & Elmadfa, I. (2004). γ- and δ-tocopherols are more effective than α-tocopherol on the autoxidation of a 10% rapeseed oil triacylglycerol-in-water emulsion with and without a radical initiator. European Journal of Lipid Science and Technology, 106, 44-51.
95. Wang, L., Song, Z., Yin, Q., & George, S. C. (2011). Paleosalinity significance of occurrence and distribution of methyltrimethyltridecylchromans in the Upper Cretaceous Nenjiang formation, Songliao Basin, China. Organic Geochemistry, 42, 1411-1419.
96. Wang, X., & Quinn, P. J. (2000). The location and function of vitamin E in membranes (Review). Molecular Membrane Biology, 17, 143-156.
97. Werne, J. P., Hollander, D. J., Lyons, T. W., & Sinninghe Damsté, J. S. (2004). Organic sulfur biogeochemistry: Recent advances and future research directions. Geological Society of America Special Paper 379, 135-150.
98. Yamauchi, R., & Matsushita, S. (1979). Products formed by photosensitized oxidation of tocopherols. Agricultural and Biological Chemistry, 43, 2151-2156.
99. Zhang, Y., Jiang. A., Sun, Y., Xie, L., & Chai, P. (2012). Stable carbon isotope compositions of isoprenoids chromans in Cenozoic saline lacustrine source rocks from the Western Qaidam Basin, NW China: Source implications. Chinese Science Bulletin, 57, 1013-1023.

2.7 Figures

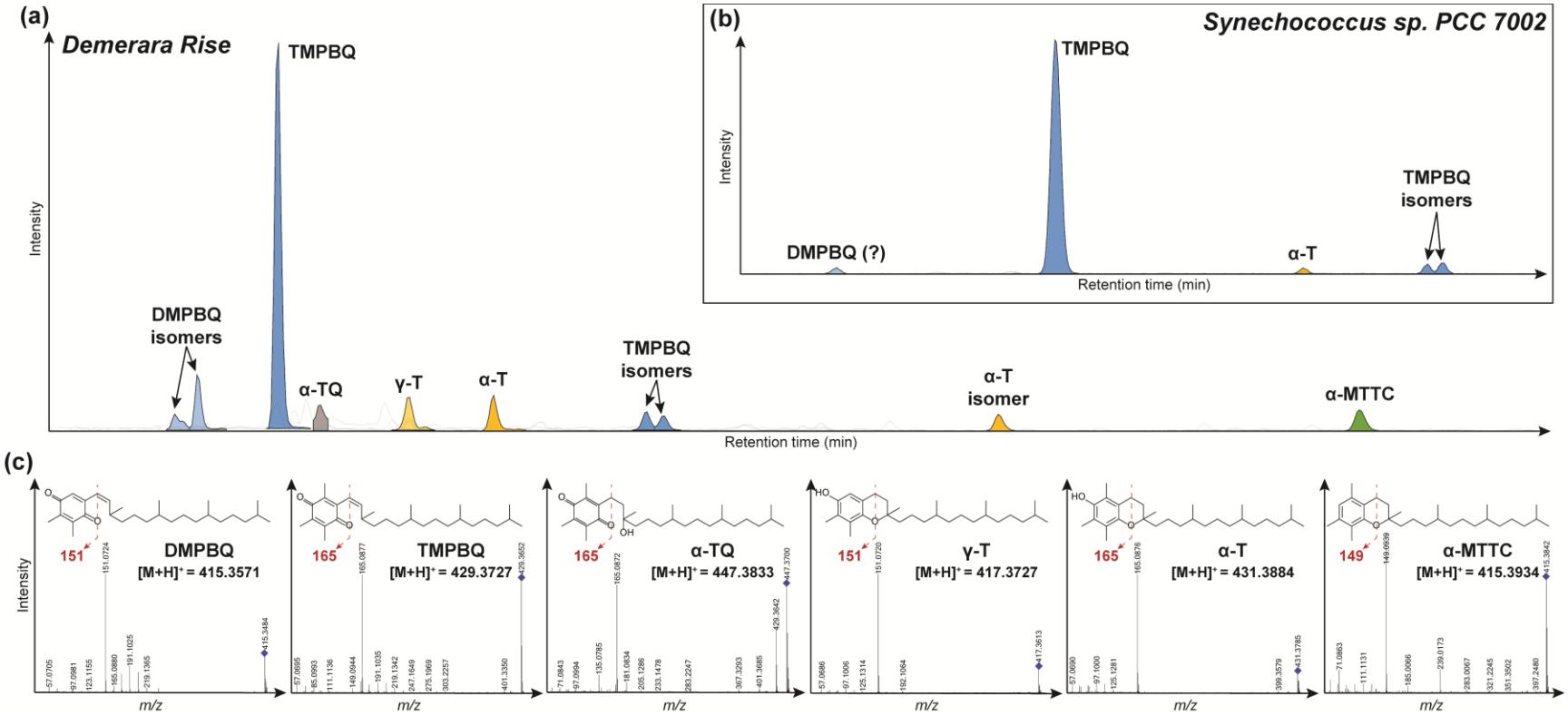

Figure 2-1. LC-qTOF-MS analysis and results of a Demerara Rise sample and cyanobacterial culture TLE kindly provided by Dr. Roger Summons of the Massachusetts Institute of Technology. (A) Summed extracted ion chromatograms (EICs) of tocol derivatives in (A) a Demerara Rise sample and (B) a *Synechococcus sp. PCC 7002* culture TLE, with (C) MS^2 mass spectra displaying characteristic fragmentation and protonated molecular masses of tocol derivatives.

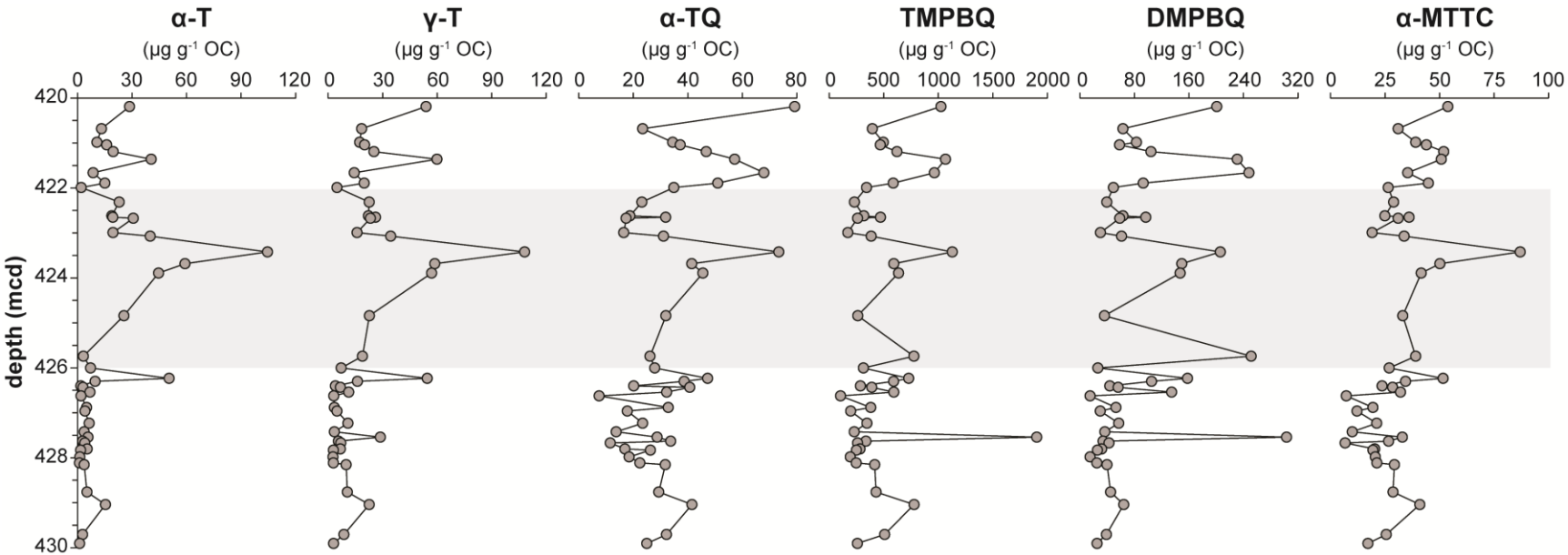

Figure 2-2. Depth profiles of tocol derivatives across OAE-2. The gray shaded region represents the OAE-2 interval as defined by the +CIE at site 1258 (Erbacher et al., 2005).

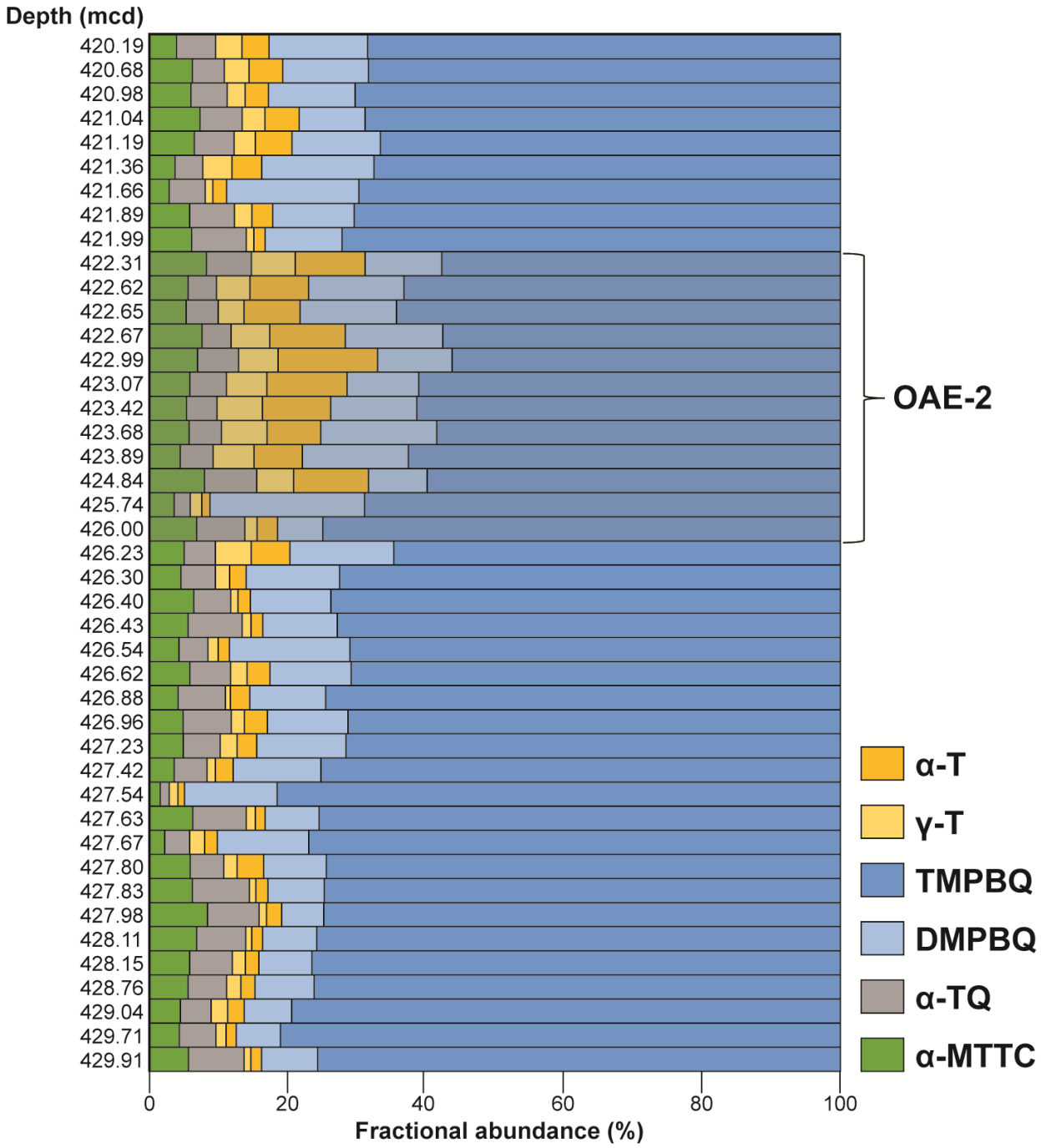

Figure 2-3. Tocol derivative fractional abundances over the sampled core interval at site 1258. Note the light gray shading denoting the OAE-2 interval. Compounds of similar structure, but varying degrees of methylation, are similar colors but different tones (e.g. dark blue for TMPBQ and light blue for DMPBQ.

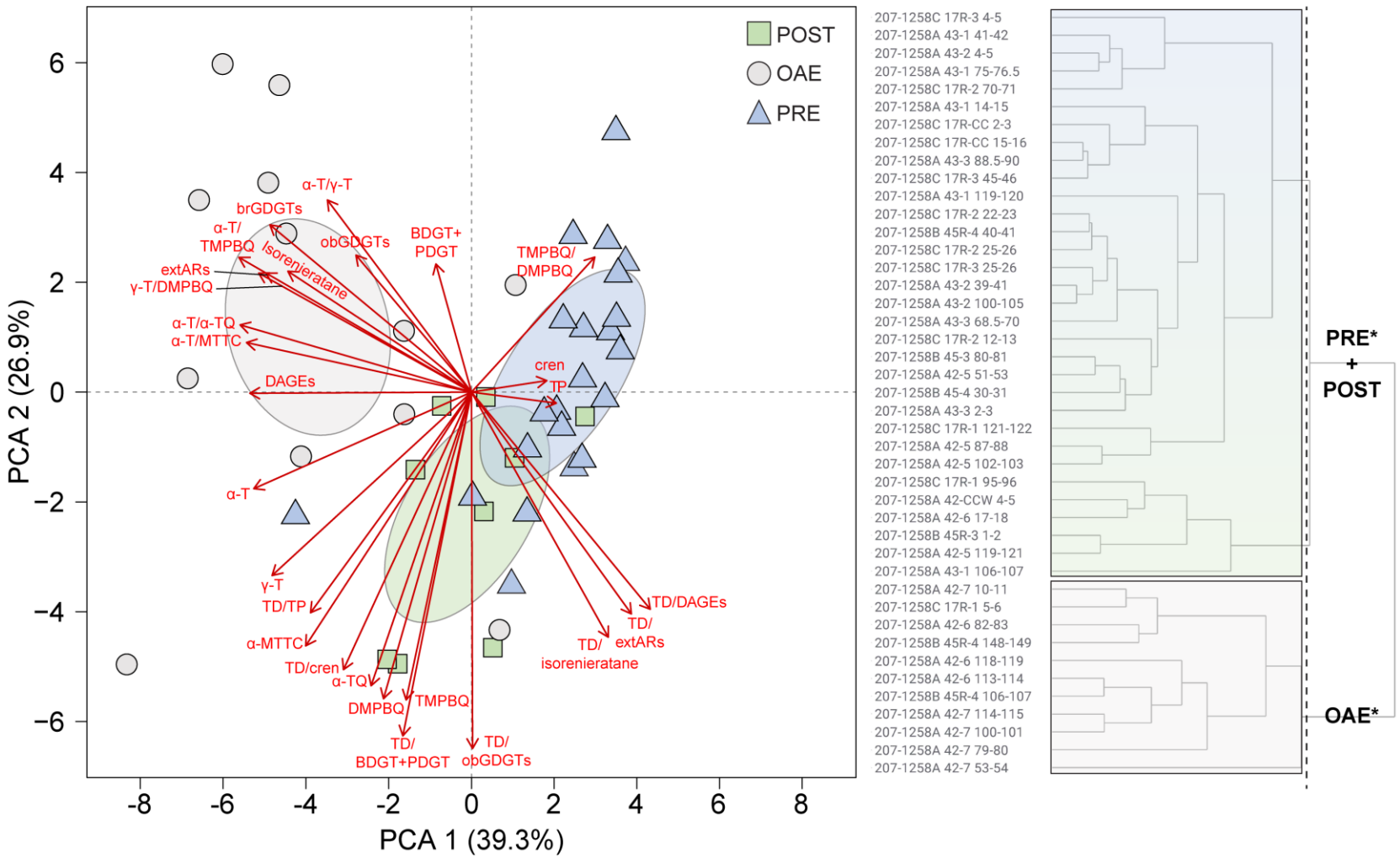

Figure 2-4. Principal component analysis (PCA) and hierarchical cluster analysis (HCA) results. The PCA biplot was generated using publicly available resources in RStudio, while the HCA dendrogram was produced in TIBCO Spotfire 11.1. Note the separation of OAE from non-OAE samples partially driven by tocol derivative ratios in both the biplot and dendrogram. Similar vector directions may suggest shared controls on compound or ratio distributions.

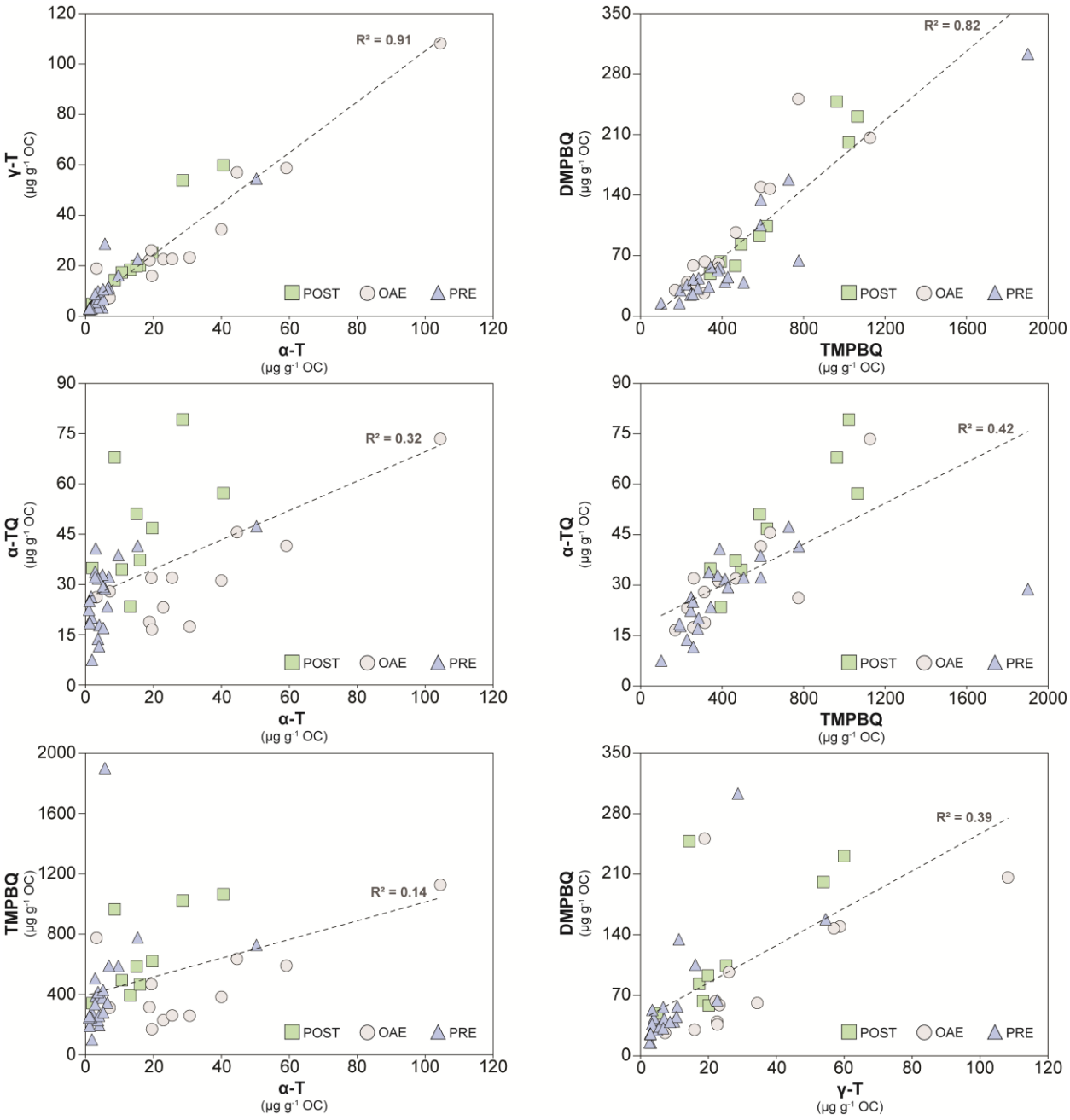

Figure 2-5. Cross plots of various tocol derivative concentrations.

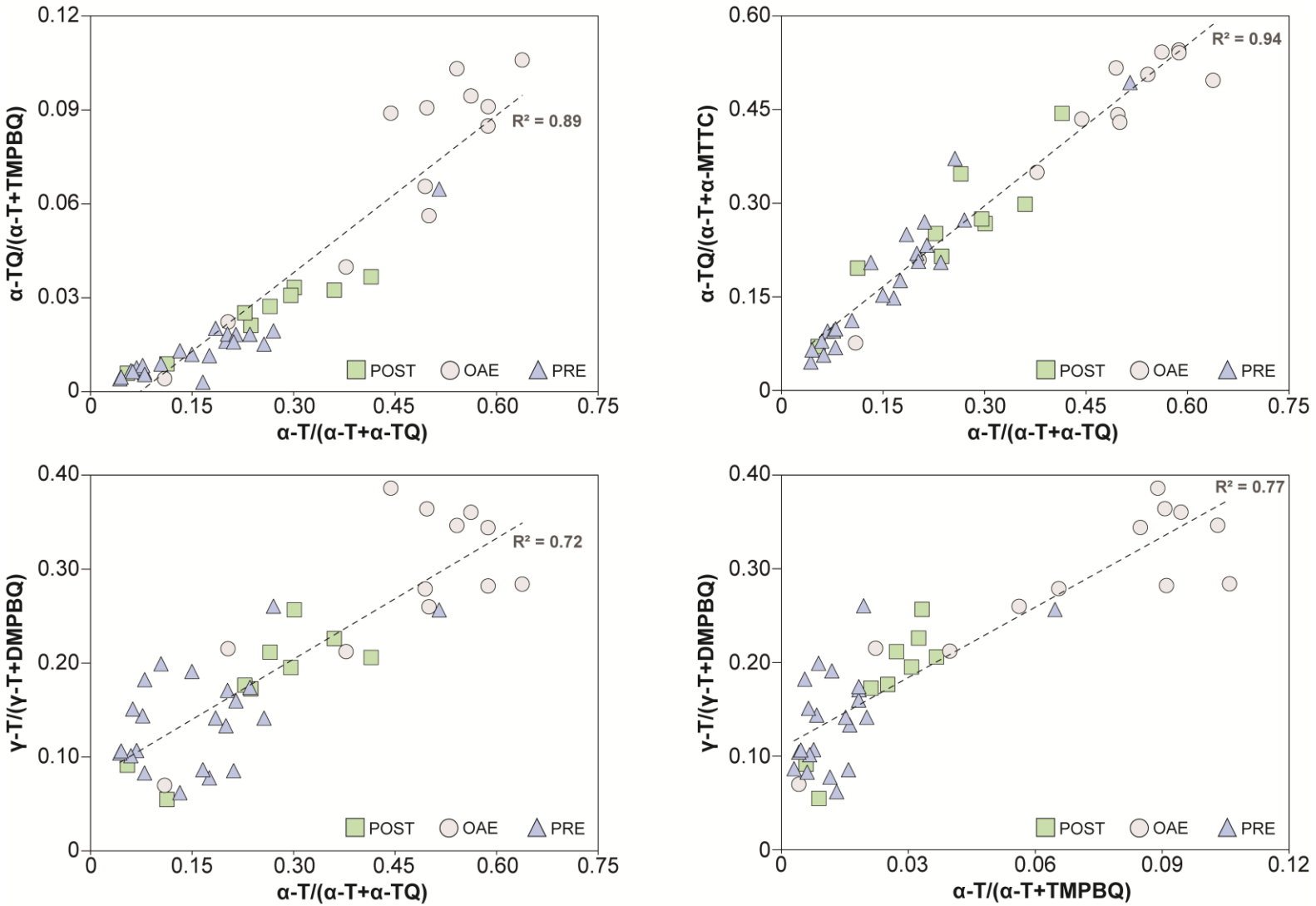

Figure 2-6. Cross plots of proposed tocol derivative ratios.

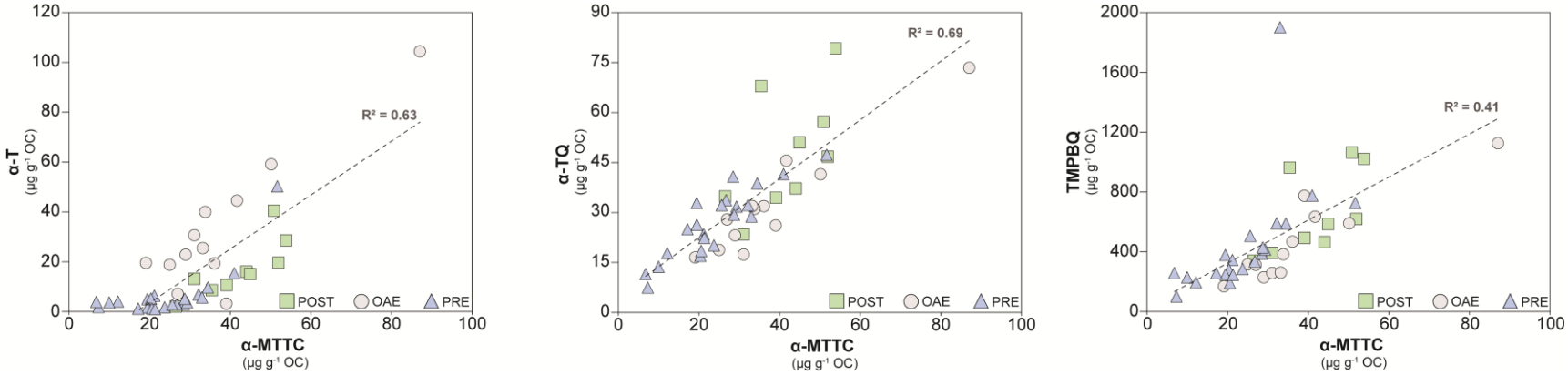

Figure 2-7. Cross plots of various tocol derivatives and α-MTTC concentrations.

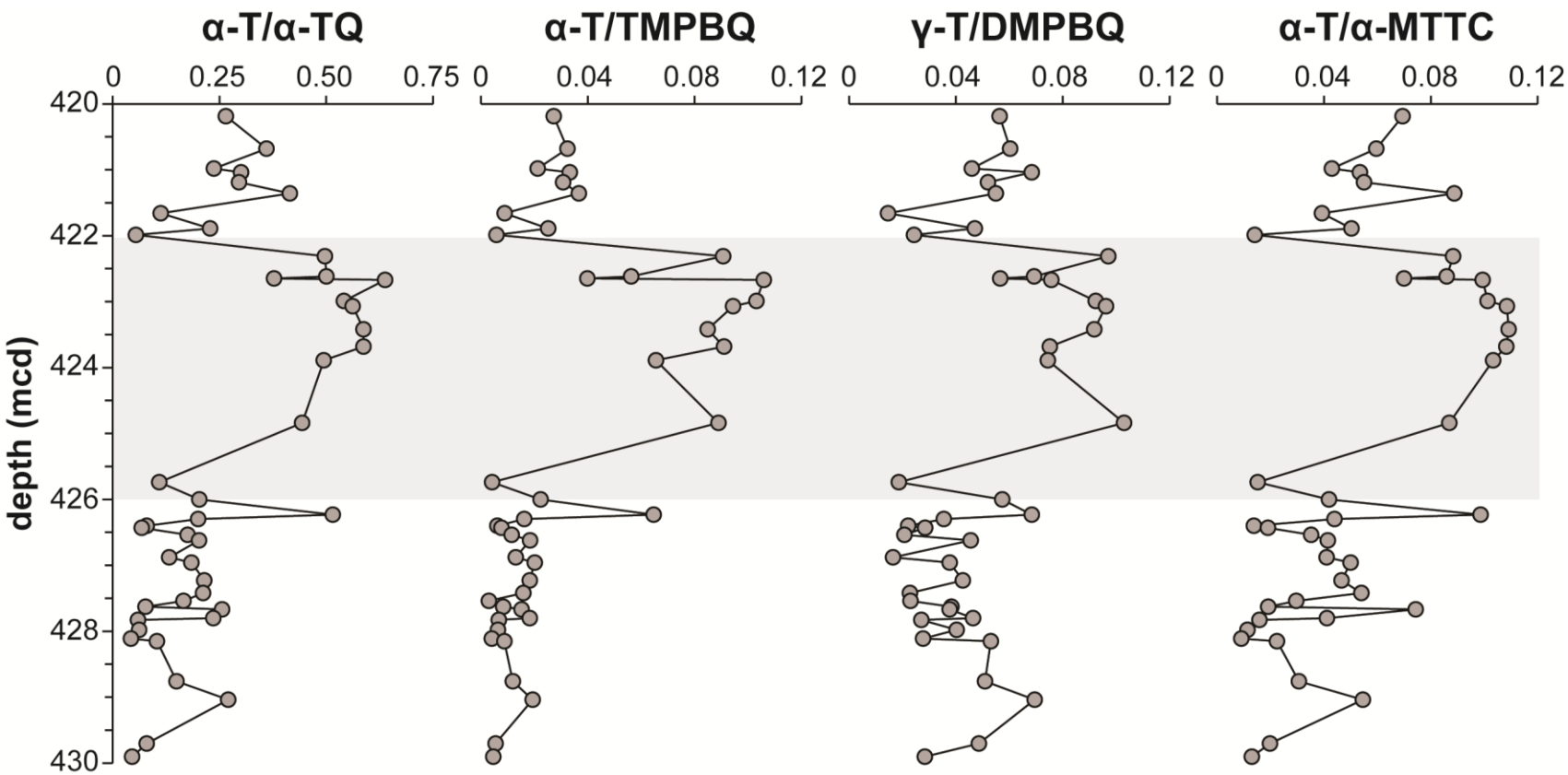

Figure 2-8. Depth profiles of proposed tocol derivative ratios. Light gray shading denotes the OAE-2 interval.

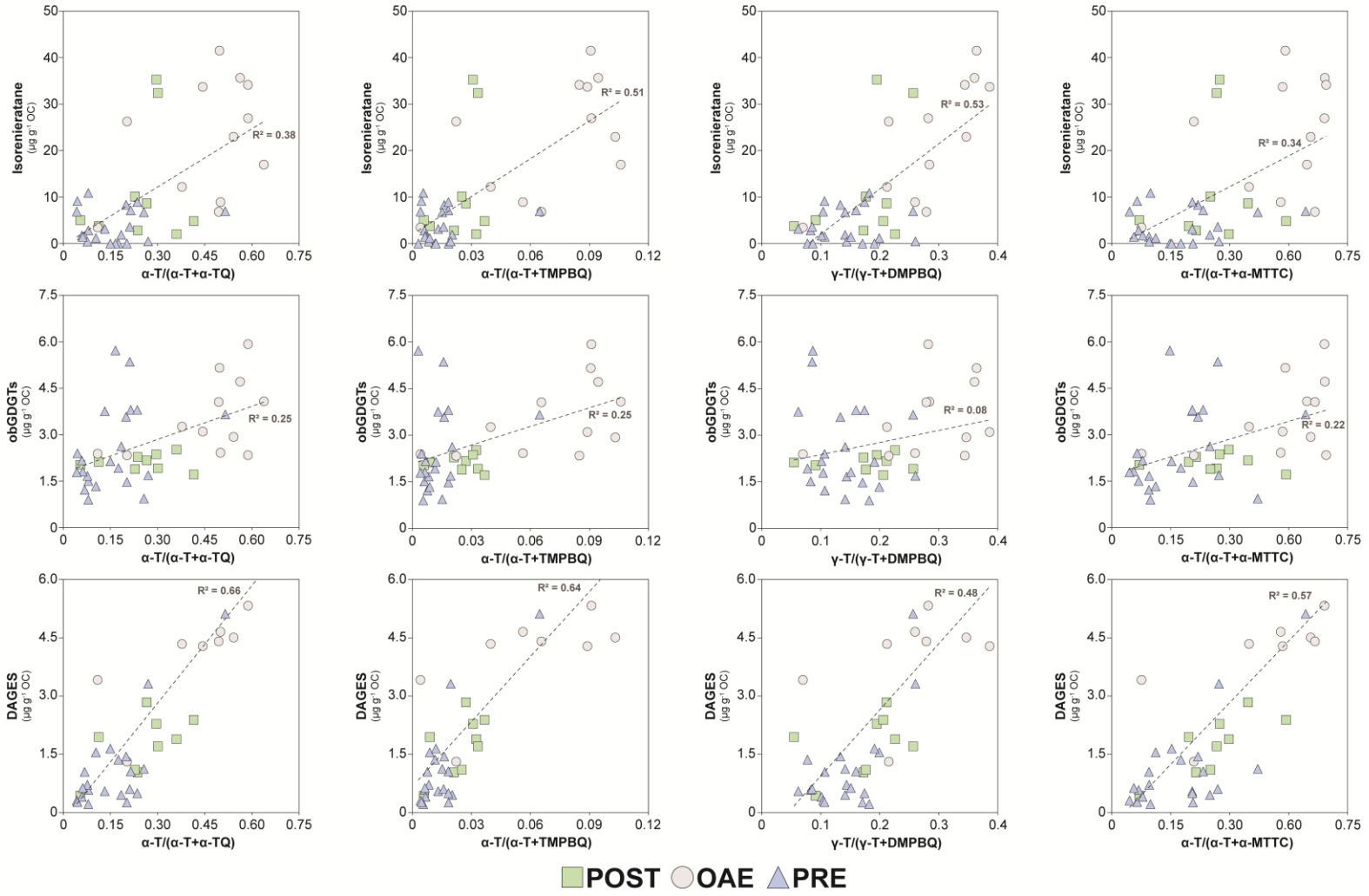

Figure 2-9. Cross plots of tocol derivative ratios against biomarkers of relatively well established paleoenvironmental significance. Note the improved correlations between biomarkers associated with sulfidic conditions (i.e. isorenieratane for PZE, and DAGEs for MSR).

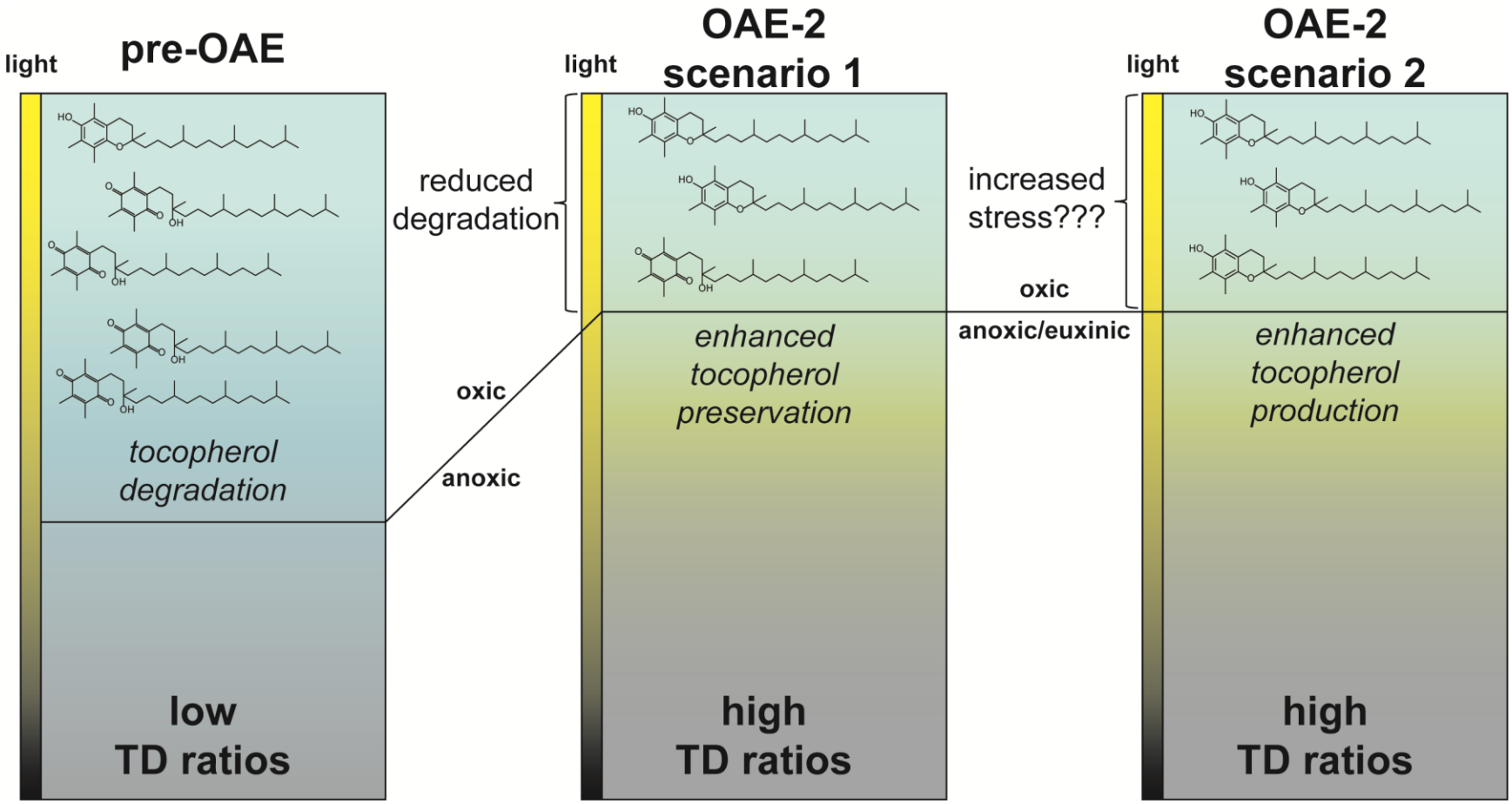

Figure 2-10. Conceptual water columns depicting potential controls on tocol derivative abundances and distributions across OAE-2. Color gradients depict water column redox gradients. Note how vertical expansion of anoxia/euxinia during OAE-2 introduced two distinct mechanisms (i.e. scenarios 1 and 2) to produce the elevated tocol derivative (TD) ratios observed.

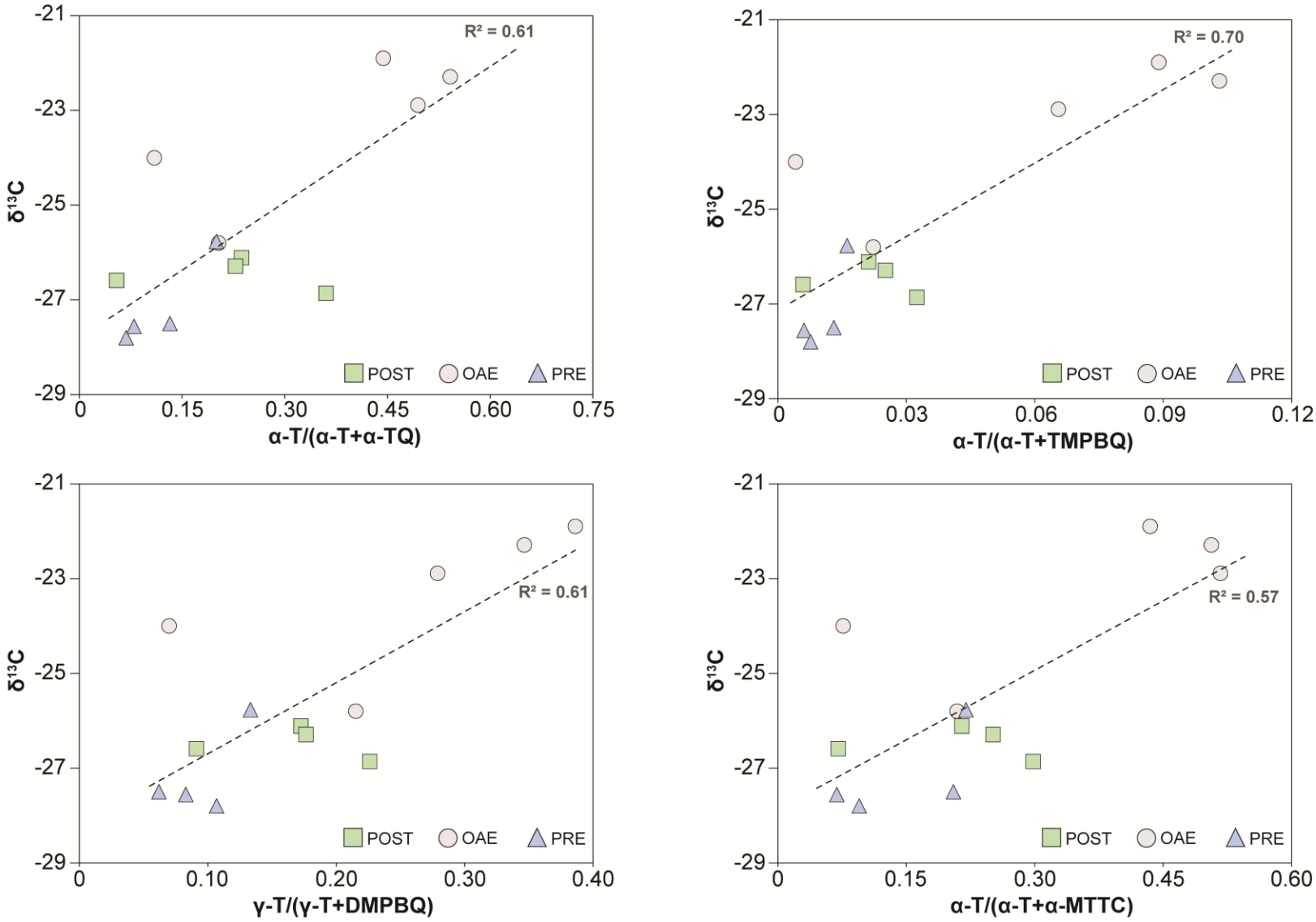

Figure 2-11. Cross plots of tocol derivative ratios and carbon isotopic compositions of organic matter. ($\delta^{13}C_{org}$ from Erbacher et al., 2005).

2.8 Supplementary Figures and Tables

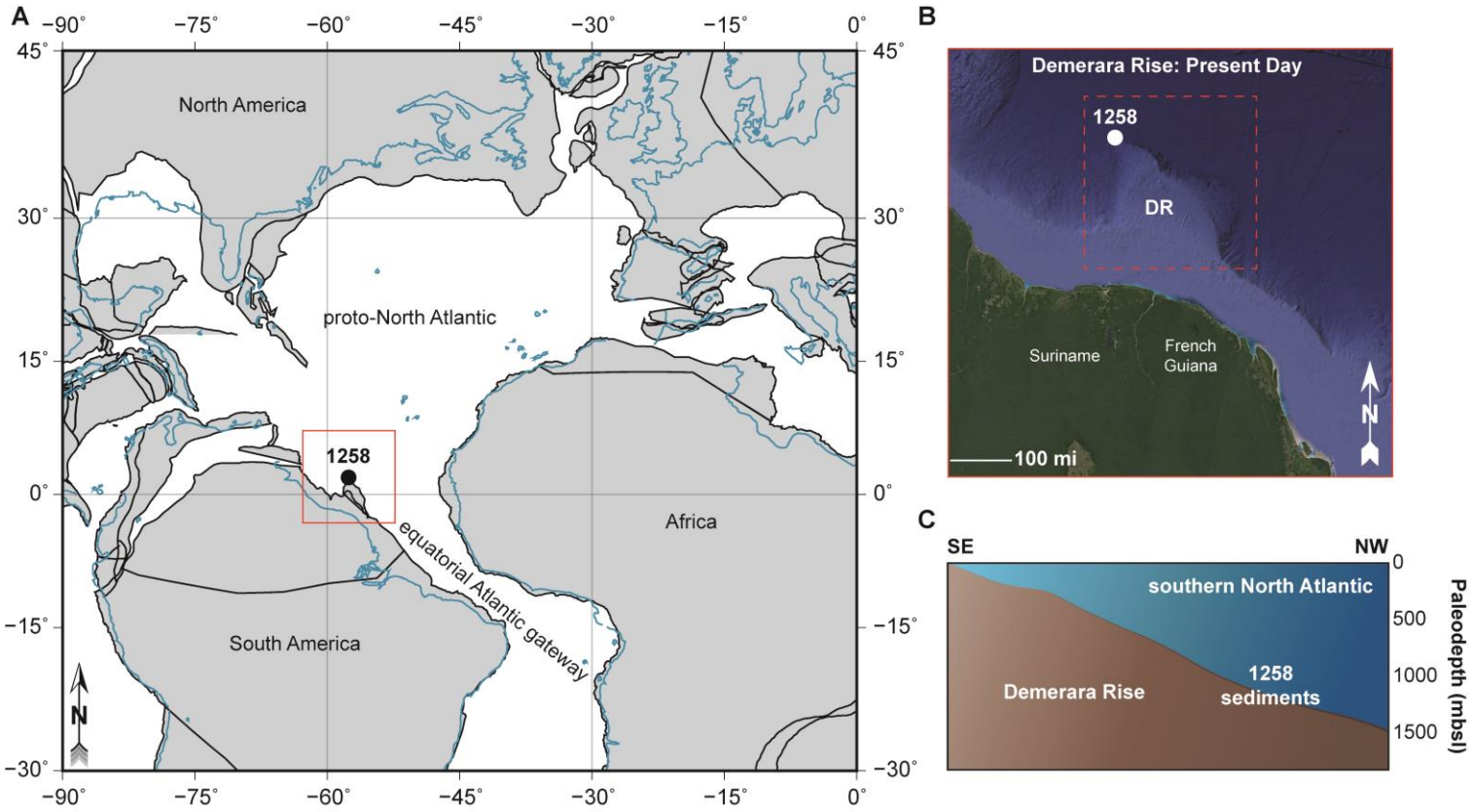

Figure S2-1. Paleogeographic context of site 1258 on the Demerara Rise, southern proto-North Atlantic Ocean. (A) Regional paleogeographic reconstruction at 93.9 Ma using the Ocean Drilling Stratigraphic Network (ODSN) plate reconstruction service (https://www.odsn.de/odsn/services/paleomap/paleomap.html). Blue lines represent modern shorelines, while gray shading bounded by black lines represents plate fragments. Site 1258 is denoted with a black dot and outlined with a red box. (B) Enlarged modern day satellite imagery of the primary study area from Google Earth Pro. (C) Cartoon depicting the relative position and paleodepths of sedimentation at site 1258 at ~93.9 Ma.

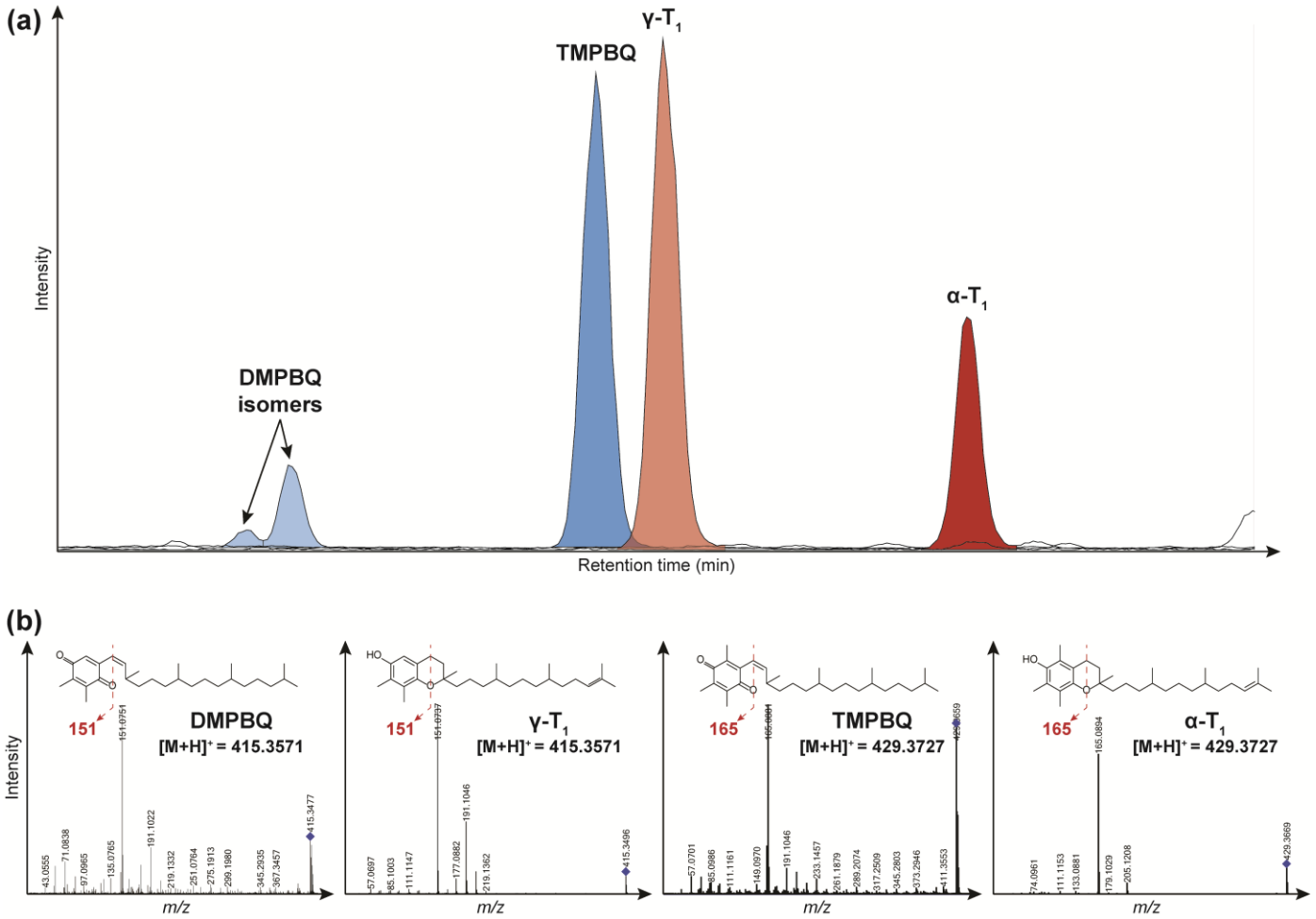

Figure S2-2. LC-qTOF-MS analysis and results of a Demerara Rise sample and tocomonoenol isolates kindly provided by Dr. Walter Vetter of the University of Hohenheim. (A) Summed extracted ion chromatograms of MPBQs in the Demerara Rise and from tocomonoenol isolates, clearly showing an absence of tocomonoenols in the natural samples. (B) MS^2 mass spectra of protonated MPBQs and tocomonoenols. While similar, note the higher intensities associated with MPBQs molecular ions, particularly TMPBQ, relative to tocomonoenols.

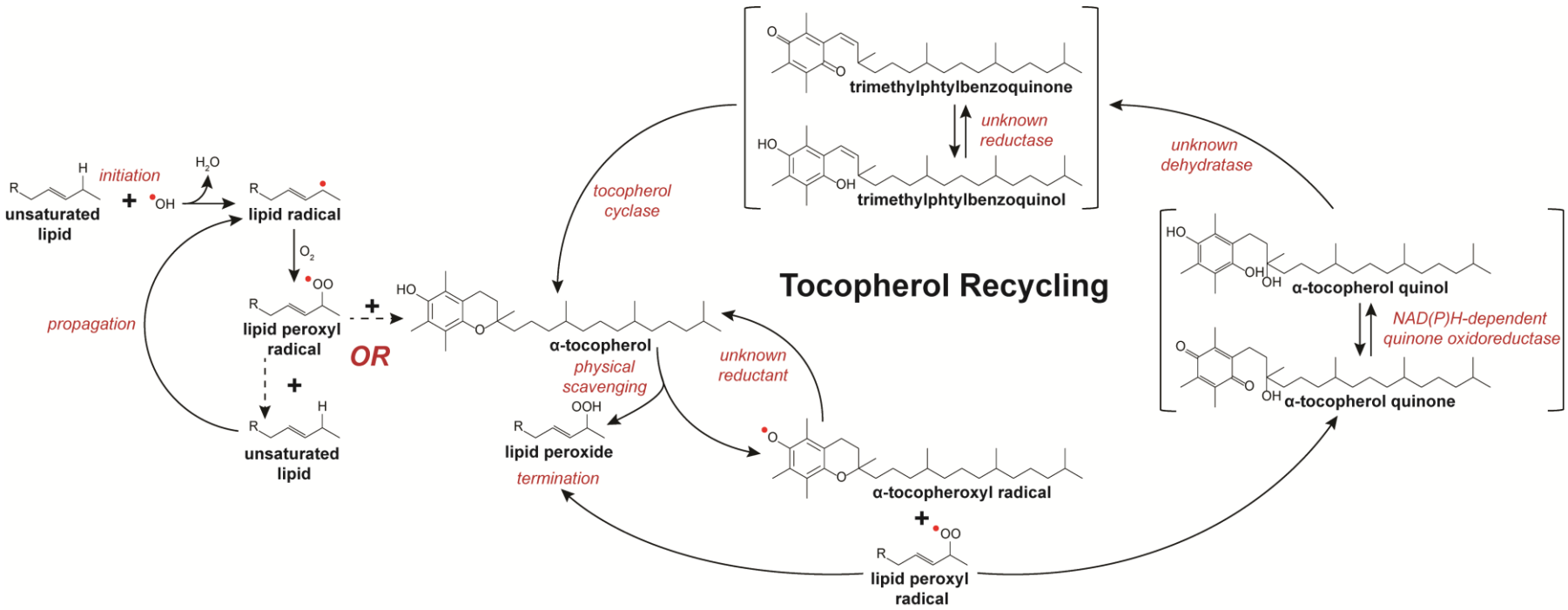

Figure S2-3. Tocopherol recycling pathway adapted from Eugeni Piller et al., (2014). Lipid peroxidation was added to provide greater context into lipid peroxyl radical formation and the mitigating role of tocopherols.

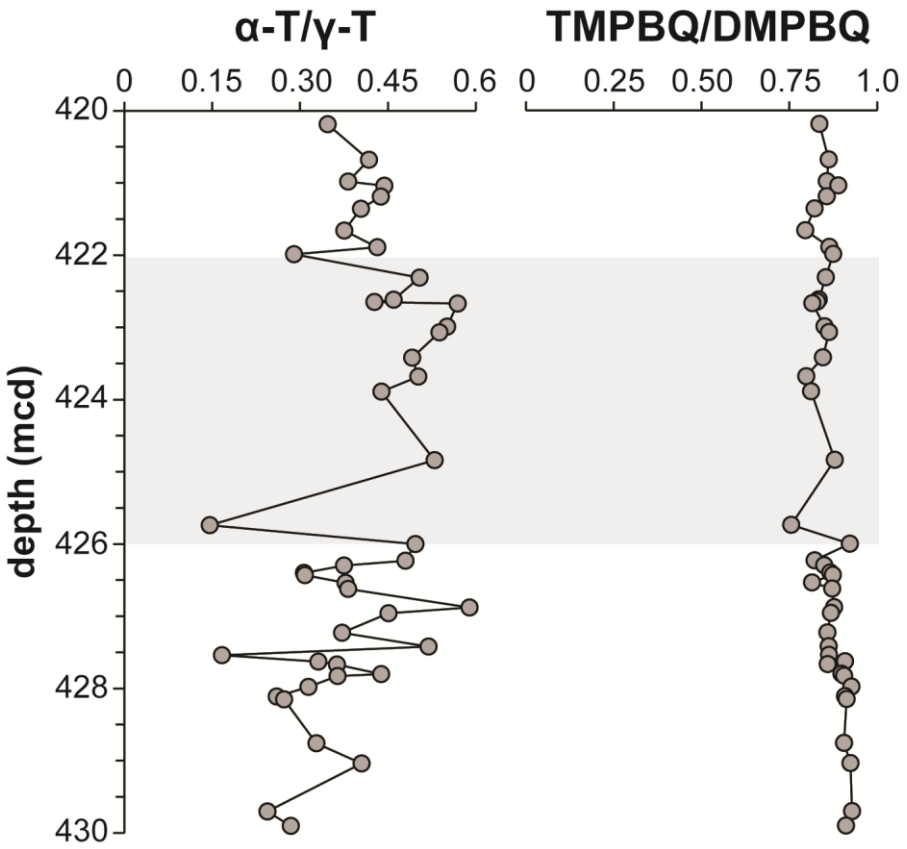

Figure S2-4. Depth profiles tocopherol and MPBQ methylation ratios.

Sample	Modified depth (mcd)	α-T (µg g-1 OC)	γ-T (µg g-1 OC)	α-TQ (µg g-1 OC)	TMPBQ (µg g-1 OC)	DMPBQ (µg g-1 OC)	α-MTTC (µg g-1 OC)	Isorenieratane (µg g-1 OC)	obGDGTs (µg g-1 OC)	DAGEs (µg g-1 OC)
207-1258B 45R-3 1-2	420.19	28.62	53.86	79.25	1022.31	200.86	53.89	8.65	2.17	2.84
207-1258A 42-5 51-53	420.68	13.20	18.45	23.46	393.73	63.16	31.08	2.03	2.52	1.89
207-1258B 45-3 80-81	420.98	10.70	17.33	34.47	494.00	83.09	39.09	2.82	2.28	1.03
207-1258A 42-5 87-88	421.04	16.05	20.10	37.26	466.18	58.21	44.01	32.40	1.92	1.71
207-1258A 42-5 102-103	421.19	19.67	25.26	46.80	619.99	104.18	51.96	35.29	2.37	2.28
207-1258A 42-5 119-121	421.36	40.56	59.92	57.27	1064.83	230.99	50.83	4.83	1.72	2.39
207-1258A 42-6 17-18	421.66	8.63	14.36	67.92	963.76	248.17	35.40	3.76	2.12	1.95
207-1258B 45-4 30-31	421.89	15.08	19.87	51.05	585.16	92.76	44.93	10.12	1.89	1.10
207-1258B 45R-4 40-41	421.99	2.01	4.93	34.89	342.06	49.11	26.45	5.04	2.03	0.44
207-1258A 42-6 82-83	422.31	22.90	22.57	23.18	229.69	39.39	28.94	41.53	5.16	6.00
207-1258A 42-6 113-114	422.62	18.81	22.14	18.81	315.92	63.04	24.96	8.90	2.42	4.66
207-1258B 45R-4 106-107	422.65	19.40	26.07	31.96	468.03	96.80	36.09	12.20	3.26	4.34
207-1258A 42-6 118-119	422.67	30.68	23.24	17.42	258.94	58.56	31.08	16.98	4.08	6.55
207-1258A 42-7 10-11	422.99	19.56	15.96	16.57	170.06	30.09	19.07	22.98	2.93	4.51
207-1258B 45R-4 148-149	423.07	40.01	34.39	31.16	383.56	60.98	33.79	35.65	4.72	8.48
207-1258A 42-7 53-54	423.42	104.49	108.18	73.44	1126.63	206.11	87.06	34.17	2.34	6.60
207-1258A 42-7 79-80	423.68	59.14	58.72	41.52	590.60	149.43	50.15	26.97	5.93	5.33
207-1258A 42-7 100-101	423.89	44.58	56.98	45.58	635.38	147.27	41.67	6.82	4.06	4.41
207-1258C 17R-1 5-6	424.84	25.52	22.66	31.99	261.28	36.02	33.17	33.73	3.10	4.29
207-1258C 17R-1 95-96	425.74	3.22	18.87	26.17	774.86	251.20	39.05	3.46	2.39	3.42
207-1258C 17R-1 121-122	426.00	7.13	7.23	27.94	312.70	26.34	26.96	26.26	2.33	1.31
207-1258A 42-7 114-115	426.23	50.32	54.53	47.36	727.57	158.05	51.69	6.94	3.66	5.12
207-1258C 17R-2 12-13	426.30	9.69	16.17	38.73	589.71	105.23	34.46	8.32	3.58	1.44
207-1258C 17R-2 22-23	426.40	1.75	3.96	20.16	285.41	43.87	23.70	2.80	1.51	0.58
207-1258C 17R-2 25-26	426.43	2.99	6.71	40.78	388.64	56.13	28.47	1.46	1.22	1.05
207-1258A 42-CCW 4-5	426.54	6.87	11.33	32.27	590.76	134.68	32.15	n.d.	1.92	1.36
207-1258A 43-1 14-15	426.62	1.91	3.09	7.50	101.87	14.99	7.30	n.d.	1.47	0.26
207-1258C 17R-2 70-71	426.88	5.01	3.49	32.88	378.81	52.93	19.45	3.13	3.76	0.55
207-1258A 43-1 41-42	426.96	4.05	4.93	17.86	196.31	29.90	12.14	1.85	2.62	0.45
207-1258A 43-1 75-76.5	427.23	6.43	10.86	23.48	345.16	57.12	21.18	7.14	3.80	1.06
207-1258C 17R-3 4-5	427.42	3.69	3.42	13.75	228.79	36.62	9.98	3.59	5.36	0.61
207-1258A 43-1 106-107	427.54	5.74	28.71	28.81	1901.69	303.27	33.00	n.d.	5.72	6.73
207-1258C 17R-3 25-26	427.63	2.82	5.71	33.76	335.83	33.97	26.72	0.40	1.67	0.72
207-1258A 43-1 119-120	427.67	3.99	7.01	11.56	258.97	42.60	6.75	6.73	0.94	1.13
207-1258A 43-2 4-5	427.80	5.25	6.72	17.02	281.10	31.88	20.32	8.90	3.80	0.50
207-1258C 17R-3 45-46	427.83	1.67	2.92	26.35	248.70	25.90	19.48	1.69	2.16	0.40
207-1258C 17R-CC 2-3	427.98	1.23	2.69	18.51	191.37	15.14	20.55	1.43	1.81	0.64
207-1258C 17R-CC 15-16	428.11	1.02	2.90	22.43	246.39	24.92	21.33	6.89	1.79	0.31
207-1258A 43-2 39-41	428.15	3.69	9.88	31.77	415.59	39.70	29.31	1.17	1.34	1.55
207-1258A 43-2 100-105	428.76	5.18	10.63	29.38	429.07	45.00	28.72	n.d.	2.14	1.65
207-1258A 43-3 2-3	429.04	15.39	22.65	41.54	776.95	64.28	41.00	0.44	1.69	3.32
207-1258A 43-3 68.5-70	429.71	2.81	8.70	32.24	506.63	39.03	25.61	10.86	0.90	0.22
207-1258A 43-3 88.5-90	429.91	1.19	3.01	25.02	257.28	25.25	17.16	9.14	2.40	0.27

Table S2-1. Biomarker concentrations of tocol derivatives, carotenoids, and glycerol ether lipids. Gray shading denotes the OAE-2 interval as defined by the +CIE (Erbacher et al., 2005).

Sample	Modified depth (mcd)	α-T/α-TQ	α-T/TMPBQ	γ-T /DMPBQ	α-T/α-MTTC	α-T/γ-T	TMPBQ/DMPBQ
207-1258B 45R-3 1-2	420.19	0.27	0.03	0.21	0.35	0.35	0.84
207-1258A 42-5 51-53	420.68	0.36	0.03	0.23	0.30	0.42	0.86
207-1258B 45-3 80-81	420.98	0.24	0.02	0.17	0.21	0.38	0.86
207-1258A 42-5 87-88	421.04	0.30	0.03	0.26	0.27	0.44	0.89
207-1258A 42-5 102-103	421.19	0.30	0.03	0.20	0.27	0.44	0.86
207-1258A 42-5 119-121	421.36	0.41	0.04	0.21	0.44	0.40	0.82
207-1258A 42-6 17-18	421.66	0.11	0.01	0.05	0.20	0.38	0.80
207-1258B 45-4 30-31	421.89	0.23	0.03	0.18	0.25	0.43	0.86
207-1258B 45R-4 40-41	421.99	0.05	0.01	0.09	0.07	0.29	0.87
207-1258A 42-6 82-83	422.31	0.50	0.09	0.36	0.44	0.50	0.85
207-1258A 42-6 113-114	422.62	0.50	0.06	0.26	0.43	0.46	0.83
207-1258B 45R-4 106-107	422.65	0.38	0.04	0.21	0.35	0.43	0.83
207-1258A 42-6 118-119	422.67	0.64	0.11	0.28	0.50	0.57	0.82
207-1258A 42-7 10-11	422.99	0.54	0.10	0.35	0.51	0.55	0.85
207-1258B 45R-4 148-149	423.07	0.56	0.09	0.36	0.54	0.54	0.86
207-1258A 42-7 53-54	423.42	0.59	0.08	0.34	0.55	0.49	0.85
207-1258A 42-7 79-80	423.68	0.59	0.09	0.28	0.54	0.50	0.80
207-1258A 42-7 100-101	423.89	0.49	0.07	0.28	0.52	0.44	0.81
207-1258C 17R-1 5-6	424.84	0.44	0.09	0.39	0.43	0.53	0.88
207-1258C 17R-1 95-96	425.74	0.11	0.00	0.07	0.08	0.15	0.76
207-1258C 17R-1 121-122	426.00	0.20	0.02	0.22	0.21	0.50	0.92
207-1258A 42-7 114-115	426.23	0.52	0.06	0.26	0.49	0.48	0.82
207-1258C 17R-2 12-13	426.30	0.20	0.02	0.13	0.22	0.37	0.85
207-1258C 17R-2 22-23	426.40	0.08	0.01	0.08	0.07	0.31	0.87
207-1258C 17R-2 25-26	426.43	0.07	0.01	0.11	0.09	0.31	0.87
207-1258A 42-CCW 4-5	426.54	0.18	0.01	0.08	0.18	0.38	0.81
207-1258A 43-1 14-15	426.62	0.20	0.02	0.17	0.21	0.38	0.87
207-1258C 17R-2 70-71	426.88	0.13	0.01	0.06	0.20	0.59	0.88
207-1258A 43-1 41-42	426.96	0.18	0.02	0.14	0.25	0.45	0.87
207-1258A 43-1 75-76.5	427.23	0.21	0.02	0.16	0.23	0.37	0.86
207-1258C 17R-3 4-5	427.42	0.21	0.02	0.09	0.27	0.52	0.86
207-1258A 43-1 106-107	427.54	0.17	0.00	0.09	0.15	0.17	0.86
207-1258C 17R-3 25-26	427.63	0.08	0.01	0.14	0.10	0.33	0.91
207-1258A 43-1 119-120	427.67	0.26	0.02	0.14	0.37	0.36	0.86
207-1258A 43-2 4-5	427.80	0.24	0.02	0.17	0.21	0.44	0.90
207-1258C 17R-3 45-46	427.83	0.06	0.01	0.10	0.08	0.36	0.91
207-1258C 17R-CC 2-3	427.98	0.06	0.01	0.15	0.06	0.31	0.93
207-1258C 17R-CC 15-16	428.11	0.04	0.00	0.10	0.05	0.26	0.91
207-1258A 43-2 39-41	428.15	0.10	0.01	0.20	0.11	0.27	0.91
207-1258A 43-2 100-105	428.76	0.15	0.01	0.19	0.15	0.33	0.91
207-1258A 43-3 2-3	429.04	0.27	0.02	0.26	0.27	0.40	0.92
207-1258A 43-3 68.5-70	429.71	0.08	0.01	0.18	0.10	0.24	0.93
207-1258A 43-3 88.5-90	429.91	0.05	0.00	0.11	0.06	0.28	0.91

Table S2-2. Tocol derivative ratios across the OAE-2 interval at site 1258 on the Demerara Rise. Gray shading denotes the OAE-2 interval as defined by the +CIE (Erbacher et al., 2005).

2.9 Structural Appendix

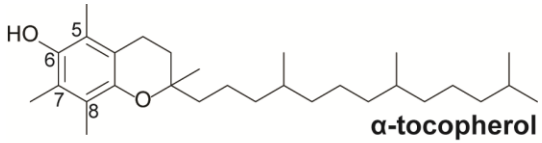

α-tocopherol

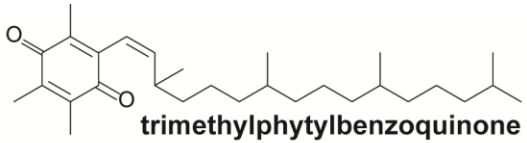

trimethylphytylbenzoquinone (TMPBQ)

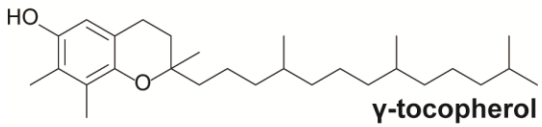

γ-tocopherol

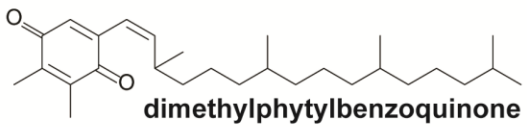

dimethylphytylbenzoquinone (DMPBQ)

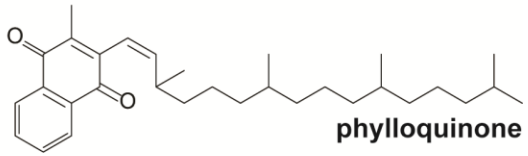

phylloquinone

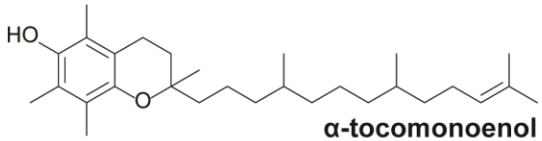

α-tocomonoenol

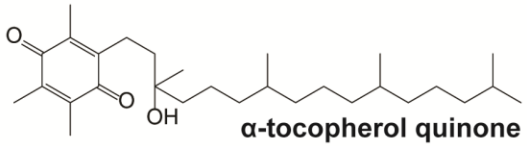

α-tocopherol quinone

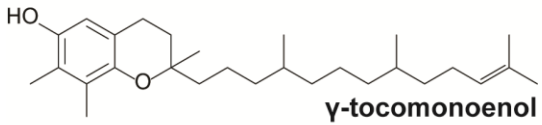

γ-tocomonoenol

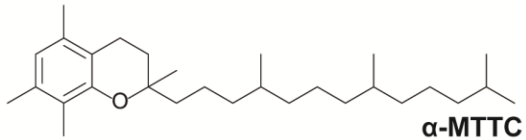

α-MTTC

Chapter 3: Impact of volcanic ash deposition on marine primary production and water chemistry in the mid-Cretaceous Western Interior Seaway

Authors: Gregory T. Connock[1*], Michael H. Engel[1], and Xiao-Lei Liu[1]

Affiliations: [1]School of Geosciences, University of Oklahoma, Norman, Oklahoma 73019, USA.

Abstract: Volcanic ash is frequently invoked to explain periods of enhanced primary production and/or organic carbon preservation in the geologic record due to the inherent fertilization potential stemming from ash composition (e.g. Fe). Although this is observed in specific regions of the oceans today, the long-term effects (i.e. thousands of years) on marine systems is poorly constrained. Here, we leveraged the stratigraphic record of the mid-Cretaceous Western Interior Seaway of North America rife with bentonites, diagenetic remnants of ancient volcanic eruptions, to determine the short- and long-term impacts of volcanic ash on marine microbial ecology and chemistry. Three intervals spanning eruptive events of varying magnitudes (VEIs of 4-7) were sampled at high resolution (~1 sample per 2 cm) to generate detailed temporal records of biomarkers (e.g. metalloporphyrins, carotenoids, and tocol derivatives) and stable isotopes ($\delta^{13}C_{org}$ and $\delta^{15}N$). All eruptions induced transient increases in primary production, consistent with rapid nutrient release upon contact with seawater, and most coincided with negative $\delta^{13}C_{org}$ excursions. Lasting shifts in redox-sensitive biomarker proxies (e.g. VO-/Ni-porphyrin ratios) followed the two major eruptions and may represent a long-term shift to euxinic bottom waters following ash deposition. This change in bottom water redox may have acted to suppress subsequent upwelling of Fe released during mineral dissolution through reactions with sulfide species, explaining the limited, protracted impact of ash on primary production. Thus, it is unlikely fertilization via volcanic ash was a prominent driver of extended elevations in primary production during the Cretaceous, requiring hyper-frequent eruptions unsupported in the geologic record to maintain a continually elevated nutrient supply. Instead, the abrupt and sustained shift in bottom water redox immediately following ash deposition likely improved organic carbon preservation, providing an alternative explanation for the apparent link between volcanism and enhanced organic carbon burial in deep time.

3.1 Introduction

Volcanism is an established climate forcing mechanism with a profound influence on climatic variability throughout geologic time by simultaneously perturbing multiple Earth systems (e.g. effects on temperature by altering atmospheric chemistry; Bray, 1974; Axelrod, 1981; Rampino, 1991; Simkin, 1993; Robock, 2000; Zielinski, 2000; Bay et al., 2004; Jicha et al., 2009). Spatiotemporal variations in eruption style (e.g. effusive vs. explosive) and frequency (e.g. superplume cycles; Sheridan, 1987; Larson, 1991) impose a range of effects on both terrestrial and

marine environments (Ayris and Delmelle, 2012 and references therein). Particularly explosive eruptions, such as those associated with subduction zone volcanism, may directly influence climate through emission of gases possessing significant radiative forcing potential (e.g. CO_2 and sulfate aerosols). While stratospheric injection of sulfur species is recognized as the most prominent, acute volcanogenic effect leading to temporary tropospheric cooling (Pollack et al., 1976; Rampino and Self, 1984; Dutton and Christy, 1992), indirect modulation of the climate system through perturbations to the biological carbon pump is increasingly invoked to explain climate variability in deep time.

Eruption ejecta are collectively referred to as tephra, with volcanic ash representing the finest material (< 2 mm) capable of traversing significant distances via eolian processes (Fisher and Schmincke, 1984; Duggen et al., 2010; Huff, 2016). Thus, proximity to active subaerial volcanism is not a prerequisite for marine systems to be perturbed by major eruptions. Nutrients, such as Fe, bound in acid salts adsorbed onto the surfaces of volcanic ash are rapidly disassociated upon contact with seawater (< 45 min; Frogner et al., 2001; Delmelle et al., 2007), alleviating [potential] limits on primary productivity associated with [micro]nutrient shortages. This process is frequently referred to as 'iron fertilization' (Martin and Fitzwater, 1988; Spirakis, 1991), whereby eolian transport of nutrient-laden volcanic ash and/or glacial/desert dust seeds the oceans with biolimiting nutrients that produce an abrupt increase in phytoplanktonic growth. However, the impact of Fe fertilization extends well beyond simply an increase in primary production. Iron is an indispensable micronutrient for all photosynthetic life, as it enables the biosynthesis of chlorophylls necessary for light-harvesting function (Martin et al., 1991). In certain regions of the ocean where Fe is a limiting nutrient (e.g. central ocean basins), exogenous delivery of Fe and other bioessential elements (Si, P, and trace metals) via eruptive events and/or continental dust

delivery has been linked with transient increases in carbon fixation (Mahowald et al., 2005; Duggen et al., 2007; Hamme et al., 2010; Langmann et al., 2010; Olgun et al., 2011; Achterberg et al., 2013; Lindenthal et al., 2013). Enhanced production of organic carbon will promote accelerated oceanic and atmospheric CO_2 drawdown (Cooper et al., 1996), which may temporally influence CO_2 sequestration and attendant cooling presuming a fraction of the biomass produced is buried. Still, attempts to delineate the long-term impacts (10^3 years) of volcanic eruptions, including Fe fertilization of marine ecosystems and long-term alteration of the oceanic biological carbon pump, are limited to conception (e.g. Watson, 1997) and coincidence (e.g. Cather et al., 2009). Continued invocation of volcanogenic Fe fertilization in deep time to explain climatic events accompanied by relatively cotemporaneous volcanism (e.g. Bains et al., 2000; Bay et al., 2004; Cather et al., 2009; Jicha et al., 2009), including Oceanic Anoxic Event 2 (OAE-2; Lee et al., 2018), necessitates an effort to constrain the duration and extent of the biotic response and chemical effects of instantaneous volcanic ash deposition in marine environments. This is particularly relevant given recent work highlighting the superior Fe bioavailability of glacial dust relative to desert dust and volcanic ash (Shoenfelt et al., 2018; Koffman et al., 2020), and inherent heterogeneity of volcanic provinces, which ultimately affects nutrient content and bioavailability (Maters et al., 2017; Capitani et al., 2018; Chen et al., 2020) that in turn affects Fe fertilization potential (e.g. Bishop and Wood, 2009; Costa et al., 2016). Further uncertainty regarding the Fe supply to ancient oceanic regions compounds these uncertainties and precludes blanket application of iron fertilization to explain past climatic perturbations, especially given that long-term impacts remain poorly characterized.

Here, we assessed the potential effects of volcanism on marine systems by delineating short- and long-term impacts of proximal volcanism on the microbial ecology and water column

chemistry of a Cretaceous epicontinental sea, the Western Interior Seaway (WIS) of North America, through high-resolution sampling of strata bounding bentonite beds of variable thicknesses. Bentonites are the diagenetic remnants of ancient ash falls, predominantly comprising smectite minerals, and represent geologically instantaneous deposition of tephra associated with a single eruption or a series of eruptions in quick succession (Obradovich and Cobban, 1975; Duggen et al., 2007; Huff, 2016). These deposits, produced by volcanism associated with the subduction of the Farallon Plate (Miall, 2009; Blakey and Raney, 2018), litter Cretaceous marine strata of the WIS (Hattin, 1985; Elder, 1988; Obradovich, 1993), which we leveraged to elucidate and temporally constrain volcanogenic effects on marine systems through a multi-proxy geochemical approach. Multiple eruptive events of varying magnitude were targeted to assess the [potentially] variable impact on WIS biogeochemistry. Transient and enduring changes coincident with ash deposition were identified, fundamentally altering how volcanism is invoked to account for past, and future, climate change.

3.1.1 Geologic setting

The WIS was a defining feature of western North America throughout the Cretaceous period, with a significant influence on greater climatic and oceanographic dynamics as a marine meridional gateway transiently connecting the Boreal and Tethyan Seas (Figure 3-1; Hay et al., 1993). No modern analog exists, as the WIS was conceived and evolved via a combination of tectonics and eustasy in a greenhouse world primed for epicontinental seas (Blakey and Raney, 2018). Isostatic flexure and crustal loading associated with the active Sevier Orogenic Belt and incipient subduction of the Farallon Plate along the western North American margin led to the formation of an elongated retroarc foreland basin bounded in the west by a rising North American Cordillera (Cross and Pilger, Jr., 1978; Jordan, 1981; Beaumont et al., 1982; Miall, 2009; Blakey

and Raney, 2018). Concordant superplume activity in the Pacific Ocean altered seafloor bathymetry, displacing large volumes of seawater that flooded the rapidly subsiding foreland basin, thereby creating the widest and deepest transcontinental seaway of the Cretaceous (Larson, 1991).

Temporal variability in subsidence rates and eustatic fluctuations, combined with orbital forcings, led to numerous 3rd order transgressive-regressive cycles (T-R) in the WIS (Kauffman, 1977). The late Cenomanian-early Turonian Greenhorn transgression (T_6-R_6 cycle in Kauffman, 1977) represented the maximum geographic and bathymetric extents of the WIS (Figure 3-1), spanning ~2000km longitudinally (IA to UT/NV) and ~5000km latitudinally (modern day Gulf of Mexico to Arctic Ocean; Cobban et al., 1994; Arthur and Sageman, 2004), with maximum depths reaching 300-500m (Hay et al., 1993; Goswami et al., 2018). The asymmetric foreland basin geometry shifted the greatest paleodepths towards the western margin along the basin axis, defined by sporadic, rapid subsidence and relatively moderate sedimentation rates (Kauffman, 1985; Kauffman and Caldwell, 1993). East of the axial basin where the RKB core is located (Figure 3-1), paleodepths progressively decreased towards the forebulge and back-bulge on the stable craton defining the eastern margin of the WIS (DeCelles and Giles, 1996; Miall et al., 2008), which was also characterized by significantly lower subsidence and sedimentation rates relative to the western margin (Kauffman, 1985). Water mass characteristics exhibited pronounced spatial variability as well, especially longitudinally. In general, the western margin was characterized by a cool, well-oxygenated southward flowing Boreal water mass, while the eastern margin was exposed to a warm, poorly oxygenated northward propagating Tethyan water mass of relatively higher salinities (Figure 3-1; Slingerland et al., 1996; Elderbak and Leckie, 2016). There is also suggestion the basin was silled at both the northern and southern openings, with deep water influx and export

subject to potentially highly variable bathymetry at the junctions with the open ocean (Scott, 1977; Kauffman, 1984; Sageman and Arthur, 1994). This created distinct circulation patterns (e.g. estuarine circulation, Slingerland et al., 1996) that affected water column properties (e.g. oxygenation, temperature, stratification) and nutrient distributions, ultimately influencing the microbial inhabitants of the WIS (Leckie et al., 1998; Fisher and Hay, 1999; Fisher and Arthur, 2002; Elderbak et al., 2014).

The Graneros Shale and Greenhorn Limestone, formations sampled in this study, represent two major depositional remnants of the Cenomanian-Turonian maximum transgression, extending across the eastern to central WIS and intertonguing with stratigraphic equivalents in the west (Dakota Sandstone and Mancos Shale; Sageman, 1991). Overall, these formations consist of fine-grained siliciclastic mudstone, calcareous shale, marlstone, limestone, and chalk, with lithologies typically repeated as rhythmic packages owing to cyclothemic deposition driven by a combination of tectonoeustatic fluxes and orbital cycles (Kauffman, 1977; Elder et al., 1994; Arthur and Sageman, 1994; Eldrett et al., 2015a). In the RKB core, black calcareous claystone and mudstone lithofacies predominate through the sampled Graneros interval, whereas the sampled Greenhorn section comprises light gray, heavily bioturbated limestone and well laminated, dark gray marlstone (Figure 3-2; Dean et al., 1995). Deposition throughout the Cenomanian-Turonian was interrupted by frequent tephra deposits, primarily in the form of volcanic ash, sourced from the western North American Cordillera. Linking ash deposits to specific regions of the Cordillera is difficult given extensive alteration of the original ash composition, preserved as highly altered smectite-rich bentonites in core and outcrop, challenging compositional correlations to candidate batholiths. Instead, correlations leverage temporal associations between bentonite ages and the timing of batholith emplacements, as well as regional geometries of mappable bentonite marker

beds given prevailing paleowind directions (Elder, 1988; Kimbrough et al., 2001; May et al., 2013). Of the three sampled intervals enveloping significant ash beds in this study, two intervals host widely observed bentonites spanning the WIS basin. The 'X' bentonite is present in the younger Graneros Shale section collected, and the 'B' bentonite (i.e. 'bentonite marker-bed B' of Elder, 1985) occurs in the Greenhorn Formation interval analyzed (Kauffman, 1977; Elder, 1988; Obradovich, 1993; Arthur and Sageman, 1994; Dean et al., 1995; Eldrett et al., 2015b). Although no formal name is given to the oldest bentonite interval sampled in the upper Graneros Shale, it is likely the ash deposit extends at least several hundred kilometers given the distance from the RKB core and the volcanic source region.

3.2. Materials and Methods

3.2.1 Study design

The Amoco Rebecca K. Bounds #1 (RKB) core was drilled in 1988 near the KS-CO border in Greeley County, KS by Amoco Production Company, and was later incorporated into the Cretaceous Western Interior Seaway Continental Scientific Drilling Project. The RKB core captures the temporality of the eastern half of the WIS throughout the Cretaceous. Excellent recovery of mid-Cretaceous strata hosting major bentonite marker beds and relatively shallow burial depths minimizing thermal alteration of organic matter and inorganic species were prominent reasons the RKB core was an excellent candidate for this study. In addition, the distal setting of the study location (western KS) relative to the volcanic arc and major deltas ensured ash deposition was exclusively subaerial in nature and sedimentation was predominantly marine, with minimal terrigenous input (Figure 3-1). Two intervals in the upper Graneros Shale and one section in the Bridge Creek Limestone member of the Greenhorn Formation were identified based on significant volcanic ash deposition inferred from compacted bentonite thickness (bentonites

greater than 2 cm in thickness, Figure 3-2). Bentonites of appreciable thickness (i.e. > 2 cm) and similar depositional age were targeted to minimize provenance and/or transport biases. The oldest sampled bentonite in the Graneros Shale is unnamed, but was deposited during the Middle Cenomanian Event as determined via carbon isotope stratigraphy of the RKB core (Patel, 2017). The base contact was gradational, while the top contact was sharp. The next interval chosen bounded the X bentonite, one of the most extensive volcanic ash deposits of the Cretaceous (Kauffman, 1977). Although no significant lithofacies change was observed, the sampled interval spanned the upper Graneros Shale-Lincoln Limestone Member of the Greenhorn Formation contact, marked by the gradational contact of the X bentonite and a thin *Ostrea* calcareous concretion. The basal contact of the X bentonite was gradational as well. Bentonite marker bed B was the youngest sampled interval in the Greenhorn Formation, specifically the Bridge Creek Limestone Member, and was deposited during OAE-2 as defined by a pronounced positive carbon isotopic excursion (Scholle and Arthur, 1980; Dean et al., 1995; Eldrett et al., 2015b). Both lower and upper contacts of the B bentonite were sharp (Figure 3-2). All bentonites were devoid of bioturbation (Dean et al., 1995). Herein these three intervals will be simply referred to as the UBI (Unnamed Bentonite Interval), XBI (X-Bentonite Interval), and BBI (B-Bentonite Interval), while each bentonite will be abbreviated UB, XB, and BB, respectively. Sampled intervals exhibiting minimal lithologic changes were targeted when possible to reduce potential biases imparted by substrate control. This was easily accommodated in the UBI and XBI, bounded by relatively persistent deposition of black calcareous claystones and mudstones. However, the BBI exhibited a distinct lithologic shift from extensively burrowed limestone to slightly bioturbated to laminated dark gray marlstone across the BB (Figure 3-2, Dean et al., 1995), and likely reflects astronomically driven climate forcings (Eldrett et al., 2015a). Multiple eruptive events of varying

magnitude were selected to assess if the marine microbial response to volcanic ash was consistent through time and how the volume of ejected ash may impact microbial life. All intervals were sampled at the highest possible resolution permitted (1 sample/2 cm on average), covering 0.3-0.45 m of strata enveloping targeted bentonites. This ensured paleoenvironmental conditions immediately preceding and following ash deposition were not overlooked.

3.2.2 Sample collection and processing

Sample collection was coordinated with staff at KGS, with candidate intervals identified through publicly available core descriptions (Dean et al., 1995) and photos (e.g. Figure 3-2). Core fragments were intentionally elongated along bedding to maximize sample mass without sacrificing temporal resolution. Sampling density was relatively constant, with strata below and above bentonites sampled equally. Where possible, sharp and gradational contacts between bentonites and adjacent strata were split to avoid contamination of organically lean ash beds with potentially organic-rich facies and isolate the conditions immediately preceding or following ash deposition. Overall, 59 samples were collected, with 18, 22, and 19 samples enveloping the UB, XB, and BB, respectively. Once collected by KGS staff, samples were shipped to the University of Oklahoma for pre-analysis preparation.

Core fragments were scraped with a pre-cleaned metal razor blade and thoroughly washed with water to remove potential contaminants, followed by rinsing with deionized water and a 1:1 azeotrope of DCM:MeOH. Samples were left to dry under a hood and wrapped in combusted aluminum foil for shipment. Pulverization to a fine rock powder was performed by the Reservoir Technology Center Lab at Chesapeake Energy using a ring and puck mill SpexSamplePrep 8530 ShatterBox. Cleaned core samples were placed in a tungsten carbide cylinder on top of a tungsten carbide puck. A steel hammer was used to further fragment samples into smaller pieces to prevent

the puck from becoming lodged in the cylinder. The cylinder was sealed and loaded into the 8530 ShatterBox for 3 minutes. Crushed rock powders were then transferred to combusted glass jars that were sealed with combusted aluminum foil and returned to the University of Oklahoma for subsequent analyses. Combusted sand was run in the cylinder followed by an acetone rinse between each sample.

3.2.3 Total organic carbon

All total organic carbon (TOC) measurements were performed by the Reservoir Technology Center Lab at Chesapeake Energy Corporation. A combusted ceramic crucible was loaded with 25 mg of rock powder followed by addition of 1mL of 5N HCl. The crucible, with sample submerged in HCl, was heated to 115^{o}C. Once the introduced 5N HCl evaporated, an additional 1mL of 5N HCl was added and left to dry. The acid-treated sample was then washed with 2mL of distilled deionized water and let completely dry. Prior to sample analysis, the LECO C-230 Carbon Determinator was calibrated using five blanks and two carbon standards (5.02%, part no. 502-319 and 1.89%, part no. 502-320) with identical accelerants used in sample measurements. One LECO metal scoop (part no. 773-579) of copper metal (part no. 501-263) and Lecocell II (part no. 501-008) accelerants were added to each sample before being loaded into the C-230 instrument. The two carbon standards were analyzed every 10 sample runs.

3.2.4 Biomarker analysis

Sample preparation was relatively identical to the procedure outlined in Chapter 1 (see section 1.2.2). Instead of 150 mg, 500 mg of rock powder was used, with 1000 mg prepared for extraction of bentonite intervals due to the poor organic content of ash beds. In addition to 100 ng of C_{46} glycerol trialkyl glycerol tetraether (GTGT) and 1000 ng of β-carotene standards, 100ng of

VO-TPP and Ni-TPP standards were introduced to each sample for relative compound quantification. Instrumental parameters and biomarker identification and quantification were consistent with methods outlined in Chapter 1 (see section 1.2.3 and 1.2.4 for isorenieratane and metalloporphyrins) and Chapter 2 (see section 2.3.1 for tocol derivatives).

3.2.5 Bulk stable carbon and nitrogen isotopes

All carbonate content was removed prior to both organic carbon and bulk nitrogen isotopic analysis. Samples were transferred to an acid-resistant tray, submerged in 3N HCl and let sit overnight. The following day, additional 3N HCl was added until no visible reaction occurred. Samples were then treated with water until a neutral pH was achieved and dried completely before analysis. Approximately 1-2 mg for $\delta^{13}C_{org}$ and 4-6 mg for $\delta^{15}N$ was transferred to tin capsules (Costech 041074) for each sample and loaded onto a Costech zero blank autosampler attached to a Costech 4010 Elemental Analyzer (EA) interfaced to a Thermo Delta V Plus isotope ratio mass spectrometer (IRMS) via a Conflo III valve. Two reagents, silvered cobalt oxide (Costech 011007) and chromium oxide (Costech 011001), were used in the quartz combustion column held at 1000^{o}C, while reduced copper wire (Costech 011013) was used in the reduction column held at 650^{o}C. The gas chromatograph (GC) oven temperature was held at 55^{o}C. Air was removed via a purge with high purity He before flash combustion, achieved by introducing a substantial O_2 pulse coincident with sample drop. Helium was used as the carrier gas at a flow rate of 100 mL/min, transporting the combusted sample to a Thermo Conflo III interface that introduced sample to the ion source of the IRMS. Organic carbon isotopic compositions ($\delta^{13}C_{org}$) were reported relative to the VPDB standard, and bulk nitrogen values ($\delta^{15}N$) were determined relative to N_2 in air. When measuring $\delta^{15}N$, a large CO_2 trap was placed between the H_2O trap and GC column to remove interference associated with CO in the ion source.

3.3 Results

3.3.1 Bulk geochemical data: TOC, $\delta^{13}C_{org}$, and $\delta^{15}N$

Most samples were relatively organic-rich and exhibited comparable TOC values before and after bentonite deposition, excluding the BBI which was defined by a marked increase in TOC after the BB and coincident with the previously described lithology shift (Figure 3-3, Table 3-1; see section 3.3.3 for more information on stratigraphic trends). The UBI was the most organic-rich interval analyzed (TOC_{avg} = 8.25 wt.%), followed by the XBI (TOC_{avg} = 2.61 wt.%) and BBI (TOC_{avg} = 2.35 wt.%). Both the UBI and XBI were characterized by relatively invariant TOC values, but exhibited sharp decreases in organic carbon within the bentonites. Many bentonite samples were organically lean, precluding biomarker and stable isotopic analysis, but adequate preservation near the contacts with overlying and underlying strata enabled the events immediately preceding and succeeding volcanic ash deposition to be reconstructed. One exception included a relatively organic-rich bentonite from the BB (BBI-8B, TOC = 5.46 wt.% at 297.44 m) that was likely contaminated with overlying organic-rich marl fragments during separation of the contrasting lithologies. However, extreme care was taken when sampling and splitting samples near the contacts, suggesting this anomalous sample could be an artifact of syndepositional reworking and mixing of calcareous muds with ash.

Organic carbon stable isotopic compositions ($\delta^{13}C_{org}$) were most depleted in the XBI ($\delta^{13}C_{org\_avg}$ = -26.65; Figure 3-3, Table 3-1). The UBI was slightly more enriched ($\delta^{13}C_{org\_avg}$ = -25.21), with the BBI defined by the heaviest $\delta^{13}C_{org}$ values ($\delta^{13}C_{org\_avg}$ = -24.12). Similar to TOC, $\delta^{13}C_{org}$ values exhibited minimal changes across the UBI and XBI, barring transiently abrupt decreases within the UB and XB, with the BBI defined by a relatively stable $\delta^{13}C_{org}$ profile excluding a brief excursion to lighter values before BB deposition. Variations in $\delta^{15}N_{bulk}$ were

small, less than 0.6 and 0.3 $^{0}/_{00}$ across the UBI and XBI, respectively. Generally low TOC values within the pre-BB limestones inhibited a complete $\delta^{15}N_{bulk}$ profile to be generated for the BBI, with the measured post-BB marlstones oscillating within a small range (less than 0.25 $^{0}/_{00}$; Figure 3-3, Table 3-1). Given much of the discussion was developed prior to obtaining isotopic results, a separate section (section 3.4.5) at the end of the discussion will attempt to reconcile interpretations founded on biomarkers with $\delta^{13}C_{org}$, and to a lesser extent, $\delta^{15}N_{bulk}$.

3.3.2 Biomarker inventory

A diverse suite of metalloporphyrins, tocol derivatives, and a C_{40} aromatic carotenoid were detected in all three analyzed intervals (Figures 3-4, 3-5, 3-6, Table 3-1; see Appendix for structures), with each interval referenced as an abbreviation of the hosted bentonite. Metalloporphyrins were composed of VO-, Ni-, and Fe-porphyrins; tocol derivatives include α- and γ-tocopherol (summed and referred to as 'tocopherols'), tri- and dimethylphytylbenzoquinones (summed and referred to as 'MPBQs'), and tri- and dimethyltridecylchromans (summed and referred to as 'MTTCs'); and the identified C_{40} aromatic carotenoid was isorenieratane. Summation of tocol derivatives was justified based on relatively consistent, positive relationships between structurally similar compounds over the three studied bentonite intervals (Figure 3-7). More specifically, VO-porphyrins included both deoxophylloerythroetioporphyrin (DPEP) and bicycloalkanoporphyrin (BiCAP) configurations, and Ni- and Fe-porphyrins included etioporphyrins (ETIO) in addition to DPEP and BiCAP structures. Overall, metalloporphyrins were the most abundant biomarker class, excluding the heavily bioturbated limestones preceding the BB which exhibited relatively low metalloporphyrin concentrations compared to tocol derivatives, specifically the MPBQs (Figure 3-8). Metalloporphyrins were chelated to VO, Ni, and Fe, with Ni-porphyrins dominant in the UBI and pre-ash BBI samples, while Fe-porphyrins and

VO-porphyrins predominated metalloporphyrin distributions in the XBI and post-ash BBI, respectively. Tocopherols and isorenieratane were present in relatively low abundances, with much higher isorenieratane concentrations observed across the UBI (Table 3-1). Both MPBQs and MTTCs comprised a significantly greater portion of the biomarker inventory detected across the BBI compared to the XBI and UBI (Figure 3-8).

3.3.3 Stratigraphic trends of geochemical proxy data

Measured TOC, $\delta^{13}C_{org}$, and $\delta^{15}N_{bulk}$ values were relatively comparable before and after ash deposition in the UBI, excluding anomalously organic-rich (21.5 wt.% at 328.89 m) and organic-lean (0.70 wt.% at 328.78 m) samples before and within the UB (Figure 3-3). The low TOC sample, UBI-8B, also displayed the most depleted $\delta^{13}C_{org}$ and $\delta^{15}N_{bulk}$ values. Note that sample UBI-8B (328.78 m) lies within the gradational contact between the UB and overlying black calcareous claystone, with sample UBI-8A (328.77 m) capturing the completed transition to pre-bentonite lithofacies (Figure 3-2). Metalloporphyrins exhibited similar temporal behavior. Concentrations of Ni- and Fe-porphyrins generally increased towards the bentonite layer, where maxima were observed in Ni- and Fe-porphyrin profiles, followed by a subsequent decline (Figure 3-9). VO-Porphyrins did not exhibit a systematic increase prior to the ash bed, but closely mirrored the post-bentonite behavior of Ni- and Fe-porphyrin profiles. Rising isorenieratane, tocopherols, and MPBQs concentrations abruptly dropped within the UB, but recovered after ash deposition ceased. The MTTCs closely followed the MPBQs, but did not display any systematic changes across the UB (Figure 3-9). No major shifts in biomarker fractional abundances were observed in the UBI (Figure 3-8).

A slight decrease in TOC values (0.55 wt.%) between pre-XB and post-XB samples was observed. Strata adjacent to the bentonite layer exhibited lower TOC and $\delta^{13}C_{org}$ values, especially

the *Ostrea* calcareous concretion layer (Sample XBI-9A, TOC = 0.15 wt.%, $\delta^{13}C_{org}$ = -27.74 $^{0}/_{00}$ at 318.80 m) above the gradational contact of the XB (Figure 3-3, Table 3-1). However, detectable biomarker distributions were recovered from this organically lean layer to constrain the immediate microbial ecological response to ash deposition. Minimal differences in metalloporphyrin concentrations were observed before and after the XB, but concentrations did abruptly increase within the *Ostrea* calcareous concretion and Ni-porphyrins precipitously rose at the onset of XB deposition captured by sample XBI-14A (Figure 3-9, Table 3-1). Significantly, this sample captured the gradational contact transitioning from black, organic-rich calcareous muds to the XB (Figure 3-2). Isorenieratane concentrations, relatively high prior to the ash deposition, displayed a marked decrease across the XB and only intermittently returned to comparable levels in post-XB samples. The MPBQs and MTTCs exhibited minimal variation in the XBI, but tocopherol concentrations did begin to decrease prior to and through the XB, followed by a progressive increase sustained well after the cessation of ash deposition (Figure 3-9). Examination of fractional abundances across the XBI revealed a relative increase in Fe-porphyrins in post-XB samples, which were also characterized by a subtle relative decrease in MPBQs and MTTCs contributions (Figure 3-8).

The BBI yielded the most variability in geochemical proxy data which, as previously described, was coincident with a distinct lithology change across the BB. Heavily bioturbated limestones preceding the BB were characterized by low TOC values (TOC_{avg} = 0.51 wt.%), while the overlying marlstones were relatively organic-rich (TOC_{avg} = 4.00 wt.%, Table 3-1). A slight enrichment in $\delta^{13}C_{org}$ was observed in the marlstone facies (+0.75 $^{0}/_{00}$, Figure 3-3). Overall, biomarker concentrations exhibited similar contrast across the BBI, highlighted by a marked shift in biomarker fractional abundances (Figure 3-8). Metalloporphyrins and tocol derivatives

increased in post-BB samples, but isorenieratane did not exhibit any systematic change throughout the BBI. It should be noted isorenieratane concentrations were very low, making it challenging to interpret the observed variations in the BBI (Figure 3-9).

3.4 Discussion

3.4.1 Determination of eruption magnitude

Estimating the relative magnitude of each eruption responsible for bentonite deposition is critical to constrain comparisons of the ensuing biotic response and environmental impact(s) between individual bentonites, as well as recent eruptions (e.g. 1991 Mount Pinatubo eruption). Although our approach is quasi-quantitative, it provided a means to assess the destabilization potential of individual eruptions and investigate possible relationships between eruption magnitude and perturbation severity. We employed the Volcanic Explosivity Index (VEI) to gauge eruption magnitude, using the most reliable criterion to calculate VEI (i.e. volume of ejecta) as other parameters were unable to be confidently calculated given these events occurred millions of years ago (Figure 3-10; Newhall and Self, 1982). A volume of ejecta minimum was determined for individual bentonite layers, interpreted as a single event or multiple events in swift succession due to the uninterrupted ash deposition observed in the RKB core, by multiplying the present-day compacted thickness at the RKB core by the known or projected areal extent. A 'maximum' estimate assumed a skewed unimodal distribution of bentonite thickness, more representative of the spatial character of ash thicknesses sourced from the western Cordillera assuming minimal submarine redistribution.

The VEI of the UB (VEI_{UB}) was the most challenging interval to quantify due to significant uncertainties surrounding the areal extent. The UB was also the thinnest bentonite, ~2 cm in the RKB core (Figure 3-2; Dean et al., 1995). Thus, based on thickness alone and assuming invariant

compaction between bentonites, the UB is likely the product of the smallest eruption in this study. However, this assumes the proximity of the RKB core to the eruption site(s) and other processes (e.g. paleowind direction) were temporally static. Consistent age dates between proximal bentonite beds, including the XB ($^{206}Pb/^{238}U$ = 95.80 ± 0.092 Ma; Eldrett et al., 2015b) and BB ($^{206}Pb/^{238}U$ = 94.33 ± 0.15 Ma; Eldrett et al., 2015b), and Cordilleran batholiths (e.g. Peninsular Ranges and Idaho batholiths; Kimbrough et al., 2001; Unruh et al., 2008; May et al., 2013), suggest ash provenance was relatively unchanged over the relatively narrow time interval analyzed. Additional compositional analyses and isopach mapping of bentonites has centered on the Idaho batholith as the likely provenance of Cenomanian-Turonian ash beds (Figure 3-1; Kauffman, 1977; Elder, 1988; Hannon and Huff, 2019; Hannon et al., 2020), with mapping efforts revealing relatively consistent areal distributions in bentonite thicknesses indicative of persistent prevailing paleowind patterns (Elder, 1988; Cadrin et al., 1995). While uncertainties do persist, the key presumptions of a consistent source region, ash distribution by eolian transport, relatively unchanged proximity to the source region, and minimal aqueous reworking inferred from the depositional setting of the RKB core are not unfounded and provide a framework to assess estimates of eruptive magnitude. Given the UB was significantly thinner than the XB or BB, and the assumption that proximity to the source region was unchanged, we presumed the UB represented a smaller volcanic eruption. Alternatively, it may also reflect derivation from a batholith spatially distinct from the Idaho batholith (e.g. Peninsular Ranges) or transport-induced biases leading to thinner ash deposits. It is difficult to assess and associate provenance contrasts with bentonite thickness, and is beyond the scope of this work to clearly define bentonite origin. As a result, a consistent source is a key assumption of this comparison and should be considered when interpreting paleoenvironmental fluctuations bounding the UB, XB, and BB. Isopach maps for bentonite marker beds A, B, C, and

D (Elder, 1988) aided areal extrapolation from the RKB, which marked the eastern limit of UB deposition. It is likely the UB extended to the western margin of the WIS, and covered a significant portion of the USA WIS west of the RKB, spanning from the southern WIS in Texas to the southern third of Alberta, Saskatchewan and Manitoba, Canada. This yielded an area of ~750,000 km^2, producing a minimum VEI_{UB} based on ejecta volume (10^9 m^3) of 4-5 (Figure 3-10).

Determination of the minimum VEI of the XB (VEI_{XB}) and BB (VEI_{BB}) involved less uncertainty surrounding geographic extents, with the XB and BB widely used marker beds in chronostratigraphic correlations across the WIS (e.g. Obradovich et al., 1993; Arthur and Sageman, 1994; Gale et al., 2008; Eldrett et al., 2015b). Both ash deposits generally thicken west to the Cordillera and exhibit a range of thicknesses between 3-100 cm for the XB (Cadrin et al., 1995) and 4-90 cm for the BB (Elder, 1988). The areal extents of the XB are greater than the BB based on published data, both spanning the southern opening of the WIS to well beyond the USA-Canada border. It is likely the BB extended to comparable northern latitudes as the XB (e.g. central Saskatchewan; Cadrin et al., 1995) based on the inferred origination from the Idaho batholith (Elder, 1988), but a lack of reported occurrences in this region precluded confident delineation of the northward extents of BB deposition. Longitudinal constraints on the XB and BB reveal both extended across a significant portion of the WIS. Thus, the XB and BB cover ~4 and ~3 million km^2, respectively. Assuming a ubiquitous thickness as observed at the RKB core (XB = 8 cm, BB = 8.5 cm; Dean et al., 1995), both bentonites were produced by eruptions of minimally 10^{10} m^3 of ash, equivalent to a minimum VEI estimate of 5 or 6 (Figure 3-10).

Two maximum estimates were derived using an idealized skewed unimodal distribution of bentonite thicknesses across the estimated depositional areas, supported by models for volcanic ash deposition and bentonite formation (e.g. Slaughter and Hamil, 1970; Carey and Sparks, 1986).

Appreciable uncertainty surrounding the spatial extents and thickness variability of UB led to the exclusion of the UB for this exercise. Present day thicknesses of 10, 25, 50, 70, 80, 90, and 100 cm were assigned to 50, 25, 12.5, 6.25, 3.12, 1.55, and 0.755% of the total areas previously outlined for the XB and BB. A minimum thickness of 10 cm was used based on isopach maps illustrating the majority of the WIS falls within the 10 cm contour for BB (Elder, 1988), which was extended to the XB based on comparable provenance histories and thicknesses at the RKB core. This yielded maximum ejecta volumes of 10^{11} and 10^{10} m^3 for the XB and BB, equivalent to a maximum VEI_{XB} of 6-7 and VEI_{BB} of 5-6. For context of recent volcanic eruptions, see Newhall and Self (1982; e.g. 1991 Mount Pinatubo was a VEI of 6). However, a true maximum estimate of VEI would include decompaction of the present-day bentonite thicknesses, further increasing the ejecta volume and potentially raising the maximum VEIs by 1 for each bentonite. This still likely does not represent an accurate depiction of eruption magnitude due to the probable ash fall beyond the WIS blanketing terrestrial environments poorly preserved in the geologic record. Regardless, VEI estimates of 5-7 are consistent with the tectonic regime of region. This VEI range is typically characterized by eruption column heights between 10 to greater than 25km above sea level (Newhall and Self, 1982), in agreement with the likely explosive, relatively silicic eruptions associated with subduction zone volcanism. Stratospheric tephra injection may also explain the expansive deposition of the XB and BB, which appear to be depositional remnants of extremely large volcanic eruptions. For context, only 4 recorded eruptions over the past half millennium have exceeded a VEI of 5 (Newhall and Self, 1982)

In summary, the bentonite intervals were produced by eruptions of varying scale. The UB represents the smallest eruption, but is shrouded in greater uncertainty than the XB and BB so estimates may be larger or smaller depending on the true areal extent of the UB. Both the XB and

BB were generated by significant volcanic event(s) of comparable magnitudes, which provided an opportunity to determine if the paleoenvironmental effects of eruptions were not solely a function of eruption magnitude. Later discussion will leverage these estimated VEIs to compare the reconstructed biogeochemical response to Cenomanian volcanism in the WIS to recent eruptions and attendant impacts.

3.4.2 Biotic impacts

Biomarkers enable a direct assessment of the marine microbial ecological response to subaerial volcanic ash deposition. These compounds may be simply thought of as molecular fossils of microbial life, which possess variable levels of diagnosticity to specific organisms and/or environmental conditions. For example, the presence of isorenieratane, detected in most RKB samples, in ancient sediments and rocks is frequently interpreted as an indicative marker for hydrogen sulfide (H_2S) in the euphotic zone (i.e. photic zone euxinia, PZE; Summons and Powell, 1987; Cui et al., 2020). This association stems from the diagenetic production of isorenieratane from isorenieratene, a biological pigment predominantly synthesized by the obligately anerobic *Chlorobiaceae* (anoxygenic phototrophic sulfur bacteria) that require both H_2S and light (i.e. PZE) to sustain metabolic function (Liaaen-Jensen et al., 1964; Imhoff, 1995; Frigaard and Dahl, 2009). In addition to isorenieratane, the metalloporphyrins and tocol derivatives complete the biomarker inventory detected via LC-qTOF-MS in the RKB core (Figures 3-4, 3-5, 3-6). Metalloporphyrins may provide a record of paleoproductivity if other environmental factors can be constrained (e.g. redox), as these tetrapyrroles represent fossil chlorophylls present in all photoautotrophs at the time of deposition (Callot et al., 1990; Sundararaman et al., 1993; Junium et al., 2015). However, metalloporphyrins are sensitive to redox variations at the sediment-water interface (SWI) that govern metal availability, ultimately affecting metal chelation to the precursor free bases and the

specific metalloporphyrins formed (Junium et al., 2015). If free base porphyrins are quantitatively converted to metalloporphyrins, leaving little to no free bases available for incorporation into the kerogen during diagenesis, then it is possible metalloporphyrin concentrations may correlate with primary production if processes biasing free base preservation are minimized (e.g. oxidation). Thus, evolving chemical states in the water column must be considered to disentangle the influences of primary productivity and redox on metalloporphyrin stratigraphic variations. Tocol derivatives, comprised of tocopherols, MPBQS, and MTTCs, may be linked to all photosynthetic organisms given the critical antioxidant function tocopherols perform in mitigating oxidative damage (Muñoz and Munné-Bosch, 2019, and references therein). However, recent work has highlighted the potential utility of tocol derivatives as proxies monitoring pelagic, potentially euphotic, redox shifts and/or the phytoplanktonic stress response to challenging environmental conditions if redox changes were relatively minimal over time (Chapter 2). Thus from a biotic perspective, the detected biomarker inventory enabled reconstruction of fluctuations in oxygenic and anoxygenic primary production, as well as the potential phytoplanktonic stress response to volcanic ash deposition. Volcanically induced environmental effects and changes (e.g. PZE) derived from biomarker proxy data will be discussed in Section 3.4.3.

Overall, the sudden introduction of [potentially] nutrient-laden volcanic ash induced biotic perturbations of varying extents and durations. The UBI, likely subjected to the smallest eruption in this study, exhibited a subtle, transient increase in primary production that was unsustained beyond the bentonite interval. It is challenging to discern if this was solely an artifact of ash deposition, as progressively increasing metalloporphyrin concentrations before the UB suggested that a sustained, gradual increase in productivity began well before any potential allochthonous nutrient delivery (Figure 3-9). Unlike the UBI, the XBI and BBI were characterized by abrupt,

large increases in primary production that collapsed after XB deposition, but were sustained following the eruption forming the BB. Recall, both the XB and BB were likely products of massive eruptive events. However, the pronounced lithology contrast in the BBI hampered confident interpretation of biomarker concentrations, including the metalloporphyrins, despite an attempt to minimize preservation biases by normalizing biomarkers to organic carbon. Further discussion surrounding the BBI will assume a predominantly paleoenvironmental signal was preserved, but alternative explanations for biomarker distributions should be considered and will be highlighted as needed. Despite the large eruption magnitude affecting the XBI, effects on primary production were relatively short-lived. Both pre- and post-XB strata were characterized by similar, nearly constant metalloporphyrin concentrations indicative of temporally invariant levels of primary production (Figure 3-9). Consistent lithofacies before and after the XB also granted confidence biomarkers faithfully recorded a paleoenvironmental signal and were minimally affected by secondary processes governing compound preservation. Thus, the XBI represented the most promising interval of those studied as it was characterized by unchanged lithologies bounding the bentonite interval, similar to the UBI, but also was subjected to a potentially massive volcanic eruption, like the BBI. The onset of the XB was marked by a slight increase in metalloporphyrin concentrations, which greatly increased just after XB gradational contact, indicative of a rapid increase in primary production in the immediate aftermath of the ash deposition. This perturbation was short-lived based on the precipitous decline of metalloporphyrin concentrations in the overlying sample, only 1.5 cm above, which were relatively constant for the remainder of the XBI (Figure 3-9). The period between the onset and termination of the XB could not be constrained due to inadequate organic carbon contents for biomarker analysis within most of the bentonite, which also affected BB samples. Unlike the XBI, the BBI displayed sustainment

of heightened metalloporphyrin concentrations in post-ash strata (Figure 3-9), signaling the potential long-term impact of volcanic ash on stimulating and supporting elevated rates of primary production. However, it is important to consider the enhanced shuttling of organic molecules via clay particles (Kennedy et al., 2002) and greater orbital forcings (e.g. Eldrett et al., 2015a), which comprised a defining difference between the relatively more siliciclastic marlstones succeeding the underlying limestones preceding the BB. Previous work has attributed limestone-marlstone cycles to Milankovitch-driven variations in solar insolation, which ultimately impacted latitudinal energy gradients and climate captured by lithology contrasts (Eldrett et al., 2015a). Interpretations of enhanced primary production during marlstone, relative to limestone, deposition are consistent with prior palynological reconstructions of paleoproductivity in the WIS (Eldrett et al., 2015a). Still, extensive bioturbation in the limestones likely compromised organic carbon preservation, including biomarkers. While the lithology contrast across the BBI complicated biomarker interpretations prone to diagenetic alteration, it did provide stark evidence for paleoenvironmental change coincident with BB deposition. However, it is challenging to disentangle volcanogenic effects from overriding processes (e.g. orbital cycles; Eldrett et al., 2015a), which should be considered during further discussion of the BBI. This does not necessarily apply to the UBI and XBI given the consistent lithologies bounding both bentonites, which reduced the possible influence of additional climate forcings that could dilute effects stemming from subaerial volcanic eruptions.

The predominantly transient increases in primary production coincident with volcanic ash introduction in the WIS were consistent with previous reports of ash impacts on marine phytoplankton (e.g. Uematsu et al., 2004; Duggen et al., 2007; Zhang et al., 2017), as well as the depositional setting of the studied intervals. Anticorrelation of isorenieratane with abrupt increases

in metalloporphyrin concentrations in the UBI and XBI provides further, indirect evidence substantiating brief periods of elevated primary production. The green sulfur bacteria, tracked using stratigraphic variations in isorenieratane concentrations, likely inhabited the lower regions of the euphotic zone beneath the overlying oxygenic photoautotrophs. Development of a thick, oxygenic photoautotrophic plate likely inhibited light penetration, decreasing light intensities and adversely impacting the anoxygenic phototrophs (Figure 3-11) reflected by the observed decline in isorenieratane concentrations (Figure 3-9). Short-term stimulation of primary production was likely an artifact of the rapid leaching of bioessential nutrients (e.g. Fe) when ash contacted seawater (Frogner et al., 2001; Delmelle et al., 2007), while it is possible eolian transport induced premature Fe extraction prior to deposition (Jones and Gislason, 2008) that stifled the protracted fertilization of the euphotic zone and produced the transient spikes in primary productivity observed. Alternatively, unfavorable chemical conditions in the eruption plume and atmosphere may have limited Fe mobilization by affecting Fe solubility (Cwiertny et al., 2008; Maters et al., 2016), confining nutrient leaching to early diagenesis (Lee et al., 2018). While short residence times of volcanic ash in the euphotic zone (minutes to days; Obradovich and Cobban, 1975; Duggen et al., 2007) favor nearly instantaneous release of nutrients to increase primary productivity (Frogner et al., 2001), it is possible that upwelling of Fe released during diagenesis could produce a similar effect. However, the shallow paleodepths (Hay et al., 1993; Goswami et al., 2018) and modeled wind field (Slingerland et al., 1996) challenge the presence of extensive upwelling in the eastern half of the WIS during the Cenomanian, as do the stratigraphic trends in metalloporphyrin concentrations. The acute productivity rise inferred from abrupt increases in metalloporphyrin concentrations in the XBI, BBI, and to a lesser extent, UBI (Figure 3-9), appear more indicative of rapid nutrient leaching in the euphotic zone than progressive disassociation of

nutrients from mineral phases during early diagenesis, which are subsequently upwelled. The latter scenario would produce a protracted period of mildly elevated primary productivity, which was not observed for any of the studied intervals. Thus, the reconstructed marine biotic response to proximal eruptions in the Cenomanian (Figure 3-11) aligns relatively well with established processes governing the delivery, mobilization, and extraction of nutrients from volcanic ash.

Although volcanic ash is widely posited as a probable stimulant enhancing primary production in certain marine systems (e.g. Spirakis, 1991; Duggen et al., 2007; Cather et al., 2009; Langmann et al., 2010; Olgun et al., 2011; Zeng et al., 2018), it hosts a variety of potentially toxic metals (e.g. Cu^{2+}) that may undermine any beneficial effects on phytoplanktonic communities (Jones and Gislason, 2008; Hoffmann et al., 2012). The abrupt introduction of metal-laden ash may induce oxidative stress (Valko et al., 2005), eliciting heightened production of antioxidants, such as the tocopherols, to mitigate cellular damage. Greater sensitivity to heavy metals by tocopherol-deficient mutants has underlined the potential role tocopherols serve in this process (Collin et al., 2008; Jin and Daniell, 2014), but application of tocopherols in deep time to assess a phytoplanktonic stress response is challenging. Disentangling metal-induced stress from other factors is nearly impossible, compounded by potential redox controls on tocopherol distributions (Chapter 2). While speculative, the tocopherols and potential derivatives, as well as tocol derivative ratios, will be discussed given their relevance to the biotic impacts of volcanic eruptions and to further constrain paleoenvironmental significance. However, the BBI will be omitted given the stark lithofacies contrast before and after the BB potentially biasing tocopherol preservation.

Consistent lithofacies bounding the UB and XB may reflect minimal redox influences on tocol derivative distributions, which have been demonstrated to possibly reflect the phytoplanktonic stress response to adverse environmental conditions if redox conditions remain

relatively static (Chapter 2). Tocopherol concentrations and tocol derivative ratios decreased through both the UB and XB (Figures 3-9 & 3-12), potentially indicative of lessened oxidative stress if this region of the WIS was iron limited during deposition. The RKB core, in the east central WIS (Figure 3-1), was relatively distal from the predominant riverine inputs in the west as well as the lesser tributaries along the eastern margin. Minimal iron delivery via riverine input, combined with documented iron limitation in the WIS during Oceanic Anoxic Event 3 (Tessin et al., 2016), suggests it was plausible iron limited conditions bounded bentonite intervals in this study. Furthermore, iron limitation induces enhanced reactive oxygen species production (Schoffman et al,. 2016), which may stimulate tocopherol synthesis to minimize oxidative damage of cellular components. The sudden delivery of nutrients (e.g. Fe) is supported by the coincident increases in primary production previously outlined, which also potentially alleviated oxidative stress tied to nutrient shortages and relaxed antioxidant (i.e. tocopherol) requirements, producing the transiently lower tocopherol concentrations observed within and adjacent to ash beds (Figure 3-9). While purely speculative, the lack of an increase in tocopherol concentrations coeval with ash deposition suggests minimal toxic effects associated with heavy metals transpired. Tocopherol concentrations and tocol derivative ratios rapidly rebounded to pre-UB levels in the UBI, but exhibited a progressive recovery following XB deposition. This may be an artifact of eruption magnitude (Figure 3-10), with the XB produced by a significantly larger volcanic event capable of destabilizing the environment for an extended period. The gradual increase in tocopherols and tocol derivative ratios in post-XB samples, if presumed to primarily reflect a stress response, signify a protracted return to pre-XB environmental conditions (e.g. iron limited). However, it is challenging to confidently extract any significance from this trend as other tocol derivatives (e.g. MPBQs, MTTCs) remain relatively unchanged and no other geochemical proxies in this study

display comparable stratigraphic behavior following the XB. In fact, tocol derivatives could reflect a compositional shift in primary producers, as tocopherol levels are not ubiquitous among phytoplankton (Haubner et al., 2014). Lack of sterane trifecta and algae-specific steroids precluded further assessment of this possibility, which is plausible given the inherent stress calcifying organisms may experience when voluminous amounts of ash [potentially] alter water chemistry (Jones and Gislason, 2008; Hoffmann et al., 2012). While some insight may be gleaned from application of tocol derivatives as a phytoplanktonic stress proxy in this study, the lack of persistent, highly reducing conditions undermines comparable application of these compounds as demonstrated elsewhere (Chapter 2) and renders tocol derivatives as primarily redox proxies in this study.

Before transitioning to the chemical effects of volcanic ash on the marine water column, the potential biotic effects of ash deposition across the BBI will be discussed. Lithology contrasts imparted distinct geochemical differences in the heavily bioturbated limestones underlying the BB and overlying organic-rich marlstones. This compromised biomarker interpretations to an extent, but allying the obvious stratigraphic changes with known eruptive effects on marine systems affords an opportunity to reconstruct potential biotic impacts of the BB eruption(s). As previously mentioned, the BBI captures an orbitally forced climatic shift induced by changes in solar insolation manifested as a rapid transition from limestone to marlstones (Eldrett et al., 2015a). However, the lithofacies change was directly coincident with a major eruption (i.e. the BB, Figure 3-2) that possibly exacerbated or accelerated oceanographic changes driven by orbital cycles. Cessation of limestone deposition following the BB may reflect a compositional shift in marine biota associated with volcanic ash introduction. Development of relatively acidic conditions in the euphotic zone affecting $CaCO_3$ saturation and polymorphs (aragonite and calcite), combined with

[potentially] toxic elements (Jones and Gislason, 2008), may have adversely affected calcifying organisms and produced the abrupt lithologic shift across the BB from limestones to marlstones. Laboratory culture experiments of diatoms and coccolithophores substantiate these claims, as diatoms exhibited higher growth rates after exposure to volcanic ash while coccolithophores were negatively impacted (Hoffmann et al., 2012). While beyond the scope of this study, future work will attempt to leverage more specific proxies (e.g. algal-specific steroids) to assess this possibility.

3.4.3 Effects on water column chemistry

Reconstruction of redox behavior concurrent with ash deposition revealed irreversible, fundamental alterations to water chemistry in specific regions of the water column for the two largest eruptions. Eruption magnitude was relatively proportional to the persistence and severity of the subsequent environmental perturbation, which was predominantly confined to deep water habitats near or within the SWI. Multiple biomarker proxies enabled specific regions of the water column to be simultaneously assessed for temporal redox changes potentially induced by volcanic eruptions. The ratio of VO- to Ni-metalloporphyrins (VO/Ni-por, VO-porphyrins/(VO-+Ni-porphyrins) was employed to monitor redox shifts near and within the SWI, leveraging the reactivity of Ni with sulfides and complexation of VO with free base porphyrins under reducing conditions to infer temporal redox variations (Lewan, 1984; Breit and Wanty, 1991). Ratios of the ETIO to DPEP porphyrin configurations tracked the relative oxicity of the pelagic water column to SWI. Oxidative degradation of chlorophylls and associated breakdown products will produce ETIO precursors, resulting in greater ETIO/DPEP values in sediments and rocks (Seely, 1966; Baker and Louda, 1983; Louda et al., 2011). Note that ETIO/DPEP values may be sensitive to thermal alteration for a variety of reasons (e.g. conversion of DPEP to ETIO porphyrins, greater thermal stability of ETIO porphyrins, preferential release of ETIO porphyrins from the kerogen

under thermal stress; Burkova et al., 1980; Barwise and Roberts, 1984; Sundararaman and Moldowan, 1993), but the narrow sampling window of intervals in this study precluded major contrasts in thermal maturity. Additionally, the shallow maximum burial depths of the Cenomanian strata in the RKB core (Dean et al., 1995) minimized the risk for thermal alteration of the indigenous environmental signal. The presence and fluctuation of isorenieratane granted insight into PZE (Summons and Powell, 1987), while tocol derivative concentrations and ratios refined interpretations of shallow water anoxia/euxinia (Chapter 2). All ratio data may be found in Table 3-2.

Marked and sustained shifts to more reducing, potentially euxinic conditions near or within the SWI occurred after deposition of the XB and BB based on abrupt increases in VO/Ni-por values (Figure 3-12). However, no pronounced change was observed across the UBI, which was defined by progressively declining VO/Ni-por values well before the UB and relatively invariant values in post-UB samples. This suggests ash deposition imposed minimal changes on bottom water redox within the UBI, which became increasingly less reducing leading into and after the UB. These findings are in relative agreement with study of bottom water redox shifts in marine settings proximal to recent eruptions. The thickness of ash deposits, as well as total Fe and bioavailable Fe (i.e. Fe^{II}/Fe^{III}), imposes direct effects on sedimentary oxygen penetration depths primarily through oxidation of silicate bound Fe^{II} (White and Yee, 1985; Haeckel et al., 2001; Hembury et al., 2012). Although Fe speciation data are currently unavailable (will be integrated with these results later) the thickness, and by extension eruption magnitude, of individual ash beds in this study and others of recent comparable eruptions (e.g. Mt. Pinatubo, VEI of 6; Newhall and Self, 1982; Hembury et al., 2012) appears to correlate with bottom water redox as well. The thinnest ash layer, the UB, had no discernible effects on pore water oxygenation, while the thicker

bentonites, XB and BB, imposed lasting deoxygenation of the SWI. A fundamental shift in bottom water redox to anoxia/euxinia may explain the lack of continued enhanced primary productivity beyond initial ash deposition. Enhanced sulfide levels likely reacted with dissolution of silicate-bound Fe^{II} forming pyrite, while the Fe^{II} that was oxidized to Fe^{III} during settling was incorporated into organic complexes such as the Fe-porphyrins. Note that the Fe ions which chelate to free base porphyrins are trivalent Fe^{III}. This may explain the marked increase in Fe-porphyrin fractional abundances in post-XB strata (Figure 3-8). Therefore, iron leaching during early diagenesis (Lee et al., 2018) may have occurred, but was inadequately transported to the euphotic zone to sustain high rates of primary production. While speculative, the transient spikes in primary productivity [theoretically] led to elevated organic carbon remineralization, which when combined with oxidation of chemical species in the ash, may have been sufficient to destabilize water column redox for a protracted period whereby sulfate reducing bacteria were able to colonize the SWI and perpetuate euxinia well beyond the primary eruption. Similar associations between euxinia and volcanic eruptions are reported for the Cretaceous (e.g. Owens et al., 2013; Zeng et al., 2018) and throughout the Phanerozoic (e.g. Shen et al., 2016; Broda et al., 2019), with volcanism even proposed as the principal external cause of euxinia (Meyer and Kump, 2008). More work is required to delineate the causal process(es) leading from volcanism to sustained marine euxinia in specific marine settings, but findings presented here substantiate a temporal link between the two environmental phenomena. Further examination of redox shifts beyond the SWI may provide insight into the extent of environmental perturbations induced by volcanism in the Cenomanian WIS.

Brief decreases in predominantly static ETIO/DPEP values were concurrent with the UB and XB, likely byproducts of abrupt increases in primary productivity inducing transiently greater

oxygen demand for organic carbon remineralization (Figure 3-12). A permanent shift to lower ETIO/DPEP values across the BB, indicative of lowered water column oxicity, aligns with the transition from heavily bioturbated limestones to slightly bioturbated and laminated marlstones, in addition to the VO/Ni-por proxy. The ubiquitous presence of isorenieratane in all UBI and XBI samples, as well as most BBI samples, underlines the persistence of PZE throughout the studied intervals. Variations in exceedingly low isorenieratane concentrations across the BBI prevents confident temporal interpretations of PZE, but the UBI and XBI will be discussed. A brief drop in isorenieratane concentrations within the UB is synchronous with similar declines in ETIO/DPEP, tocopherols, and tocol derivative ratios, which is accompanied by increases in Ni- and Fe-metalloporphyrin profiles interpreted as short-lived productivity spikes (Figures 3-9 & 3-12). Increased turbidity associated with large volumes of volcanic ash precipitating through the water column combined with a dense, thriving plate of oxygenic photoautotrophs likely inhibited adequate light intensities from reaching the chemocline, adversely affecting the *Chlorobiaceae* and leading to decreased isorenieratane concentrations. Alternatively, enhanced sedimentation rates of organically lean ash diluted isorenieratane and tocopherol concentrations within the UB. However, concomitant drops in tocol derivative ratios, indicative of retreating anoxic-euxinic waters from the photic zone, support a temporary decline in *Chlorobiaceae* populations. Thus, it seems the pelagic anoxic/euxinic waters temporarily migrated to deeper depths, but did not impact bottom water conditions, during UB deposition. In addition, the tocol derivative ratios appear to primarily record pelagic redox fluctuations near the euphotic zone based on stratigraphic similarities with isorenieratane in the UBI and XBI (Figures 3-9 & 3-12).

Unlike the UBI, isorenieratane concentrations did not return to pre-ash levels in the XBI despite evidence for expanded bottom water anoxia/euxinia (e.g. VO/Ni-por). While tocopherol

concentrations and tocol derivative ratios track the isorenieratane profile initially, a departure from this covariation in post-XB samples (where isorenieratane remains relatively low and tocopherols and tocol derivative ratios progressively rise) reflects shoaling anoxic, but not euxinic, waters (Figures 3-9 & 3-12). Otherwise, phototrophic sulfur bacteria may be more sensitive to volcanic ash and recover over longer timescales uncaptured by the narrow stratigraphic window analyzed. Another possibility involves pelagic sulfide depletion via reactions with volcanic ash (e.g. $Fe^{II}S + H_2S \rightarrow Fe^{II}S_2 + H_2$; Rickard and Luther, 2007), leading to inorganic competition for H_2S that negatively impacted the phototrophic sulfur bacteria. Regardless of the mechanism by which PZE was altered, the volcanic eruption producing the XB fundamentally altered redox conditions throughout the entire water column to varying extents. While the bottom waters transitioned from an oxic-suboxic state to anoxic-euxinic, the intermediate and near-surface waters below the oxygenated surface layer became less euxinic but remained anoxic. Interestingly, this means the XBI was defined by variable redox states in space and time that were perturbed by a massive volcanic eruption (Figure 3-11).

The redox evolution across the BBI was similarly affected by, or at least coincident with, ash deposition. However, a key difference between the BBI and XBI was that redox shifts within the BBI varied in time, but were consistent in vertical space. Post-BB samples record an abrupt transition to euxinia near the SWI, highlighted by a pronounced shift in VO/Ni-por values, which were also characterized by a vertical expansion of anoxic/euxinic conditions to the lower euphotic zone. The continued presence of isorenieratane, albeit detected in low concentrations, confirms the presence of PZE, but the marked shifts in ETIO/DPEP values and tocol derivative concentrations and ratios highlight an appreciable expansion of reducing conditions well above the SWI in post-BB samples (Figures 3-9 & 3-12). This interpretation leverages the lability of chlorophylls and

tocopherols in the water column, where they are prone to rapid abiotic and biotic degradation (Louda et al., 2000; Mawson and Keely, 2008; Nassiry et al., 2009; Rontani et al., 2010). Thus, a relative decrease in chlorophyll oxidation products (i.e. ETIO porphyrins) and increases in the absolute abundance of tocopherols, as well as their abundance relative to degradation products (i.e. captured by the tocol derivative ratios), is indicative of substantially expanded pelagic anoxia in conjunction with highly reducing bottom waters following BB deposition, similar to the post-ash environment reconstructed across the XBI (Figure 3-11) and previous work on limestone-marlstone cycles (Eldrett et al., 2015a).

3.4.4 Implications for paleoenvironmental and modern study

The reconstructed biotic impacts and chemical effects of proximal volcanism in the WIS were roughly proportional to eruption magnitude (i.e. VEI) inferred from compacted bentonite thickness and areal extents. All eruptions produced transiently increased primary production that was not sustained significantly beyond ash deposition. However, the two major eruptions imparted lasting changes (minimally thousands of years) on water column chemistry spanning the SWI to lower euphotic zone, highlighting the long-term destabilization potential of volcanism on marine environments. While reconstructed short-term effects (e.g. enhanced primary production) were in general agreement with modern reports of volcanogenic impacts (e.g. Fe fertilization), this study highlighted the potentially transient nature of a direct eruptive influence on marine primary production. Thus, continued invocation of volcanism as a causal mechanism for widespread, enhanced organic carbon burial driven by oceanic ash fertilization requires clarification.

Iron fertilization associated with subaerial volcanic eruptions is rooted in conceptual logic (Martin and Fitzwater, 1988; Spirakis, 1991) and observation of recent, major eruptions (e.g. 1991 Mt. Pinatubo, Sarmiento, 1993; Watson, 1997; Langmann et al., 2010). However, the potential

long-term effects of eruptive events are poorly constrained due to a lack of observational data, making the process subject to misapplication. This issue is exacerbated by nearly ubiquitous application of the Fe fertilization concept as a mechanism to produce enhanced carbon burial when volcanic activity and major Earth events (e.g. extinctions, climate change) are contemporaneous, such as OAE-2 (e.g. Lee et al., 2018; Zeng et al., 2018), despite little evidence for stimulated primary productivity in idealized oceanographic regions prone to this phenomenon (e.g. high-nutrient low chlorophyll regions). This is not a significant issue with present day study of iron fertilization, but endemic in many paleoenvironmental reconstructions. Further, predominantly appropriate, associations between volcanism and climate (Bay et al., 2006; Jicha et al., 2009), linked by the ability for intense volcanism to affect the biological carbon pump (e.g. Langmann et al., 2010), exacerbate continued misapplication of Fe fertilization, and by extension volcanism, as the principal trigger inducing protracted periods of heightened primary productivity that destabilized the ocean-atmosphere system across various periods of Earth history. The time interval of this study, the Cenomanian epoch of the Cretaceous period, provides an excellent forum to address this issue amidst the backdrop of our assessment of short- and long-term effects of proximal volcanism on the WIS.

As previously outlined, the WIS was adjacent to active subduction zone volcanism, which is significant when considering the potential fertilization effects of ejected ash. Subduction zone volcanism is relatively explosive compared to hot spot or divergent plate volcanism, capable of stratospheric ash injection that results in extensive coverage and impact by the eruptive plume (Duggen et al., 2010). However, this is offset by inferior reactivity of ash associated with silicic magmas (Jones and Gislason, 2008), which are also predisposed to relatively greater amounts of Fe^{III} relative to Fe^{II} (Hoshyaripour et al., 2014), ultimately affecting the fertilizing potential on

marine phytoplankton. This is further compounded by how Fe solubility is affected within the eruptive plume and atmosphere prior to contact with seawater, which remains enigmatic (e.g. Maters et al., 2017), but may impart considerable effects on fertilization potential by impacting Fe bioavailability. Furthermore, it is challenging to delineate iron limited regions in deep time, which served a greater role in destabilizing the climate system than preexisting, high productivity regions such as coastal shelf environments (e.g. Demerara Rise, ~400 km north of Suriname). These uncertainties have not prevented previous workers from invoking volcanic ash as a key mechanism stimulating primary productivity, and subsequent enhanced organic carbon sequestration, in the Cretaceous period (e.g. Lee et al., 2018; Zeng et al., 2018). While we do not contest the rationale of these propositions, our results necessitate the addition of several contingencies to maintain consistency with the observed biotic response to ash deposition in this study.

It is apparent, based on the results presented here, previous experimental work (e.g. Frogner et al., 2001; Jones and Gislason, 2008; Olgun et al., 2011), and satellite observations (e.g. Duggen et al., 2007; Westberry et al., 2013), that subduction zone volcanism may stimulate phytoplankton growth in susceptible regions. However, few studies (typically of geologically ancient eruptions, e.g. Kuhnt et al., 2005; Perrier et al., 2012) can evaluate long-term trends (10^3 years or more), leading to potentially erroneous interpretations of geochemical proxy data. Our findings demonstrate that volcanic ash led to only temporarily elevated primary production in the WIS. Thus, invocation of volcanic ash as the ultimate driver of enhanced organic carbon burial during OAE-2 requires either hyper-frequent eruptions providing a constant supply of nutrients to marine ecosystems, which is unsubstantiated in the sedimentary record, or fertilization of other regions capable of sustaining elevated productivity well after a major eruption. While the former scenario is unlikely, the latter may account for the presently unconstrained organic carbon burial required

to produce the widely observed positive carbon isotope excursion (+CIE) defining OAE-2 (Scholle and Arthur, 1980; Owens et al., 2018). Concurrent subaerial volcanism, producing not only the BB but also extensive deposition of bentonite marker beds A and C (Elder, 1985; 1988) within the OAE-2 interval (Eldrett et al., 2015b), was previously proposed as a causal mechanism initiating the +CIE and widespread deoxygenation of OAE-2 (Lee et al., 2018). Although the frequency of ash deposition remains inadequate to sustain elevated primary production for the duration of OAE-2 (~600 kyr; Sageman et al., 2006; du Vivier et al., 2015), seeding high-nutrient low chlorophyll regions of the global ocean with nutrient-laden ash beyond the WIS and proto-North Atlantic possibly increased deep ocean organic carbon burial that may account for the 'missing' organic carbon needed to produce the +CIE (Owens et al., 2018). Still, vast regions of the Pacific Ocean remain uncharacterized, and the few studied regions revealed that oxic conditions prevailed (Takashima et al., 2011; Gangl et al., 2019). This, combined with unfavorable paleowind fields transporting ash eastward across North America (Elder, 1988; Slingerland et al., 1996), challenges interpretations reliant on long-term elevations in marine primary production caused by iron fertilization via volcanic ash in the Cretaceous. Acute spikes in primary production, as observed here, rather than a protracted response better align with the established rapid settling rates of volcanic ash (minutes to days; Obradovich and Cobban, 1975; Duggen et al., 2007) and the nearly instantaneous dissolution of acid salts rendering Fe bioavailable (Frogner et al., 2001; Delmelle et al., 2007). Therefore, conceptual reasoning paired with the reconstructed biotic response to volcanic ash deposition in the Cenomanian Western Interior Seaway articulate the transient effects of iron fertilization on primary production, necessitating a reevaluation of past geologic events and refining expectations for future eruptive events.

Volcanism may still indirectly impact primary productivity in the short- and long-term via established feedbacks representing the greater influences of eruptions on climate (e.g. volcanism ↑ → pCO_2 ↑ → temperature ↑ → physical/chemical weathering ↑ → nutrient input ↑ → primary productivity ↑ → deoxygenation ↑), with sustained elevations in primary production likely produced in this manner. We are simply proposing the direct fertilization of marine environments with volcanic ash is a transient process, unable to be sustained without continual renewal of allochthonous nutrients via repeated eruptions, and thus challenging to invoke over long periods of geologic time without circumstantial evidence. In certain instances, Fe fertilization may lower primary production or have no stimulatory effect (e.g. Bishop and Wood, 2009; Costa et al., 2016; Chen et al., 2020), or perturb elemental cycling and create nutrient shortages (e.g. P scavenging; Jones and Gislason, 2008). However, we documented enduring shifts in bottom water redox coevally initiated with ash deposition that may facilitate the enhanced preservation of organic carbon (Figure 3-11). As previously discussed, a 'permanent' transition to anoxic/euxinic bottom waters across the XBI and BBI parallels the deoxygenation observed within ash layers of modern analogs (1991 Mt. Pinatubo; Haeckel et al., 2001; Hembury et al., 2012). Similarly delayed recovery of benthic foraminifera following Ordovician (Perrier et al., 2012) and K/T boundary ash beds (Kuhnt et al., 2005), indicative of persistent bottom water anoxia caused by poor deep-water circulation, mirror post-bentonite reconstructions in this study. Although causal mechanisms are challenging to constrain beyond an association with major eruptions, this seemingly ubiquitous marine redox shift coincident with ash deposition provides a mechanism to enhance organic carbon burial. No significant TOC changes were observed across the analyzed intervals in this study (Figure 3-3, Table 3-1), but organic carbon enrichment in sediments following ash deposition may serve to extensively alter carbon cycling as previously proposed (Hembury et al., 2012). Thus, an

association between subaerial volcanism and enhanced organic carbon burial during specific periods of Earth history may reflect a causal relationship for different reasons (i.e. enhanced preservation) than initially proposed (enhanced productivity via Fe fertilization). More work is needed to disentangle effects of subaerial from submarine volcanism though, as onset of the Caribbean large igneous province (LIP) was relatively coincident with eruptive events in this study (Turgeon and Creaser, 2008; du Vivier et al., 2015), in agreement with the proposed global synchroneity of igneous bodies (Larson, 1991). Submarine release of metal-rich hydrothermal fluids may induce progressive marine deoxygenation (Kerr, 1998) and remove limits on primary production (Sinton and Duncan, 1997). If LIP activity began just before, or was simultaneous with the XB and BB eruptions, then it is possible regional circulation patterns pulling the deoxygenated Tethyan water mass from the proto-Gulf of Mexico into the WIS (Slingerland et al., 1996; Elderbak and Leckie, 2016) induced lasting, regional shifts in bottom water redox that were coincident with, but not directly or solely a product of, subaerial volcanism. Regardless of cause (subaerial and/or submarine volcanism), the delineated transient and persistent impacts on the eastern WIS following major eruptions represent significant perturbations to the marine environment, necessitating further investigation to properly constrain and elucidate the role(s) volcanism serves in climatic evolution. Later acquisition and integration of Fe speciation results over the studied bentonite intervals will enable a direct assessment of temporal changes in iron availability and attendant impacts on primary productivity and water column chemistry.

3.4.5 Reconciliation with bulk stable isotopes

Overall, variations in bulk organic carbon and nitrogen stable isotopes were minimal across all volcanic ash deposits (Figure 3-3). However, abrupt depletions in bulk carbon values were observed immediately after the UB and XB, while a similar negative excursion occurred prior to

the BB. As stated before, the BBI is challenging to interpret owing to the stark contrast in lithologies before and after the BB, likely a product of astronomically driven climate change (Eldrett et al., 2015a), and as a result will be omitted accordingly from this discussion. Consistent, negative excursions in bulk organic carbon isotopes may reflect a multitude of processes aligning with previous reconstruction of the biochemical response to volcanic eruptions. Both negative excursions were coincident with transient increases in primary production and deepening of the chemocline, as well as the onset of intensified bottom water anoxia/euxinia (Figure 3-11). Prior study has attributed negative carbon isotope excursions in $\delta^{13}C_{org}$ to a rapid, voluminous injection of volcanogenic CO_2 into the atmosphere and/or ocean (e.g. Kump and Arthur, 1999). Synchronicity between eruptions, inferred from the presence of bentonites, and depleted $\delta^{13}C_{org}$ values from samples residing in or immediately following ash beds in this study (Figure 3-3), intimates a volcanogenic effect as a potential causal factor for stratigraphic anomalies in $\delta^{13}C_{org}$ profiles. This aligns with the reconstructions of primary production using the metalloporphyrins, with a single eruptive event supported by an isolated spike in productivity and $\delta^{13}C_{org}$ (Figures 3-3 & 3-9). However, direct injection of volcanogenic CO_2 as the principal cause of the negative $\delta^{13}C_{org}$ excursions is unlikely ($\delta^{13}C$ of mantle ~ -5 to -8 $^{0}/_{00}$; Javoy et al., 1986), as additional factors likely contributed to the negative $\delta^{13}C_{org}$ excursions in the UBI and XBI.

Enhanced primary production, interpreted to cooccur with a negative $\delta^{13}C_{org}$ excursion in this study, has previously been attributed to positive carbon isotope excursions in the geologic record (e.g. OAE-2; Scholle and Arthur, 1980). This association stems from the prerequisite heightened organic carbon burial to produce a positive excursion in both organic and inorganic carbon reservoirs, by preferentially sequestering ^{12}C initially, producing a relatively ^{13}C-enriched dissolved inorganic carbon (DIC) pool. Yet, no apparent enrichment in TOC was observed (Figure

3-3) across the UBI or XBI, likely due to the transient nature of the productivity increase and/or dilution effects due to voluminous ash deposition. Thus, the abrupt negative $\delta^{13}C_{org}$ excursion may reflect the transient increase in primary production initially favoring ^{12}C, which produced no subsequent enrichment in the DIC pool given the brevity of the event. Other [potential] explanations for the negative $\delta^{13}C_{org}$ excursion include a compositional change in phytoplankton, with a shift from calcareous to siliceous phytoplankton most likely based on ash-leachate and culture experiments (Jones and Gislason, 2008; Hoffmann et al., 2012) and potentially captured by the delayed recovery of tocol derivative profiles in the XB. The anticipated shift in $\delta^{13}C_{org}$ tied to shifts in primary producer composition, if any, is challenging to constrain and may be slightly positive given the ability for some diatoms to perform C_4 photosynthesis (Reinfelder et al., 2000), although the role of C_4 metabolism in diatom carbon fixation is contentious (Haimovich-Dayan et al., 2012). Consideration of other coincident changes brings the distinct shift in bottom water redox after the XB into focus (Figure 3-11). This likely impacted benthic organisms intolerant to anoxic/euxinic conditions, which may have lessened microbial reworking of organic matter and produced the negative $\delta^{13}C_{org}$ value observed. Indeed, high benthic respiration of precipitating biomass may produce enrichments of 3-4 $^{0}/_{00}$ in $\delta^{13}C_{org}$ (Fischer, 1991), so an attenuation of heterotrophy could produce the negative $\delta^{13}C_{org}$ excursion. However, the sustainment of anoxia/euxinia near the SWI was not accompanied by persistently low $\delta^{13}C_{org}$ values. This signifies either an adaptation of benthic organisms to evolving redox conditions, or that microbial reworking of organic matter was not a prominent control on temporal $\delta^{13}C_{org}$ changes. Alternatively, the negative $\delta^{13}C_{org}$ excursions may be produced by preferential adsorption of ^{13}C-depleted organic molecules over ^{13}C-enriched molecules during ash diagenesis, but this is challenging to constrain. Although several processes may impact $\delta^{13}C_{org}$, it seems the negative $\delta^{13}C_{org}$ excursions coincident

with volcanic ash deposition may be a composite artifact of transiently enhanced primary production favoring isotopically depleted DIC and preferential complexation of ^{13}C-depleted organic molecules with chemical species in the ash during diagenesis (e.g. reactive Fe; Longman et al., 2019).

Interpretation of $\delta^{15}N_{bulk}$ is challenging, both from the perspective of disentangling potential controls and analytical error. Low TOC values in samples within or adjacent to bentonites required large sample amounts to obtain reproducible $\delta^{15}N_{bulk}$ values, while $\delta^{15}N_{bulk}$ recorded the nitrogen isotopic composition of precipitating organic matter that may be altered via microbial reworking and diagenesis (Robinson et al., 2012). Contribution from inorganic nitrogen may impact $\delta^{15}N_{bulk}$ values as well, but these were unable to be determined since total nitrogen was not measured and likely had minimal influence on $\delta^{15}N_{bulk}$ values in organic-rich samples (Fulton et al., 2012). Therefore, interpretation of $\delta^{15}N_{bulk}$ profiles in the UB and XB presumes nitrogen isotopic compositions reflect the original primary producers. This is a fair presumption in organic-rich samples, as previous work highlighted $\delta^{15}N_{bulk}$ will predominantly mirror primary producer $\delta^{15}N$ values (Robinson et al., 2012).

All $\delta^{15}N_{bulk}$ values were negative across all eruption horizons, with minimal changes in concert with ash deposition (Figure 3-3). Negative $\delta^{15}N_{bulk}$ values may indicate N_2-fixation via diazotrophy due to minimal fractionation associated with cleavage of the N_2 triple bond (e.g. Bauersachs et al., 2009), assuming conventional Mo-nitrogenases were active (Zhang et al., 2014), in agreement with previous work on Cenomanian-Turonian marine settings (Kuypers et al., 2004; Kashiyama et al., 2008; Ohkouchi et al., 2015). These negative $\delta^{15}N_{bulk}$ values are frequently attributed to enhanced cyanobacterial contribution to fixed nitrogen supply, especially during OAEs, but typically coincide with other proxies for cyanobacteria (e.g. 2-methylhopanoids;

Summons et al., 1999). Additionally, alternative viable models to account for depleted $\delta^{15}N_{bulk}$ values exist (e.g. upwelling of ^{15}N-depleted NH_4^+; Higgins et al., 2012) and a lack of porphyrin $\delta^{15}N$ values hampers confidence in interpretations founded on solely $\delta^{15}N_{bulk}$. Nevertheless, contextual information provided by biomarker-based reconstructions highlighted the relative persistence of shallow anoxia/euxinia, which likely created ideal conditions for denitrification and annamox. Removal of fixed nitrogen species via these processes in anoxic regions of the water column (e.g. Lam et al., 2007) potentially induced sustained fixed nitrogen shortages in the greater WIS that produced a persistent reliance on N_2-fixation and ultimately, the negative $\delta^{15}N_{bulk}$ values observed across all intervals. Further work allying $\delta^{15}N_{bulk}$ with compound-specific isotopic analyses (e.g. porphyrins, $\delta^{15}N_{por}$) is essential given the potential impacts of volcanic ash on nitrogen cycling. For example, anammox rates decrease with high ash loadings in marine environments at recent eruption sites (Song et al., 2014). Since anammox is a major sink for fixed nitrogen, suppression of anammox may perturb nitrogen cycling and enable the transiently enhanced rates of primary production reconstructed. Alternatively, indirect evidence exists for reduction of NO_2^- and NO_3^- to NH_4^+ within and below the SWI via oxidation of silicate bound Fe^{II} (Song et al., 2014), providing a mechanism for sustained NH_4^+ production invoked by some models of nitrogen cycling during OAE-2 (Higgins et al., 2012). These relationships between volcanism and nitrogen, as well as other elemental cycles, remain critical to elucidate and assess if the extent of major eruptions on various Earth systems is to be realized and applied in deep time reconstructions.

3.5 Conclusions

High resolution sampling across three bentonite intervals, produced by eruptions of varying estimated magnitudes, revealed some consistencies in biomarker and stable isotope trends

following ash deposition. Transient increases in primary production were associated with all eruptions, aligning with modern ash-leachate experiments, which also account for the lack of long-term fertilization effects observed. Negative $\delta^{13}C_{org}$ excursions were observed across both bentonite intervals unaffected by a major lithology change, likely due to atmospheric injection of isotopically depleted volcanogenic CO_2. As with recent eruptions, ash thickness correlated with perturbations to bottom water redox. A major, sustained increase in VO-/Ni-porphyrin values followed the two largest eruptions, likely capturing the development of anoxia/euxinia near the SWI. While these findings do substantiate a link between volcanism and enhanced organic carbon burial, they do not align with the preexisting explanations for this coincidence. Current invocations of volcanism as an ultimate driver of enhanced organic carbon burial rely on the presumption that ash will act as a stimulant for primary production by alleviating shortages in biolimiting elements (e.g. Fe). Our results confirm this phenomenon, but underscore its transiency which necessitates caution of continued misapplication and discourages blanket application of iron fertilization via volcanic ash in paleoenvironmental study. However, distinct shifts to redox states favoring enhanced organic carbon sequestration in the immediate aftermath of ash deposition perpetuates the link between volcanism and black shale deposition, albeit via a different process (i.e. preservation) then typically invoked (i.e. productivity). This highlights the innate complexities of natural systems, and warrants further investigation to determine how volcanic ash variably impacts contrasting depositional settings subjected to distinct climatic regimes.

3.6 References

1. Achterberg, E. P., Moore, C. M., Henson, A., Steigenberger, S., Stohl, A., Eckhardt, S., Avendano, L. C., Cassidy, M., Hembury, D., Klar, J. K., Lucas, M. I., Macey, A. I., Marsay, C. M., & Ryan-Keogh, T. J. (2013). Natural iron fertilization by the Eyjafjallajökull volcanic eruption. Geophysical Research Letters, 40, 921-926.

2. Arthur, M. A., & Sageman, B. B. (2004). Sea-level control on source-rock development: Perspectives from the Holocene Black Sea, the mid-Cretaceous Western Interior Basin of North America, and the late Devonian Appalachian Basin. SEPM Special Publication No. 82, 35-59.
3. Axelrod, D. I. (1981). Role of volcanism in climate and evolution. Special Paper 185, Geological Society of America, Boulder CO.
4. Ayris, P. M., & Delmelle, P. (2012). The immediate environmental effects of tephra emission. Bulletin of Volcanology, 74, 1905-1936.
5. Bains, S., Norris, R. D., Corfield, R. M., & Faul, K. L. (2000). Termination of global warmth at the Palaeocene/Eocene boundary through productivity feedback. Nature, 407, 171-174.
6. Baker, E. W., & Louda, J. W. (1983). Thermal aspects of chlorophyll geochemistry. Advances in Organic Geochemistry, 1981, 401-421.
7. Bauersachs, T., Schouten, S., Compaoré, J., Wollenzien, U., Stal, L. J., & Sinninghe Damsté, J. S. (2009). Nitrogen isotopic fractionation associated with growth on dinitrogen gas and nitrate by cyanobacteria. Limnology and Oceanography, 54, 1403-1411.
8. Barwise, A. J. G., & Roberts, I. (1984). Diagenetic and catagenetic pathways for porphyrins in sediments. Organic Geochemistry, 6, 167-176.
9. Bay, R. C., Bramall, N., & Price, P. B. (2004). Bipolar correlation of volcanism with millennial climate change. Proceedings of the National Academy of Sciences, 101, 6341-6345.
10. Bay, R. C., Bramall, N. E., Price, P. B., Clow, G. D., Hawley, R. L., Udisti, R., & Castellano, E. (2006). Globally synchronous ice core volcanic tracers and abrupt cooling during the last glacial period. Journal of Geophysical Research, 111, D11108.
11. Beaumont, C., Keen, C. E., & Boutilier, R. (1982). A comparison of foreland and rift margin sedimentary basins. Royal Society of London, Philosophical Transactions, 305, 295-317.
12. Bishop, J. K. B., & Wood, T. J. (2009). Year-round observations of carbon biomass and flux variability in the Southern Ocean. Global Biogeochemical Cycles, 23, GB003206.
13. Blakey, R. C. (2014). Paleogeography and paleotectonics of the Western Interior Seaway, Jurassic-Cretaceous of North America. Presentation at Tulsa Geological Society.
14. Blakey, R. C., & Raney, W. D. (2018). The continental arc, Sevier Orogeny, Western Interior Seaway and flat-slab subduction: Cretaceous Period: Ca. 145-65. Ancient Landscapes of Western North America, 8, 103-130.
15. Bray, J. R. (1974). Glacial advance relative to volcanic activity since A.D. 1500. Nature, 248, 42-43.
16. Breit, G. N., & Wanty, R. B. (1991). Vanadium accumulation in carbonaceous rocks – a review of geochemical controls during deposition and diagenesis. Chemical Geology, 91, 83-97.
17. Broda, K., Marynowski, L., Rakociński, M., & Zatoń, M. (2019). Coincidence of photic zone euxinia and impoverishment of arthropods in the aftermath of the Frasnian-Famennian biotic crisis. Scientific Reports, 9, 16996.
18. Burkova, U. N., Ryadova, O. V., Serebrennikova, O. W., & Titov, V. I. (1980). Geoporphyrin composition as an indication of organic matter transformation. Geokhimiya, 9, 1417-1421.

19. Cadrin, A. A. J., Kyser, T. K., Caldwell, W. G. E., & Longstaffe, F. J. (1995). Isotopic and chemical compositions of bentonites as paleoenvironmental indicators of the Cretaceous Western Interior Seaway. Palaeogeography, Palaeoclimatology, Palaeoecology, 119, 301-320.
20. Callot, H. J., Ocampo, R., & Albrecht, P. (1990). Sedimentary porphyrins: Correlations with biological precursors. Energy & Fuels, 4, 635-639.
21. Capitani, G., Miyajima, N., Sulpizio, R., D'Addabbo, M., Galimberti, L,. Guidi, M., & Andreozzi, G. B. (2018). Iron release in aqueous environment by fresh volcanic ash from Mount Etna (Italy) and Popocatépetl (Mexico) volcanoes. Environmental Earth Sciences, 77.
22. Carey, S., & Sparks, R. S. J. (1986). Quantitative models of the fallout and dispersal of tephra from volcanic eruption columns. Bulletin of Volcanology, 48, 109-125.
23. Cather, S. M., Dunbar, N. W., McDowell, F. W., McIntosh, W. C., & Scholle, P. A. (2009). Climate forcing by iron fertilization from repeated ignimbrite eruptions: The icehouse-silicic large igneous province (SLIP) hypothesis. Geosphere, 5, 315-324.
24. Chen, T., Liu, Q., Roberts, A. P., Shi, X., & Zhang, Q. (2020). A test of the relative importance of iron fertilization from aeolian dust and volcanic ash in the stratified high-nitrate low-chlorophyll subarctic Pacific Ocean. Quaternary Science Reviews, 248, 106577.
25. Cobban, W. A., Merewether, E. A., Fouch, T. D., & Obradovich, J. D. (1992). Some Cretaceous shorelines in the Western Interior of the United States. Mesozoic Systems of the Rocky Mountain Region, 393-414.
26. Collin, V. C., Eymery, F., Genty, B., Rey, P., & Havaux, M. (2008). Vitamin E is essential for the tolerance of Arabidopsis thaliana to metal-induced oxidative stress. Plant, Cell & Environment, 31, 244-257.
27. Connock, G. T., & Liu, X.-L. (2020). Clarifying the significance of tocopherols and associated derivatives in the geosphere. Ph.D. Thesis, Chapter 2, University of Oklahoma.
28. Cooper, D. J., Watson, A. J., & Nightingale, P. D. (1996). Large decrease in ocean-surface CO_2 fugacity in response to in situ iron fertilization. Nature, 383, 511-513.
29. Costa, K. M., McManus, J. F., Anderson, R. F., Ren, H., Sigman, D. M., Winckler, G., Fleisher, M. Q., Marcantonio, F., & Ravelo, A. C. (2016). No iron fertilization in the equatorial Pacific Ocean during the last ice age. Nature, 529, 519-522.
30. Coulson, A., Kohn, M., & Barrick, R. (2011). Isotopic evaluation of ocean circulation in the Late Cretaceous North American seaway. Nature Geoscience, 4, 852-855.
31. Cross, T. A., & Pilger Jr., R. H. (1978). Tectonic controls of late Cretaceous sedimentation, western interior, USA. Nature, 274, 653-657.
32. Cui, X., Liu, X.-L., Shen, G., Ma, J., Husain, F., Rocher, D., Zumberge, J. E., Bryant, D. A., & Summons, R. E. (2020). Niche expansion for phototrophic sulfur bacteria at the Proterozoic-Phanerozoic transition. Proceedings of the National Academy of Sciences, 117, 17599-17606.
33. Cwiertny, D. M., Young, M. A., Grassian, V. H. (2008). Chemistry and photochemistry of mineral dust aerosol. Annual Review of Physical Chemistry, 59, 27-51.
34. Dean, W. E., Arthur, M. A., Sageman, B. B., & Lewan, M. D. (1995). Core descriptions and preliminary geochemical data from the Amoco Production Company Rebecca K. Bounds #1 well, Greeley Country, Kansas. U.S. Geological Survey Open-File Report 95-209.

35. DeCelles, P. G., & Giles, K. A. (1996). Foreland basin systems. Basin Research, 8, 105-123.
36. Delmelle, P., Lambert, M, Dufrêne, Y., Gerin, P., Óskarsson, N. (2007). Gas/aerosol-ash interaction in volcanic plumes: new insights from surface analysis of fine volcanic ash. Earth and Planetary Science Letters, 259, 159-170.
37. Duggen, S., Crott, P., Schacht, U., & Hoffmann, L. (2007). Subduction zone volcanic ash can fertilize the surface ocean and stimulate phytoplankton growth: Evidence from biogeochemical experiments and satellite data. Geophysical Research Letters, 34, L01612.
38. Duggen, S., Olgun, N., Croot, P., Hoffmann, L., Dietze, H., Delmelle, P., & Teschner, C. (2010). The role of airborne volcanic ash for the surface ocean biogeochemical iron-cycle: a review. Biogeosciences, 7, 827-844.
39. Dutton, E. G., & Christy, J. R. (1992). Solar radiative forcing at selected locations and evidence for global lower tropospheric cooling following the eruptions of El Chichón and Pinatubo. Geophysical Research Letters, 19, 2313-2316.
40. du Vivier, A. D. C., Selby, D., Condon, D. J., Takashima, R., & Nishi, H. (2015). $^{187}Os/^{188}Os$ isotope chemistry and U-Pb geochronology: Synchroneity of global Os isotope change across OAE 2. Earth and Planetary Science Letters, 428, 204-216.
41. Elder, W. P. (1985). Biotic patterns across the Cenomanian-Turonian extinction boundary near Pueblo, Colorado. Fine-grained deposits and biofacies of the Cretaceous Western Interior Seaway: Evidence of cyclic sedimentary processes, FG4, 157-169.
42. Elder, W. P. (1988). Geometry of upper Cretaceous bentonite beds: Implications about volcanic source areas and paleowind patterns, western interior, United States. Geology, 16, 835-838.
43. Elder, W. P., Gustason, E. R., & Sageman, B. B. (1994). Correlation of basinal carbonate cycles to nearshore parasequences in the late Cretaceous Greenhorn seaway, Western Interior U.S.A. Geological Society of America Bulletin, 106, 892-902.
44. Elderbak, K., Leckie, R. M., & Tibert, N. E. (2014). Paleoenvironmental and paleoceanographic changes across the Cenomanian-Turonian Boundary Event (Oceanic Anoxic Event 2) as indicated by foraminiferal assemblages from the eastern margin of the Cretaceous Western Interior Sea. Palaeogeography, Palaeoclimatology, Palaeoecology, 413, 29-48.
45. Elderbak, K., & Leckie, R. M. (2016). Paleocirculation and foraminiferal assemblages of the Cenomanian-Turonian Bridge Creek Limestone bedding couplets: Productivity vs. dilution during OAE2. Cretaceous Research, 60, 52-77.
46. Eldrett, J. S., Ma, C., Bergman, S. C., Ozkan, A., Minisini, D., Lutz, B., Jackett, S.-J., Macaulay, C., & Kelly, A. E. (2015a). Origin of limestone-marlstone cycles: Astronomic forcing of organic-rich sedimentary rocks from the Cenomanian to early Coniacian of the Cretaceous Western Interior Seaway, USA. Earth and Planetary Science Letters, 423, 98-113.
47. Eldrett, J. S., Ma. C., Bergman, S. C., Lutz, B., John Gregory, F., Dodsworth, P., Phipps, M., Hardas, P., Minisini, D., Ozkan, A., Ramenzani, J., Bowring, S. A., Kamo, S. L., Ferguson, K., Macaulay, C., & Kelly, A. E. (2015b). An astronomically calibrated stratigraphy of the Cenomanian, Turonian and earliest Coniacian from the Cretaceous Western Interior Seaway, USA: Implications for global chronostratigraphy. Cretaceous Research, 56, 316-344.

48. Eldrett, J.S., Dodsworth, P., Bergman, S.C., Wright, M. & Minisini, D. (2017). Water-mass evolution in the Cretaceous western interior seaway of North America and equatorial Atlantic. Climate of the Past, 13, 855-878.
49. Fischer, G. (1991). Stable carbon isotope ratios of plankton carbon and sinking organic matter from the Atlantic sector of the Southern Ocean. Marine Chemistry, 35, 581-596.
50. Fisher, R. V., & Schmincke, H.-U. (1984). Pyroclastic Rocks. Springer-Verlag Berlin Heidelberg New York Tokyo.
51. Fisher, C. G., & Hay, W. W. (1999). Calcareous nannofossils as indicators of mid-Cretaceous paleofertility along an ocean front, U. S. Western Interior. Geological Society of America Special Paper 332, 161-180.
52. Fisher, C. G., & Arthur, M. A. (2002). Water mass characteristics in the Cenomanian US Western Interior seaway as indicated by stable isotopes of calcareous organisms. Palaeogeography, Palaeoclimatology, Palaeoecology, 188, 189-21.
53. Frigaard, N. U., & Dahl, C. (2009). Sulfur metabolism in phototrophic sulfur bacteria. Advances in Microbial Physiology, 54, 103-200.
54. Frogner, P., Gíslason, S. R., & Óskarsson, N. (2001). Fertilizing potential of volcanic ash in ocean surface water. Geology, 29, 487-490.
55. Fulton, J. M., Arthur, M. A., & Freeman, K. H. (2012). Black Sea nitrogen cycling and the preservation of phytoplankton $\delta^{15}N$ signals during the Holocene. Global Biogeochemical Cycles, 26, GB2030.
56. Gale, A. S., Voigt, S., Sageman, B. B., & Kennedy, W. J. (2008). Eustatic sea-level record for the Cenomanian (Late Cretaceous) – Extension to the Western Interior Basin, USA. Geology, 36, 859-862.
57. Gangl, S. K., Moy, C. M., Stirling, C. H., Jenkyns, H. C., Crampton, J. S., Clarkson, M. O., Ohneiser, C., & Porcelli, D. High-resolution records of Oceanic Anoxic Event 2: Insights into the timing, duration and extent of environmental perturbations from the palaeo-South Pacific Ocean. Earth and Planetary Science Letters, 518, 172-182.
58. Goswami, A., Hinnov, L., Gnanadesikan, A., & Young, T. (2018). Realistic paleobathymetry of the Cenomanian-Turonian (94Ma) boundary global ocean. Geosciences, 8, 8010021.
59. Haeckel, M., van Beusekom, J., Wisner, M. G., & König, I. (2001). The impact of the 1991 Mount Pinatubo tephra fallout on the geochemical environment of deep-sea sediments in the South China Sea. Earth and Planetary Science Letters, 193, 151-166.
60. Haimovich-Dayan, M., Garfinkel, N., Ewe, D., Marcus, Y.., Gruber, Y., Wagner, H., Kroth, P. G., & Kaplan, A. (2012). The role of C_4 metabolism in the marine diatom *Phaeodactylum tricornutum*. New Phytologist, 197, 177-185.
61. Hamme, R. C., Webley, P. W., Crawford, W. R., Whitney, F. A., DeGrandpre, M. D., Emerson, S. R., Eriksen, C. C., Giesbrecht, K. E., Gower, J. F. R., Kavanaugh, M. T., Peña, M. A., Sabine, C. L., Batten, S. D., Coogan, L. A., Grundle, D. S., & Lockwood, D. (2010). Volcanic ash fuels anomalous plankton bloom in subarctic Northeast Pacific. Geophysical Research Letters, 37, GL044629.
62. Hattin, D. E. (1985). Distribution and significance of widespread, time-parallel pelagic limestone beds in Greenhorn Limestone (Upper Cretaceous) of the Central Great Plains and Southern Rocky Mountains. Fine-grained deposits and biofacies of the Cretaceous Western Interior Seaway: Evidence of Cyclic Sedimentary Processes, SEPM Field Trip Guide, 4.

63. Häubner, N., Sylvander, P., Vuori, K., & Snoeijs, P. (2014). Abiotic stress modifies the synthesis of alpha-tocopherol and beta-carotene in phytoplankton species. Journal of Phycology, 50, 753-759.
64. Hay, W. W., Eicher, D. L., & Diner, R. (1993). Physical oceanography and water masses in the Western Interior Seaway. Evolution of the Western Interior Basin. Geological Association of Canada Special Paper, 39, 297-318.
65. Hembury, D. J., Palmer, M. R., Fones, G. R., Mills, R. A., Marsh, R., & Jones, M. T. (2012). Uptake of dissolved oxygen during marine diagenesis of fresh volcanic material. Geochimica et Cosmochimica Acta, 84, 353-368.
66. Higgins, M. B., Robinson, R. S., Husson, J. M., Carter, S. J., & Pearson, A. (2012). Dominant eukaryotic export production during ocean anoxic events reflects the importance of recycled NH_4^+. Proceedings of the National Academy of Sciences, 109. 2269-2274.
67. Hoffmann, L. J., Breitbarth, E., Ardelan, M. V., Duggen, S., Olgun, N., Hassellöv, Wängberg, S.- Å. (2012). Influence of trace metal release from volcanic ash on growth of *Thalassiosira psedonana* and *Emiliania huxleyi*. Marine Chemistry, 132-133, 28-33.
68. Hoshyaripour, G., Hort, M., Langmann, B., & Delmelle, P. (2014). Volcanic controls on ash iron solubility: New insights from high-temperature gas-ash interaction modeling. Journal of Volcanology and Geothermal Research, 286, 67-77.
69. Huff, W. (2016). K-bentonites: A review. American Mineralogist, 101, 43-70.
70. Imhoff, J. F. (1995). Taxonomy and physiology of phototrophic purple bacteria and green sulfur bacteria. Anoxygenic Photosynthetic Bacteria, New York, Kluwer Academic Press, 1-15.
71. Javoy, M., Pineau, F., & Delorme, H. (1986). Carbon and nitrogen isotopes in the mantle. Chemical Geology, 57, 41-62.
72. Jicha, B. R., Scholl, D. W., & Rea, D. K. (2009). Circum-Pacific arc flare-ups and global cooling near the Eocene-Oligocene boundary. Geology, 37, 303-306.
73. Jin, S., & Daniell, H. (2014). Expression of γ-tocopherol methyltransferase in chloroplasts results in massive proliferation of the inner envelope membrane and decreases susceptibility to salt and metal-induced oxidative stresses by reducing reactive oxygen species. Plant Biotechnology Journal, 12, 1274-1285.
74. Jones, M. T., & Gíslason, S. R. (2008). Rapid releases of metal salts and nutrients following the deposition of volcanic ash into aqueous environments. Geochimica et Cosmochimica Acta, 72, 3661-3680.
75. Jordan, T. E. (1981). Thrust loads and foreland basin evolution, Cretaceous, western United States. American Association of Petroleum Geologists Bulletin, 65, 2506-2520.
76. Junium, C. K., Freeman, K. H., & Arthur, M. A. (2015). Controls on the stratigraphic distribution and nitrogen isotopic composition of zinc, vanadyl and free base porphyrins through Oceanic Anoxic Event 2 at Demerara Rise. Organic Geochemistry, 80, 60-71.
77. Kashiyama, Y., Ogawa, N. O., Kuroda, J., Shiro, M., Nomoto, S., Tada, R., Kitazato, H., & Ohkouchi, N. (2008). Diazotrophic cyanobacteria as the major photoautotrophs during mid-Cretaceous oceanic anoxic events: Nitrogen and carbon isotopic evidence from sedimentary porphyrin. Organic Geochemistry, 29, 532-549.
78. Kauffman, E. G. (1977). Geological and biological overview: Western interior Cretaceous basin. Rocky Mountain Association of Geologists, The Mountain Geologist, 75-99.
79. Kauffman, E. G. (1984). Paleobiogeography and evolutionary response dynamic in the Cretaceous Western Interior Seaway of North America. Jurassic-Cretaceous

Biochronology and Paleogeography of North America, Geological Association of Canada Special Paper 27, 273-306.
80. Kauffman, E. G. (1985). Cretaceous evolution of the Western Interior Basin of the United States. Society of Economic Paleontologists and Mineralogists 1985 Midyear Meeting, Golden, CO., Field Trip Guidebook, 4, 4-13.
81. Kauffman, E. G., & Caldwell, W. G. E. (1993). The Western Interior Basin in space and time. Evolution of the Western Interior Basin. Geological Association of Canada Special Paper, 39, 1-30.
82. Kennedy, M. J., Pevear, D. R., & Hill, R. J. (2002). Mineral surface control of organic carbon in black shale. Science, 295, 657-660.
83. Kerr, A. C. (1998). Oceanic plateau formation: a cause of mass extinction and black shale deposition around the Cenomanian-Turonian boundary. Journal of the Geological Society of London, 155, 619-626.
84. Kimbrough, D. L., Smith, D. P., Mahoney, J. B., Moore, T. E., Grove, M., Gastil, R. G., Ortega-Rivera, A., & Fanning, C. M. (2001). Forearc-basin sedimentary response to rapid late Cretaceous batholith emplacement in the Peninsular Ranges of southern and Baja California. Geology, 29, 491-494.
85. Kuhnt, W., Hess, S., Holbourn, A., Paulsen, H., & Salomon, B. (2005). The impact of the 1991 Mt. Pinatubo eruption on deep-sea foraminiferal communities: A model for the Cretaceous-Tertiary (K/T) boundary? Palaeogeography, Palaeoclimatology, Palaeoecology, 224, 83-107.
86. Kump, L. R., & Arthur, M. A. (1999). Interpreting carbon-isotope excursions: carbonates and organic matter. Chemical Geology, 161, 181-198.
87. Kuypers, M. M. M., van Breugel, Y., Schouten, S., Erba, E., & Sinninghe Damsté, J. S. (2004). N_2-fixing cyanobacteria supplied nutrient N for Cretaceous oceanic anoxic events. Geology, 853-856.
88. Lam, P., Jensen, M. M., Lavik, G., McGinnis, D. F., Müller, B., Schubert, C. J., Amann, R., Thamdrup, B., & Kuypers, M. M. M. (2007). Linking crenarchaeal and bacterial nitrification to anammox in the Black Sea. Proceedings of the National Academy of Sciences, 104, 7104-7109.
89. Langmann, B., Zakšek, K., Hort, M., & Duggen, S. (2010). Volcanic ash as fertiliser for the surface ocean. Atmospheric Chemistry and Physics, 10, 3891-3899.
90. Larson, R. L. (1991). Latest pulse of Earth: Evidence for a mid-Cretaceous superplume. Geology, 19, 547-550.
91. Leckie, R. M., Yuretich, R. F., West, O. L. O., Finkelstein, D., & Schmidt, M. (1998). Paleoceanography of the southwestern Western Interior Sea during the time of the Cenomanian-Turonian Boundary (late Cretaceous). Society for Sedimentary Geology, Concepts in Sedimentology and Paleontology, 6, 101-126.
92. Lee, C.-T. A., Jiang, H., Ronay, E., Minisini, D., Stiles, J., & Neal, M. (2018). Volcanic ash as a driver of enhanced carbon burial in the Cretaceous. Scientific Reports, 8, 4197.
93. Lewan, M. D. (1984). Factors controlling the proportionality of vanadium to nickel in crude oils. Geochimica et Cosmochimica Acta, 48, 2231-2238.
94. Liaaen-Jensen, S., Hegge, E., & Jackman, L. M. (1964). Bacterial carotenoids XVIII, The carotenoids of photosynthetic bacteria, Acta Chemica Scandinavica, 18, 1703-1718.

95. Lindenthal, A., Langmann, B., Paetsch, J., Lorkorwski, I., & Hort, M. (2013). The ocean response to volcanic iron fertilization after the eruption of Kasatochi volcano: a regional biogeochemical model study. Biogeosciences, 10, 3715-3729.
96. Longman, J., Palmer, M. R., Gernon, T. M., & Manners, H. R. (2019). The role of tephra in enhancing organic carbon preservation in marine sediments. Earth-Science Reviews, 192, 480-490.
97. Louda, J. W., Loitz, J. W., Rudnick, D. T., & Baker, E. W. (2000). Early diagenetic alteration of chlorophyll-a and bacteriochlorophyll-a in a contemporaneous marl ecosystem; Florida Bay. Organic Geochemistry, 31, 1561-1580.
98. Louda, J. W., Mongkhonsri, P., & Baker, E. W. (2011). Chlorophyll degradation during senescence and death-III: 3-10 yr experiments, implications for ETIO series generation. Organic Geochemistry, 42, 688-699.
99. Lowery, C. M., Leckie, R. M., Bryant, R., Elderbak, K., Parker, A., Polyak, D. E., Schmidt, M., Snoeyenbos-West, O., & Sterzinar, E. (2018). The Late Cretaceous Western Interior Seaway as a model for oxygenation change in epicontinental restricted basins. Earth-Science Reviews, 177, 545-564.
100. Mahowald, N. M., Baker, A. R., Bergametti, G., Brooks, N., Duce, R. A., Jickells, T. D., Kubilay, N., Prospero, J. M., & Tegen, I. (2005). Atmospheric global dust cycle and iron inputs to the ocean. Global Biogeochemical Cycles, 19, GB002402.
101. Martin, J. H., & Fitzwater, S. E. (1988). Iron deficiency limits phytoplankton growth in the north-east Pacific subarctic. Nature, 331, 341-343.
102. Martin, J. H., Gordon, R. M., & Fitzwater, S. E. (1991). The case for iron. Limnology and Oceanography, 36, 1793-1802.
103. Maters, E. C., Delmelle, P., & Bonneville, S. (2016). Atmospheric processing of volcanic glass: effects on iron solubility and redox speciation. Environmental Science and Technology, 50, 5033-5040.
104. Maters, E. C., Delmelle, P., & Gunnlaugsson, H. P. (2017). Controls on iron mobilisation from volcanic ash at low pH: Insights from dissolution experiments and Mössbauer spectroscopy. Chemical Geology, 449, 73-81.
105. Mawson, D. H., & Keely, B. J. (2008). Novel functionalised chlorins in sediments of the Messinian Vena del Gesso evaporitic sequence: Evidence for a facile route to reduction for biomarkers. Organic Geochemistry, 39, 203-209.
106. May, S. R., Gray, G. G., Summa, L. L., Stewart, N. R., Gehrels, G. E., & Pecha, M. E. (2013). Detrital zircon geochronology from Cenomanian-Coniacian strata in the Bighorn Basin, Wyoming, U.S.A.: Implications for stratigraphic correlation and paleogeography. Rocky Mountain Geology, 48, 41-61.
107. Meyer, K. M., and Kump, L. R, Oceanic euxinia in Earth history: Causes and consequences. Annual Reviews of Earth and Planetary Sciences, 36, 251-288.
108. Miall, A. D. (2009). Initiation of the Western Interior foreland basin. Geology, 37, 383-384.
109. Miall, A. D., Catuneanu, O., Vakarelov, B. K., & Post, R. (2008). The Western Interior Basin. Sedimentary Basins of the World, 5, 329-362.
110. Muñoz, P., & Munné-Bosch, S. (2019). Vitamin E in Plants: Biosynthesis, Transport, and Function. Trends in Plant Science, 24, 1040-1051.

111. Nassiry, M., Aubert, C., Mouzdahir, A., & Rontani, J.-F. (2009). Generation of isoprenoid chromans, notably prist-1-ene, via photo- and autoxidative degradation of vitamin E. Organic Geochemistry, 40, 38-50.
112. Newhall, C. G., & Self, S. (1982). The Volcanic Explosivity Index (VEI): An estimate of explosive magnitude and historical volcanism. Journal of Geophysical Research, 87, 1231-1238.
113. Obradovich, J. D. (1993). A Cretaceous time scale. Geological Association of Canada, Evolution of the Western Interior Seaway, Special Paper 39, 379-396.
114. Obradovich, J. D., & Cobban, W. A. (1975). A time-scale for the late Cretaceous of the Western Interior of North America. The Cretaceous system in the Western Interior of North America, Geological Association of Canada, Special Paper 13, 31-54.
115. Ohkouchi, N., Kuroda, J., & Taira, A. (2015). The origin of Cretaceous black shales: a change in surface ocean ecosystem and its triggers. Proceedings of the Japan Academy, Series B Physical and Biological Sciences, 91, PMC4631894.
116. Olgun, M., Duggen, S., Croot, P. L., Delmelle, P., Dietze, H., Schacht, U., Óskarsson, N., Sibe, C., Auer, A., & Garbe-Schönberg, D. (2011). Surface ocean iron fertilization: The role of airborne volcanic ash from subduction zone and hot spot volcanoes and related iron fluxes into the Pacific Ocean. Global Biogeochemical Cycles, 25, GB4001.
117. Owens, J. D., Gill, B. C., Jenkyns, H. C., Bates, S. M., Severmann, S., Kuypers, M. M. M., Woodfine, R. G., & Lyons, T. W. (2013). Sulfur isotopes track the global extent and dynamics of euxinia during Cretaceous Oceanic Anoxic Event 2. Proceedings of the National Academy of Sciences, 110, 18407-18412.
118. Owens, J. D., Lyons, T. W., & Lowery, C. M. (2018). Quantifying the missing sink for global organic carbon burial during a Cretaceous oceanic anoxic event. Earth and Planetary Science Letters, 499, 83-94.
119. Patel, S. Y. (2017). Characterising carbon cycle perturbations in the Cenomanian Western Interior Seaway of North America. Ph.D. Thesis, University of Southampton, 127.
120. Perrier, V., Meidla, T., Tinn, O., & Ainsaar, L. (2012). Biotic response to explosive volcanism: Ostracod recovery after Ordovician ash-falls. Palaeogeography, Palaeoclimatology, Palaeoecology, 365, 166-183.
121. Pollack, J. B., Toon, O. B., Sagan, C., Summers, A., Baldwin, B., & van Camp, W. (1976). Volcanic explosions and climatic change: A theoretical assessment. Journal of Geophysical Research, 81, 1071-1083.
122. Rampino, M. R. (1991). Volcanism, climatic change, and the geologic record. Sedimentation in Volcanic Settings, SEPM Special Publication 45, 9-18.
123. Rampino, M. R., & Self, S. (1984). Sulphur-rich volcanic eruptions and stratospheric aerosols. Nature, 310, 677-679.
124. Reinfelder, J. R., Kraepiel, A. M., & Morel, F. M. (2000). Unicellular C_4 photosynthesis in a marine diatom. Nature, 407, 996-999.
125. Rickard, D., & Luther, G. W. (2007). Chemistry of iron sulfides. Chemical Reviews, 107, 514-562.
126. Robinson, R. S., Kienast, M., Albuquerque, A. L., Altabet, M., Contreras, S., de Pol Holz, R., Dubois, N., Francois, R., Galbrath, E., Hsu, T.-C., Ivanochko, T., Jaccard, S., Kao, S.-J., Kiefer, T., Kienast, S., Lehmann, M., Martinez, P., McCarthy, M., Möbius, J., Pedersen, T., Quan, T. M., Ryabenko, E., Schmittner, A., Schneider, R., Schneider-Mor, A.,

Shigemitsu, M., Sinclair, D., Somes, C., Studer, A., Thunell, R., & Yang, J.-Y. (2012). A review of nitrogen isotopic alteration in marine sediments. Paleoceanography, 27, PA4203.
127. Robock, A. (2000). Volcanic eruptions and climate. Reviews of Geophysics, 38, 191-219.
128. Rontani, J-F., Nassiry, M., Michotey, V., Guasco, S., Bonin, P. (2010). Formation of pristane from α-tocopherol under simulated anoxic sedimentary conditions: A combination of biotic and abiotic degradative processes. Geochimica et Cosmochimica Acta, 74, 252-263.
129. Sageman, B. B. (1991). High-resolution even stratigraphy, carbon geochemistry and paleobiology of the upper Cenomanian Harland Shale Member, Greenhorn Formation (Cretaceous), Western Interior Basin, US. Ph.D. Thesis, University of Colorado, 572.
130. Sageman, B. B., & Arthur, M. A. (1994). Controls on the accumulation of organic matter in Western Interior Sea; evidence from late Cenomanian Hartland Shale Member. American Association of Petroleum Geologists and Society of Economic Paleontologists and Mineralogists, Annual Meeting Abstracts, 249.
131. Sageman, B. B., Meyers, S. R., & Arthur, M. A. (2006). Orbital time scale and new C-isotope record for Cenomanian-Turonian boundary stratotype. Geology, 34, 125-128.
132. Sarmiento, J. L. (1993). Atmospheric CO_2 stalled. Nature, 365, 697-698.
133. Scholle, P. A., & Arthur, M. A. (1980). Carbon isotope fluctuations in Cretaceous pelagic limestones: potential stratigraphic and petroleum exploration tool. American Association of Petroleum Geologists Bulletin, 64, 67-87.
134. Schoffman, H., Lis, H., Shaked, Y., & Keren, N. (2016). Iron-nutrient interactions within phytoplankton. Frontiers in Plant Science, 7, 1223.
135. Scott, R. W. (1977). Early Cretaceous environments and paleocommunities in the southern Western Interior. Rocky Mountain Association of Geologists, 14, 155-168.
136. Seely, G. R. (1966). The structure and chemistry of functional groups. The Chlorophylls, 1, 67-110.
137. Shen, J., Feng, Q., Algeo, T. J., Li, C., Planavsky, N. J., Zhou, L., Zhang, M. (2016). Two pulses of oceanic environmental disturbance during the Permian-Triassic boundary crisis. Earth and Planetary Science Letters, 443, 139-152.
138. Sheridan, R. E. (1987). Pulsation tectonics as the control on long-term stratigraphic cycles. Paleoceanography and Paleoclimatology, 2, 97-118.
139. Shoenfelt, E. M., Winckler, G., Lamy, F., Anderson, R. F., & Bostick, B. C. (2018). Highly bioavailable dust-borne iron delivered to the Southern Ocean during glacial periods. Proceedings of the National Academy of Sciences, 115, 11180-11185.
140. Simkin, T. (1993). Terrestrial volcanism in space and time. Annual Reviews of Earth and Planetary Sciences, 21, 427-452.
141. Sinton, C. W., & Duncan, R. A. (1997). Potential links between ocean plateau volcanism and global ocean anoxia at the Cenomanian-Turonian boundary. Economic Geology, 92, 836-842.
142. Slaughter, M., & Hamil, M. (1970). Model for deposition of volcanic ash and resulting bentonite. Geological Society of America Bulletin, 81, 961-968.
143. Slingerland, R., Kump, L. R., Arthur, M. A., Fawcett, P. J., Sageman, B. B., & Barron, E. J. (1996). Estuarine circulation in the Turonian Western Interior seaway of North America. Geological Society of America Bulletin, 108, 941-952.

144. Song, B., Buckner, C. T., Hembury, D. J., Mills, R. A., & Palmer, M. R. (2014). Impact of volcanic ash on anammox communities in deep sea sediments. Environmental Microbiology Reports, 6, 159-166.
145. Spirakis, C. S. (1991). Iron fertilization with volcanic ash? Eos, 72, 525.
146. Summons, R. E., & Powell, T. G. (1987). Identification of aryl isoprenoids in source rocks and crude oils: Biological markers for the green sulphur bacteria. Geochimica et Cosmochimica Acta, 51, 557-566.
147. Summons, R. E., Jahnke, L. L., Hope, J. M., & Logan, G. A. (1999). 2-Methylhopanoids: Biomarkers for cyanobacteria and for oxygenic photosynthesis. Nature, 400, 554-557.
148. Sundararaman, P., & Moldowan, J. M. (1993). Comparison of maturity based on steroid and vanadyl porphyrin parameters: A new vanadyl porphyrin maturity parameter for higher maturities. Geochimica et Cosmochimica Acta, 57, 1379-1386.
149. Sundararaman, P., Schoell, M., Littke, R., Baker, D. R., Leythaeuser, D., & Rullkötter, J. (1993). Depositional environment of Toarcian shales from northern Germany as monitored with porphyrins. Geochimica et Cosmochimica Acta, 57, 4213-4218.
150. Takashima, R., Nishi, H., Yamanaka, T., Tomosugi, T., Fernando, A. G., Tanabe, K., Moriya, K., Kawabe, F., & Hayashi, K. (2011). Prevailing oxic environments in the Pacific Ocean during the mid-Cretaceous Oceanic Anoxic Event 2. Nature Communications, 2, 234.
151. Tessin, A., Sheldon, N. D., Hendy, I., & Chappaz, A. (2016). Iron limitation in the Western Interior Seaway during the late Cretaceous OAE 3 and its role in phosphorus recycling and enhanced organic matter preservation. Earth and Planetary Science Letters, 449, 135-144.
152. Turgeon, S. C., & Creaser, R. A. (2008). Cretaceous oceanic anoxic event 2 triggered by a massive magmatic episode. Nature, 454, 323-328.
153. Uematsu, M., Toratani, M., Kajino, M., Narita, Y., Senga, Y., & Kimoto, T. (2004). Enhancement of primary productivity in the western North Pacific caused by the eruption of the Miyake-jima Volcano. Geophysical Research Letters, 31, L06106.
154. Valko, M., Morris, H., & Cronin, M. T. (2005). Metals, toxicity and oxidative stress. Current Medicinal Chemistry, 12, 1161-1208.
155. Watson, A. J. (1997). Volcanic Fe, CO_2, ocean productivity and climate. Nature, 385, 587-588.
156. Westberry, T. K., Behrenfeld, M. J., Milligan, A. J., & Doney, S. C. (2013). Retrospective satellite ocean color analysis of purposeful and natural ocean iron fertilization. Deep Sea Research Part I: Oceanographic Research Papers, 73, 1-16.
157. White, A. F., & Yee, A. (1985). Aqueous oxidation-reduction kinetics associated with coupled electron-cation transfer from iron-containing silicates at 25°C. Geochimica et Cosmochimica Acta, 49, 1263-1275.
158. Zeng, Z., Pike, M., Tice, M. M., Kelly, C., Marcantonio, F., Xu, G., & Maulana, I. (2018). Iron fertilization of primary productivity by volcanic ash in the late Cretaceous (Cenomanian) Western Interior Seaway. Geology, 46, 859-862.
159. Zhang, X., Sigman, D. M., Morel, F. M. M., & Kraepiel, A. M. L. (2014). Nitrogen isotope fractionation by alternative nitrogenases and past ocean anoxia. Proceedings of the National Academy of Sciences, 111, 4782-4787.

160. Zhang, R., Jiang, T., Tian, Y., Xie, S., Zhou, L., Li, Q., & Jiao, N. (2017). Volcanic ash stimulates growth of marine autotrophic and heterotrophic microorganisms. Geology, 45, 679-682.
161. Zielinski, G. 2000. Use of paleo-records in determining variability within the volcanic-climate system. Quaternary Science Reviews, 19, 417-438.

3.7 Figures

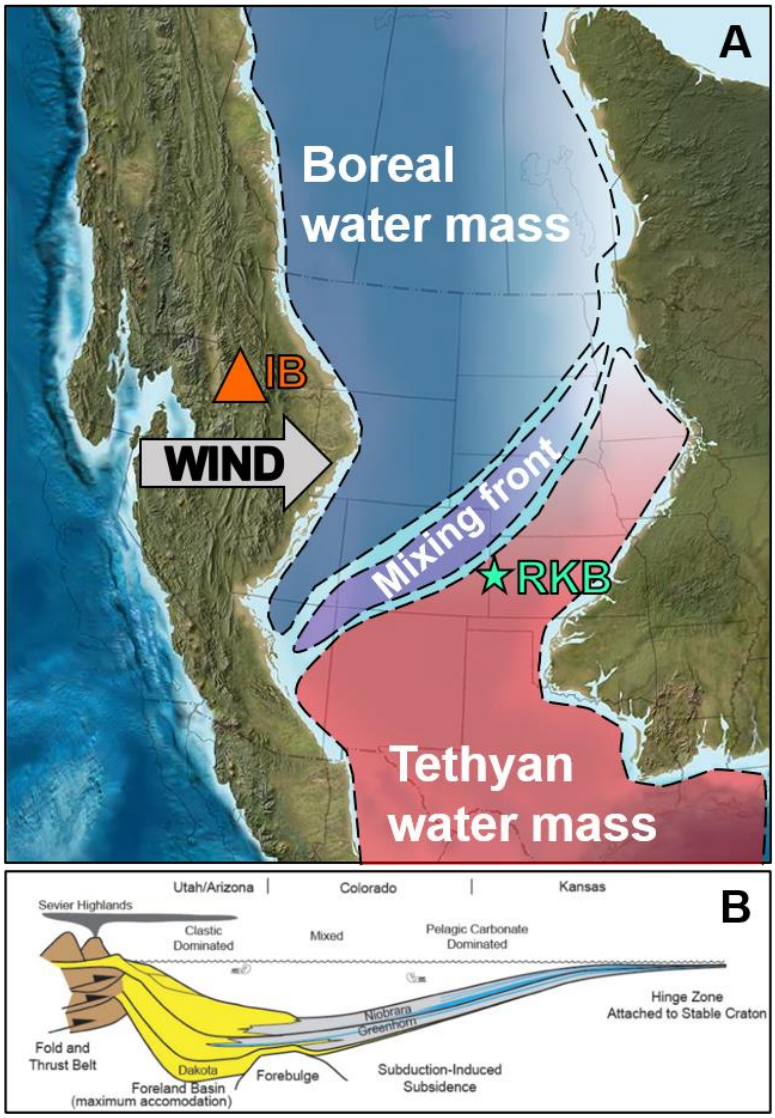

Figure 3-1. Paleogeography of the mid-Cretaceous and tectonic regime of western North America. (A) Paleogeography depicting the Western Interior Seaway of North America (Blakey, 2014). Study site (RKB core) is depicted by the green star, with generalized paleowind direction derived from Elder, (1988). IB is an abbreviation for the Idaho Batholith marked by an orange triangle, where eruptions were likely centralized (Kauffman, 1977; Elder, 1988; Hannon and Huff, 2019; Hannon et al., 2020). Water mass areal delineations were modified from Lowery et al., (2018) using a personally compiled database from publicly available fossil assemblage and $\delta^{18}O$ $CaCO_3$ data (Leckie et al., 1998; Fisher and Arthur, 2002; Coulson et al., 2011; Elderbak et al., 2014; Elderbak and Leckie, 2016; Eldrett et al., 2017), with color denoting relative temperatures. (B) Generalized cross section of the WIS basin, with idealized sedimentation and paleodepth distributions (from Lowery et al., 2018).

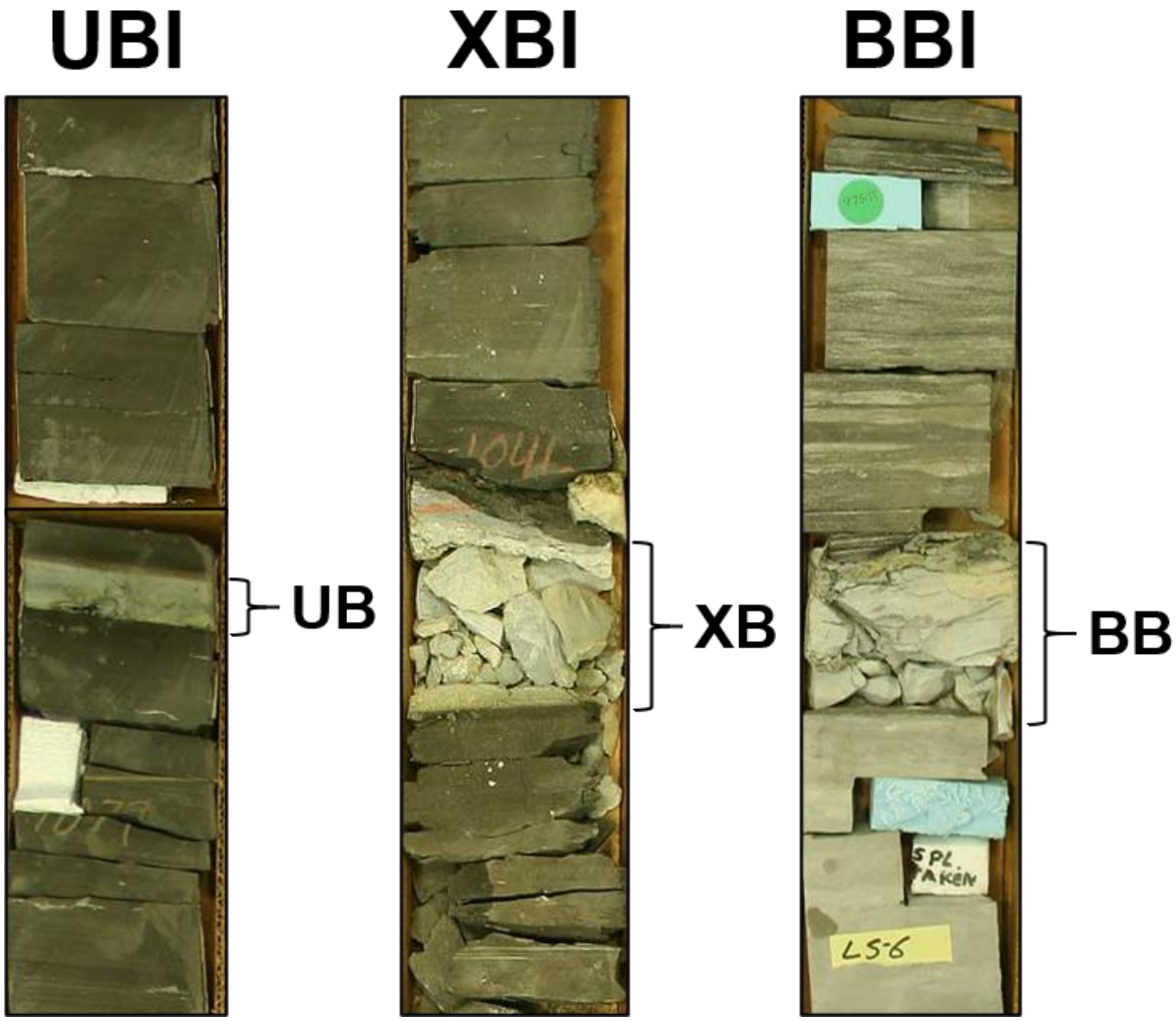

Figure 3-2. Core photographs of the three sampled bentonites. Each image is scaled independently, but general comparisons are retained (e.g. the UB is thinner than the XB or BB). For reference use bentonites as a measure of scale (UB = 2 cm; XB = 8 cm; BB = 8.5 cm). All core photos were taken from a publicly accessible repository kindly provided and maintained by the Kansas Geological Survey (http://www.kgs.ku.edu/Magellan/CoreLibrary/image.html).

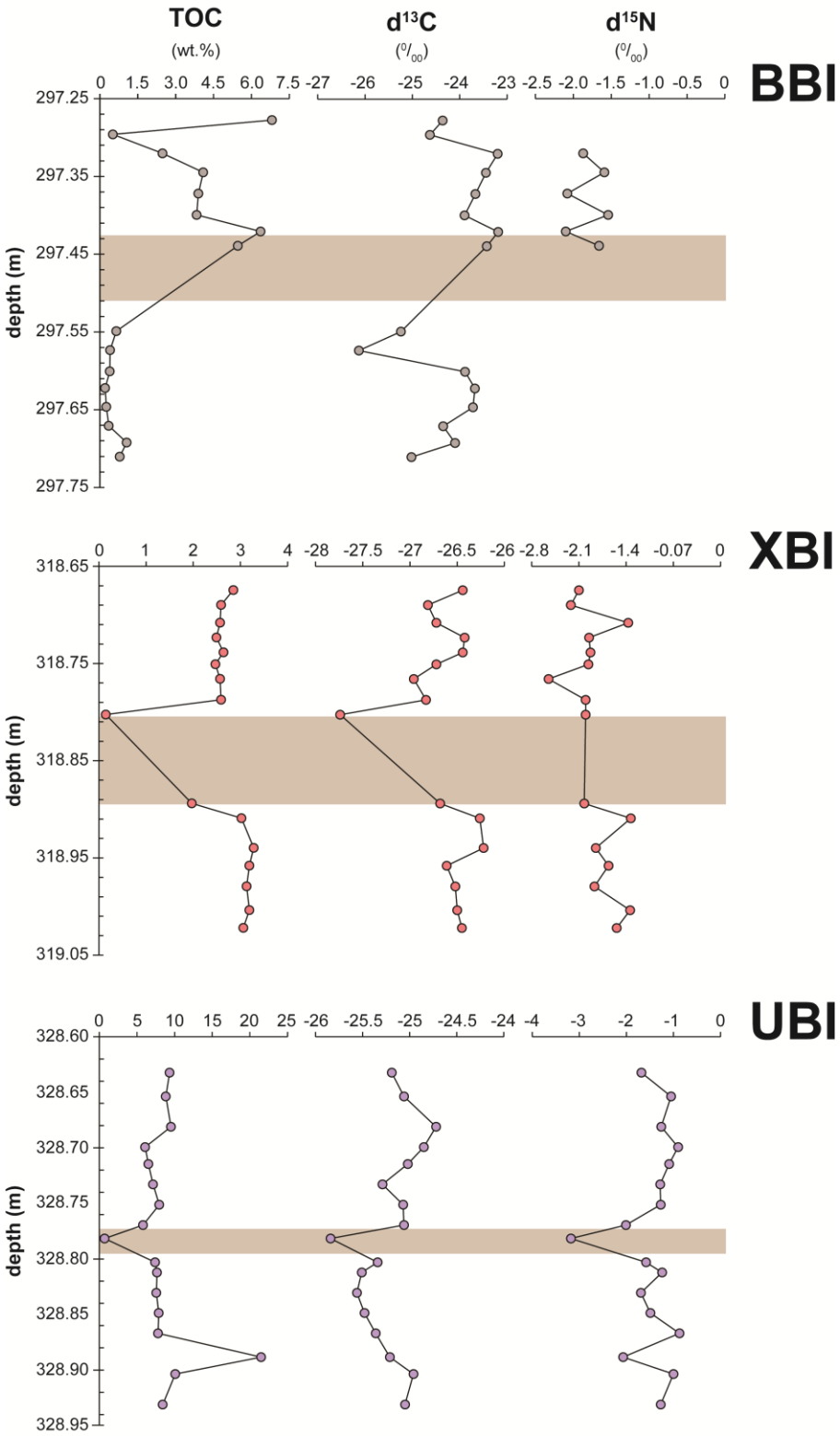

Figure 3-3. Depth profiles of bulk organic and isotopic data. The brown rectangles denote respective bentonites.

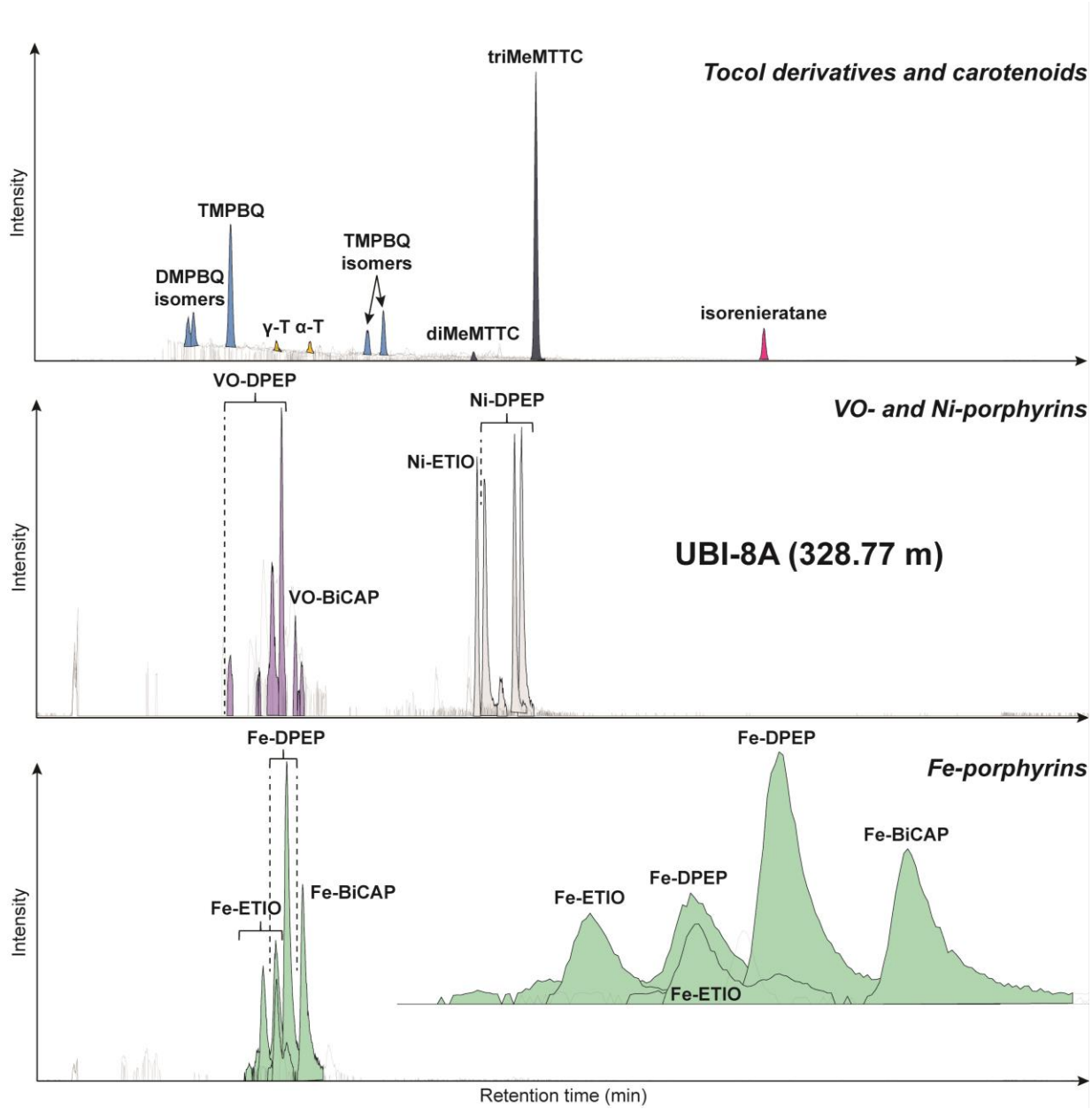

Figure 3-4. LC-qTOF-MS analysis and results of a sample from the UBI in the RKB core. Summed extracted ion chromatograms (EICs) of detected biomarkers are shown. Combination of EICs was dependent on distinct chromatographic elution time and similar signal intensities to improve summed EIC clarity.

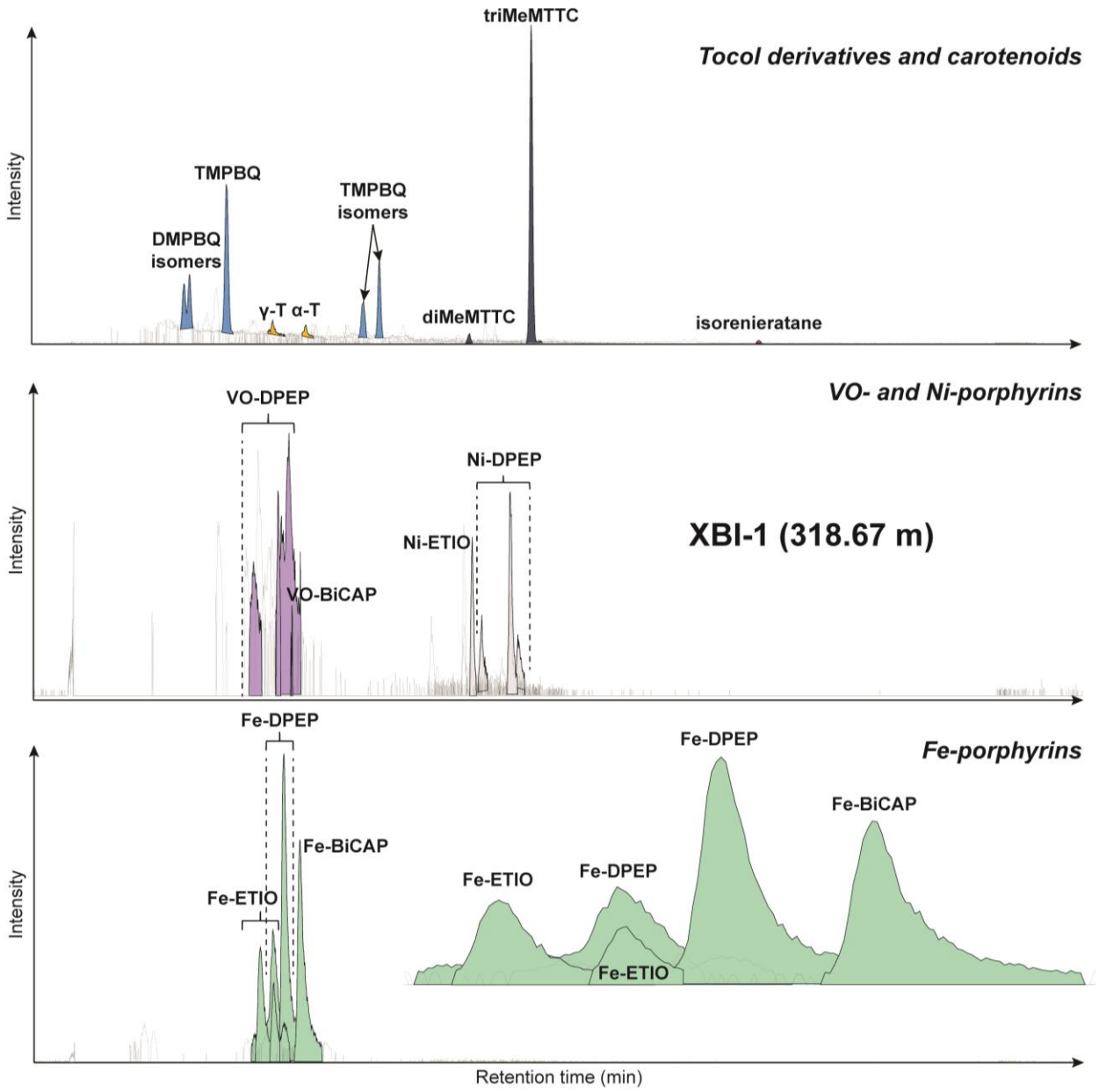

Figure 3-5. LC-qTOF-MS analysis and results of a sample from the XBI in the RKB core. Summed extracted ion chromatograms (EICs) of detected biomarkers are shown. Combination of EICs was dependent on distinct chromatographic elution time and similar signal intensities to improve summed EIC clarity.

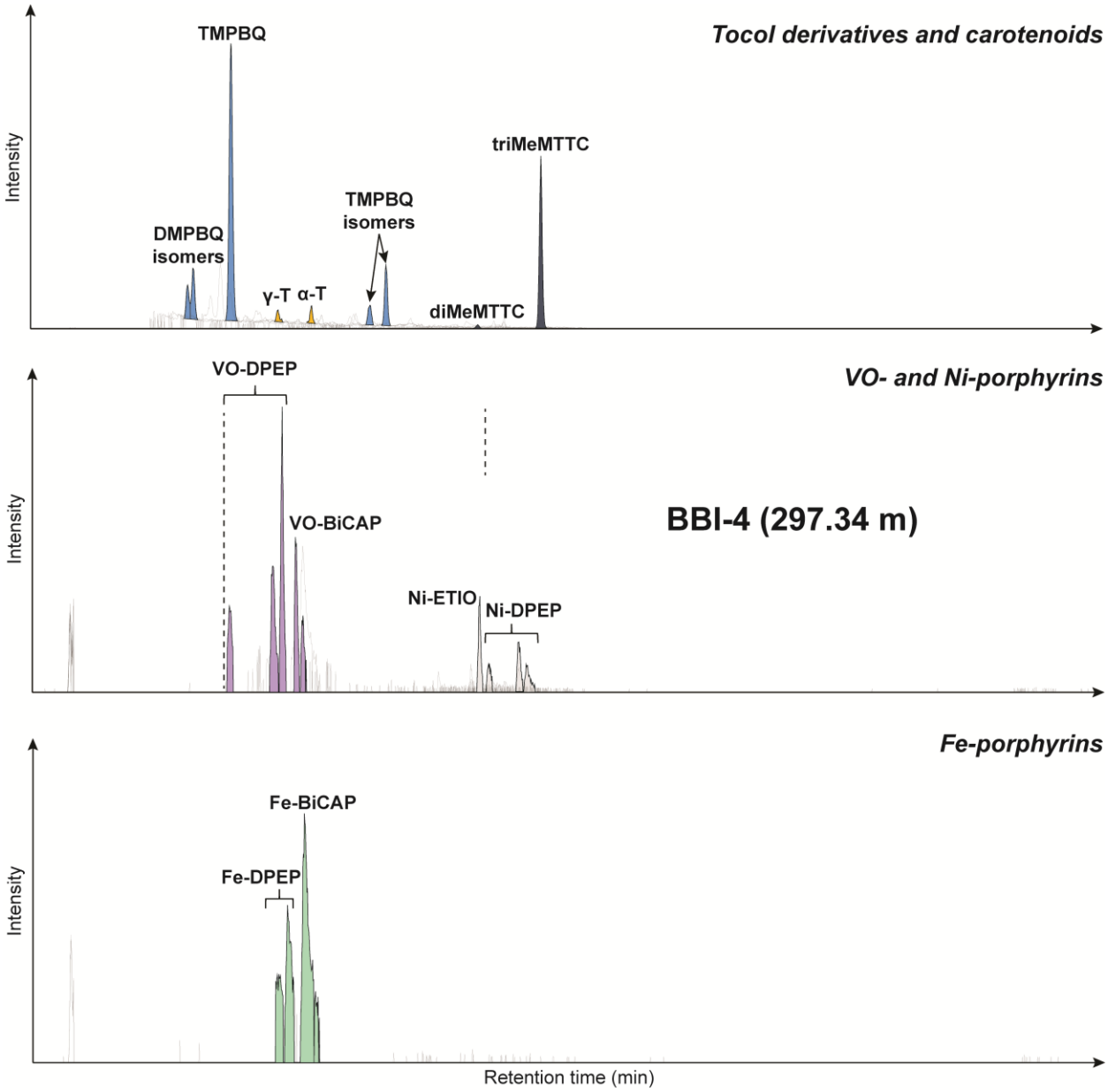

Figure 3-6. LC-qTOF-MS analysis and results of a sample from the BBI in the RKB core. Summed extracted ion chromatograms (EICs) of detected biomarkers are shown. Combination of EICs was dependent on distinct chromatographic elution time and similar signal intensities to improve summed EIC clarity.

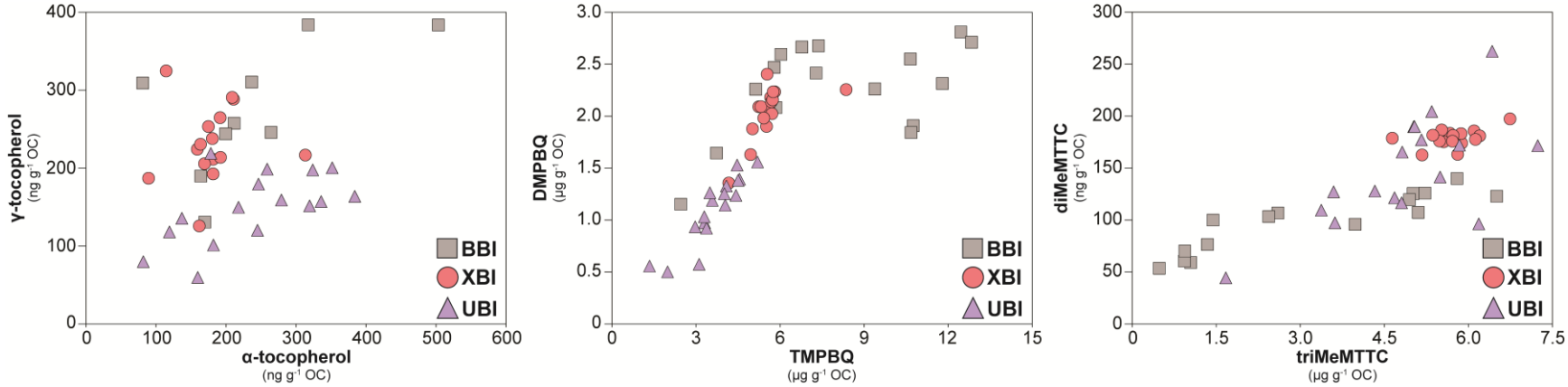

Figure 3-7. Cross plots of tocol derivatives in the intervals bounding bentonite beds in the RKB core.

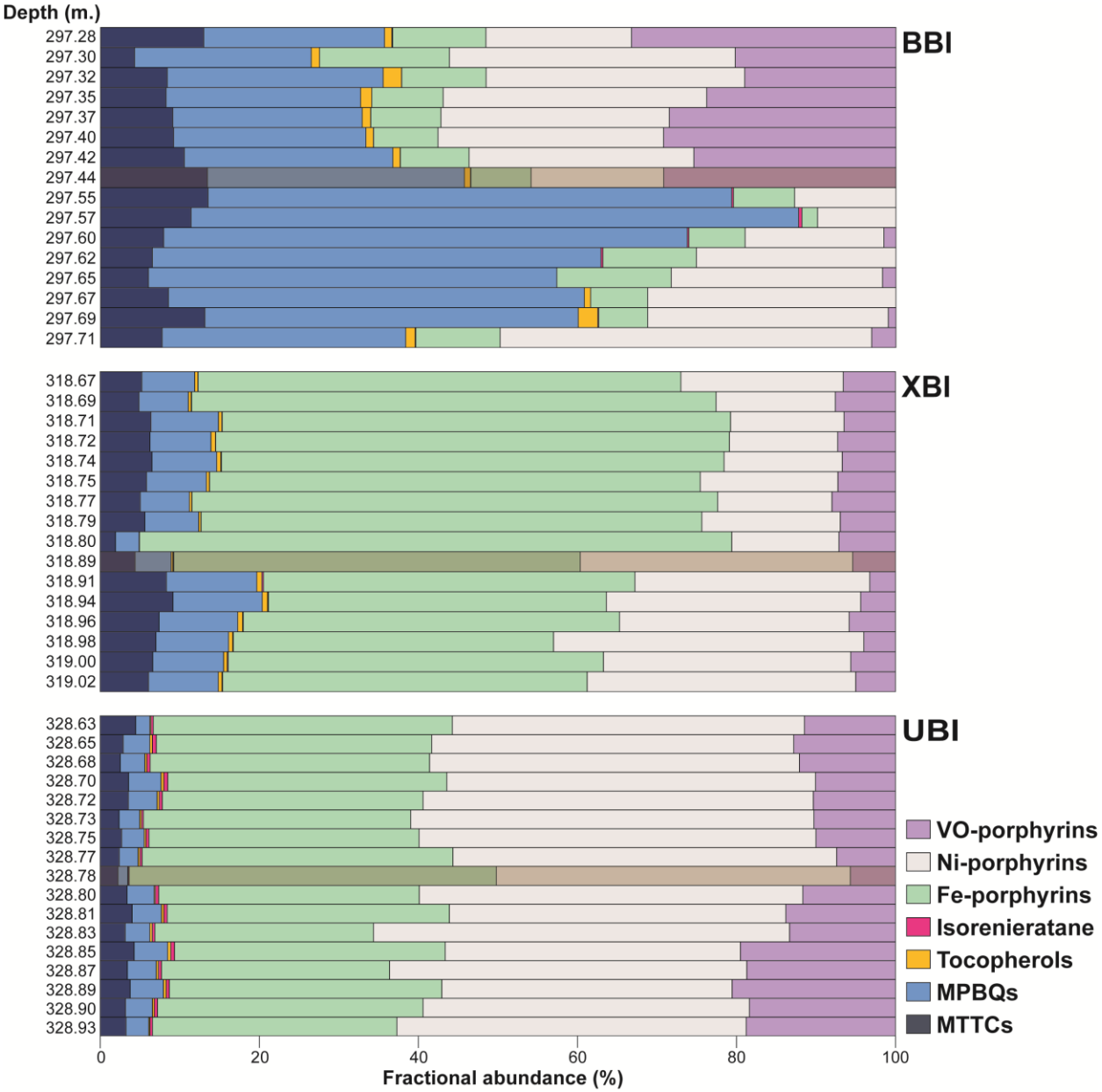

Figure 3-8. Biomarker fractional abundances across the three sampled intervals in the RKB core. The light brown shading denotes samples within the bentonite beds. More than 1 sample was taken per ash bed, but poor organic carbon preservation compromised biomarker preservation and recovery. Intervals are ordered stratigraphically (i.e. oldest to youngest from bottom to top).

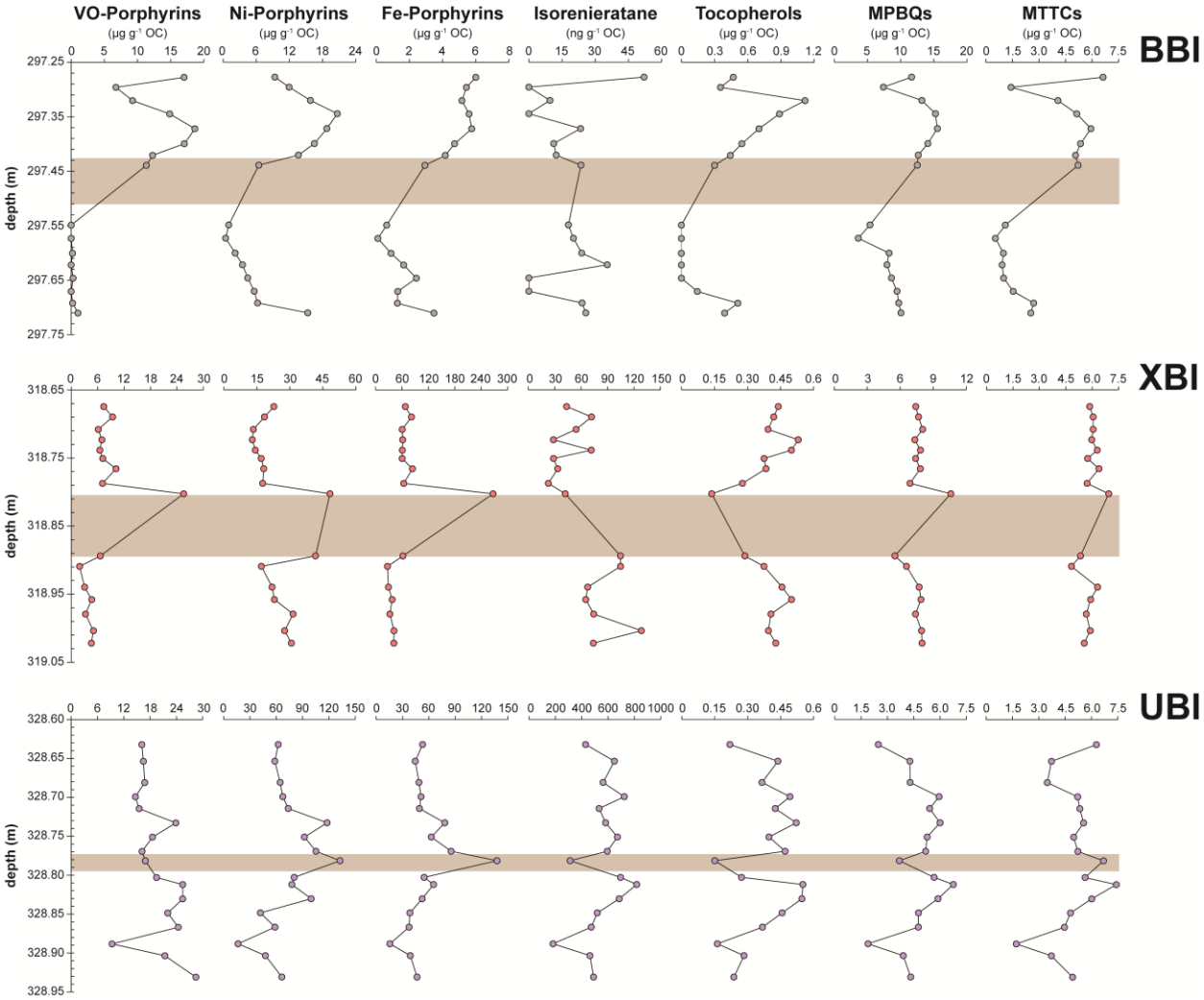

Figure 3-9. Biomarker concentration depth profiles across bentonite intervals in the RKB core. Light brown shading depicts the bentonite (i.e. ash bed). Note isorenieratane concentrations are presented in ng g^{-1} OC.

Bentonite Interval	Bentonite thickness (cm)	Areal extents (km^2)	Ejecta volume (m^3)	VEI (Newhall and Self, 1982)
BBI	8.5	3,000,000	25500000000	5 to 6
XBI	8	4,000,000	32000000000	5 to 6
UBI	2	750,000	1500000000	4 to 5

VEI ***≈*** *ejecta volume ≈ thickness * areal extents*

Figure 3-10. Parameters and formula used to calculate VEI for each bentonite (i.e. ash bed).

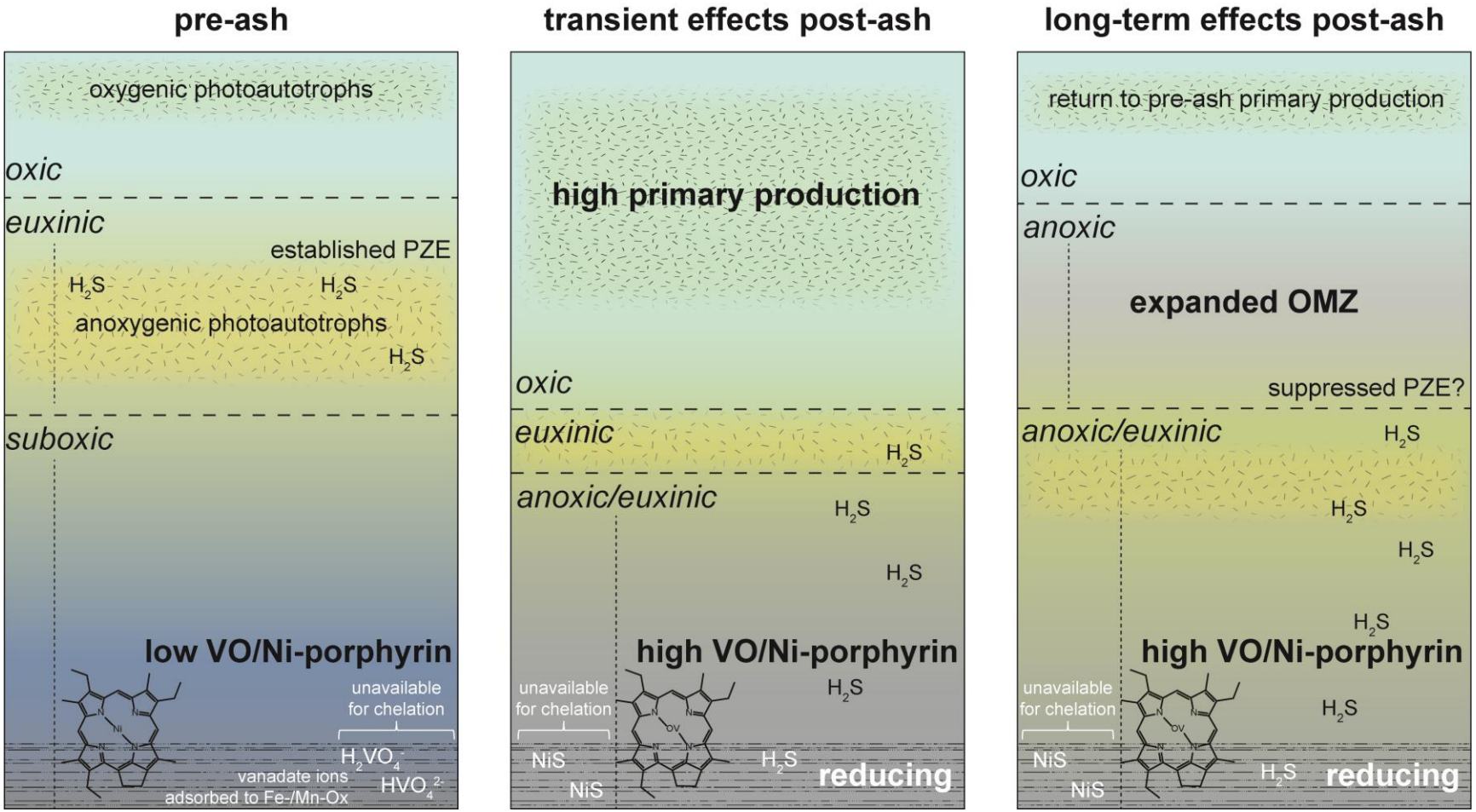

Figure 3-11. Two-dimensional cross sections of the water column depicting short- and long-term biogeochemical impacts of volcanic ash in the WIS. Color gradients correspond to water column redox gradients. Mechanisms affecting metal availability for porphyrin chelation are highlighted in white text. Oxygenic and anoxygenic photoautotrophs are depicted with green and yellow hashed regions, respectively.

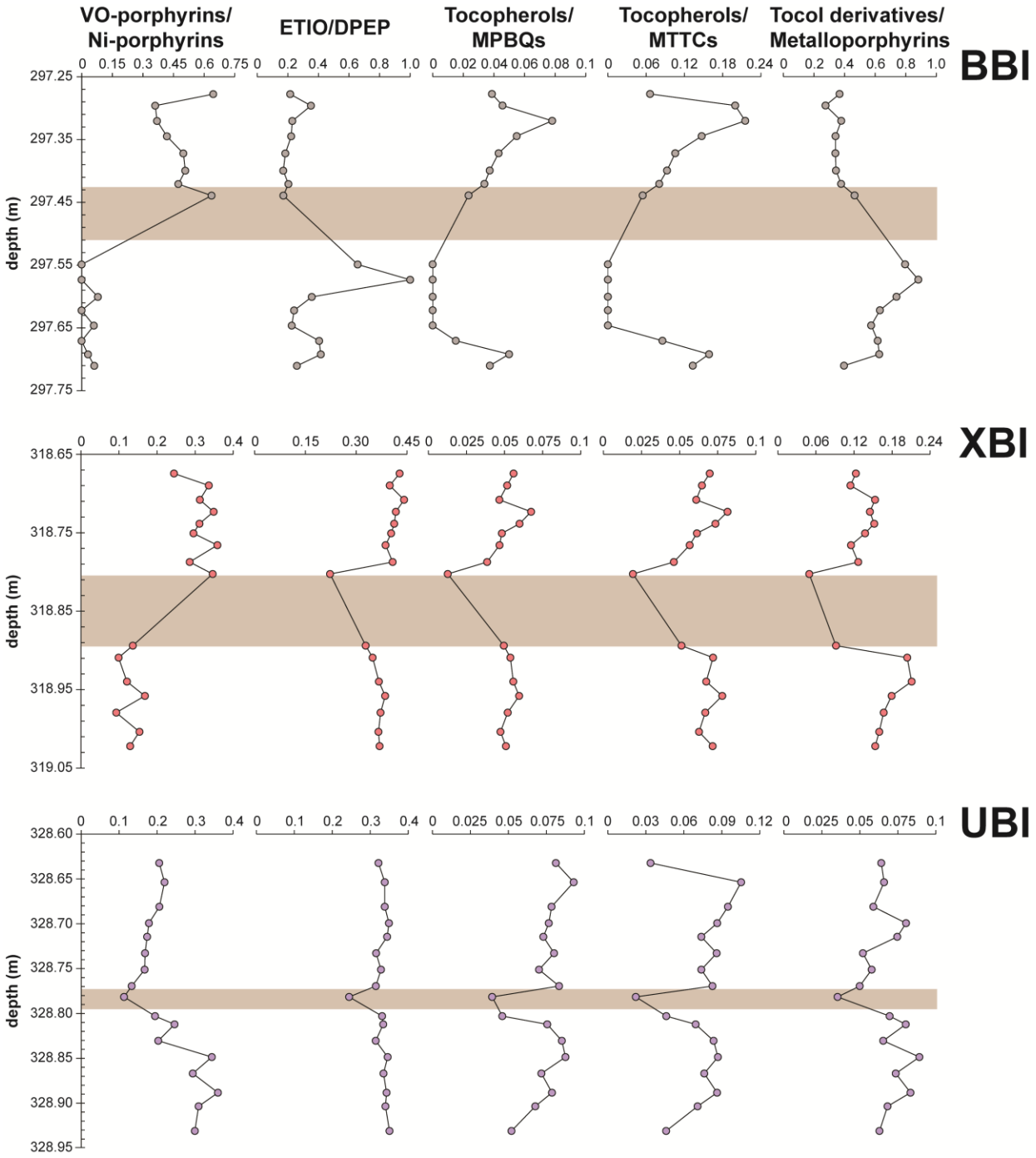

Figure 3-12. Depth profiles of biomarker ratios sensitive to paleoenvironmental change across the three sampled intervals in the RKB core. Light brown shading depicts the bentonites (i.e. ash beds).

3.8 Tables

Sample	Depth (m)	TOC (wt.%)	$d^{13}C_{org}$ ($^0/_{00}$)	$d^{15}N_{bulk}$ ($^0/_{00}$)	VO-porphyrins (µg g^{-1} OC)	Ni-porphyrins (µg g^{-1} OC)	Fe-porphyrins (µg g^{-1} OC)	Isorenieratane (ng g^{-1} OC)	Tocopherols (µg g^{-1} OC)	MPBQs (µg g^{-1} OC)	MTTCs (µg g^{-1} OC)
BBI-1	297.28	6.81	-24.36	-1.76	17.02	9.37	6.00	52.10	0.47	11.65	6.63
BBI-2	297.30	0.52	-24.63		6.73	11.95	5.44	0.00	0.35	7.39	1.42
BBI-3	297.32	2.48	-23.20	-1.87	9.26	15.81	5.17	9.56	1.12	13.20	4.07
BBI-4	297.34	4.09	-23.45	-1.59	14.86	20.68	5.59	0.00	0.89	15.26	5.14
BBI-5	297.37	3.90	-23.67	-2.08	18.63	18.77	5.76	23.40	0.70	15.55	5.94
BBI-6	297.40	3.83	-23.90	-1.54	17.06	16.53	4.72	11.22	0.55	14.11	5.35
BBI-7	297.42	6.36	-23.19	-2.10	12.26	13.64	4.16	12.40	0.44	12.66	5.07
BBI-8B	297.44	5.46	-23.43	-1.66	11.32	6.47	2.93	23.60	0.30	12.52	5.21
BBI-11	297.55	0.65	-25.24		0.00	1.04	0.63	17.88	0.00	5.38	1.10
BBI-12	297.57	0.41	-26.13		0.00	0.47	0.09	20.19	0.00	3.61	0.54
BBI-13	297.60	0.39	-23.89		0.19	2.19	0.89	23.93	0.00	8.26	0.99
BBI-14	297.62	0.21	-23.68		0.00	3.53	1.65	35.48	0.00	7.93	0.92
BBI-15	297.65	0.25	-23.72		0.28	4.46	2.42	0.00	0.00	8.62	1.01
BBI-16	297.67	0.35	-24.35		0.00	5.64	1.30	0.00	0.14	9.44	1.54
BBI-17	297.69	1.06	-24.10		0.20	6.25	1.27	24.08	0.51	9.70	2.71
BBI-18	297.71	0.79	-25.02		1.01	15.33	3.48	25.77	0.39	10.05	2.54
XBI-1	318.67	2.85	-26.44	-2.10	7.36	22.79	67.76	43.41	0.44	7.42	5.85
XBI-2	318.69	2.59	-26.81	-2.22	9.38	18.55	81.63	71.79	0.42	7.67	6.05
XBI-3	318.71	2.57	-26.72	-1.37	6.13	13.52	60.52	54.30	0.39	8.04	6.05
XBI-4	318.72	2.49	-26.42	-1.95	6.94	13.00	61.62	28.42	0.53	7.33	5.97
XBI-5	318.74	2.64	-26.44	-1.93	6.47	14.35	60.96	71.46	0.50	7.84	6.29
XBI-6	318.75	2.47	-26.72	-1.96	7.14	17.03	60.69	28.68	0.37	7.40	5.73
XBI-7	318.77	2.57	-26.96	-2.55	10.15	18.18	83.77	33.46	0.38	7.83	6.38
XBI-8	318.79	2.59	-26.83	-2.00	7.07	17.70	64.03	22.66	0.28	6.89	5.71
XBI-9A	318.80	0.15	-27.74	-2.00	25.52	48.30	266.94	41.97	0.14	10.61	6.94
XBI-14A	318.89	1.97	-26.68	-2.02	6.57	41.71	62.27	104.68	0.29	5.52	5.33
XBI-15	318.91	3.02	-26.26	-1.33	1.87	17.10	27.06	104.80	0.37	6.58	4.82
XBI-16	318.94	3.28	-26.22	-1.85	3.03	22.01	29.25	67.44	0.46	7.73	6.30
XBI-17	318.96	3.19	-26.61	-1.66	4.65	23.05	37.76	65.23	0.50	7.89	5.91
XBI-18	318.98	3.13	-26.52	-1.87	3.22	31.55	32.56	74.22	0.41	7.40	5.66
XBI-19	319.00	3.19	-26.50	-1.34	5.03	27.71	42.05	128.33	0.39	7.94	5.89
XBI-20	319.02	3.06	-26.45	-1.54	4.56	30.77	41.77	73.85	0.43	7.99	5.55
UBI-1	328.63	9.33	-25.19	-1.68	16.13	62.26	52.86	429.12	0.22	2.48	6.28
UBI-2	328.65	8.83	-25.06	-1.05	16.48	58.50	44.51	647.89	0.44	4.28	3.72
UBI-3	328.68	9.52	-24.72	-1.26	16.76	64.56	48.77	562.04	0.37	4.30	3.48
UBI-4	328.70	6.09	-24.85	-0.90	14.66	67.51	51.11	723.89	0.49	5.94	5.21
UBI-5	328.71	6.53	-25.02	-1.09	15.52	73.73	49.28	532.31	0.43	5.41	5.34
UBI-6	328.73	7.15	-25.29	-1.28	23.87	117.99	78.18	581.57	0.52	6.00	5.55
UBI-7	328.75	7.96	-25.07	-1.27	18.53	92.18	62.78	671.00	0.40	5.26	4.99
UBI-8A	328.77	5.82	-25.06	-2.01	16.17	105.40	85.40	594.39	0.47	5.18	5.23
UBI-8B	328.78	0.70	-25.84	-3.18	16.92	132.67	137.58	311.85	0.15	3.68	6.69
UBI-10	328.80	7.41	-25.34	-1.58	19.46	80.45	54.70	694.76	0.27	5.66	5.64
UBI-11	328.81	7.67	-25.51	-1.24	25.43	77.86	65.33	817.69	0.55	6.75	7.41
UBI-12	328.83	7.57	-25.56	-1.69	25.44	99.81	52.47	685.34	0.55	5.88	6.01
UBI-13	328.85	7.90	-25.48	-1.49	22.01	41.92	38.45	518.57	0.46	4.77	4.80
UBI-14	328.87	7.80	-25.36	-0.87	24.41	58.66	37.47	472.19	0.37	4.76	4.46
UBI-15	328.89	21.50	-25.21	-2.07	9.34	16.58	15.56	182.37	0.16	1.90	1.71
UBI-16	328.90	10.10	-24.96	-1.00	21.37	47.72	38.81	462.73	0.28	3.90	3.72
UBI-17	328.93	8.43	-25.05	-1.27	28.43	66.49	46.47	490.02	0.24	4.33	4.92

Table 3-1. Bulk (TOC, $\delta^{13}C_{org}$ $\delta^{15}N_{bulk}$) and molecular geochemical data.

Sample	Depth (m)	VO-porphyrins/ Ni-porphyrins	ETIO/DPEP	Tocopherols/MPBQs	Tocopherols/MTTCs	Tocol derivatives/ Metalloporphyrins
BBI-1	297.28	0.64	0.23	0.04	0.07	0.37
BBI-2	297.30	0.36	0.36	0.05	0.20	0.28
BBI-3	297.32	0.37	0.26	0.08	0.22	0.38
BBI-4	297.34	0.42	0.24	0.05	0.15	0.34
BBI-5	297.37	0.50	0.21	0.04	0.11	0.34
BBI-6	297.40	0.51	0.19	0.04	0.09	0.34
BBI-7	297.42	0.47	0.24	0.03	0.08	0.38
BBI-8B	297.44	0.64	0.20	0.02	0.05	0.47
BBI-11	297.55	0.00	0.66	0.00	0.00	0.79
BBI-12	297.57	0.00	1.00	0.00	0.00	0.88
BBI-13	297.60	0.08	0.46	0.00	0.00	0.74
BBI-14	297.62	0.00	0.37	0.00	0.00	0.63
BBI-15	297.65	0.06	0.34	0.00	0.00	0.57
BBI-16	297.67	0.00	0.50	0.02	0.09	0.62
BBI-17	297.69	0.03	0.49	0.05	0.16	0.63
BBI-18	297.71	0.06	0.32	0.04	0.13	0.40
XBI-1	318.67	0.24	0.39	0.06	0.07	0.12
XBI-2	318.69	0.34	0.37	0.05	0.06	0.11
XBI-3	318.71	0.31	0.41	0.05	0.06	0.15
XBI-4	318.72	0.35	0.39	0.07	0.08	0.14
XBI-5	318.74	0.31	0.39	0.06	0.07	0.15
XBI-6	318.75	0.30	0.37	0.05	0.06	0.14
XBI-7	318.77	0.36	0.36	0.05	0.06	0.12
XBI-8	318.79	0.29	0.37	0.04	0.05	0.13
XBI-9A	318.80	0.35	0.21	0.01	0.02	0.05
XBI-14A	318.89	0.14	0.33	0.05	0.05	0.09
XBI-15	318.91	0.10	0.36	0.05	0.07	0.20
XBI-16	318.94	0.12	0.37	0.06	0.07	0.21
XBI-17	318.96	0.17	0.37	0.06	0.08	0.18
XBI-18	318.98	0.09	0.35	0.05	0.07	0.17
XBI-19	319.00	0.15	0.34	0.05	0.06	0.16
XBI-20	319.02	0.13	0.35	0.05	0.07	0.15
UBI-1	328.63	0.21	0.28	0.08	0.03	0.06
UBI-2	328.65	0.22	0.28	0.09	0.11	0.07
UBI-3	328.68	0.21	0.28	0.08	0.09	0.06
UBI-4	328.70	0.18	0.30	0.08	0.09	0.08
UBI-5	328.71	0.17	0.30	0.07	0.07	0.07
UBI-6	328.73	0.17	0.25	0.08	0.09	0.05
UBI-7	328.75	0.17	0.27	0.07	0.07	0.06
UBI-8A	328.77	0.13	0.26	0.08	0.08	0.05
UBI-8B	328.78	0.11	0.21	0.04	0.02	0.04
UBI-10	328.80	0.19	0.29	0.05	0.05	0.07
UBI-11	328.81	0.25	0.28	0.08	0.07	0.08
UBI-12	328.83	0.20	0.27	0.09	0.08	0.07
UBI-13	328.85	0.34	0.29	0.09	0.09	0.09
UBI-14	328.87	0.29	0.28	0.07	0.08	0.07
UBI-15	328.89	0.36	0.29	0.08	0.09	0.08
UBI-16	328.90	0.31	0.29	0.07	0.07	0.07
UBI-17	328.93	0.30	0.27	0.05	0.05	0.06

Table 3-2. Biomarker ratios of metalloporphyrins and tocol derivatives.

3.9 Structural Appendix

Tocol derivatives and carotenoids

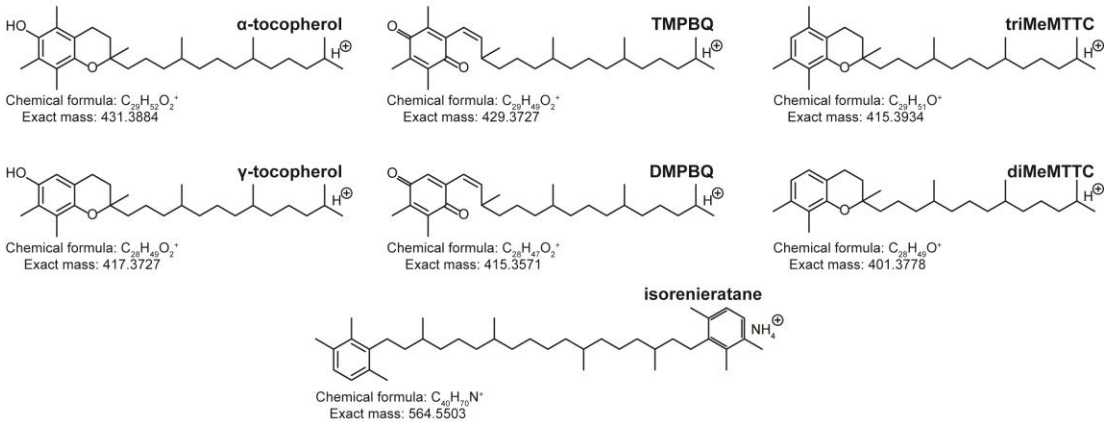

Metalloporphyrins

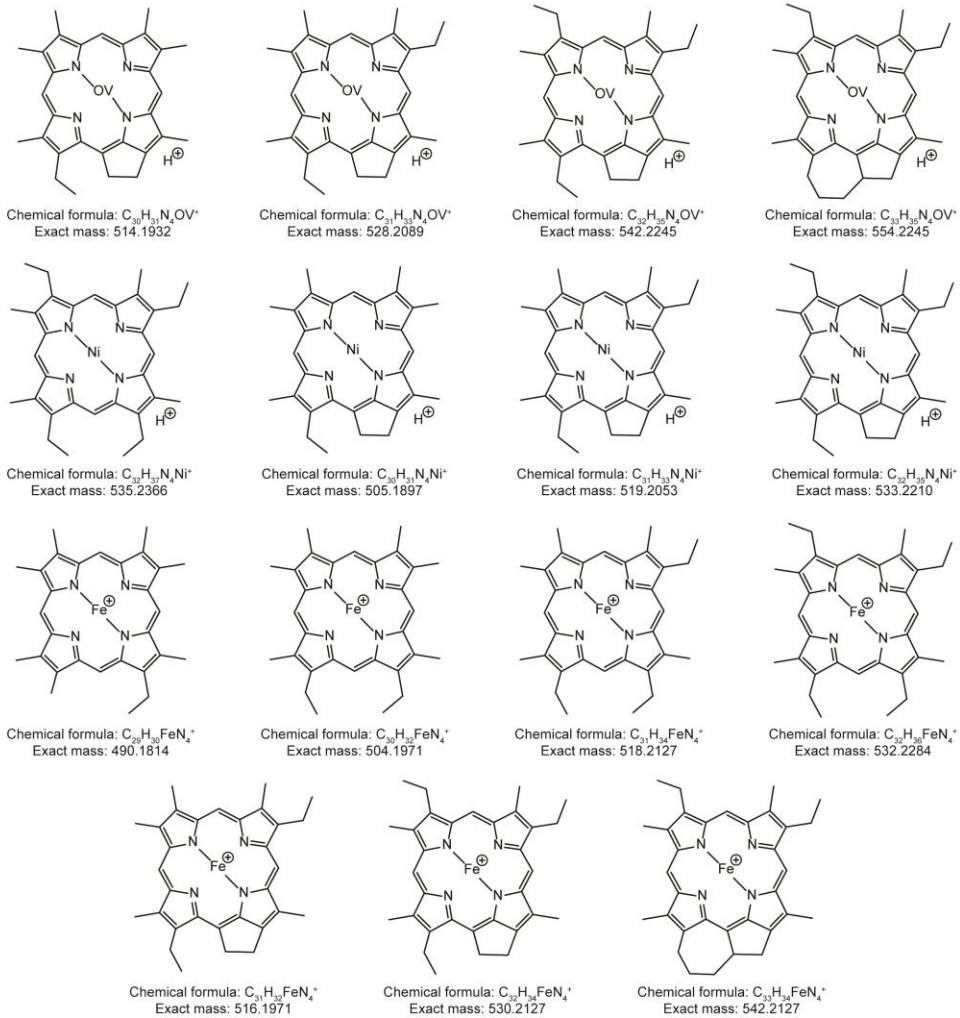

Chapter 4: Latitudinal variations in marine microbial ecological dynamics unravel the lifecycle of Oceanic Anoxic Event 2 (OAE-2)

Authors: Gregory T. Connock[1*], Jeremy D. Owens[2], and Xiao-Lei Liu[1]

Affiliations: [1]School of Geosciences, University of Oklahoma, Norman, Oklahoma 73019, USA. [2]Department of Earth, Ocean, and Atmospheric Science, Florida State University, and National High Magnetic Field Laboratory, Tallahassee, Florida 32306, USA.

Abstract

A positive carbon isotope excursion (+CIE) attributed to enhanced organic carbon burial defines one of the most extensive Oceanic Anoxic Events (OAEs) of the Cretaceous spanning the Cenomanian-Turonian boundary (OAE-2). Despite thorough investigation, the processes governing the lifecycle of OAE-2 are grossly oversimplified. This is compounded by a lack of spatiotemporal delineation of organic carbon burial drivers on a local to regional scale, which is only recorded as a composite in the isotopic record reflecting the temporal evolution of global reservoirs. Here we generated comprehensive biomarker inventories at multiple sites spanning the proto-North Atlantic (p-NA) to reconstruct the microbial ecological dynamics sensitive to environmental change spanning OAE-2. Water column redox gradients, specifically photic zone impingement by oxygen minimum zones (OMZs), was integral to overall microbial community structure and subsequent production and/or preservation of organic carbon by affecting nutrient shuttling to the euphotic zone. Established OMZs in the southern p-NA facilitated the regional development of prolific primary production that destabilized carbon cycling and served as a mechanism to consume marine oxygen and initiate the +CIE. During OAE-2, organic carbon factories shifted north to continental margins in the central p-NA due to expanded OMZs, which offset attenuated primary production and enhanced preservation in the southern p-NA. This acted to perpetuate the +CIE, which ultimately ended because of continued, pervasive OMZ intensification and photic zone euxinia that led to nutrient deficiencies in surface waters and a collapse in primary production, analogous to reconstructions of the southern p-NA during OAE-2 onset. The simultaneous synchroneity and diachroneity of organic carbon burial drivers across the p-NA reveals unseen complexities in the +CIE driven by an amalgam of local environmental states modulating the expanse of marine deoxygenation in the mid-Cretaceous.

4.1 Introduction

Marine environments were subjected to recurrent periods of pervasive deoxygenation throughout the Cretaceous period termed Oceanic Anoxic Events (OAEs; Schlanger and Jenkyns, 1976). The most extensively studied event, OAE-2 (Cenomanian-Turonian, ~93.9 Ma), was defined by a pronounced carbon cycle perturbation driven by a sustained period of enhanced organic carbon burial, inferred from the globally observed positive carbon isotope excursion

(+CIE) in both organic and inorganic carbon reservoirs (e.g. Pratt and Threlkeld, 1984; Arthur et al., 1988; Thurow et al., 1992; Hasegawa, 1997; Tsikos et al., 2004; Erbacher et al., 2005; Jarvis et al., 2006; Jenkyns, 2010; Bomou et al., 2013). Proposed, principal causal mechanisms of the +CIE and OAE-2 include enhanced primary productivity linked with relatively coeval igneous activity and attendant effects (e.g. CO_2 outgassing → warmer global climate → intensified weathering), as well as associated or independent expansion of marine anoxia/euxinia increasing organic carbon burial (Schlanger and Jenkyns, 1976; Arthur et al., 1987; Sinninghe Damsté and Köster, 1998; Kuypers et al., 2002; Turgeon and Creaser, 2008; Pogge von Strandmann et al., 2013; Du Viver et al., 2014, 2015; Owens et al., 2018). However, recent work has elucidated environmental and biogeochemical dynamicity during OAE-2 that intimates unappreciated complexities necessitating further investigation (Owens et al., 2012; van Bentum et al., 2012; Clarkson et al., 2018; Raven et al., 2018). Further delineation of progressive deoxygenation preceding OAE-2 (Owens et al., 2016; Ostrander et al., 2017; Raven et al., 2019), attributed to localized increases in primary production (e.g. the pre-OAE biotic perturbation, pre-OAE BP; Connock et al., in review, Chapter 1), necessitates an improved understanding of how localized phenomena contributed to the greater OAE and coeval +CIE.

Here, we reconstructed microbial ecological dynamics enveloping OAE-2 by applying a novel analytical method and approach (liquid chromatography – quadrupole time-of-flight – mass spectrometry, LC-qTOF-MS) to generate diverse biomarker inventories sensitive to environmental change at distinct latitudes and depositional settings across the proto-North Atlantic (p-NA). Biomarkers represent the molecular fossils of past microbial life, and are thus sensitive to the oceanographic and climatic shifts spanning OAE-2. Significantly, biomarkers capture localized depositional variations, albeit amidst the backdrop of the global climate state, and may help

disentangle localized influences on proxy data predominantly reflecting regional/global trends. Paleoenvironmental context relevant to the determination of local organic carbon burial drivers, and how they contribute to the greater +CIE, may be inferred by assessing trends in depth-specific microbial communities (e.g. pelagic vs. benthic) through time and space. We targeted two primary objectives to achieve an original conception outlining the lifecycle of OAE-2, and perhaps other periods of marine deoxygenation: 1) spatial delineation of the pre-OAE BP and 2) reconstruction and correlation of microbial ecological and oceanographic dynamics throughout OAE-2. Environmental consistencies predisposing regions to the pre-OAE BP were identified, which reemerged at other localities later during OAE-2 and acted to perpetuate pervasive anoxia and euxinia in the greater p-NA. Recognition of synchronous and diachronous microbial ecological shifts across the p-NA emphasized how local biases in organic carbon burial drivers varied temporally, ultimately recording a sequence events articulating the spatiotemporal character of the +CIE and OAE-2.

4.2 Methods

4.2.1 Sample collection, preparation, and analysis

In addition to the 43 samples collected at ODP Site 1258 in Chapter 1, three additional sites were sampled at varying resolutions. DSDP Site 367 was the most sparsely sampled locality (n = 10), with improved sampling density at Shell International/Office National de Recherches et d'Exploitations Pétrolières well S75 (n = 28) and IODP Site U1407 (n = 23). Samples were prepared for LC-qTOF-MS using the same procedure outlined in Chapter 1 (see section 1.2.2), except additional standards (VO-TPP, Ni-TPP) were included to improve metalloporphyrin quantification. The analytical method was consistent with previous analysis of OAE-2 sediments

(e.g. site 1258) outlined in Chapter 1 (see section 1.2.3), as were biomarker identifications and quantification (see sections 1.2.4 and 2.3.1).

4.3 Results

4.3.1 Paleogeographic context

Three additional localities of distinct paleolatitudes in the proto-North Atlantic (p-NA, ~5^{o}N, 15^{o}N, and 35^{o}N; Figure 4-1) were studied to assess the spatial extents and potential synchroneity of reconstructed events bounding OAE-2 at the Demerara Rise. Previously published delineations of OAE-2 leveraging the characteristic +CIE ensured samples were coeval with those analyzed in Chapter 1 (Arthur et al., 1988; Kuhnt et al., 2001; Kuypers et al., 2002; Kuhnt et al., 2005; Bornemann and Friedrich, unpublished results) Recall, ODP Site 1258 on the Demerara Rise was situated near the equator (0^{o}) and represents a highly productive, persistently anoxic upwelling center along the northern continental margin of Suriname (South America) at paleodepths of ~500-1500 m (Figure 4-1). Laminated black shales predominate Albian to Campanian strata, underscoring the persistent anoxia unbound by globally observed OAEs at this site defined by exceptional organic matter preservation (Erbacher et al., 2004; 2005).

Like the Demerara Rise, organic-rich deposits were not solely exclusive to OAE-2 at DSDP Site 367 (paleolatitude ~5^{o}N), drilled in the Cape Verde Basin off the west coast of Senegal. (Figure 4-1). Although a greater distance separates sites 1258 and 367 today, both sites were significantly closer in the Cenomanian-Turonian and record equatorial oceanographic conditions in the southwest (1258) and southeast (367) p-NA, respectively. Extensively laminated, organic-rich sediments precede the onset of OAE-2 at site 367, with TOC values up to 50 wt.% observed during the event (Herbin et al., 1986). This provided direct evidence for anoxic deep water in the

p-NA given site 367 paleodepths, capturing abyssal plain sedimentation at ~3700 m near the ancestral mid-ocean ridge (Kuypers et al., 2002).

Conversely, Shell International/Office National de Recherches et d'Exploitations Pétrolières well S75 (herein simply referred to as 'site S75') was characterized by the shallowest paleodepths of this study (~100-300 m; Kuhnt et al., 1997). Positioned along the northwestern African coast in the Tarfaya Basin (present day Morocco, paleolatitude ~15^{o}N; Figure 4-1), the Cenomanian-Turonian interval of site S75 consisted of two organic-rich facies, calcareous black shales and gray-brown laminated chalks, interbedded with light gray limestones (Leine, 1986; Kolonic et al., 2005). Deposition of these predominant lithofacies is periodically interrupted by tempestites exhibiting diagnostic hummocky cross-stratification (Albani El et al., 1999). Exceptionally high sedimentation rates surpassing 10 cm/kyr enabled site S75 to achieve unmatched organic matter accumulation rates during the Cenomanian-Turonian, including OAE-2 (Leine, 1986; Kuhnt et al., 1997). This has permitted high-resolution temporal investigations of OAE-2 at proximal wells (e.g. SN^{o}4; Kuhnt et al., 2017) and a significantly expanded OAE-2 interval in most cores from the Tarfaya Basin, such as site S75.

IODP Site U1407 provides paleoenvironmental context of the northern p-NA margin (~35^{o}N) at paleodepths of ~2600 m on the Newfoundland Ridge (Figure 4-1). However, this paleodepth is tentative as it was intended for the region at 50Ma (Tucholke and Vogt, 1979), not ~94Ma. Given a maximum transgression was relatively coeval with OAE-2 and a comparably warm climatic state to Cretaceous hothouses was in place ~50Ma (e.g. Early Eocene Climatic Optimum; Zachos et al., 2008), it is likely paleodepths were similar. Further validation of this key presumption is challenging as very little published literature exists for site U1407, which primarily targeted Paleogene strata to constrain Paleocene and Eocene climate transitions (Norris et al.,

2014). A combination of sedimentology and biostratigraphy aided in the initial delineation of OAE-2, with later carbon isotopic analysis clearly showing the characteristic +CIE (Bornemann and Friedrich, unpublished results). The OAE is preceded by deposition of green to white nannofossil chalks and thin intercalations of dark gray clays. Interestingly, nannofossil biostratigraphy and carbon isotope stratigraphy revealed the onset of OAE-2 began within these nannofossil chalks and was not coincident with the sharp transition to finely laminated/massive black shales littered with small (sub-mm) pyrite framboids. This signifies site U1407 lagged the initial globally enhanced burial of organic carbon driving the +CIE. Duration estimates of OAE-2 are likely impossible due to drilling disturbances when coring, but the shift to facies indicative of localized deoxygenation (i.e. black shales) span only ~30 cm and are separated by a band of dark gray claystone. Onboard biostratigraphic analysis revealed the entirety of OAE-2 was captured and is thus highly condensed at site U1407. A brief transitory period succeeded black shale deposition, reflected by a narrow (26 cm) section of laminated green-gray clays and dark gray radiolarian tests. This is followed by a reappearance of green to white chalks, but now intercalated with siliceous limestone and chert (Norris et al., 2014). These lithofacies transitions are consistent with those observed at other global sites (e.g. Bonarelli horizon; Arthur and Premoli Silva, 1982), but the proximity of the black shale in site U1407 to established biostratigraphic zonations is consistent with a delayed onset of localized anoxia at the Newfoundland Ridge relative to other regions (e.g. Tethys Ocean, southern p-NA).

4.3.2 Biomarker inventories

Biomarker preservation and stratigraphic distributions were primarily controlled by distinct, site-specific environmental conditions. Post-depositional alteration of biomarkers via thermal maturity was likely minimal since all samples were immature (Kuhnt et al., 1997; Forster

et al., 2004; Kolonic et al., 2005; Meyers et al., 2006; Sinninghe Damsté et al., 2008; Norris et al., 2014), meaning temporal variations in biomarker inventories predominantly reflect the evolution of microbial inhabitants, controlled by environmental changes, in the p-NA. However, preservation of the indigenous microbial signal is subject to degradative processes post-senescence operative under both oxidative and reductive conditions within the water column and sediments. Biomarker interpretations from localities exhibiting major lithologic shifts indicative of contrasting redox states and depositional environments (e.g. sites S75 and U1407) may be adversely affected by the absence of specific compounds or altered distributions of those preserved. This will be evident when comparing the biomarker diversity between sites, with subsequent interpretations attempting to account for potential biases and mitigate erroneous interpretations. Still, biomarker preservation across all 4 sites exceeds that observed in the overwhelming majority of paleoenvironmental investigations employing biomarker proxies.

Sites 1258, 367, and U1407 exhibited exceptional biomarker preservation. Both free-base tetrapyrroles and metalloporphyrins were present, as well as isoprenoidal (isoGDGTs), branched (brGDGTs), and overly branched (obGDGTs) GDGTs. The C_{40} aromatic carotenoid isorenieratane was detected in samples from all three sites, in addition to dialkyl glycerol ethers (DAGEs), butanetriol/pentanetriol dialkyl glycerol tetraethers (BDGT/PDGT), and a diverse suite of tocol derivatives composed of α- and γ-tocopherol, α-tocopherol quinone, di- and tri-methylphytylbenzoquinones (MPBQs), and the 5,7,8-methyltrimethyltridecylchroman (MTTC, Figure 4-2). Only the MPBQs and MTTC were ubiquitously present, with tocopherols and α-tocopherol quinone absent from site U1407 and γ-tocopherol exclusive to site 1258. Biomarker diversity markedly shifts in post-OAE U1407 samples characterized by minimal to no tetrapyrroles (free bases or metalated) and a substantial decrease in crenarchaeol fractional abundances offset

by a large increase in DAGEs (Figure 4-3). In contrast to sites 1258, 367, and U1407, site S75 exhibited less diversity in biomarker classes owing to the absence of all glycerol ether lipids. Metalloporphyrins were the most dominant, followed by free base tetrapyrroles, tocol derivatives (excluding γ-tocopherol) and isorenieratane (Figure 4-2). Biomarker fractional abundances were similar at site 367, predominated by tetrapyrroles, while tocol derivatives were the most abundant at site 1258 followed by tetrapyrroles and crenarchaeol. Appreciable fractional abundances of isorenieratane were relatively exclusive to OAE-2 at sites 1258, 367, and to a lesser extent site S75, where isorenieratane was unbound by the OAE. Interestingly, isorenieratane was detected in relatively trace amounts in a pre-OAE sample from site U1407, which exhibited an overall predominance of crenarchaeol in pre-/intra-OAE strata that shifted to DAGEs in the post-OAE interval (Figure 4-3).

Depth profiles of biomarker concentrations were possible for sites 1258 (previously discussed in Chapter 1, Figure 4-4), 367 (Figure 4-5), and S75 (Figure 4-6). Lack of TOC values for site U1407 (still pending) precluded normalization to organic carbon and thus, biomarker depth profiles were unable to be discussed. While normalization to the mass of sediment extracted was an option, it was determined biomarker concentrations were heavily biased towards greater TOC values and quantification using sediment mass was inappropriate at site U1407. Tetrapyrroles, crenarchaeol, and to a lesser extent, obGDGTs, rapidly increase in pre-OAE samples from site 367 before declining to relatively lower concentrations that were sustained throughout OAE-2 (Figure 4-5), mirroring observations at site 1258 (Figure 4-4). Isorenieratane, in low concentrations before OAE-2, remained elevated during the event, which was also characterized by spikes in obGDGTs, DAGEs, BDGT/PDGT, and tocol derivatives. Biomarker trends following OAE-2 at site 367 were challenging to interpret due to the low sample count ($n = 2$), and will not be discussed. Tetrapyrrole

concentrations, in contrast to sites 1258 and 367, were generally elevated during OAE-2 at site S75 (Figure 4-6). An overall increase was observed during the first half of the OAE, followed by a brief decline and recovery to maximum tetrapyrrole concentrations in the last sample within the OAE-2 interval. Post-OAE tetrapyrrole concentrations were comparable to those observed pre-OAE. The presence of isorenieratane was typically transient, characterized by isolated concentration spikes throughout the sampled interval. However, a sustained increase in isorenieratane concentrations marked the latter half of OAE-2 and briefly extended into post-OAE samples where maximum values were observed. Tocol derivatives remained relatively unchanged across the onset of OAE-2, but exhibited a progressive rise during the latter half of the OAE. This was not sustained beyond OAE-2, but a rapid, transient increase in tocol derivatives in younger post-OAE samples was observed (Figure 4-6).

4.4 Discussion

4.4.1 Spatial extrapolation of the pre-OAE biotic perturbation

The paleoenvironmental significance of all biomarkers was addressed in Chapter 1 (see section 1.3.1) and Chapter 2 (see section 2.4.3), with a complete discussion proposing and outlining the pre-OAE biotic perturbation (pre-OAE BP) at site 1258 found in Chapter 1 (see section 1.3.2). Recognition of the pre-OAE BP at site 1258 (Connock et al., in review, Chapter 1), defined by a localized, protracted (~100 kyr) phase of enhanced primary production and attendant expansion of marine anoxia, revealed the potential biotic induction of OAE-2 and progressive deoxygenation recently identified to antedate the +CIE and OAE inception (Owens et al., 2016; Ostrander et al., 2017). Substantiation of the pre-OAE BP is supported by a concomitant, minor positive $\delta^{13}C_{org}$ excursion (Erbacher et al., 2005) likely indicative of elevated primary productivity, as well as an abrupt, coincident $\delta^{34}S_{pyrite}$ decline attributed to an expansion of anoxic conditions

(Raven et al., 2019) potentially related to the spike in organic matter remineralization at site 1258. Relatively concurrent onset of large igneous province (LIP) activity (~200-300 kyr before OAE-2; Du Vivier et al., 2014) with the pre-OAE BP (~220 ± 4 kyr before OAE-2; Connock et al., in review, Chapter 1) suggests a potential causal relationship, especially given the modern marine microbial ecological response to submarine interactions with volcanic fluids (Wilson et al., 2019). Thus, identification of the pre-OAE BP revealed how antecedent spikes in primary productivity locally facilitated the initiation of the OAE as a mechanism to consume marine oxygen and subsequently enhance organic carbon preservation globally.

Although identification of the pre-OAE BP refined current understandings of how marine deoxygenation develops in deep time, it was based on a single locality (site 1258) and unable to be spatially extrapolated to coeval, published biomarker records from other regions of the p-NA given the novelty of the applied LC-qTOF-MS method (Connock et al., in review, Chapter 1). To address this shortcoming, all sites in this study were subjected to the same LC-qTOF-MS method as site 1258 to generate comparative biomarker inventories and delineate the spatial character of the pre-OAE BP, as well as the spatiotemporal variance of primary productivity spanning OAE-2. Unfortunately, lack of TOC values for site U1407 limited interpretations to biomarker fractional abundances and/or ratios, which do not capture the pre-OAE BP as well as concentration profiles. Still, lithology contrasts across the OAE-2 interval at site U1407 may hamper confident interpretations on solely biomarker profiles given redox and diagenetic effects on compound preservation. Similar factors may compromise interpretations of biomarker concentrations at site S75, and will be addressed accordingly throughout the discussion. Characteristic features of the pre-OAE at site 1258 included spikes in tetrapyrrole, crenarchaeol, and obGDGTs concentrations attributed to enhanced primary production by photo- (tetrapyrroles) and chemoautotrophs

(crenarchaeol) producing an expanded oxygen minimum zone hosting a prolific anaerobic bacterial community (obGDGTs, Figure 4-4). Site 367, although less extensively sampled compared to site 1258, exhibited similar pre-OAE stratigraphic trends in tetrapyrroles, crenarchaeol, and obGDGTs that may correlate to the pre-OAE BP (Figures 4-2 & 4-5). Note that both sites 1258 and 367 displayed sharp increases in MPBQs concomitant with pre-OAE BP onset, although an explanation for this observation remains elusive. Conversely, site S75 did not exhibit any diagnostic pre-OAE trends consistent with the pre-OAE BP, reliant on solely tetrapyrroles as crenarchaeol and obGDGTs were undetected. This may be an artifact of variable biomarker preservation tied to lithologic changes reflecting dynamic environmental conditions, or inadequate sampling prior to OAE-2. However, elevated tetrapyrrole concentrations throughout OAE-2, potentially indicative of heightened primary productivity at site S75 (Figure 4-6), provide a mechanism to sustain the +CIE as primary production at other sites (e.g. sites 1258 and 367) decreased during OAE-2 highlighted by a relative decline in tetrapyrrole profiles (Figures 4-4 & 4-5).

Recognition of the pre-OAE BP at site 367 was not surprising given the proximity to site 1258 (Figure 4-1), paleogeographic positioning along the western margin of Africa enabling efficient nutrient distribution via upwelling (Handoh et al., 1999; Trabucho Alexandre et al., 2010), and persistently reducing bottom waters ensuring biomarkers primarily reflect microbial ecological variations. The only difference between the two sites was the reconstructed response of deep water (i.e. bathypelagic to benthic) microbial communities. At site 1258, only a transient increase in microbial sulfate reduction (MSR) was identified, based on a spike in DAGEs concentrations, and inferred to represent depletion of energetically favorable electron acceptors by enhanced organic matter remineralization (Figure 4-4). Further descension of the redox ladder was

observed at site 367 where contribution from methanogenic archaea, or possibly heterotrophic archaea (BDGT/PDGT) increased in tandem with characteristic biomarkers of the pre-OAE BP (Figure 4-5). Subsequent decline in biomass production by photo- and chemoautotrophs (i.e. tetrapyrroles and crenarchaeol) leading into the onset of OAE-2 led to an attenuation of remineralization rates, and a decline in BDGT/PDGT concentrations as methanogenic/heterotrophic archaeal communities collapsed. This reflects the considerable organic carbon production that characterized both sites 367 and 1258 during the pre-OAE BP. The relatively proximity between both sites likely meant subjection to similar environmental conditions, one of which may include exogenous nutrient delivery from submarine LIPs or hydrothermal fluids associated with the nearby mid-ocean ridge (MOR; Sinninghe Damsté and Köster, 1998; Kuypers et al., 2002). Coincidence between the onset of LIP and MOR activity is not beyond the realm of possibility given the general synchroneity of igneous events during superplume events (Larson, 1991). Indeed, Sr isotopes have elucidated accelerated spreading rates, enhanced submarine volcanism, and increased emission of hydrothermal fluids characterized the Cenomanian-Turonian (Ingram et al., 1994; Frijia and Parente, 2008), corroborated by Nd (MacLeod et al., 2008) and Os (Turgeon and Creaser, 2008) isotopic excursions. Thus, the vicinity of sites 1258 and 367 to the MOR likely predisposed both sites to upwelling of bioessential elements released from igneous activity, ultimately playing a role in pre-OAE BP initiation.

Further correlation of the pre-OAE BP to other regions will be challenged by contrasting redox states preceding the pervasive marine anoxia/euxinia defining OAE-2. The persistently reducing bottom waters enveloping the OAE-2 interval at sites 1258 and 367 may explain why the pre-OAE BP was detected at both localities, but not at site S75. However, all three sites exhibited persistently elevated VO/Ni-porphyrin values (> 0.8, calculated as VO-porphyrins/(VO-

porphyrins+Ni-porphyrins), Figure 4-7; Tables 4-1, 4-2, 4-3) indicative of euxinic bottom water/SWI conditions whereby available VO complexed with free base porphyrins as Ni was drawn down by reactions with sulfides (Lewan, 1984; Breit and Wanty, 1991). This suggests there may be additional diagenetic effects unrelated to redox (e.g. matrix effects, reviewed in Wakeham and Canuel, 2005) impacting biomarker retention in sediments and subsequent rocks. The lack of a comparable biomarker inventory at site S75, devoid of GDGTs and other glycerol ether lipids, does not signify an absence of GDGT-producing organisms, but rather the poor preservation or selective degradation of these compounds. Preferential degradation of glycerol ether lipids relative to the less labile compounds preserved (e.g. tetrapyrroles, tocol derivatives, isorenieratane) likely occurred and fits the depositional setting of site S75. The presence of interbedded tempestites and hummocky cross-stratification (Albani El et al., 1999) confirms the shallow estimated paleodepths (~100-300 m; Kuhnt et al., 1997) that predisposed sediments to reworking and transient oxygenation of the SWI, potentially compromising biomarker indigeneity and preservation of glycerol ether lipids. Further analysis (e.g. GC-MS) is required to determine if potential degradation products (Liu et al., 2016) are present, but the lack of comparable biomarker preservation at site S75 is concerning and may compromise interpretations solely founded on biomarker proxies. However, based on the biomarker distributions and stratigraphic trends preceding OAE-2, the pre-OAE BP did not extend to the northwestern coast of Africa (Tarfaya Basin). This parallels $\delta^{34}S_{pyrite}$ records from site S75 that reveal expansion of anoxia/euxinia was concurrent with the +CIE and OAE-2 onset, which contrasts $\delta^{34}S_{pyrite}$ stratigraphy at site 1258 reflective of intensified anoxia before OAE-2 (Raven et al., 2019) and linked to the pre-OAE BP (Connock et al., review, Chapter 1) presaging the global development of widespread euxinia during the event (Owens et al., 2013).

The presence of the pre-OAE BP in the northern p-NA (U1407) was unable to be evaluated, but a brief period of PZE inferred from the sudden occurrence of isorenieratane and slight decline in crenarchaeol fractional abundances preceded the onset of OAE-2 (Figure 4-3). This is consistent with the progressive development of PZE prior to OAE-2 initiation, but after cessation of the pre-OAE BP, at site 1258, as well as potentially sites 367 and S75 where increases in isorenieratane concentrations occur across the +CIE (Figures 4-4, 4-5, 4-6). Appreciable MSR was already active before OAE-2 at site U1407, reflected by relatively consistent DAGEs contribution to the total biomarker pool (Figure 4-3). VO/Ni-porphyrin values provide an alternative perspective on bottom water redox at site U1407, exhibiting high variability throughout the entire sampled interval (Figure 4-7). Bottom water redox, inferred from VO/Ni-porphyrin values, ranged from oxic to euxinic due to the complete absence of VO- or Ni-porphyrins in some samples, but was predominantly consistent with anoxia/euxinia at the SWI before OAE-2 ($VO/Ni\text{-}porphyrin_{avg}$ = 0.47). A complete absence of Ni-porphyrins, producing a VO/Ni-porphyrin value of 1, coincided with the appearance of isorenieratane. Thus, a period of intensified upwelling may have transported sulfidic waters to the lower euphotic zone and enabled the transient development of PZE prior to OAE-2 at site U1407. Altered nutrient cycling and enhanced environmental stressors associated with transitioning water chemistry may have destabilized established microbial community gradients and explain the abrupt drop in crenarchaeol, but coincident rise in tocol derivatives sensitive to redox fluctuations, leading into OAE-2 (Figure 4-3). However, it is perplexing as to why pervasive PZE did not develop at sites 1258 and 367 given the invocation of upwelled, potentially hydrothermally derived nutrients to initiate and sustain the pre-OAE BP. Contrasting water chemistry between sites 1258/367 and U1407 may have inhibited efficient nutrient transport to the upper euphotic zone, or a lack of sustained upwelling at site U1407 may

have facilitated the stabilization of the water column and chemocline formation. In addition, prolific primary production in the oxygenated photic zone supported by a protracted phase of intensified upwelling at sites 1258 and 367 may have suppressed the development of phototrophic sulfur bacteria by limiting light availability to the lower euphotic zone. While the exact mechanism is challenging to identify currently, the key takeaway is PZE was a transient feature along the northern margin of the p-NA prior to OAE-2. Future evaluation of site U1407 for the presence of the pre-OAE BP may be possible despite potential preservation biases given comparable biomarker inventories before and during OAE-2 at this site (Figure 4-3).

4.4.2 Microbial ecological and oceanographic dynamics during OAE-2

Evolving climatic and oceanographic conditions during OAE-2 induced pronounced microbial ecological shifts in the southern p-NA (site 1258) defined by an expansion of intermediate and deep water microbial communities (Connock et al., in review, Chapter 1). Shoaling of a euxinic OMZ fueled by high rates of MSR led to recurrent PZE and sustained anoxia in the euphotic zone as water mass density gradients stabilized the water column, causing persistent stratification that sustained persistent PZE. This enabled the development of a distinct microbial ecology during OAE-2 in the southern p-NA, whereby organisms tolerant to the expanding euxinic environment thrived (e.g. phototrophic sulfur bacteria, Figure 4-2). Pervasive anoxia/euxinia, combined with a well-stratified water column, fundamentally altered biogeochemical cycling that led to nutrient (e.g. fixed N) shortages in supra-chemocline (i.e. oxygenated surface waters) communities where primary productivity declined (Kuypers et al., 2002; van Bentum et al., 2009; Jiménez Berrocoso et al., 2010; Martin et al., 2012; Owens et al., 2013; Raven et al., 2019; Connock et al., in review, Chapter 1). Application of the same LC-qTOF-MS method on additional sites has now enabled the microbial ecological dynamics, and by extension the overriding

oceanographic state, to be reconstructed across the greater p-NA to constrain the biotic response to OAE-2, as well as interpretations of other geochemical proxy records.

Previous consistencies between both southern p-NA localities (sites 1258 and 367) were maintained when assessing the microbial ecological changes throughout OAE-2 (Figure 4-2). The biotic response outlined above for site 1258 is directly applicable to site 367 based on temporal changes in biomarker distributions coeval with OAE-2. Declines in tetrapyrrole and crenarchaeol concentrations capture photo- and chemoautotrophic communities adversely affected by the development of PZE and OMZ expansion, inferred from abrupt increases in isorenieratane and obGDGTs profiles (Figure 4-5), particularly at 639.39 mbsf where a major shift in fractional abundances occurred (Figure 4-3). As reconstructed at site 1258, sharp positive excursions in the DAGEs are indicative of enhanced MSR sustaining PZE in the euphotic zone. A coeval spike in BDGT/PDGT concentrations is the only distinct feature of site 367 relative to site 1258, potentially a product of greater organic matter production and subsequent remineralization. While tocol derivatives remain relatively low during OAE-2, a brief increase was observed at site 367 (Figure 4-5) with relatively low sampling density potentially belying a greater frequency of elevated concentrations as observed at site 1258 (Figure 4-4). It is possible the spike in tocol derivatives captures a phytoplanktonic stress response to increasingly adverse conditions during the OAE, as proposed for site 1258 (see Chapter 2), given site 367 was subjected to highly reducing conditions beyond the OAE-2 interval,. These findings concur with and expand on previous work on site 367, which primarily highlighted the presence of shallow PZE and euxinia (Sinninghe Damsté and Köster, 1998; Kuypers et al., 2002; Owens et al., 2012).

Reconstruction of microbial ecological changes was limited and potentially compromised by preferential degradation of glycerol ether lipids at site S75. However, biomarker preservation

is still excellent compared to most paleoenvironmental studies, only alongside the exceptional biomarker records at sites 1258 and 367 is site S75 relatively inferior. Further discussion will make a key assumption that degradation was temporally consistent, based on no significant stratigraphic differences in biomarker inventories (e.g. sample-dependent preservation) and no apparent relationship between specific lithofacies and perceivably enhanced biomarker preservation. Unlike sites 1258 and 367, no major microbial reorganization marked OAE-2 at site S75 as shown by biomarker fractional abundances (Figure 4-2). Interestingly, fractional abundances appeared to exhibit cyclical trends characterized by increases in tocol derivatives relative to tetrapyrroles, followed by a systematic 'rebound' whereby tetrapyrroles increased relative to tocol derivatives (Figure 4-3). This was repeated throughout the sampled interval, most pronounced during OAE-2, and may be related to obliquity-driven changes in carbonate and organic matter production (Kuhnt et al., 2017). Tetrapyrrole concentrations generally increased throughout OAE-2, but exhibited a progressive decline and rise between ~75-65 m (Figure 4-6). This could reflect an initial increase in primary production during the first half of OAE-2, followed by a brief reduction inferred from attenuated chlorophyll synthesis and subsequent degradation to the sedimentary tetrapyrroles. Episodic PZE, deduced from the erratic behavior of isorenieratane (Figure 4-6) in agreement with previous reports (Sinninghe Damsté and Köster, 1998; Kuypers et al., 2002; Kolonic et al., 2005), did not have comparable effects on the overlying oxygenic photoautotrophs as seen at sites 1258 and 367 and thus, is unable to explain the tetrapyrrole profile. Instead, the progressive increase in tocol derivatives coincident with the initial drop in tetrapyrrole concentrations suggests gradual, but sustained, expansion of the OMZ.

Recall, tocol derivatives may record the phytoplanktonic stress response in settings characterized by persistent anoxia (e.g. sites 1258 and 367), but may also be sensitive to redox

shifts given the proclivity of tocopherols to rapidly degrade under oxidizing conditions (Grams et al., 1972; Liebler et al., 1990, Rontani et al., 2007; Nassiry et al., 2009), which was likely the case for site S75. The initial expansion of the OMZ may have negatively impacted preexisting oxygenic photoautotrophs by altering the transport and/or bioavailability of essential nutrients. However, this may have led to a phytoplanktonic reorganization and/or an enhanced cyanobacterial presence, a widely proposed biotic response during OAE-2 (Kuypers et al., 2002; Kashiyama et al., 2008; Junium et al., 2015; Owens et al., 2016) better suited to the increasingly anoxic water column. Sterane trifecta data, not included in this study or published elsewhere, for site S75 and the greater Tarfaya Basin would greatly assist in substantiation of this tentative interpretation by tracking potential coeval shifts in algal community composition as demonstrated elsewhere during OAE-2 (e.g. site 1258; Owens et al., 2016). Continually increasing tocol derivatives were eventually accompanied by rising tetrapyrrole and isorenieratane concentrations (~70 m, Figure 4-6), signifying the development of PZE and a simultaneous, relative increase in primary production [and/or preservation][3]. A cooccurrence of PZE and enhanced primary production may result from OMZ impingement on the photic zone, which has previously been invoked and demonstrated to improve nutrient advection to oxic surface waters via modulation of elemental cycling (e.g. N cycle; Higgins et al., 2012; Naafs et al., 2019). However, continued shoaling and sustainment of euxinic waters in the photic zone, partially an artifact of intensified stratification, will eventually promote quantitative loss of fixed N species through denitrification and/or anammox, as well as inhibit efficient upwelling of NH_4^+. This may explain why stratigraphic trends in tetrapyrroles and isorenieratane eventually decouple (Figure 4-6), with primary production adversely impacted by

[3] It is challenging to confidently differentiate the effects of enhanced production of tetrapyrrole precursors overlying and/or within euxinic waters from the coincident enhanced preservation of tetrapyrroles in an expanded euxinic environment.

nutrient shortages as isorenieratane concentrations continue to increase towards maximum values beyond the termination of OAE-2 as defined by the +CIE. The Black Sea, frequently referenced as a modern analog for past marine anoxia, exhibits similar water column characteristics (Kuypers et al., 2003) observed during this period at site S75, which also resembled the prevailing conditions during OAE-2 in the southern p-NA (sites 1258 and 367). Thus, while the development and/or expansion of the OMZ initially facilitated enhanced primary production for most of OAE-2 at site S75, continued vertical migration of euxinic waters ultimately led to the precipitous collapse of the prolific oxygenic photoautotrophic community coeval with OAE-2 termination.

Variation in microbial community dynamics along the northern margin of the p-NA (site U1407) is currently restricted to fractional abundances of biomarker classes. Later acquisition of organic carbon content will enable biomarkers to be quantified, although site U1407 possesses the greatest risk of disparate biomarker preservation given the organically lean, highly oxidized lithofacies (e.g. green chalks) enveloping the black shales of OAE-2, particularly in the post-OAE interval which is not a focus of subsequent discussion (Norris et al., 2014). Unlike all other sites predominated by photoautotrophic biomarkers (i.e. tetrapyrroles or tocol derivatives), glycerol ether lipids were the most abundant biomarkers at site U1407 (Figure 4-2). Crenarchaeol was the most prominent in pre-OAE and OAE strata, while the DAGEs were the relatively most abundant lipid following the OAE. Like site 1258, a shift in fractional abundances at site U1407 was initiated prior to the +CIE and was sustained throughout the majority of OAE-2 (Figure 4-3). Similar trends were not observed at site 367, where marked changes to biomarker fractional abundances were confined to OAE-2, or at site S75, where no apparent shift in fractional abundances was coeval with the event. However, at site 1258, tocol derivatives overwhelmed tetrapyrroles as the dominant biomarker class in the aftermath of the pre-OAE BP but before the onset of OAE-2. Although not

identical to the pre-OAE shift at site 1258, an abrupt increase in the relative abundance of tocol derivatives was coincident with the appearance of isorenieratane and a significant reduction in tetrapyrroles composed of solely metalloporphyrins in pre-OAE strata of U1407 (269.66 m, Figure 4-3). This pre-OAE shift at site U1407 is somewhat analogous to fractional abundances observed during OAE-2 at site 1258, with previous interpretations of biomarker distributions at both reconstructing similar environmental conditions. In short, the development of a well-stratified water column enabled the establishment of thick, euxinic OMZ where photoautotrophic sulfur bacteria, as well as other low-oxygen tolerant organisms, thrived. However, reducing conditions were likely confined to the OMZ and potentially SWI (based on VO/Ni-porphyrin values) given the observed lag in black shale deposition relative to the onset of the +CIE at site U1407 (Norris et al., 2014). This still may have altered biogeochemical cycling, leading to nutrient scarcity in the oxygenated surface waters that adversely impacted primary production. Examination of fractional abundances following this abrupt microbial shift, presumedly related to evolving oceanographic conditions, grants valuable context into the microbial ecological dynamics defining OAE-2 along the northern p-NA margin.

Following the brief phase of PZE and immediately before OAE-2 initiation, tocol derivatives remained elevated, tetrapyrroles returned in greater abundance, but the relative abundance of crenarchaeol markedly declined (Figure 4-3). This was maintained during the initial phase of OAE-2, but was accompanied by progressively enhanced contributions from DAGEs, BDGT/PDGT and tocol derivatives, alongside declining tetrapyrroles (Figure 4-3). During this period, relatively static fractional abundances of crenarchaeol remained low compared to the pre-PZE interval. However, as DAGEs, BDGT/PDGT, and tocol derivatives declined, crenarchaeol began to increase as tetrapyrrole contributions were persistently depressed. These temporal trends

in biomarker fractional abundances may represent initial intensification of the OMZ during the first half of OAE-2 and subsequently enhanced shuttling of organic matter to the SWI that supported expanded deep water communities of sulfate reducing bacteria (i.e. DAGEs) and methanogenic/heterotrophic archaea (BDGT/PDGT). However, it is unlikely the OMZ impinged upon the photic zone given the lack of fossil pigments produced by phototrophic sulfur bacteria (i.e. isorenieratane). Thus, certain bioessential elements (e.g. fixed N) were not efficiently transported to the upper euphotic zone and lost to biologically mediated reactions (e.g. denitrification; Naafs et al., 2019). This explains the progressive collapse of primary production (i.e. tetrapyrroles), and the relatively low crenarchaeol abundances representing *Thaumarchaeota* more tolerant to oligotrophic settings (Könneke et al., 2014). Compared to sites 1258, 367, and to a lesser extent, S75, OMZ expansion was not as pervasive at site U1407, which may explain the lasting presence of crenarchaeol at site U1407 during OAE-2 and very low fractional abundances and concentrations at sites 1258 and 367 (Figures 4-3, 4-4, 4-5, 4-6). The subsequent contraction of the OMZ, highlighted by declining tocol derivatives, reduced environmental stressors on overlying microbial communities and produced the progressively increasing crenarchaeol abundances during the second half of OAE-2 at site U1407 (Figure 4-3). Preferential exposure to upwelled nutrients enabled the initial recovery of *Thaumarchaeota*, and suppressed the latter rebound in primary production observed just before the cessation of OAE-2 (268.99 m, Figure 4-3). Declining rain rates of organic matter, resulting from enhanced pelagic oxidation reactions due to OMZ contraction, led to the decline of MSR and other forms of heterotrophy in deep water environments. Therefore, U1407 exhibited dynamic microbial ecological changes driven by a fluctuating OMZ that began prior to globally enhanced organic carbon burial (i.e. the +CIE) and continued to evolve throughout OAE-2.

4.4.3 OAE-2 inception, perpetuation, and termination

Delineating the extents of the pre-OAE BP and spatiotemporal dynamics of marine microbial ecological change bounding OAE-2 provided both direct and indirect evidence to posit the mechanism(s) inducing, perpetuating, and terminating the event. Many studies have attempted to determine causal factors contributing to the propagation of widespread marine deoxygenation during OAE-2, as well as how it was sustained for ~600 kyr and ultimately collapsed (e.g. Schlanger and Jenkyns, 1976; Demaison and Moore, 1980; Scholle and Arthur, 1980; Pedersen and Calvert, 1990; Kuypers et al., 2002, 2004; Nederbragt et al., 2004; Turgeon and Creaser, 2008; Trabucho Alexandre et al., 2010; Monteiro et al., 2012; Du Vivier et al., 2014, 2015; Jenkyns et al., 2017; Owens et al., 2018; Raven et al., 2018). Even more characterize the environmental perturbations preceding, coinciding with, or following the event (e.g. Erbacher et al., 2005; Jenkyns et al., 2007; Friedrich et al., 2008; Kashiyama et al., 2008; van Bentum et al., 2009; Higgins et al., 2012; Martin et al., 2012; Owens et al., 2013, 2016; Ostrander et al., 2017; Raven et al., 2019), providing an excellent foundation comprised of diverse approaches for future study. However, the +CIE, classically used to demarcate OAE-2, represents a phase of sustained, *globally* enhanced carbon burial (Scholle and Arthur, 1980). Thus, many studies overlook how local to regional perturbations may destabilize carbon cycling, favoring oversimplified global shifts in productivity and/or preservation as principal forcings of the +CIE and, by extension, the formally delineated OAE-2. Only recently have localized phenomena (e.g. pre-OAE BP, Connock et al., in review, Chapter 1) been invoked to explain the progressive deoxygenation of the greater ocean basins preceding OAE-2 (Owens et al., 2016; Ostrander et al., 2017). Here, we address an ongoing enigma surrounding how an OAE is conceived, nourished, and eventually ‘ends’.

The spatial character of the pre-OAE BP is important. Limited to the southern p-NA sites (sites 1258 and 367), it seems the pre-OAE BP was dependent on regions predisposed to developed, persistent OMZs and highly reducing bottom water conditions. Therefore, the association between the pre-OAE BP and the southern p-NA, where pervasive black shale deposition occurred beyond OAE-2, was likely not a coincidence. Presuming exogenous nutrients derived from LIPs or the MOR were released during the enhanced period of igneous activity relatively coeval with pre-OAE BP initiation (Du Vivier et al., 2014), subsequent upwelling in anoxic settings would aid shuttling of [hydrothermal] Fe and other bioessential metals (Owens et al., 2012) to stimulate primary production, a defining feature of the pre-OAE BP. The lack of shallow pelagic euxinia at sites 1258 and 367 during the pre-OAE BP, with euxinia likely restricted to within the SWI based on high VO/Ni-porphyrin values (Figure 4-7, Tables 4-1 & 4-2) and an absence of sulfate reducing bacterial lipids (i.e. DAGEs, Figures 4-4 & 4-5), only enhanced vertical advection of critical nutrients that may be rendered unavailable under oxic or euxinic conditions (e.g. Fe; Owens et al., 2012). Furthermore, the southern p-NA OMZ was probably persistently shallow, proximal to the euphotic zone based on the pronounced increase in primary production at both sites (sites 1258 and 367) and critical for favored models explaining $\delta^{15}N$ systematics with upwelling of fixed N species predominated by NH_4^+ (Higgins et al., 2012; Naafs et al., 2019). Neither site S75 nor U1407 exhibited a persistently reducing redox state prior to OAE-2 onset, which explains the lack of the pre-OAE BP at these localities. Thus, the localized water column redox gradient possessed a profound influence on the spatial extents of the pre-OAE BP, but also the greater microbial ecological response concomitant with OAE-2.

The shift from a productivity-driven system (i.e. pre-OAE BP) to a preservation dominant system at site 1258, and by extension site 367, during OAE-2 has been previously discussed in

Chapter 1 (see section 1.3.4). Both southern p-NA sites were subjected to pervasive, recurrent PZE and sustained photic zone anoxia enabled by the development of pronounced density stratification. However, despite the clear intrusion of the OMZ into the lower euphotic zone, primary production was depressed for the entirety of OAE-2 in the southern p-NA. Regional shoaling and sustainment of the euxinic OMZ enabled a significant expansion of microbial communities tolerant to the sulfidic environment, and led to habitat constriction of the photo- and chemoautotrophs residing in the overlying oxygenated waters. Since upwelling was the primary mechanism of nutrient delivery along the continental margins in the southern p-NA (Trabucho Alexandre et al., 2010), organisms tolerant to the underlying euxinic conditions gained preferential exposure to upwelled nutrients. This exacerbated biologically mediated nutrient sinks thriving in the expanded anoxic/euxinic water column (e.g. denitrification or anammox; Devol, 2015 and references therein) and chemical depletion of trace metals (Hetzel et al., 2009; Owens et al., 2016), with stark density gradients (Jiménez Berrocoso et al., 2010; Martin et al., 2012; Connock et al., in review, Chapter 1) further compounding nutrient stress by limiting upwelling efficiency. Yet, the persistence of the +CIE necessitates continued, elevated production and enhanced preservation of organic carbon elsewhere across the p-NA as previously proposed (Connock et al., in review, Chapter 1). Results from the central p-NA along the northwestern coast of Africa (site S75) highlighted a relative increase in primary production during OAE-2 initially linked with a shoaling OMZ. As during the pre-OAE BP, this enabled improved nutrient transport to primary producers from depth and facilitated periods of enhanced primary production for the majority of OAE-2 at site S75. However, continued shoaling and/or intensification of a now euxinic OMZ enabled the progressive development of similarly expanded euxinia-tolerant microbial communities as observed earlier during OAE-2 in the southern p-NA. Parallels between the initial biotic response

to OAE-2 in the southern p-NA eventually manifested at higher latitudes like site S75, with a subsequent collapse in primary production as PZE maintained prolific anoxygenic photoautotrophic sulfur bacterial populations in progressively stratified waters. Significantly, maximum isorenieratane concentrations marked the end of OAE-2 (Figures 4-4, 4-5, 4-6), as defined by the +CIE, at all sites where present during OAE-2 (sites 1258, 367, and S75). This is substantiated by previous biomarker study at these sites (Kuypers et al., 2002; Kolonic et al., 2005; van Bentum et al., 2009), and provides a mechanism to end the +CIE, but not necessarily the widespread deoxygenation, consistent with reports of lasting euxinia and marine deoxygenation after OAE-2 (Owens et al., 2013; Ostrander et al., 2017; Connock et al., in review, Chapter 1). The following discussion will place these findings in greater context by addressing how the +CIE was initiated, perpetuated, and terminated, as well as how this relates to the lifecycle of OAE-2.

The Cretaceous, particularly the Cenomanian-Turonian, was primed for OAEs. High pCO_2 (2 to 8x greater than today; Barclay et al., 2010; Wang et al., 2014) drove elevated sea surface temperatures exceeding 30^{o}C (O'brien et al., 2017) that reduced marine O_2 solubility in greatly expanded, highly productive continental shelf environments linked with seafloor swelling and high production rates of oceanic crust (Larson, 1991; Kaiho and Saito, 1994; Bjerrum et al., 2006). As a result, marine deoxygenation and euxinia was not confined to OAEs (Erbacher et al., 2005; Owens et al., 2013; Owens et al., 2016; Ostrander et al., 2017; Raven et al., 2019; Connock et al., in review, Chapter 1), which is precisely how OAE-2 and the attendant +CIE were conceived. Preexisting OMZs in the southern p-NA enabled the efficient upwelling of exogenous, LIP-/MOR-derived nutrients to the euphotic zone ~220 ± 4 kyr prior to OAE-2. This event, termed the pre-OAE BP (Connock et al., in review, Chapter 1), represented a regional increase in organic carbon production (i.e. primary production) and, more importantly, export that acted as a marine oxygen

sink via enhanced remineralization reactions to initiate the progressive marine deoxygenation antedating OAE-2. Continued development and expansion of OMZs across the p-NA, Tethyan Sea, and [potentially] global oceans resulted in rampant organic carbon burial producing the initial +CIE excursion. However, highly productive settings in the southern p-NA were adversely impacted by intensified, persistent shallow water anoxia and euxinia during OAE-2 that ultimately imposed constraints on primary production, while simultaneously enhancing organic carbon sequestration. Other regions where OMZs were not temporal constants prior to OAE-2, such as the northwestern African coast, acted as compensatory mechanisms to sustain the +CIE through elevated primary production driven by the development and expansion of nutrient-shuttling OMZs. However, similarly abrupt declines in primary production towards the end of OAE-2 were eventually encountered in these settings as observed in the southern p-NA coeval with OAE-2 initiation. Expanded euxinia, likely confined to continental margins (Owens et al., 2013; Raven et al., 2019), and extensive deoxygenation across the p-NA for nearly 600 kyr (i.e. OAE-2 duration; Sageman et al., 2006) led to severe micronutrient shortages through drawdown of the marine trace metal reservoir (Hetzel et al., 2009; Owens et al., 2016). This was compounded by habitat constriction and nutrient (e.g. fixed N) loss associated with shoaling sulfidic conditions, which peaked (based on the observed isorenieratane maxima at multiple sites) across [minimally] the southern and central p-NA continental margins just before OAE-2 'ended' based on the +CIE. Coincident collapses in primary production occurred, leading to the cessation of heightened organic carbon production and the conclusion of the +CIE. However, regional anoxia and euxinia lingered beyond the +CIE, as evinced by sulfur isotopes (Owens et al., 2013; Raven et al., 2019), biomarkers (Connock et al., in review, Chapter 1; this study), carbon isotopes (Erbacher et al., 2005), thallium isotopes (Ostrander et al., 2017), and trace metals (Owens et al., 2016). Thus, the

OAE did not exhibit a spatially universal 'end', with significant regions of the p-NA and [potentially] greater ocean basins still subject to extensive anoxia/euxinia priming the marine realm for the next OAE. In summary, diachronous microbial ecological shifts across the p-NA, principally driven by evolving water column chemistry and structure, signify how simultaneously distinct forcings across space (i.e. productivity and preservation) operated along a continuum locally to initiate, modulate and terminate OAE-2 and produce the spatiotemporal behavior of the +CIE.

4.5 Conclusions

Application of a novel LC-qTOF-MS method revealed unseen microbial ecological dynamics, captured by comprehensive biomarker inventories, reflective of evolving oceanographic conditions spanning OAE-2 in the p-NA. Significantly, biomarker distributions revealed marked sensitivity to the development and expansion of anoxia, and eventually euxinia, which accounted for the initiation, perpetuation, and termination of enhanced carbon burial producing the stratigraphic behavior of the +CIE and coincident OAE. Our findings highlight the influence of vertical redox gradients on organic carbon burial drivers, with key implications emphasizing how localized heterogeneities in depositional conditions may be masked by proxies recording fluctuations in global biogeochemical cycles. Although we address the +CIE in this work, future study must target other proxy records (e.g. $\delta^{15}N$) to further disentangle local from global influences if we are to mechanistically ascertain an accurate model for not just OAE-2, but marine deoxygenation throughout geologic time.

4.6 References

1. Albani El., A. E., Vachard, D., Kuhnt, W., & Chellai, E. H. (1999). Signature of hydrodynamic activity caused by rapid sea level changes in pelagic organic-rich sediments, Tarfaya basin (southern Morocco). Earth and Planetary Science Letters, 329, 397-404.
2. Arthur, M. A., & Premoli-Silva, I. (1982). Development of widespread organic carbon-rich strata in the Mediterranean Tethys. Nature and Origin of Cretaceous Carbon-Rich Facies, 7-54.
3. Arthur, M. A., Schlanger, S. O., & Jenkyns, H. C. (1987). The Cenomanian-Turonian Oceanic anoxic event II, Palaeoceanographic controls on organic-matter production and preservation, Geol. Soci. Spec. Publ., 26, 401-420.
4. Arthur, M. A., Dean, W. E., & Pratt, L. M. (1988). Geochemical and climatic effects of increased marine organic carbon burial at the Cenomanian/Turonian boundary, Nature 335, 714-717.
5. Barclay, R. S., McElwain, J. C., & Sageman, B. B. (2010). Carbon sequestration activated by a volcanic CO2 pulse during Oceanic Anoxic Event 2. Nature Geoscience 3, 205-208.
6. Bjerrum, C. J., Bendtsen, J., & Legarth, J. J. F. (2006). Modeling organic carbon burial during sea level rise with reference to the Cretaceous. Geochemistry, Geophysics, Geosystems, 7, 1-24.
7. Bomou, B., Adatte, T., Tantawy, A. A., Mort, H., Fleitmann, D., Huang, Y. & Föllmi, K. B. (2013). The expression of the Cenomanian-Turonian oceanic anoxic event in Tibet. Palaeogeography, Palaeoclimatology, Palaeoecology, 369, 466–481.
8. Breit, G. N., & Wanty, R. B. (1991). Vanadium accumulation in carbonaceous rocks – a review of geochemical controls during deposition and diagenesis. Chemical Geology, 91, 83-97.
9. Clarkson, M. O., Stirling, C. H., Jenkyns, H. C., Dickson, A. J., Porcelli, D., Moy, C. M., Pogge von Strandmann, P. A. E., Cooke, I. R., & Lenton, T. M. (2018). Uranium isotope evidence for two episodes of deoxygenation during Oceanic Anoxic Event 2. Proceedings of the National Academy of Sciences, 115, 2918-2923.
10. Connock, G. T., Liu, X.-L., & Owens, J. D. (in review). Biotic induction and microbial ecological dynamics of Oceanic Anoxic Event 2 (OAE-2). Communications Earth & Environment.
11. Demaison, G. J., & Moore, G. T. (1980). Anoxic environments and oil source bed genesis. Organic Geochemistry, 2, 9-31.
12. Devol, A. H. (2015). Denitrification, anammox, and N_2 production in marine sediments. Annual Review of Marine Science, 7, 403-423.
13. Du Vivier, A. D. C., Selby, D., Sageman, B. B., Jarvis, I., Gröcke, D. R. & Voigt, S. (2014). Marine $^{187}Os/^{188}Os$ isotope stratigraphy reveals the interaction of volcanism and ocean circulation during Oceanic Anoxic Event 2. Earth Planet. Sci. Lett. 389, 23–33.
14. Du Vivier, A. D. C., Jacobson, A. D., Lehn, G. O., Selby, D., Hurtgen, M. T. & Sageman, B. B. (2015). Ca isotope stratigraphy across the Cenomanian-Turonian OAE 2: Links between volcanism, seawater geochemistry, and the carbonate fractionation factor. Earth Planet. Sci. Lett. 416, 121–131.
15. Erbacher, J., Mosher, D. C., Malone, M. J., & Expedition 207 Scientists. (2004). Chapter 5, Site 1258. Proceedings of the Ocean Drilling Program, Initial Reports, 207, 1-117.

16. Erbacher, J., Friedrich, O., Wilson, P. A., Birch, H. & Mutterlose, J. (2005). Stable organic carbon isotope stratigraphy across Oceanic Anoxic Event 2 of Demerara Rise, western tropical Atlantic. Geochemistry, Geophysics Geosystems, 6, 1–9.
17. Forster, A., Sturt, H., Meyers, P. A., & Expedition 207 Scientists. (2004). Molecular biogeochemistry of Cretaceous blacks shales from Demerara Rise: Preliminary shipboard results from sites 1257 and 1258, Leg 207. Proceedings of the Ocean Drilling Program, 207, 1-22.
18. Friedrich, O., Erbacher, J., Moriya, K., Wilson, P. A., & Kuhnert, H. (2008). Warm saline intermediate waters in the Cretaceous tropical Atlantic Ocean. Nature Geoscience, 1, 453-457.
19. Frijia, G. & Parente, M. (2008). Strontium isotope stratigraphy in the upper Cenomanian shallow-water carbonates of the southern Apennines: Short-term perturbations of marine 87Sr/86Sr during the oceanic anoxic event 2. Palaeogeography, Palaeoclimatology, Palaeoecology. 261, 15-29.
20. Grams, G. W., Eskins, K., & Inglett, G. E. (1972). Dye-sensitized photooxidation of α-tocopherol. Journal of the American Chemical Society, 94, 866-868.
21. Handoh, I. C., Bigg, G. R., Jones, E. J. W., & Inoue, M. (1999). An ocean modeling study of the Cenomanian Atlantic: Equatorial paleo-upwelling, organic-rich sediments and the consequences for a connection between the proto-North and South Atlantic. Geophysical Research Letters, 26, 223-226.
22. Hasegawa, T. (1997). Cenomanian-Turonian carbon isotope events recorded in terrestrial organic matter from northern Japan. Palaeogeography, Palaeoclimatology, Palaeoecology, 130, 251–273.
23. Herbin, J. P., Montadert, L., Müller, C., Gomez, R., Thurow, J. W., & Wiedmann, J. (1986). Organic-rich sedimentation at the Cenomanian-Turonian boundary in oceanic and coastal basins in the North Atlantic and Tethys. Geological Society Special Publications, 21, 389-422.
24. Hetzel, A., Böttcher, M. E., Wortmann, U. G., & Brumsack, H.-J. (2009). Paleo-redox conditions during OAE 2 reflected in Demerara Rise sediment geochemistry (ODP Leg 207). Palaeogeography, Palaeoclimatology, Palaeoecology, 273, 302-328.
25. Higgins, M. B., Robinson, R. S., Husson, J. M., Carter, S. J., & Pearson, A. (2012). Dominant eukaryotic export production during ocean anoxic events reflects the importance of recycled NH_4^+. Proceedings of the National Academy of Sciences, 109. 2269-2274.
26. Ingram, B.L., Coccioni, R., Montanari, A. & Richter, F.M. (1994). Strontium isotopic composition of mid-Cretaceous seawater. Science, 264, 546-550.
27. Jarvis, I., Gale, A. S., Jenkyns, H. C., & Pearce, M. A. (2006). Secular variation in Late Cretaceous carbon isotopes: A new δ13C carbonate reference curve for the Cenomanian-Campanian (99.6-70.6). Geol. Mag., 143, 561-608.
28. Jenkyns, H.C., Matthews, A., Tsikos, H., & Erel, Y. (2007). Nitrate reduction, sulfate reduction, and sedimentary iron isotope evolution during the Cenomanian-Turonian oceanic anoxic event. Paleoceanography, 22, PA3208.
29. Jenkyns, H. C. (2010). Geochemistry of oceanic anoxic events. Geochemistry, Geophysics Geosystems, 11, 1–30.
30. Jenkyns, H.C., Dickson, A.J., Ruhl, M., & Van den Boorn, S.H. (2017). Basalt-seawater interaction, the Plenus Cold Event, enhanced weathering and geochemical change:

deconstructing Oceanic Anoxic Event 2 (Cenomanian–Turonian, Late Cretaceous). Sedimentology, 64, 16-43.
31. Jiménez Berrocoso, A., MacLeod, K. G., Martin, E. E., Bourbon, E., Londoño, C. I., & Basak, C. (2010). Nutrient trap for Late Cretaceous organic-rich black shales in the tropical North Atlantic. Geology, 38, 1111-1114.
32. Junium, C. K., Freeman, K. H., & Arthur, M. A. (2015). Controls on the stratigraphic distribution and nitrogen isotopic composition of zinc, vanadyl and free base porphyrins through Oceanic Anoxic Event 2 at Demerara Rise. Organic Geochemistry, 80, 60-71.
33. Kaiho, K. & Saito, S. (1994). Oceanic crust production and climate during the last 100 Myr. Terra Nova, 6, 376-384.
34. Kashiyama, Y., Ogawa, N. O., Kuroda, J., Shiro, M., Nomoto, S., Tada, R., Kitazato, H., & Ohkouchi, N. (2008). Diazotrophic cyanobacteria as the major photoautotrophs during mid-Cretaceous oceanic anoxic events: Nitrogen and carbon isotopic evidence from sedimentary porphyrin. Organic Geochemistry, 29, 532-549.
35. Kolonic, S., Wagner, T., Forster, A., Sinninghe Damsté, J. S., Walsworth-Bell, B., Erba, E., Turgeon, S., Brumsack, H.-J., Chellai, E. H., Tsikos, H., Kuhnt, W., & Kuypers, M. M. M. (2005). Black shale deposition on the northwest African Shelf during the Cenomanian/Turonian oceanic anoxic event: Climate coupling and global organic carbon burial. Paleoceanography, 20, PA1006.
36. Könneke, M., Schubert, D.M., Brown, P.C., Hügler, M., Standfest, S., Schwander, T., von Borzyskowski, L.S., Erb, T.J., Stahl, D.A., & Berg, I.A. (2014). Ammonia-oxidizing archaea use the most energy-efficient aerobic pathway for CO2 fixation. Proceedings of the National Academy of Sciences, 111, 8239-8244.
37. Kuhnt, W., Nederbragt, A., & Leine, L. (1997). Cyclicity of Cenomanian-Turonian organic-carbon-rich sediments in the Tarfaya Atlantic Coastal Basin (Morocco). Cretaceous Research, 18, 587-601.
38. Kuhnt, W., Chellai, E. H., Holbourn, A., Luderer, F., Thurow, J., Wagner, T., El Albani, A., Beckmann, B., Herbin, J.-P., Kawamura, H., Kolonic, S., Nederbragt, S., & Ravilious, K. (2001). Morocco Basin's sedimentary record may provide correlations for Cretaceous paleoceanographic events worldwide. EOS Transactions, American Geophysical Union, 82, 361-368.
39. Kuhnt, W., Luderer, F., Nederbragt, S., Thurow, J., & Wagner, T. (2005). Orbital-scale record of the late Cenomanian-Turonian oceanic anoxic event (OAE-2_ in the Tarfaya Basin (Morocco). International Journal of Earth Sciences, 94, 147-159.
40. Kuhnt, W., Holbourn, A. E., Beil, S., Aquit, M., Krawczyk, T., Flögel, S., Chellai, E. H., & Jabour, H. (2017). Unraveling the onset of Cretaceous Oceanic Anoxic Event 2 in an extended sediment archive from the Tarfaya-Laayoune Basin, Morocco. Paleoceanography, PA003146.
41. Kuypers, M. M. M., Pancost, R. D., Nijenhuis, I. A. & Sinninghe Damsté, J. S. (2002). Enhanced productivity led to increased organic carbon burial in the euxinic North Atlantic basin during the late Cenomanian oceanic anoxic event. Paleoceanography, 17, 3, 3–13.
42. Kuypers, M. M. M., Sliekers, A. O., Lavik, G., Schmid, M., Jørgensen, B. B., Kuenen, J. G., Sinninghe Damsté, J. S., Strous, M., & Jetten, M. S. M. (2003). Anaerobic ammonium oxidation by anammox bacteria in the Black Sea. Nature, 422, 608-611.

43. Kuypers, M. M. M., van Breugel, Y., Schouten, S., Erba, E. & Sinninghe Damsté, J. S. (2004). N_2-fixing cyanobacteria supplied nutrient N for Cretaceous oceanic anoxic events. Geology, 32, 853-856.
44. Larson, R. L. (1991). Latest pulse of Earth: Evidence for a mid-Cretaceous superplume. Geology, 19, 547-550.
45. Leine, L. (1986). Geology of the Tarfaya oil shale deposit, Morocco. Geol. Mijnbouw, 65, 57-74.
46. Lewan, M. D. (1984). Factors controlling the proportionality of vanadium to nickel in crude oils. Geochimica et Cosmochimica Acta, 48, 2231-2238.
47. Liebler, D. C., Baker, P. F., & Kaysen, K. L. (1990). Oxidation of vitamin E: evidence for competing autoxidation and peroxyl radical trapping reactions of the tocopheryl radical. Journal of the American Chemical Society, 112, 6995-7000.
48. Liu, X.-L., Birgel, D., Elling, F., Sutton, P. A., Lipp, J. S., Zhu, R., Zhang, C., Könneke, M., Peckmann, J., Rowland, S. J., Summons, R. E., & Hinrichs, K.-U. (2016). From ether to acid: A plausible degradation pathway of glycerol dialkyl glycerol tetraethers. Geochimica et Cosmochimica Acta, 183, 138-152.
49. Macleod, K. G., Martin, E. E., & Blair S. W. (2008). Nd isotopic excursion across Cretaceous ocean anoxic event 2 (Cenomanian-Turonian) in the tropical North Atlantic. Geology, 36, 811–814.
50. Martin, E. E., MacLeod, K. G., Jiménez Berrocoso, A., & Bourbon, E. (2012). Water mass circulation on Demerara Rise during the Late Cretaceous based on Nd isotopes. Earth and Planetary Science Letters, 327-328, 111-120.
51. Meyers, P. A., Bernasconi, S. M., & Forster, A. (2006). Origins and accumulations of organic matter in expanded Albian to Santonian black shale sequences on the Demerara Rise, South American margin. Organic Geochemistry, 37, 1816-1830.
52. Monteiro, F.M., Pancost, R.D., Ridgwell, A., & Donnadieu, Y. (2012). Nutrients as the dominant control on the spread of anoxia and euxinia across the Cenomanian-Turonian oceanic anoxic event (OAE2): Model-data comparison. Paleoceanography, 27, PA4209.
53. Naafs, B. D. A., Monteiro, F. M., Pearson, A., Higgins, M. B., Pancost, R. D., & Ridgwell, A. (2019). Fundamentally different global marine nitrogen cycling in response to severe ocean deoxygenation. Proceedings of the National Academy of Sciences, 116, 24979-24984.
54. Nassiry, M., Aubert, C., Mouzdahir, A., & Rontani, J.-F. (2009). Generation of isoprenoid chromans, notably prist-1-ene, via photo- and autoxidative degradation of vitamin E. Organic Geochemistry, 40, 38-50.
55. Nederbragt, A. J., Thurow, J. W., Vonhof, H., & Brumsack, H. (2004). Modeling oceanic carbon and phosphorus fluxes: implications for the cause of the late Cenomanian Oceanic Anoxic Event (OAE2). Journal of the Geological Society, 161, 721-728.
56. Norris, R. D., Wilson, P. A., Blum, P., & Expedition 342 Scientists. (2014). Site U1407. Proceedings of the Integrated Ocean Drilling Program, 342, 1-106.
57. O'Brien, C. L., Robinson, S. A., Pancost, R. D., Sinninghe Damsté, J. S., Schouten, S., Lunt, D. J., Alsenz, H., Bornemann, A., Bottini, C., Brassell, S. C., Farnsworth, A., Forster, A., Huber, B. T., Inglis, G. N., Jenkyns, H. C., Linnert, C., Littler, K., Markwick, P., McAnena, A., Mutterlose, J., Naafs, B. D. A., Püttmann, W., Sluijs, A., van Helmond, N. A. G. M., Vellekoop, J., Wagner, T., & Wrobel N. E. (2017). Cretaceous sea-surface

temperature evolution: Constraints from TEX 86 and planktonic foraminiferal oxygen isotopes. Earth-Science Reviews, 172, 224–247.
58. Ostrander, C. M., Owens, J. D. & Nielsen, S. G. (2017). Constraining the rate of oceanic deoxygenation leading up to a Cretaceous Oceanic Anoxic Event (OAE-2: ~94 Ma). Sci. Adv. 3, 1–6.
59. Owens, J. D., Lyons, T. W., Li, X., Macleod, K. G., Gordon, G., Kuypers, M. M. M., Anbar, A., Kuhnt, W., & Severmann, S. (2012). Iron isotope and trace metal records of iron cycling in the proto-North Atlantic during the Cenomanian-Turonian oceanic anoxic event (OAE-2). Paleoceanography, 27, 1-13.
60. Owens, J. D., Gill, B. C., Jenkyns, H. C., Bates, S. M., Severmann, S., Kuypers, M. M. M., Woodfine, R. G., & Lyons T. W. (2013). Sulfur isotopes track the global extent and dynamics of euxinia during Cretaceous Oceanic Anoxic Event 2. Proc. Natl. Acad. Sci. 110, 18407–18412.
61. Owens, J. D., Reinhard, C. T., Rohrssen, M., Love, G. D., & Lyons T. W. (2016). Empirical links between trace metal cycling and marine microbial ecology during a large perturbation to Earth's carbon cycle. Earth Planet. Sci. Lett. 449, 407–417.
62. Owens, J. D., Lyons, T. W., & Lowery, C. M. (2018). Quantifying the missing sink for global organic carbon burial during a Cretaceous oceanic anoxic event. Earth Planet. Sci. Lett. 499, 83–94.
63. Pedersen, T. F., & Calvert, S. E. (1990). Anoxia vs. Productivity: What controls the formation of organic-carbon-rich sediments and sedimentary rocks? AAPG Bulletin, 74, 454-466.
64. Pogge Von Strandmann, P. A. E., Jenkyns, H. C. & Woodfine, R. G. (2013). Lithium isotope evidence for enhanced weathering during Oceanic Anoxic Event 2. Nature Geoscience, 6, 668–672.
65. Pratt, L. M., & Threlkheld, C. N. (1984) Stratigraphic significance of 13C/12C ratios in Mid-Cretaceous rocks of the Western Interior, U.S.A. Mem. Can. Soc. Pet. Geol., 9, 305-312.
66. Raven, M. R., Fike, D. A., Gomes, M. L., Webb, S. A., Bradley, A. S., & McClelland, H.-L. O. (2018). Organic carbon burial during OAE2 driven by changes in the locus of organic matter sulfurization. Nature Communications, 9:3409, 1-9.
67. Raven, M. R., Fike, D. A., Bradley, A. S., Gomes, M. L., Owens, J. D., & Webb, S. A. (2019). Paired organic matter and pyrite $\delta^{34}S_{pyrite}$ records reveal mechanisms of carbon, sulfur, and iron cycle disruption during Oceanic Anoxic Event 2. Earth and Planetary Science Letters, 512, 27-38.
68. Rontani, J-F., Nassiry, M., & Mouzdahir, A. (2007). Free radical oxidation (autoxidation) of α-tocopherol (vitamin E): a potential source of 4,8,12-16-tetramethylheptadecan-4-olide in the environment. Organic Geochemistry, 38, 37-47.
69. Sageman, B. B., Meyers, S. R., & Arthur, M. A. (2006). Orbital time scale and new C-isotope record for Cenomanian-Turonian boundary stratotype. Geology, 34, 125-128.
70. Schlanger, S. O., & Jenkyns, H. C. (1976). Cretaceous Oceanic Anoxic Events: Causes and consequences. Geologie en Mijnbouw, 55, 179-184.
71. Scholle, P. A., & Arthur, M. A. (1980). Carbon isotope fluctuations in Cretaceous pelagic limestones: potential stratigraphic and petroleum exploration tool. AAPG Bulletin, 64, 67-87.

72. Sinninghe Damsté, J. S., & Köster, J. (1998). A euxinic southern North Atlantic Ocean during the Cenomanian/Turonian oceanic anoxic event. Earth and Planetary Science Letters, 158, 165-173.
73. Sinninghe Damsté, J. S., Kuypers, M. M. M., Pancost, R. D., & Schouten, S. (2008). The carbon isotopic response of algae, (cyano)bacteria, archaea and higher plants to the late Cenomanian perturbation of the global carbon cycle: Insights from biomarkers in black shales from the Cape Verde Basin (DSDP Site 367). Organic Geochemistry, 39, 1703-1718.
74. Thurow J., Brumsack, H.-J., Rullkötter, J., Littke, R. & Meyers, P. (1992). The Cenomanian/Turonian Boundary Event in the Indian Ocean: a Key to Understand the Global Picture. Geophysical Monograph. 70, 253–273.
75. Trabucho Alexandre, J., Tuenter, E., Henstra, G.A., van der Zwan, K.J., van de Wal, R.S., Dijkstra, H.A., & de Boer, P.L. (2010). The mid-Cretaceous North Atlantic nutrient trap: black shales and OAEs. Paleoceanography, 25, PA4201.
76. Tsikos H., Jenkyns H. C., Walsworth-Bell B., Petrizzo M. R., Forster A., Kolonic S., Erba E., Silva I. P., Baas M., Wagner T., and Sinninghe Damsté, J. S. (2004). Carbon-isotope stratigraphy recorded by the Cenomanian–Turonian Oceanic Anoxic Event: correlation and implications based on three key localities. J. Geol. Soc. London. 162, 576.1-576.
77. Tucholke, B. E., & Bogt, P. R. (1979). Western North Atlantic: sedimentary evolution and aspects of tectonic history. Initial Reports DSDP, 43, 791-825.
78. Turgeon, S. C., & Creaser, R. A. (2008). Cretaceous oceanic anoxic event 2 triggered by a massive magmatic episode. Nature, 454, 323-328.
79. van Bentum, E. C., Hetzel, A., Brumsack, H.-J., Forster, A., Reichart, G.-J., & Sinninghe Damsté J. S. (2009). Reconstruction of water column anoxia in the equatorial Atlantic during the Cenomanian-Turonian oceanic anoxic event using biomarker and trace metal proxies. Palaeogeography, Palaeoclimatology, Palaeoecology, 280, 489-498.
80. van Bentum, E. C., Reichart, G. J., Forster, A., & Sinninghe Damsté J. S. (2012). Latitudinal differences in the amplitude of the OAE-2 carbon isotopic excursion: pCO_2 and paleo productivity. Biogeosciences, 9, 717–731.
81. Wang, Y., Huang, C., Sun, B., Quan, C., Wu, J., & Lin, Z. (2014). Paleo-CO2 variation trends and the Cretaceous greenhouse climate. Earth Science Reviews 129, 136-147.
82. Wakeham, S. G., & Canuel, E. C. (2005). Degradation and preservation of organic matter in marine sediments. The Handbook of Environmental Chemistry, 2, 295-321.
83. Wilson, S.T., Hawco, N.J., Armbrust, E.V., Barone, B., Björkman, K.M., Boysen, A.K., Burgos, M., Burrell, T.J., Casey, J.R., DeLong, E.F. and Dugenne, M. (2019). Kīlauea lava fuels phytoplankton bloom in the North Pacific Ocean. Science, 365, 1040-1044.
84. Zachos, J. C., Dickens, G. R., & Zeebe, R. E. (2008). An early Cenozoic perspective on greenhouse warming and carbon-cycle dynamics. Nature, 451, 279-283.

4.7 Figures

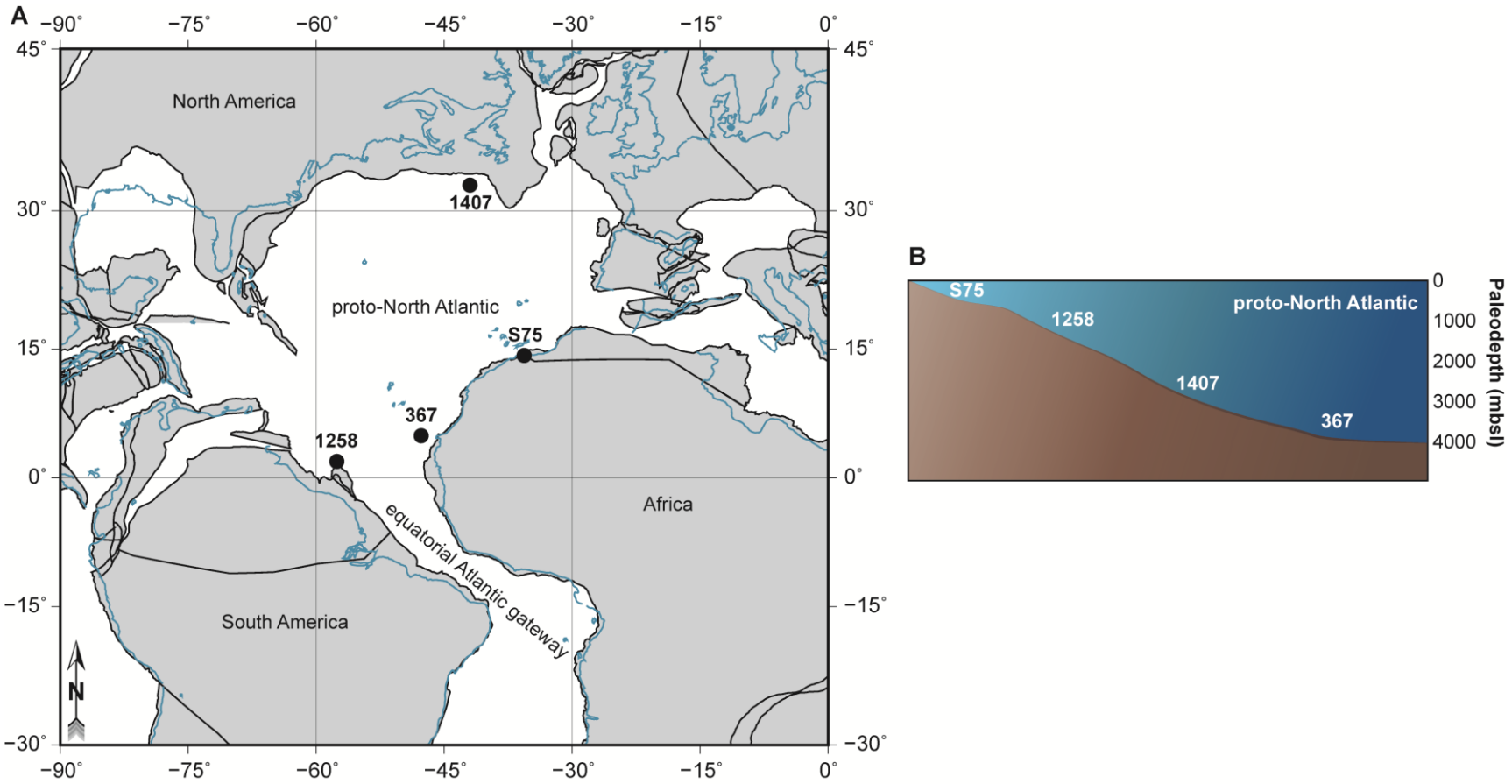

Figure 4-1. Paleogeographic and depositional context of study sites in the proto-North Atlantic Ocean. (A) Regional paleogeographic reconstruction at 93.9 Ma using the Ocean Drilling Stratigraphic Network (ODSN) plate reconstruction service (https://www.odsn.de/odsn/services/paleomap/paleomap.html). Blue lines represent modern shorelines, while gray shading bounded by black lines represents plate fragments. Sites are denoted with black dots and labeled accordingly. (B) Generalized cartoon of depositional setting and paleodepth of study sites.

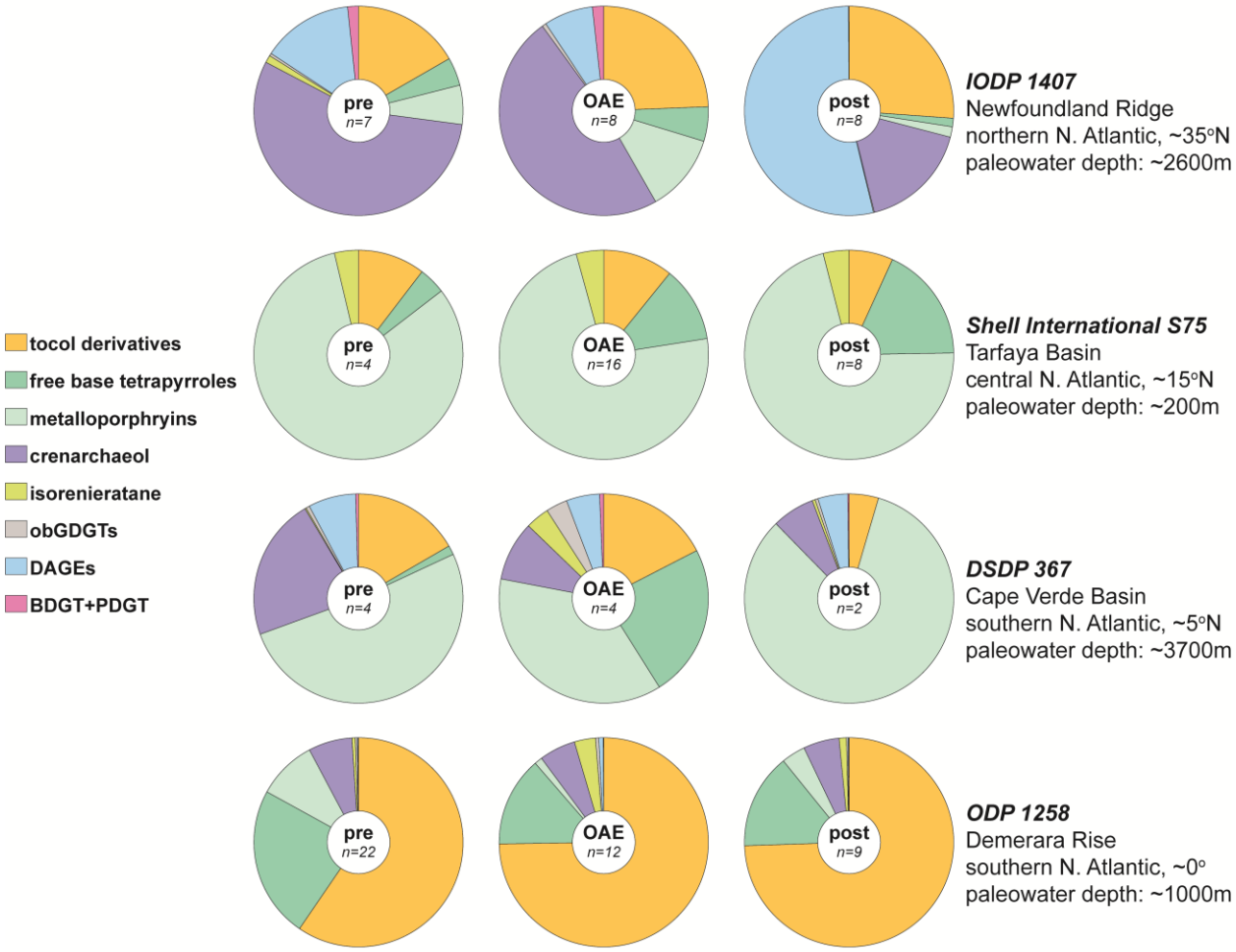

Figure 4-2. Averaged biomarker fractional abundance pie charts for pre-OAE, OAE, and post-OAE samples. Note the number of samples averaged for each respective pie chart, as this was not consistent between sites or time intervals. Sites are ordered by latitude (i.e. ascending latitude from bottom to top).

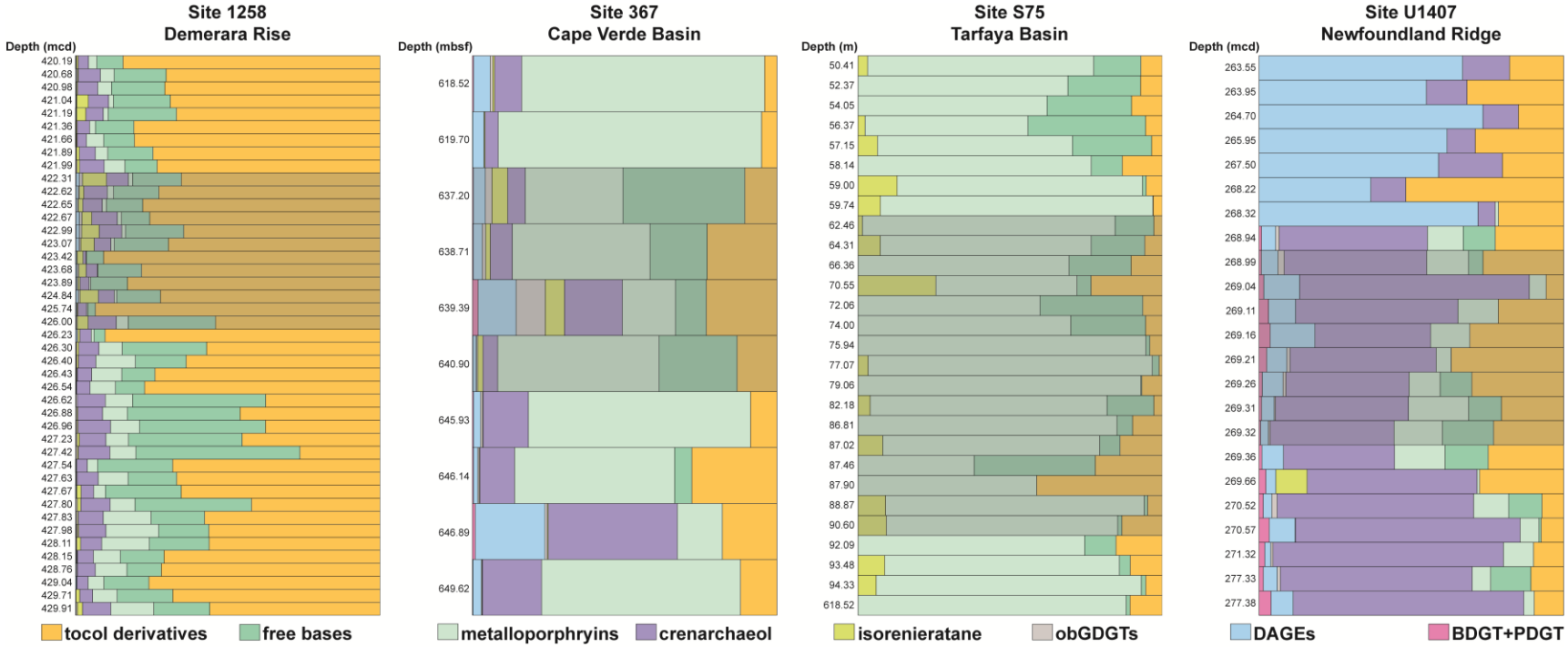

Figure 4-3. Biomarker fractional abundances preceding, during, and following OAE-2 at individual sites. Light gray shading corresponds to OAE-2 as defined by the site-specific +CIE.

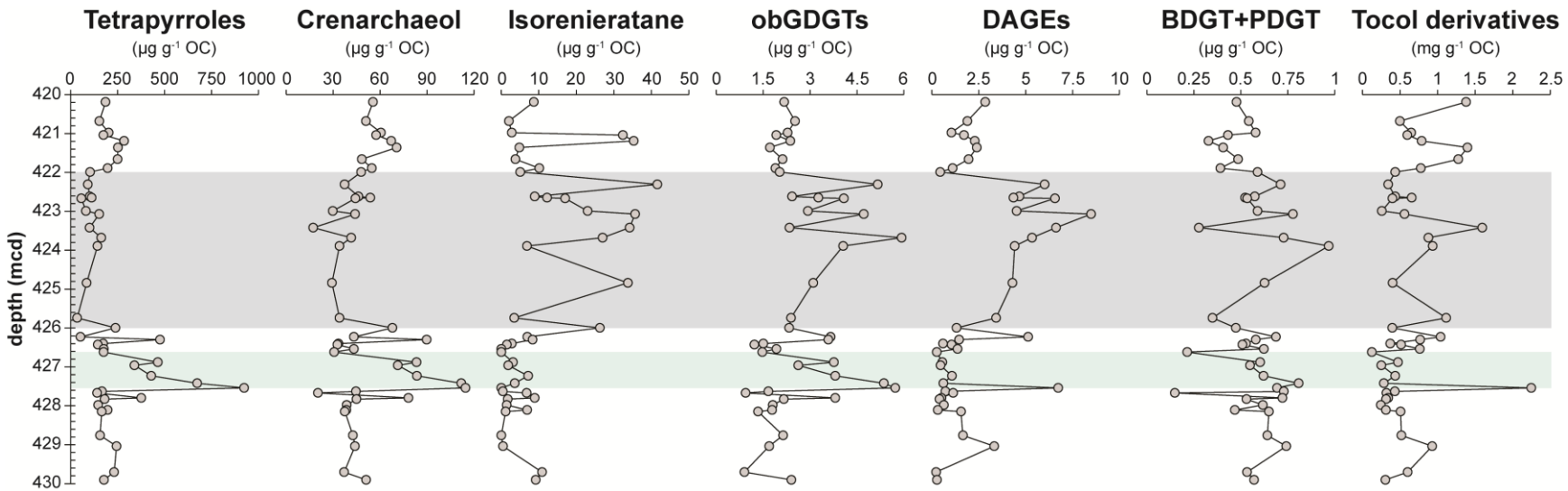

Figure 4-4. Depth profiles of biomarker concentrations at ODP Site 1258. The blue line represents the pre-OAE BP as determined by biomarker distributions and the gray shading denotes the OAE-2 interval.

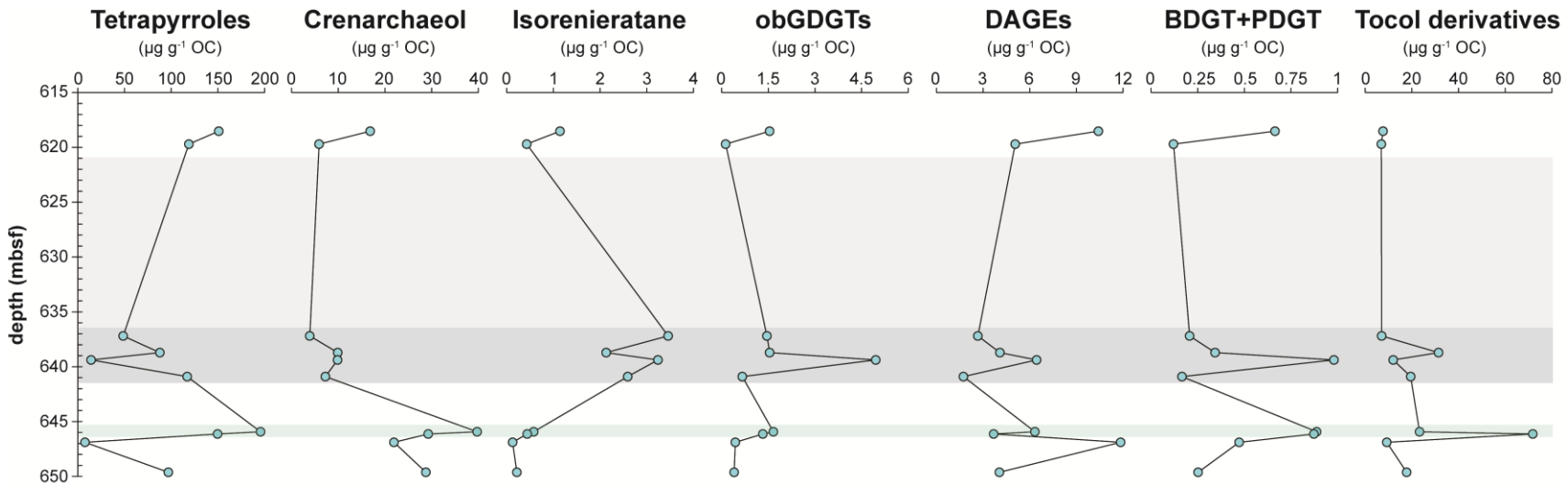

Figure 4-5. Depth profiles of biomarker concentrations at DSDP Site 367. The blue line represents the pre-OAE BP as determined by biomarker distributions. The darker gray shading denotes the OAE-2 interval, with light gray signifying maximum possible extents of OAE-2 unresolved due to poor core recovery leading to a stratigraphic void.

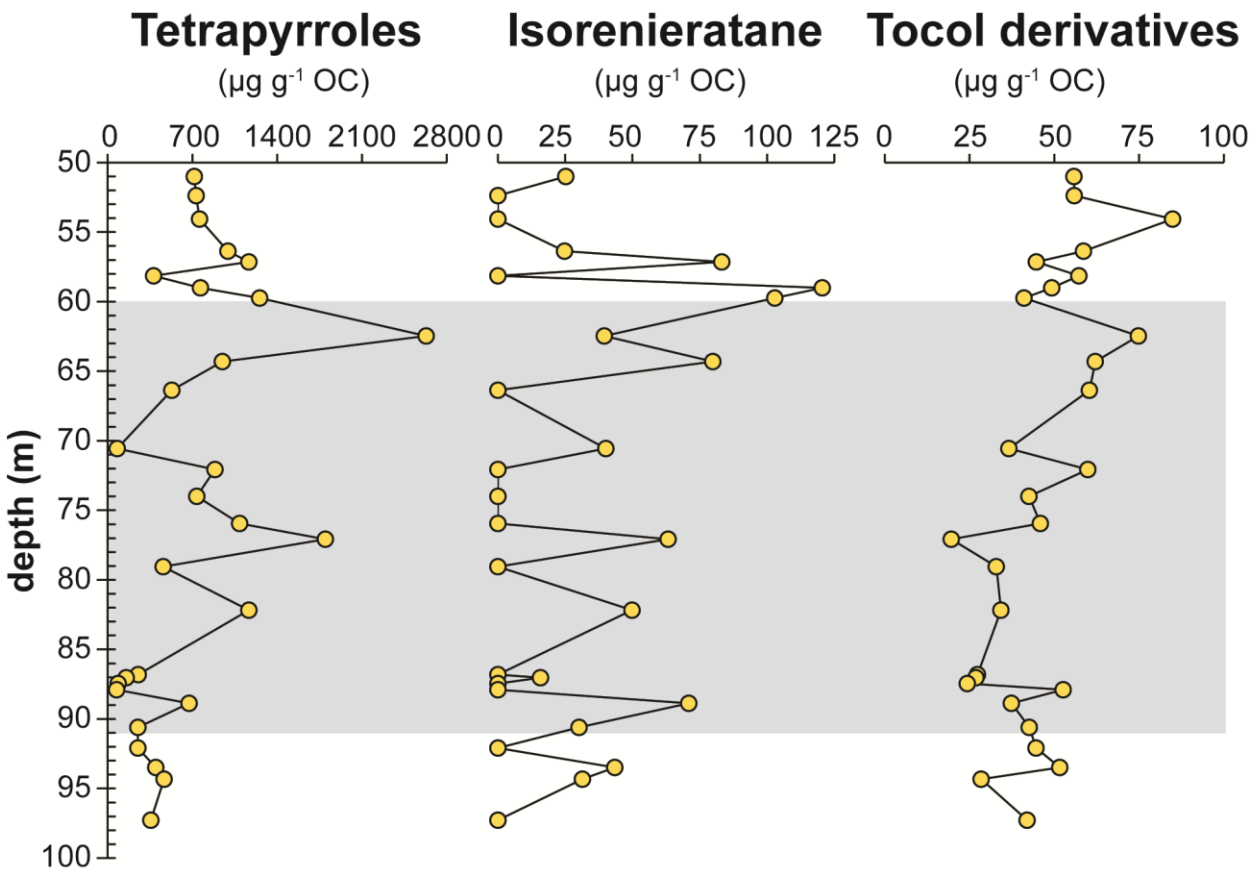

Figure 4-6. Depth profiles of biomarker concentrations at Site S75. Gray shading highlights the OAE-2 interval.

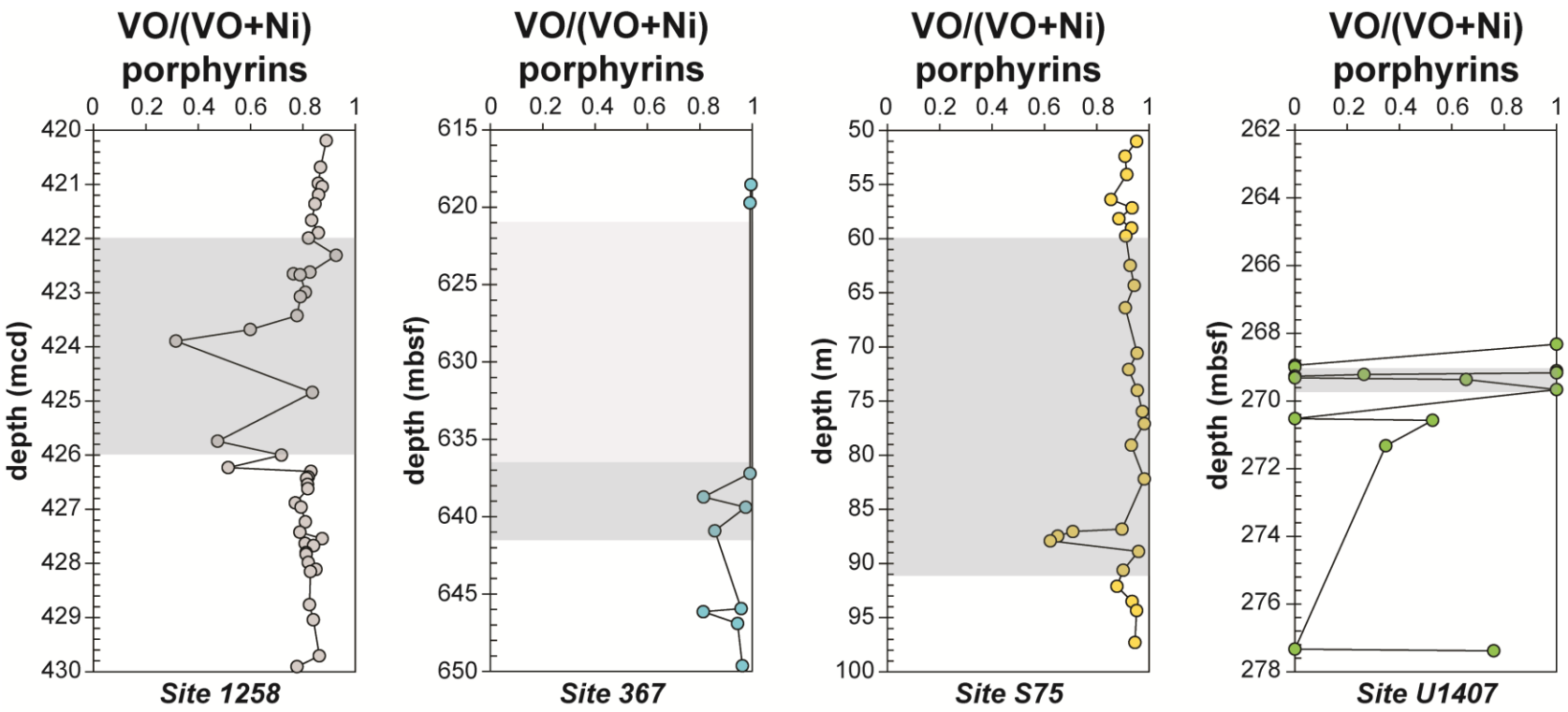

Figure 4-7. VO/Ni metalloporphyrin ratios across the four studied OAE-2 sites. Dark gray shading denotes the OAE-2 interval, light gray shading represents the potential temporal extents of OAE-2 at site 367 where a void in the cored interval precluded complete delineation of OAE-2.

4.8 Tables

Sample	Modified depth (mcd)	Tetrapyrroles (µg g-1 OC)	Crenarchaeol (µg g-1 OC)	Isorenieratane (µg g-1 OC)	obGDGTs (µg g-1 OC)	DAGEs (µg g-1 OC)	BDGT+PDGT (µg g-1 OC)	Tocol derivatives (µg g-1 OC)	VO/(VO+Ni) Porphyrins
207-1258B 45R-3 1-2	420.19	185.54	55.54	8.65	2.17	2.84	0.48	1380.88	0.89
207-1258A 42-5 51-53	420.68	153.17	50.94	2.03	2.52	1.89	0.54	497.52	0.87
207-1258B 45-3 80-81	420.98	202.22	60.55	2.82	2.28	1.03	0.58	649.81	0.86
207-1258A 42-5 87-88	421.04	175.09	57.47	32.40	1.92	1.71	0.43	595.68	0.87
207-1258A 42-5 102-103	421.19	284.28	67.18	35.29	2.37	2.28	0.33	789.99	0.86
207-1258A 42-5 119-121	421.36	251.62	70.51	4.83	1.72	2.39	0.41	1399.04	0.85
207-1258A 42-6 17-18	421.66	249.57	48.36	3.76	2.12	1.95	0.49	1277.46	0.83
207-1258B 45-4 30-31	421.89	197.09	54.75	10.12	1.89	1.10	0.39	778.21	0.86
207-1258B 45R-4 40-41	421.99	103.57	47.90	5.04	2.03	0.44	0.59	436.02	0.82
207-1258A 42-6 82-83	422.31	91.52	37.32	41.53	5.16	6.00	0.71	342.25	0.93
207-1258A 42-6 113-114	422.62	101.60	46.14	8.90	2.42	4.66	0.57	436.39	0.83
207-1258B 45R-4 106-107	422.65	111.63	53.70	12.20	3.26	4.34	0.52	655.65	0.76
207-1258A 42-6 118-119	422.67	56.33	44.27	16.98	4.08	6.55	0.53	399.46	0.79
207-1258A 42-7 10-11	422.99	81.46	29.80	22.98	2.93	4.51	0.59	257.90	0.81
207-1258B 45R-4 148-149	423.07	151.95	44.11	35.65	4.72	8.48	0.78	559.59	0.79
207-1258A 42-7 53-54	423.42	100.63	17.21	34.17	2.34	6.60	0.28	1595.46	0.78
207-1258A 42-7 79-80	423.68	163.18	41.50	26.97	5.93	5.33	0.73	878.42	0.60
207-1258A 42-7 100-101	423.89	142.44	34.04	6.82	4.06	4.41	0.97	935.93	0.31
207-1258C 17R-1 5-6	424.84	84.57	29.20	33.73	3.10	4.29	0.63	402.35	0.84
207-1258C 17R-1 95-96	425.74	34.36	34.06	3.46	2.39	3.42	0.35	1113.37	0.47
207-1258C 17R-1 121-122	426.00	238.45	67.94	26.26	2.33	1.31	0.47	396.46	0.72
207-1258A 42-7 114-115	426.23	52.22	43.27	6.94	3.66	5.12	0.69	1040.44	0.51
207-1258C 17R-2 12-13	426.30	476.04	89.80	8.32	3.58	1.44	0.58	767.52	0.83
207-1258C 17R-2 22-23	426.40	172.97	33.43	2.80	1.51	0.58	0.53	371.03	0.82
207-1258C 17R-2 25-26	426.43	144.30	32.72	1.46	1.22	1.05	0.51	514.21	0.81
207-1258A 42-CCW 4-5	426.54	177.06	43.25	-	1.92	1.36	0.62	764.89	0.82
207-1258A 43-1 14-15	426.62	175.32	30.69	-	1.47	0.26	0.21	125.07	0.82
207-1258C 17R-2 70-71	426.88	464.13	83.28	3.13	3.76	0.55	0.60	472.76	0.77
207-1258A 43-1 41-42	426.96	339.51	71.30	1.85	2.62	0.45	0.55	251.46	0.79
207-1258A 43-1 75-76.5	427.23	429.68	83.48	7.14	3.80	1.06	0.62	435.25	0.81
207-1258C 17R-3 4-5	427.42	673.73	111.88	3.59	5.36	0.61	0.81	284.34	0.79
207-1258A 43-1 106-107	427.54	924.20	114.68	0.00	5.72	6.73	0.69	2248.94	0.87
207-1258C 17R-3 25-26	427.63	166.50	44.65	0.40	1.67	0.72	0.73	430.93	0.81
207-1258A 43-1 119-120	427.67	140.57	20.37	6.73	0.94	1.13	0.15	319.69	0.84
207-1258A 43-2 4-5	427.80	375.94	78.13	8.90	3.80	0.50	0.72	341.86	0.81
207-1258C 17R-3 45-46	427.83	181.63	44.96	1.69	2.16	0.40	0.53	314.63	0.81
207-1258C 17R-CC 2-3	427.98	146.56	38.72	1.43	1.81	0.64	0.62	243.43	0.82
207-1258C 17R-CC 15-16	428.11	196.85	38.48	6.89	1.79	0.31	0.47	313.10	0.85
207-1258A 43-2 39-41	428.15	166.03	37.49	1.17	1.34	1.55	0.65	507.98	0.83
207-1258A 43-2 100-105	428.76	156.29	42.66	0.00	2.14	1.65	0.64	518.49	0.83
207-1258A 43-3 2-3	429.04	244.70	43.92	0.44	1.69	3.32	0.74	929.21	0.84
207-1258A 43-3 68.5-70	429.71	231.72	37.03	10.86	0.90	0.22	0.53	600.40	0.86
207-1258A 43-3 88.5-90	429.91	177.79	51.13	9.14	2.40	0.27	0.57	306.35	0.78

Table 4-1. Biomarker concentrations and metalloporphyrin VO/Ni values at ODP Site 1258. Gray shading denotes OAE-2.

Sample	Modified depth (mbsf)	Tetrapyrroles (µg g-1 OC)	Crenarchaeol (µg g-1 OC)	Isorenieratane (µg g-1 OC)	obGDGTs (µg g-1 OC)	DAGEs (µg g-1 OC)	BDGT+PDGT (µg g-1 OC)	Tocol derivatives (µg g-1 OC)	VO/(VO+Ni) Porphyrins
367_17-2_102-107	618.52	150.94	16.84	1.14	1.55	10.42	0.66	7.66	1.00
367_17-3_68-74	619.70	118.90	5.89	0.43	0.13	5.07	0.12	6.93	0.99
367_18-1_120-124	637.20	48.54	3.87	3.46	1.46	2.67	0.21	7.09	0.99
367_18-2_121-125	638.71	87.78	9.89	2.13	1.54	4.09	0.34	31.40	0.81
367_18-3_39-42	639.39	14.26	9.85	3.24	4.95	6.44	0.98	11.99	0.98
367_18-4_40-43	640.90	117.14	7.22	2.59	0.67	1.74	0.17	19.52	0.86
367_19-1_143-147	645.93	195.66	39.76	0.58	1.66	6.33	0.89	23.27	0.96
367_19-2_14-18	646.14	149.63	29.26	0.44	1.33	3.68	0.87	71.84	0.81
367_19-2_89-94	646.89	7.63	21.92	0.13	0.45	11.84	0.47	9.28	0.94
367_19-4_62-66	649.62	96.90	28.74	0.22	0.41	4.06	0.25	17.76	0.96

Table 4-2. Biomarker concentrations and metalloporphyrin VO/Ni values at DSDP Site 367. Gray shading denotes OAE-2.

Sample	Modified depth (m)	Tetrapyrroles (µg g-1 OC)	Isorenieratane (µg g-1 OC)	Tocol derivatives (µg g-1 OC)	VO/(VO+Ni) Porphyrins
S75_34	51.00	716.04	25.21	55.81	0.95
S75_36	52.37	731.82	0.00	55.91	0.91
S75_40	54.05	759.78	0.00	84.89	0.91
S75_43	56.37	993.58	24.71	58.65	0.85
S75_44	57.15	1167.08	83.15	44.71	0.93
S75_45	58.14	378.76	0.00	57.23	0.88
S75_46	59.00	766.75	120.48	49.24	0.93
S75_48	59.74	1255.73	102.85	41.10	0.91
S75_52	62.46	2631.52	39.51	74.83	0.93
S75_54	64.31	947.95	79.89	62.09	0.94
S75_59	66.36	530.00	0.00	60.38	0.91
S75_64	70.55	80.01	40.11	36.59	0.95
S75_65AI	72.06	885.48	0.00	59.93	0.92
S75_65BE	74.00	736.10	0.00	42.55	0.96
S75_67	75.94	1090.16	0.00	45.86	0.97
S75_68	77.07	1799.03	63.20	19.64	0.98
S75_72	79.06	458.14	0.00	32.90	0.93
S75_76B	82.18	1167.56	49.90	34.28	0.98
S75_77K	86.81	253.19	0.00	27.29	0.90
S75_77R	87.02	151.65	15.84	26.86	0.71
S75_77U	87.46	86.37	0.00	24.34	0.65
S75_77X	87.90	74.99	0.00	52.65	0.62
S75_79	88.87	673.11	70.92	37.38	0.96
S75_81	90.60	249.15	30.13	42.58	0.90
S75_84	92.09	249.42	0.00	44.61	0.88
S75_85	93.48	397.06	43.41	51.57	0.93
S75_86	94.33	465.39	31.37	28.44	0.95
S75_90	97.28	355.83	0.00	41.99	0.95

Table 4-3. Biomarker concentrations and metalloporphyrin VO/Ni values at Site S75. Gray shading denotes OAE-2.

Concluding remarks and future work

The findings presented in this work underscore the potential of the applied LC-qTOF-MS method in paleoenvironmental study. Generation of comprehensive biomarker inventories, especially in well-preserved sediments and rocks (e.g. DSDP, ODP, IODP cores), enabled reanimation of marine microbial dynamics sensitive to environmental fluxes surrounding OAE-2. Outstanding enigmas pertaining to periods of enhanced organic carbon burial were partially resolved and seeds for an updated perspective on marine deoxygenation in the geologic record were planted. For the first time, the potential biotic induction of pre-OAE deoxygenation was recognized and spatially defined. Diachroneity in organic carbon burial drivers was also identified, and an updated interpretation of the widely observed positive carbon isotope excursion was proposed. The impact of volcanic ash in marine systems was critically assessed, with transient stimulation of primary productivity and a lasting transition to reducing bottom waters challenging current understandings surrounding the association between volcanism and enhanced organic carbon burial. Biomarkers relegated to insignificance (i.e. tocopherols) were revitalized and discovered to possess significant paleoenvironmental potential delineating pelagic redox fluctuations and/or phytoplanktonic health. This dissertation is an exclusive product of the novel LC-qTOF-MS method applied, and would not exist in its current form if preexisting techniques were used.

Data generation for all chapters was reliant on the negligible sample requirements for LC-qTOF-MS analysis. The DSDP, ODP, and IODP core samples were very limited in quantity, while the high-resolution aims of Chapter 3 significantly reduced sample size. For samples of comparable organic richness, conventional GC-MS preparation requires one to two orders of magnitude more sample (10-50 g) than the method applied here (150-500 mg). Additionally, biomarker inventories were predominantly comprised of large, polar molecules of insufficient

volatility for GC-based analyses (excluding high temperature GC). Not only would derivatization greatly extend sample preparation time, but also could introduce the risk for experimental biases altering the indigeneity of molecular signatures. Additionally, the relatively streamlined preparatory procedure for LC-qTOF-MS enabled rapid sample processing, and it is no exaggeration this dissertation would not be complete if the extensive fractionation required for GC-MS or GC-MS/MS was performed. The biggest challenge has been data condensation, as the LC-qTOF-MS method provided an abundance of tangents to pursue. Those underdeveloped or not mentioned in the preceding chapters will be briefly described as reference for future study.

The most significant emergent discovery, which will require years to constrain, was the relative ease of tetrapyrrole characterization via LC-qTOF-MS. However, alkylation patterns are predominantly unknown, precluding confident associations with precursor chlorophylls and bacteriochlorophylls. Future work will mainly focus on chlorophyll/bacteriochlorophyll degradation experiments and improved determination of alkylation patterns. This will permit compositional changes in chlorophyll/bacteriochlorophyll variants, and by extension [potentially] primary producer composition, to be reconstructed in deep time, providing insight into microbial responses to rapid environmental change and how pigment composition evolved through time.

A novel series of extended archaeols ($C_{20,30}$; $C_{20,35}$; $C_{20,40}$) were identified and discussed as potential markers for halophilic archaea, which permitted temporal variations in water mass density gradients and possible stratification to be assessed at the Demerara Rise. These compounds were also detected at site 367. Further work is needed to constrain source organisms, ultimately affecting their paleoenvironmental significance.

Vitamin K (phylloquinone) and potential derivatives, phyllochromanol and phyllochroman, were detected in all studied sites. Phyllochroman exhibited excellent preservation

potential, comparable to the MTTCs, and correlated very well with MTTCs. If phyllochromanol and phyllochroman are true derivatives of Vitamin K, these compounds may provide similar environmental context as the tocol derivative ratios outlined in Chapter 3.

This new method has also provided a way critically evaluate commonly used organic geochemical proxies (e.g. TEX_{86}, BIT index). Compounds involved in these proxies are simultaneously measured alongside other biomarkers indicative of specific paleoenvironmental conditions. The expanded focus of this work, unrestricted to a specific compound class, revealed interesting covariations between GDGT ring distributions and biomarkers not related to sea surface temperatures. While this does not suggest TEX_{86} fails to capture temperature histories, it may indicate additional controls on the number of GDGT cyclopentane moieties. For example, the inferred sea surface temperature increase coincident with OAE-2 onset at Demerara Rise was accompanied by a marked microbial ecological shift driven by expanding euxinic waters. Perhaps GDGTs do faithfully record temperature, but simply reflect the shoaling of archaeal communities to shallower, warmer waters in response to the vertical advance of sulfidic conditions captured by increases in isorenieratane and DAGEs. Similar peculiarities were observed between the BIT indices and the OAE-2 interval, as briefly discussed in the Supplementary Information of Chapter 1.

Finally, a few notes for continuation and validation of key findings presented in Chapters 1-4. Additional periods of widespread marine deoxygenation need to be evaluated to determine if the pre-OAE BP was unique to OAE-2, or a recurrent mechanism acting to drawdown marine oxygen throughout Earth's history. The proposal of diachronous organic carbon burial drivers would greatly benefit from carbon and nitrogen bulk isotopes, which would permit reconciliation with a simple box model to validate interpretations currently founded on biomarker distributions.

Additionally, further sampling of pre-OAE strata from sites 367 and S75 combined with age constraints is necessary to confidently extrapolate the pre-OAE BP to other sites, and confirm its apparent exclusivity to the southern proto-North Atlantic. Lastly, although multiple bentonites were examined in Chapter 3, additional bentonites of distinct age and depositional setting must be assessed to establish the variability of volcanic ash impacts in marine environments.